

**A NEW TYPE CURVE APPROACH TO THE CONSTRUCTION OF TYPE WELLS
FOR THE ANALYSIS OF MULTI-FRACTURED HORIZONTAL WELLS IN LOW
PERMEABILITY PLAYS**

A Thesis

by

ALEXANDER CHARLES ELEIOTT

Submitted to the Office of Graduate and Professional Studies of
Texas A&M University
in partial fulfillment of the requirements for the degree of

MASTER OF SCIENCE

Chair of Committee,
Committee Members,

Head of Department,

W. John Lee
Duane A. McVay
Zenon Medina-Cetina
Jeff Spath

December 2018

Major Subject: Petroleum Engineering

Copyright 2018 Alexander Charles Eleiott

ABSTRACT

The oil and gas industry has urgent need for accurate methods to forecast performance of future wells and of those without extensive production histories producing from unconventional plays. Reliable assessment of potential future wells allows producers to evaluate their drilling programs and enables them to arrive upon economically sound development strategies. Similarly, accurate forecasting of those wells already drilled but with short production histories is critical for portfolio management, as it enables evaluation of the existing portfolio's current performance and additionally serves as a critical review of decision-making methodology. By constructing type wells at varying levels of uncertainty (P90, P50, and P10), producers will be able to approach these matters statistically and thus avoid the pitfalls associated with deterministic methods and the means by which they address uncertainty.

This thesis presents a newly-developed type curve that may be used to assess reservoir and completions properties and forecast future production from multi-fractured horizontal wells in unconventional, low permeability formations. Additionally, a methodology for the construction of statistical type wells by applying the aforementioned type curve analysis to a large set of wells from a given resource play is proposed. To construct the type wells, all individual wells from a data set are first analyzed individually and then scaled to a common set of reference parameters. Once scaled, wells are ranked by EUR, after which type wells are constructed for each chosen level of uncertainty using the production profile of wells of the corresponding percentile.

Results of this research suggest the new type curve is an effective means by which matrix permeability and fracture half-length may be determined and by which future production may be

forecast. The inclusion of early-time data may distort these results, however, and as such analysis of wells with production histories of less than one year may yield inaccurate results. Additionally, it is critically important to develop a representative set of reference parameters when scaling wells, as any type wells constructed from the set of scaled production profiles will only be fully-representative for wells with properties similar to the reference parameters.

DEDICATION

I dedicate this thesis to my parents, without whom I would be nothing and to whom I owe everything. I additionally dedicate this work to the boys. Thanks for keeping morale high and the ship afloat. Finally, I dedicate this to Shelby. I don't deserve her even at my best, and yet she somehow manages to handle me at my worst.

ACKNOWLEDGEMENTS

I would like to thank Dr. Lee, my advisor and committee chair, for his guiding hand throughout this research process. His sage wisdom and limitless patience were undeniably crucial to this project's success. Additionally, I would like to thank my other committee members, Dr. McVay and Dr. Medina-Cetina, for their input and guidance.

CONTRIBUTORS AND FUNDING SOURCES

Contributors

This study was supervised by a thesis committee consisting of Dr. W. John Lee and Dr. Duane A. McVay of the Harold Vance Department of Petroleum Engineering and Dr. Zenon Medina-Cetina of the Zachry Department of Civil Engineering.

Field data was provided by Romaine Lemoine and Liuyi Jin of the Harold Vance Department of Petroleum Engineering.

All other work conducted for the thesis was completed by the student independently.

Funding Sources

All work was completed independently without outside financial support.

TABLE OF CONTENTS

	Page
ABSTRACT.....	ii
DEDICATION.....	iv
ACKNOWLEDGEMENTS.....	v
CONTRIBUTORS AND FUNDING SOURCES	vi
TABLE OF CONTENTS.....	vii
LIST OF FIGURES	ix
LIST OF TABLES.....	xi
1. INTRODUCTION	1
1.1 Problem Statement.....	1
1.2 Literature Review	1
1.3 Objectives of Research	3
2. ANALYSIS AND METHODOLOGY	4
2.1 Development of New Type Curve.....	4
2.2 Making the Match and Calculation of Parameters.....	10
2.2.1 Outlier Detection and Removal.....	10
2.2.2 Diagnostic Plots.....	11
2.2.3 Making the Match	11
2.2.4 Calculation of Parameters	14
2.3 Forecasting Future Production.....	17
2.4 Scaling	21
2.5 Constructing the Type Wells	25
3. RESULTS	26
3.1 Validation.....	26
3.2 Field Study – Midland Basin Data Set.....	30
3.2.1 Input Parameters.....	31

3.2.2 “Good” Wells	32
3.2.3 “Bad” Wells.....	43
3.2.4 “Early” Wells	48
3.3 The Issue of Uncertainty.....	54
4. CONCLUSIONS AND RECOMMENDATIONS FOR FUTURE WORK....	57
4.1 Conclusions.....	57
4.2 Recommendations for Future Work	58
NOMENCLATURE	59
REFERENCES	61
APPENDIX A.....	62
“Good” Well Set Plots and Results	62
“Bad” Well Set Plots and Results	88
“Early” Well Set Plots and Results.....	101
APPENDIX B.....	141
Derivation of Eq. 2.4.....	141
Derivation of Eq. 2.9.....	143
Derivation of Eqs. 2.22 and 2.23	146
Derivation of Eq. 2.30.....	147
Derivation of Eq. 2.31.....	149
Derivation of Eq. 2.54.....	151

LIST OF FIGURES

	Page
Fig. 2.1: Modified Type Curve	8
Fig. 3.1: Simulated Oil Well Type Curve Match.....	27
Fig. 3.2: Simulated Oil Well – Forecast Testing	28
Fig. 3.3: Simulated Gas Well Type Curve Match.....	29
Fig 3.4: Simulated Gas Well – Forecast Testing	30
Fig. 3.5: Well 119 Diagnostic Plot.....	33
Fig. 3.6: Well 119 Type Curve Match.	34
Fig. 3.7: Well 119 Production History and Forecast	34
Fig. 3.8: Histogram of b_{TR} -Values – “Good” Well Set.....	36
Fig. 3.9: Histogram of Calculated Permeabilities – “Good” Well Set.....	36
Fig. 3.10: Histogram of Calculated Fracture Half-Lengths – “Good” Well Set.....	36
Fig. 3.11: Histogram of Unscaled EURs – “Good” Well Set	38
Fig. 3.12: Histogram of Scaled EURs – “Good” Well Set	39
Fig. 3.13: Unscaled Production Profiles of all Wells – “Good” Well Set	41
Fig. 3.14: Scaled Production Profiles of all Wells – “Good” Well Set	42
Fig. 3.15: P90, P50, and P10 Type Wells – “Good” Well Set.....	43
Fig. 3.16: Histogram of b_{TR} -Values – “Bad” Well Set	44
Fig. 3.17: Histogram of Calculated Permeabilities – “Bad” Well Set	45
Fig. 3.18: Histogram of Calculated Fracture Half-Lengths – “Bad” Well Set	45
Fig. 3.19: Histogram of Unscaled EURs – “Bad” Well Set.....	46
Fig. 3.20: Histogram of Scaled EURs – “Bad” Well Set	46

Fig. 3.21: P90, P50, and P10 Type Wells – “Bad” Well Set	48
Fig. 3.22: Histogram of b_{TR} -Values – “Early” Well Set	50
Fig. 3.23: Histogram of Calculated Permeabilities – “Early” Well Set.....	50
Fig. 3.24: Histogram of Calculated Fracture Half-Lengths – “Early” Well Set	51
Fig. 3.25: Histogram of Unscaled EURs – “Early” Well Set	52
Fig. 3.26: Histogram of Scaled EURs – “Early” Well Set.....	52
Fig. 3.27: P90, P50, and P10 Type Wells – “Early” Well Set	54

LIST OF TABLES

	Page
Table 3.1: Simulated Wells Input Parameters.....	26
Table 3.2: Range of Input Parameters for Wolfcamp Formation Data Set.....	32
Table 3.3: Scaling Reference Parameters – “Good” Well Set.....	38
Table 3.4: Scaled and Unscaled EURs, MSTB – “Good” Well Set	40
Table 3.5: Scaling Reference Parameters – “Bad” Well Set	46
Table 3.6: Scaled and Unscaled EURs, MSTB – “Bad” Well Set.....	47
Table 3.7: Scaling Reference Parameters – “Early” Well Set	52
Table 3.8: Scaled and Unscaled EURs, MSTB – “Early” Well Set	53

1. INTRODUCTION

1.1 Problem Statement

This research seeks to develop a statistical method to construct type wells in order to forecast production of future MFHWs and those with short histories producing from unconventional oil and gas plays. By employing type curves, completion and formation properties may be determined and future production may be forecast for hundreds or thousands of individual wells from a particular play. These analyses can then be used to develop representative type wells at varying levels of uncertainty that will allow for prediction of future production from new and currently drilled wells within that play. This is invaluable to the industry, as it will allow producers to establish economically sound development strategies and critically evaluate the performance of their current portfolios.

The methodology proposed by this research seeks to provide the desired accuracy when predicting the performance of newly drilled or soon-to-be drilled wells with relative ease and without the requirement of extensive and costly testing and data collection. By integrating type curve analysis into the proposed methodology, completion and formation properties can be determined solely from production data, which is easily obtainable and requires no substantial investment.

1.2 Literature Review

The research proposed builds upon the work of Fetkovich (1980) and his development of type curves describing the flow behavior of slightly compressible fluids. Fetkovich (1980) pioneered

the usage of type curves in production data analysis, combining analytical solutions for early time radial transient flow with the empirical Arps' decline equations describing boundary dominated flow. Following Fetkovich, Carter (1985) developed the so-called Carter type curves, bridging an important gap by describing gas flow for finite radial and linear systems. The work proposed in this thesis draws substantial inspiration from the work of Chen and Teufel (2000), as was presented in their paper on the modification of Fetkovich (1980) type curves. Their modification (Chen and Teufel, 2000) includes the addition of transient stems for pure- and near-linear flow, which are expected when producing MFHWs from tight formations. Wattenbarger's type curve (1998) is the primary basis for this research, which describes the behavior of linear flow in fractured wells. This thesis will expand upon Wattenbarger's work, adding transient stems for near-linear flow in a similar fashion to Chen and Teufel (2000) while additionally incorporating hyperbolic BDF stems for the purpose of production forecasting.

As the oil and gas industry becomes increasingly reliant upon unconventional resources, the need for accurate analysis methods becomes all the more pressing. Traditional decline curve analysis methods, developed and useful for assessing conventional reservoirs, are inappropriate for unconventional reservoirs, and as such new analysis techniques are required. In response to this need, type wells have emerged as a useful and effective tool. In their 2012 paper, Freeborn et al. discuss type wells and industry standards for their usage, addressing a number of inadequacies with their current application. Per Freeborn (2012), type wells are often incorrectly constructed by evaluating the arithmetic average of only currently producing wells. However, this practice leads to survivor bias and subsequent overestimation of production and reserves. Additionally, Freeborn (2012) found that the ubiquitous "time-slice" method, commonly used in commercial

software, often yields inaccurate results. Russell et al. (2012) further explored the inaccuracy issues associated with the “time-slice” method, discovering that issues arise when well-rate time profiles are not parallel but instead cross one another. Rastogi and Lee (2015) affirm Freeborn’s assertions regarding the proper averaging of wells when constructing type wells and proposed further modifications to the construction process, suggesting the exclusion of early-time (typically the first six months) data and outliers more than one standard deviation away from the best fit decline trend. Additionally, they recommend the usage of normalized rates based upon the average rate over a given period of time once a stabilized trend is identified (Rastogi and Lee, 2015). In their 2016 paper, Freeborn and Russell discuss the incorporation of aggregation principles and Monte Carlo simulation into the construction of type wells. They show that a probability distribution depends upon the sample size taken from a distribution, with the width of the probability distribution decreasing with increasing sample size (i.e. the uncertainty associated with the mean EUR of 5 wells is higher than that of 10 wells) (Freeborn and Russell 2016).

1.3 Objectives of Research

The objective of this work is to expand upon Wattenbarger’s work on linear flow in fractured wells by developing a new type curve that maintains the utility of Wattenbarger’s type curve while additionally enabling future production to be forecast (1998). Furthermore, the objective is to establish a procedure for using the newly developed type curve to analyze hundreds to thousands of wells from a particular resource play, scale their respective production profiles to a common set of reference parameters, and construct representative type wells that may then be used to predict performance of future wells or wells with short production histories.

2. ANALYSIS AND METHODOLOGY

2.1 Development of New Type Curve

This proposed methodology required modification of Wattenbarger's original type curve, as was presented in his paper on linear flow in fractured tight gas wells (1998). Wattenbarger's type curve consists of two distinct flow periods - early-time pure linear flow, plotted as a negative half-slope logarithmic straight line, followed by exponential decline once the drainage boundaries have all been felt - and serves as an effective tool for reservoir and completions characterization, allowing for the calculation of matrix permeability and fracture half-length. Its inability to provide any basis for the forecasting of future production, however, proves a major limitation. Therefore, the new type curve presented in this work was developed in such a way as to maintain the utility of Wattenbarger's unmodified curve while additionally incorporating elements that overcome this shortcoming.

The new type curve modifies the original in two main ways – first by incorporating additional “infinite-acting” transient stems and second by the addition of multiple hyperbolic boundary dominated flow stems, with an end result resembling Fetkovich's original type curves (1980) and Chen and Teufel's modification thereof (2000). The transient stems consist of a set of logarithmic straight lines with slopes ranging from -1 to -1/4. More generally, a transient stem can be generated for any arbitrary value of b_{TR} between 1 and 4, with the corresponding logarithmic line exhibiting a slope equal to $-1/b_{TR}$. These stems were based upon Wattenbarger's “short-term” approximation for the solution to the constant pressure infinite reservoir outer boundary case, which is shown below (1998).

$$\frac{1}{q_D} = \frac{\pi}{2} \sqrt{\pi \left(\frac{y_e}{x_f}\right)^2 t_{Dye}} \quad (2.1)$$

Rearranging Eq. 2.1 and substituting in q_{Ds_f} for q_D , t_{Ds_f} for t_{Dye} , and $s_f/2$ for y_e , we arrive upon the equation for the transient stem corresponding to $b_{TR} = 2$:

$$\left(\frac{s_f}{x_f}\right) q_D = \left(\frac{4}{\pi^{1.5}}\right) (t_{Ds_f})^{-0.5} \quad (2.2)$$

Defining $t_{Ds_f,Con}$ as the convergence point for all transient stems, the general equation was found to be

$$\left(\frac{s_f}{x_f}\right) q_D = \left(\frac{4}{\pi^{1.5}}\right) (t_{Ds_f,Con})^{\frac{1}{b_{TR}} - \frac{1}{2}} (t_{Ds_f})^{-\frac{1}{b_{TR}}} \quad (2.3)$$

Per Wattenbarger, transient flow concludes at a dimensionless time of 0.25 (1998). Substituting this value into Eq. 2.3, we arrive upon the final form of the general equation for the transient stems:

$$\left(\frac{s_f}{x_f}\right) q_D = \left(\frac{4}{\pi^{1.5}}\right) (0.25)^{\frac{1}{b_{TR}} - \frac{1}{2}} (t_{Ds_f})^{-\frac{1}{b_{TR}}} \quad (2.4)$$

A complete derivation of the Eq. 2.4 can be found in Appendix B.

The addition of hyperbolic BDF stems allows for the forecasting of future production, as it provides a means by which to characterize the flow during the late-time BDF regime. These stems are based upon and are of the same form as the ubiquitous Arps' decline equations, an empirical set of equations presented by J.J. Arps in the mid-20th century (1944). Restated in more familiar terms, Arps' exponential and hyperbolic rate-time decline relations are given by, respectively:

$$q(t) = q_i \exp(-dt) \quad (2.5)$$

where $d = d_i = \text{constant}$ (only in the case of exponential flow), and

$$q(t) = \frac{q_i}{(1 + b_{BDF} d_i t)^{\frac{1}{b_{BDF}}}} \quad (2.6)$$

Values of b_{BDF} can range from 0 to 1. Eq. 2.5 is applicable only when b_{BDF} equals zero, with Eq. 2.6 being appropriate for all other values. However, it should be noted that Eq. 2.6 equals Eq. 2.5 in the limit as b_{BDF} goes to zero. This is significant as it is one of the primary criteria by which the hyperbolic BDF stems for the modified type curve were derived.

Wattenbarger's long-term approximation of the constant pressure closed reservoir solution, given below, defines the late-time exponential flow regime (1998).

$$\frac{1}{q_D} = \frac{\pi}{4} \exp\left(\frac{\pi^2}{4} t_{Dye}\right) \quad (2.7)$$

Rearranging and substituting in q_{Dsf} for q_D , t_{Dsf} for t_{Dye} , and $s_f/2$ for y_e , we arrive upon the equation for the BDF stem corresponding to $b = 0$:

$$\left(\frac{s_f}{x_f}\right) q_D = \frac{8}{\pi} \exp\left(-\frac{\pi^2}{4} t_{Dsf}\right) \quad (2.8)$$

Observing that this equation is of the same form as Arps' equation for exponential decline, it follows logically that the hyperbolic stems will similarly be of the same form as Arps' hyperbolic equation. Under this assumption, the general form of the hyperbolic stems is

$$\left(\frac{s_f}{x_f}\right) q_D = \frac{8}{\pi} / \left(1 + \frac{\pi^2}{4} b_{BDF} t_{Dsf}\right)^{\frac{1}{b_{BDF}}} \quad (2.9)$$

As was the case for Arps' exponential and hyperbolic relations, the general equation for the hyperbolic stems collapses onto Wattenbarger's original exponential stem in the limit as b_{BDF} goes to zero. A complete derivation of Eq. 2.9 is given in Appendix B. The new type curve presented in this thesis can be constructed entirely from Eqs. 2.4 and 2.9. Eq. 2.4 can be used to generate transient stems at all dimensionless times prior to the convergence point, taken to be 0.25, after which the BDF stems can be plotted using Eq. 2.9. **Fig. 2.1** shows the new type curve with a selection of transient and BDF b -values

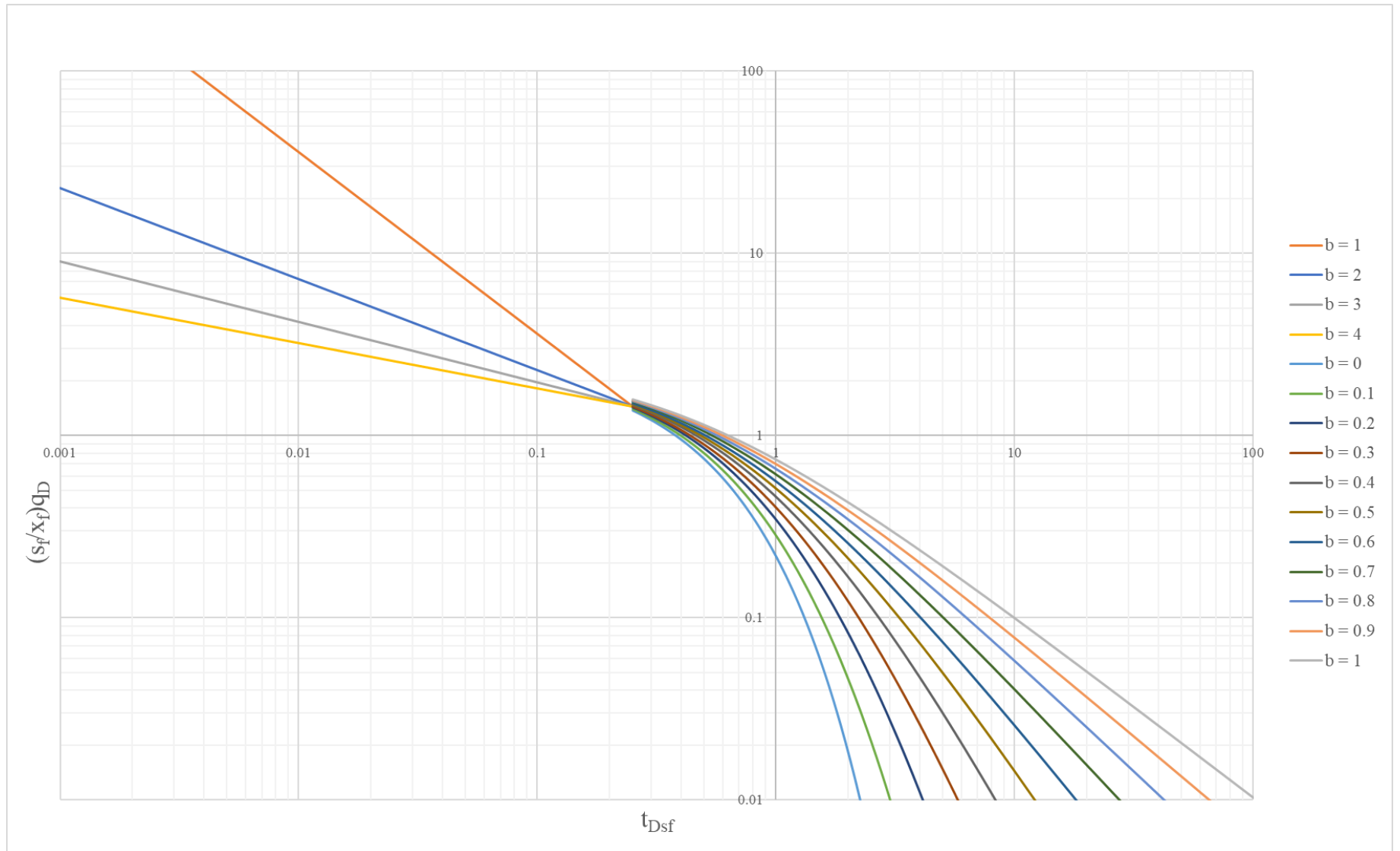


Fig. 2.1: Modified Type Curve. Rate/time data should be plotted on logarithmic paper with log-cycles of the same size as the above and overlaid onto the type curve. Once the best visual match is determined, the time match point, rate match point, and corresponding b_{TR} and b_{BDF} values should be recorded.

By design and as confirmed by Fig. 2.1, the transient stems consist of logarithmic straight lines that converge to a single point at a dimensionless time of 0.25, at which point the BDF stems begin. A slight discontinuity can be observed at the start of BDF; although the transient stems all end at the same dimensionless rate, the same cannot be said for the beginning of the BDF stems. Upon inspection of Eq. 2.9, the general equation for the BDF stems, the reason for this discontinuity becomes apparent – the stems truly converge only at a dimensionless time of zero, and, as consequence of their form, the BDF stems have diverged to a discernible degree by the time the transient stems have converged. This result was not entirely unexpected, however, as the same behavior manifests in Fetkovich's type curve (1980), although it is slightly more noticeable in this case. Validation of the type curve using simulated data suggests this discontinuity is of no practical significance and should not be cause for concern.

2.2 Making the Match and Calculation of Parameters

2.2.1 Outlier Detection and Removal

Prior to discussing how data is matched to the type curve, the issue of outliers must be addressed. In order to ensure the validity of the match and any calculated parameters, outliers must be properly detected and resolved, either via adjustment or removal. The methodology proposed in this thesis employs two separate outlier detection protocols – an automated first-pass method followed by visual detection.

The local outlier factor (LOF) algorithm was used for automated first-pass outlier detection. LOF does not necessitate *a priori* knowledge of a model to detect outliers, instead relying upon comparisons of a point's relative density to the relative densities of that point's k-nearest neighbors (Chaudhary and Lee, 2016). As such, LOF proves advantageous over many other commonly used algorithms, which require assumptions to be made regarding the underlying model prior to seeking outliers and thus introduce biases into the process. Further detail regarding LOF can be found in the referenced Chaudhary and Lee paper (2016). Although LOF serves well in a first-pass capacity, it may on its own prove insufficient when working with clusters of outliers and/or relatively small datasets and consequently should be paired with another outlier detection mechanism in order to ensure optimal results. In the case of this methodology, visual detection of outliers was deemed sufficient.

Once outliers have been detected, they must be resolved. For this work, all individual rate/time outliers - high or low - and early-time (prior to the start of transient flow) outliers were removed from consideration, although their contribution to cumulative production was kept. Consecutive

series of low outliers, corresponding to periods of aberrantly low production, were adjusted for, however, rather than being removed outright. An expected average rate was calculated based upon the production rates from on-trend datapoints prior to and following each low period, after which an “adjusted” producing time could be determined by dividing total production during the period by the expected average rate. At this point, the aberrant points were removed and all subsequent datapoints were adjusted by the difference between actual low period time and the “adjusted” producing time.

2.2.2 Diagnostic Plots

Diagnostic plots can be used to identify the flow regimes present in the data. A logarithmic plot of rate versus material balance time (MBT) is most effective for determining when a well is exhibiting signs of BDF, which manifests as a negative unit-slope straight line (Jha and Lee, 2017). Due to factors such as changing operational conditions or fracture fluid cleanup, early-time production data often deviates from the transient trend. To determine the correct starting time of the transient regime, a logarithmic rate versus time plot can be used, which will show a clear straight-line trend once transient flow has begun that continues until the well begins to transition from the transient regime to BDF. A logarithmic rate versus MBT plot is not recommended for characterization of the transient period as the appearance of the straight-line trend can be delayed or distorted by the early off-trend data (Jha and Lee, 2017).

2.2.3 Making the Match

Once the flow regimes have been identified, the data can be matched to the type curve. The transient b-value, b_{TR} , can be determined either visually or by using simple linear regression on the logarithms of the data determined to be during the transient period. The BDF b-value, b_{BDF}

of wells determined to be in BDF should be determined visually based upon a best-fit match to the type curve.

For wells exhibiting BDF, the matching procedure is quite simple. After ensuring the log-cycles are plotted to the same size, the production data is overlaid onto the type curve and moved until the best visual fit is found. The time match point (TMP) and rate match point (RMP) can then be determined from the ratio of dimensionless time to real time and dimensionless rate to real rate, respectively, read from both plots at any matched point.

Determining the match points for wells still undergoing transient flow is substantially more complicated, as any match made for such wells will be nonunique; in order to find a unique match, the transition to BDF must occur. Consequently, a transition to BDF must be forced to occur at an assumed time, and a b_{BDF} value must be assumed. The most conservative course of action would be to assume an immediate transition to an exponential ($b_{BDF} = 0$) BDF regime, but this would yield unreasonably low production in the vast majority of cases. Instead, it is more reasonable to assume the transient period continues to a specified minimum decline rate, at which point the transition occurs. Nominal decline rate is defined as follows:

$$d = -\frac{1}{q} \frac{dq}{dt} \quad (2.10)$$

For a well still experiencing transient flow, the decline rate at any given time is given by:

$$d = \frac{1}{b_{TR}t} \quad (2.11)$$

And therefore, the time and the end of the transient regime, for a given minimum decline rate, is:

$$t_{transition} = \frac{1}{b_{TR}d_{min}} \quad (2.12)$$

Thus, the time match point is:

$$TMP = \frac{t_{Dsf,Con}}{t_{transition}} = (0.25)(b_{tr}d_{min}) \quad (2.13)$$

Calculating the rate match point requires the determination of the transient rate/time model. The transient rate/time model is defined as:

$$q(t)_{TR} = q_{i,TR}t^{-\frac{1}{b_{TR}}} \quad (2.14)$$

The logarithm of the coefficient, $q_{i,TR}$, is the intercept of the best fit straight-line with a forced slope of $-1/b_{TR}$ through the logarithms of the transient data. Once this value is determined, rates can be calculated at any time during the transient period. The rate at the end of the transient regime is given by:

$$q_{transition} = (q_{i,TR})t_{transition}^{-\frac{1}{b_{TR}}} \quad (2.15)$$

The corresponding dimensionless rate, where all transient stems converge, is:

$$\left(\frac{s_f}{x_f}\right) q_{D,Con} = \left(\frac{4}{\pi^{1.5}}\right) (t_{Dsf,Con})^{-0.5} = \left(\frac{4}{\pi^{1.5}}\right) (0.25)^{-0.5} = \left(\frac{8}{\pi^{1.5}}\right) \quad (2.16)$$

Using these values, the rate match point can then be determined:

$$RMP = \frac{\left(\frac{s_f}{x_f}\right) q_D}{q} = \frac{\left(\frac{8}{\pi^{1.5}}\right)}{(q_{i,TR}) \frac{1}{b_{TR} t_{transition}}} \quad (2.17)$$

2.2.4 Calculation of Parameters

Once the match points have been determined, matrix permeability and fracture half-length can be calculated using modified definitions of Wattenbarger's dimensionless variables. Wattenbarger (1998) defines dimensionless time, t_{Dye} , as:

$$t_{Dye} = \frac{0.00633kt}{\phi \mu c_t y_e^2} \quad (2.18)$$

Modifying this definition to include s_f ($=2y_e$) and renaming the variable to t_{Dsf} , dimensionless time becomes:

$$t_{Dsf} = t_{Dye} = \frac{0.02532kt}{\phi \mu c_t s_f^2} \quad (2.19)$$

The definition of dimensionless time is the same for both oil and gas wells. Dimensionless rate, however, is defined differently for each. Wattenbarger (1998) defines dimensionless oil rate as:

$$q_D = \frac{141.2qB\mu}{kh(p_i - p_{wf})} \quad (2.20)$$

And dimensionless gas rate as:

$$q_D = \frac{1424q_gT}{kh(m(p_i) - m(p_{wf}))} \quad (2.21)$$

These definitions, however, presume production from a single fracture. As such, they must be modified to correct for the presence of multiple fractures. This correction yields a dimensionless oil rate of

$$q_D = \left(\frac{s_f}{L_w}\right) \frac{141.2qB\mu}{kh(p_i - p_{wf})} \quad (2.22)$$

and a dimensionless gas rate of

$$q_D = \left(\frac{s_f}{L_w}\right) \frac{1424q_gT}{kh(m(p_i) - m(p_{wf}))} \quad (2.23)$$

Further details regarding the corrected Eqs. 2.22 and 2.23 can be found in Appendix B.

The modified definition of dimensionless time is used in conjunction with the TMP to calculate matrix permeability. Starting with Eq. 2.19 and rearranging:

$$\frac{t_{Dsf}}{t} = TMP = \frac{0.02532k}{\phi\mu c_t s_f^2} \quad (2.24)$$

Therefore, permeability can be calculated as:

$$k = \frac{\phi\mu c_t s_f^2 (TMP)}{0.02532} \quad (2.25)$$

The RMP can then be used with the calculated permeability to determine fracture half-length.

Rearranging the definition of dimensionless rate, Eq. 2.22 for oil wells, and multiplying through by (s_f/x_f) yields:

$$\frac{\left(\frac{s_f}{x_f}\right)q_D}{q} = RMP = \left(\frac{s_f^2}{x_f L_w}\right) \frac{141.2B\mu}{kh(p_i - p_{wf})} \quad (2.26)$$

which can then be rearranged to solve for fracture half-length:

$$x_f = \left(\frac{s_f^2}{(RMP)L_w}\right) \frac{141.2B\mu}{kh(p_i - p_{wf})} \quad (2.27)$$

Following the same procedure for gas wells yields

$$\frac{\left(\frac{s_f}{x_f}\right)q_D}{q_g} = RMP = \left(\frac{s_f^2}{x_f L_w}\right) \frac{1424T}{kh(m(p_i) - m(p_{wf}))} \quad (2.28)$$

and

$$x_f = \left(\frac{s_f^2}{(RMP)L_w}\right) \frac{1424T}{kh(m(p_i) - m(p_{wf}))} \quad (2.29)$$

2.3 Forecasting Future Production

The procedure for forecasting future production differs for wells already exhibiting signs of BDF and those still in the transient period.

The rate/time behavior of wells that have already transitioned to BDF can be modeled by Arps' decline relations, Eqs. 2.5 and 2.6 from above. Eq. 2.6 (and Eq. 2.5, implicitly), includes three unknowns – b_{BDF} , q_i , and d_i . The b -value is already known from the type curve match, but q_i and d_i must still be determined. Using the RMP, q_i can be calculated rather straightforwardly:

$$q_i = \left(\frac{8}{\pi}\right) \left(\frac{1}{RMP}\right) \quad (2.30)$$

Initial decline rate, d_i , can be calculated similarly by using the TMP:

$$d_i = \left(\frac{\pi^2}{4}\right) TMP \quad (2.31)$$

Complete derivations for Eqs. 2.30 and 2.31 are provided in Appendix B.

Once q_i and d_i are determined, production rates at any given time can be calculated using Eq. 2.5 or 2.6, and thus future production may be forecast. To forecast cumulative production at an arbitrary time, Arps' cumulative/time relations must be used, which can be derived by integrating Eqs. 2.5 and 2.6 with respect to time. The predicted cumulative production at any given time is the sum of cumulative production during production history, N_p , and the incremental production to that point.

$$N_{p,forecast} = N_p + \frac{q_i}{(b-1)d_i} \left[(1 + bd_i t)^{1-\frac{1}{b}} - (1 + bd_i t_{hist})^{1-\frac{1}{b}} \right] \quad (2.32)$$

Therefore, the EUR can be calculated by

$$EUR = N_p + \frac{q_i}{(b-1)d_i} \left[(1 + bd_i t_{life})^{1-\frac{1}{b}} - (1 + bd_i t_{hist})^{1-\frac{1}{b}} \right] \quad (2.33)$$

Forecasting future production for wells still experiencing transient flow, as discussed in the previous section, requires determining when to transition from transient flow and selecting an appropriate value of b_{BDF} . In such cases, three flow regimes are modeled – transient, transition, and BDF. The rate/time relation prior to the end of transient flow is described by Eq. 2.14 and can be used to predict rates up until the transition point. Cumulative production at any point during the transient flow regime (after the end of production history), can be calculated as

$$N_{p,forecast} = N_p + \frac{q_{i,TR}}{1 - \frac{1}{b_{TR}}} \left[t^{1 - \frac{1}{b_{TR}}} - t_{hist}^{1 - \frac{1}{b_{TR}}} \right] \quad (2.34)$$

with the total cumulative production by the end of the transient period equaling

$$N_{p,TR,forecast} = N_p + \frac{q_{i,TR}}{1 - \frac{1}{b_{TR}}} \left[t_{transition}^{1 - \frac{1}{b_{TR}}} - t_{hist}^{1 - \frac{1}{b_{TR}}} \right] \quad (2.35)$$

The transition regime begins once the transient flow period ends. The transition region is modeled similarly to the BDF region, but instead uses an intermediate b-value, b^* , which is the average of b_{TR} and b_{BDF} , and a modified definition of time, t^* ($t^* = t - t_{transition}$). The general hyperbolic form describing the rate/time relation of the transition region is given by

$$q(t^*) = q_i^* / (1 + b^* d_i^* t^*)^{\frac{1}{b^*}} \quad (2.36)$$

The purpose of the transition region is to smoothly transition from end of transient flow to the beginning of BDF, and both q_i^* and d_i^* are defined with this purpose in mind. In order to ensure continuity, q_i^* is equal to the final rate at the end of the transient period, $q_{transition}$, which can be calculated using Eq. 2.15, and d_i^* is equal to the specified minimum decline rate. Selection of these values guarantees the transition region begins from the same point and with the same slope as the end of the transient region. This transition region continues until the intersection between it and the BDF model, which occurs at t_{BDF} and after which BDF begins. Determination of this intersection point will be discussed later.

Cumulative production at any point during the transition regime is equal to the forecast production at the end of transient flow plus the incremental transition regime production accrued to that point and is given by

$$N_{p,forecast} = N_{p,TR,forecast} + \frac{q_i^*}{(b^*-1)d_i^*} [(1 + b^*d_i^*t^*)^{1-\frac{1}{b^*}} - 1] \quad (2.37)$$

At the end of the transition regime, cumulative production is therefore given by

$$N_{p,transition,forecast} = N_{p,TR,forecast} + \frac{q_i^*}{(b^*-1)d_i^*} [(1 + b^*d_i^*t_{BDF}^*)^{1-\frac{1}{b^*}} - 1] \quad (2.38)$$

Where $t_{BDF}^* = t_{BDF} - t_{transition}$.

The BDF region is modeled in precisely the same way as for wells already exhibiting BDF. Eqs. 2.30 and 2.31 define q_i and d_i , respectively, b_{BDF} is the previously assumed value, and the rate/time relation is still modeled by Eq. 2.5 or 2.6. The sole difference is determining when BDF begins, t_{BDF} . This point can be determined by finding the intersection between the transition model and the BDF model. Equating Eqs. 2.6 and 2.36 at $t = t_{BDF}$ (and $t^* = t_{BDF}^*$) yields

$$\frac{q_i^*}{(1+b^*d_i^*t_{BDF}^*)^{\frac{1}{b^*}}} = \frac{q_i}{(1+bd_it_{BDF})^{\frac{1}{b}}} \quad (2.39)$$

The value of t that satisfies Eq. 2.39 will be t_{BDF} . This value can be easily calculated by defining a function as the difference between R.H.S. and L.H.S. of Eq. 2.39 and seeking the first root larger than $t_{transition}$. Once t_{BDF} has been determined, future production can be forecast at times beyond this point using the aforementioned BDF model.

Calculation of future cumulative production and EUR is largely equivalent to the process outlined for wells already exhibiting BDF and requires only minimal modifications to Eqs. 2.32 and 2.33. The cumulative production at any point during BDF is equal to the sum of the cumulative production through the end of the transition period and the incremental production that has occurred during BDF. It is given by

$$N_{p,forecast} = N_{p,transition,forecast} + \frac{q_i}{(b-1)d_i} \left[(1 + bd_i t)^{1-\frac{1}{b}} - (1 + bd_i t_{BDF})^{1-\frac{1}{b}} \right] \quad (2.40)$$

Similarly, the EUR can be calculated as

$$EUR = N_{p,transition,forecast} + \frac{q_i}{(b-1)d_i} \left[(1 + bd_i t_{life})^{1-\frac{1}{b}} - (1 + bd_i t_{BDF})^{1-\frac{1}{b}} \right] \quad (2.41)$$

2.4 Scaling

An individual well's production profile is a function of its unique combination of reservoir, completion, and operational properties. No two wells are exactly alike, and, as such, no two production profiles are identical. When preparing and analyzing a set of wells in order to construct a type well, it is critical that only wells with similar properties and similar production profiles be considered in order to ensure the type well is truly representative, and, thus, wells are placed into distinct bins and kept separate from dissimilar wells. Stringent “similarity” requirements, however, are likely to result in a large number of bins for a given play, with each bin consequently containing only a few wells. These small bins result in non-representative sample sizes, largely invalidating any attempts to construct accurate type wells.

To mitigate this issue, the number of bins must decrease, and bin size must increase accordingly. Scaling wells to a set of reference properties and conditions is an effective way to accomplish this. By employing scaling techniques, previously dissimilar wells can now be placed within the same bin, resulting in increasingly representative sample sizes and increasingly accurate type wells.

Both time and rate can be scaled to a common set of production parameters via scaling factors. These scaling factors can be derived from the definitions of dimensionless time and dimensionless rate and are summarized below:

$$t'_{perm} = \frac{k}{k_{ref}} \quad (2.42)$$

$$t'_{spacing} = \left(\frac{S_{f,ref}}{S_f} \right)^2 \quad (2.43)$$

$$q'_{perm} = \frac{k_{ref}}{k} \quad (2.44)$$

$$q'_{spacing} = \left(\frac{S_f}{S_{f,ref}} \right)^2 \quad (2.45)$$

$$q'_{half-length} = \frac{x_{f,ref}}{x_f} \quad (2.46)$$

$$q'_{lat\ length} = \frac{L_{w,ref}}{L_w} \quad (2.47)$$

$$q'_{net\ pay} = \frac{h_{ref}}{h} \quad (2.48)$$

$$q'_{drawdown} = \frac{\Delta p_{,ref}}{\Delta p} \quad (2.49)$$

Combined total scaling factors are calculated by multiplying all other factors together and for time and rate, respectively, are

$$t' = t'_{perm} t'_{spacing} \quad (2.51)$$

and

$$q' = q'_{perm} q'_{spacing} q'_{half-length} q'_{lat\ length} q'_{net\ pay} q'_{drawdown} \quad (2.51)$$

Once total scaling factors have been calculated, a well's scaled production profile can be found by multiplying its time values by the total time scaling factor and its rates by the total rate scaling factor.

$$t_{sc} = t' t \quad (2.52)$$

$$q_{sc} = q' q \quad (2.53)$$

Calculation of scaled EUR requires both time and rate total scaling factors. In addition, the cumulative production at an unscaled time corresponding to the scaled well lifetime must be known (e.g., if the lifetime of scaled wells is 30 scaled years and t' is 0.5, N_p after $30/0.5 = 60$ unscaled years must be calculated). Eq. 2.54 below shows the scaled EUR calculation:

$$EUR_{sc} = q' t' N_p \left(t = \frac{t_{life,sc}}{t'} \right) \quad (2.54)$$

A complete derivation Eq. 2.54 is provided in Appendix B.

2.5 Constructing the Type Wells

Type wells can be constructed once all wells in a dataset have been analyzed and scaled. There are a number of industry practices regarding the construction of type wells, ranging from simply arithmetically averaging production rates to performing Monte Carlo simulation and employing probabilistic methods. For the purpose of this work, it was deemed sufficient to rank wells by scaled EUR and construct P90, P50, and P10 type wells using the scaled production profiles of wells of the corresponding percentile. For example, in a dataset of 100 wells, the P90 type well would be the scaled profile of the well with the 10th lowest scaled EUR, the P50 type well would be the scaled profile of the well with the median scaled EUR, and the P10 type well would be the scaled profile of the well with the 10th highest scaled EUR.

3. RESULTS

3.1 Validation

In order to validate the type curve and forecasting procedures outlined in the previous section, simulations of two wells, one oil and one gas, were run using IHS Harmony's RTA software package. Input parameters for each well are summarized in **Table 3.1** below.

Oil Well 1			Gas Well 1		
μ	1.151	cP	μ	0.025	cP
B	1.19	RB/STB	B	6.69E-04	RB/scf
ϕ	0.06		ϕ	0.06	
p_i	3000	psia	p_i	5000	psia
T_r	200	°F	T_r	200	°F
h	200	ft	h	200	ft
c_t	1.08E-05	psi ⁻¹	c_t	4.07E-05	psi ⁻¹
L_w	10000	ft	L_w	10000	ft
s_f	400	ft	s_f	400	ft
Δp	2500	psi	Δp	4500	psi
k	3.56E-04	mD	k	3.56E-04	mD
x_f	200.0	ft	x_f	200.0	ft

Table 3.1: Simulated Wells Input Parameters

Once the simulations were run, the generated data was matched to the type curve, permeability and fracture half-length were calculated. To assess the forecasting procedures, the simulated data was truncated at an arbitrary point following the transition to BDF. Production was then forecast from this point onward until the end of simulated production history, at which time rates and produced volumes were compared to the simulated values. The results of these validation efforts are discussed below.

Fig. 3.1 shows the simulated oil well's type curve match. The well exhibits a transient flow period corresponding to a b_{TR} -value of 2, suggesting pure linear flow. This transient flow period continues for approximately 9 years, after which the well transitions to exponential decline.

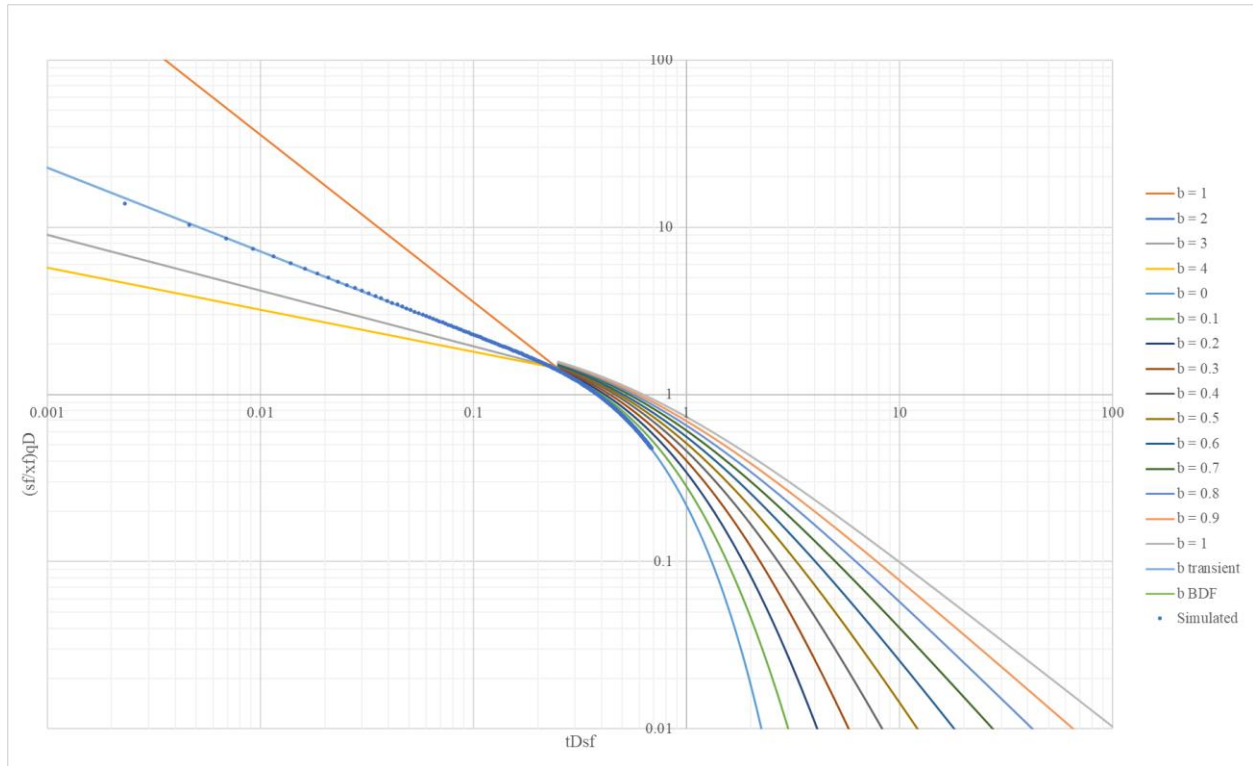


Fig. 3.1: Simulated Oil Well Type Curve Match. The well exhibited pure-linear flow during the transient period and later transitioned to exponential flow. The presence of the BDF regime allowed for a unique match to be made.

The TMP and RMP for this well were determined from the best visual match of the data to the type curve. Using these values, permeability was calculated to be 3.58×10^{-4} mD and fracture half-length 198.9 ft, corresponding to errors of 0.45% and -0.54%, respectively.

To assess the forecasting procedure, the simulated dataset was truncated after 4,000 days of production, and production was then re-forecast to the original end of simulated production

history, slightly over 9,000 days. This is visualized in **Fig. 3.2**, which is identical to Fig. 3.1 save for the replacement of the tail of the data with the newly forecast values, shown in red.

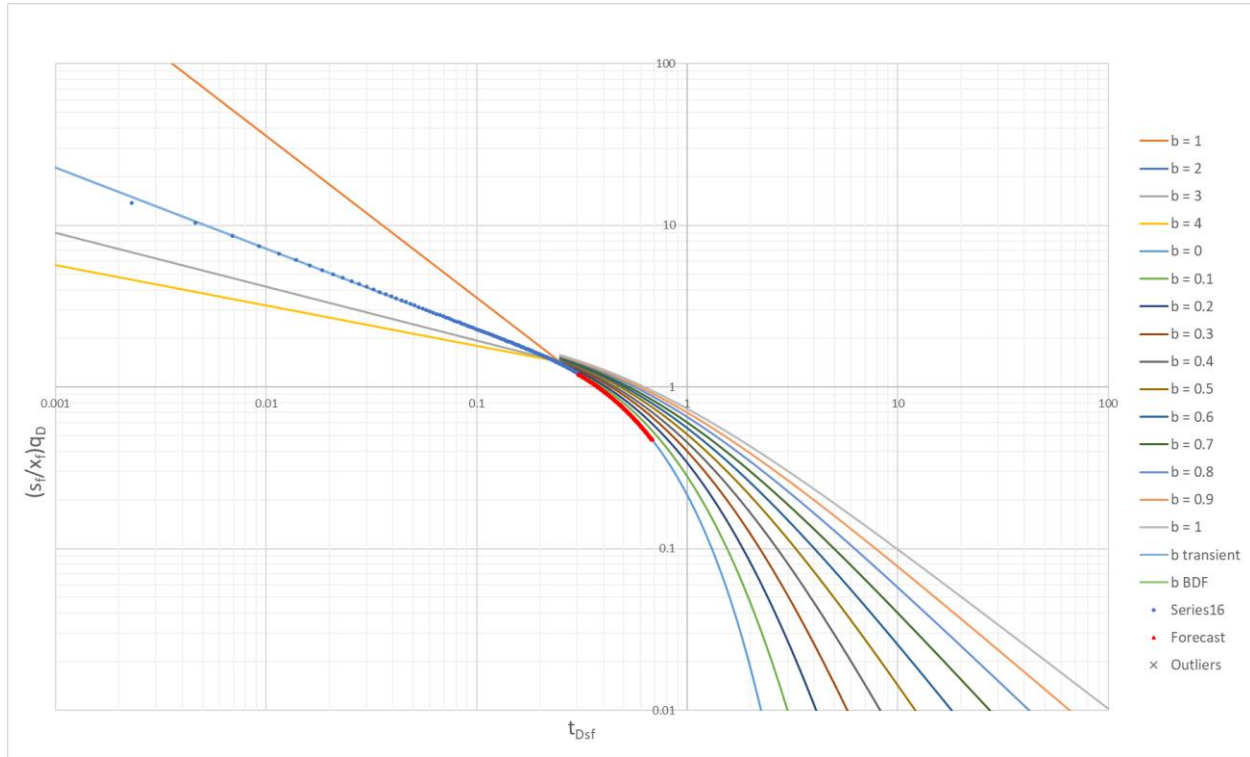


Fig. 3.2: Simulated Oil Well – Forecast Testing. The simulated data was truncated after approximately 4,000 days and then re-forecast to the end of the original simulated history. As can be seen by comparing this figure to Fig. 3.1, there is excellent agreement between the original data and the forecast.

Per the simulation, the well's cumulative production at the end of its history was 165.2 MSTB.

Recalculating cumulative production using the forecasting procedure resulted in a value of 163.7

MSTB, an error of less than one percent.

The simulated gas well was analyzed in precisely the same fashion. To avoid the additional complexity of the pseudopressure calculation required to use the gas equation, Eq. 2.23, the oil equation, Eq. 2.22, was deemed a sufficient approximation. The similarly exhibits a period of

transient linear flow, lasting for approximately 9 months, before transitioning to a hyperbolic BDF regime corresponding to a b_{BDF} value of 0.525. Based upon the visual match, permeability was calculated to be 3.48×10^{-4} mD and fracture half-length 176.5 ft, corresponding to errors of -2.4% and -11.8%, respectively. The relatively high error in the fracture half-length calculation is likely attributable to the usage of the oil equation as an approximation. It is expected that the more tedious gas equation would yield more accurate results. Cumulative production calculated using the forecasting procedure was determined to be 2,874.8 MMscf, as compared to a simulated value of 2,916.4 MMscf, an error of -1.4%. The visual match of production data and the test of the forecasting procedure are shown in **Figs. 3.3 and 3.4**, respectively.

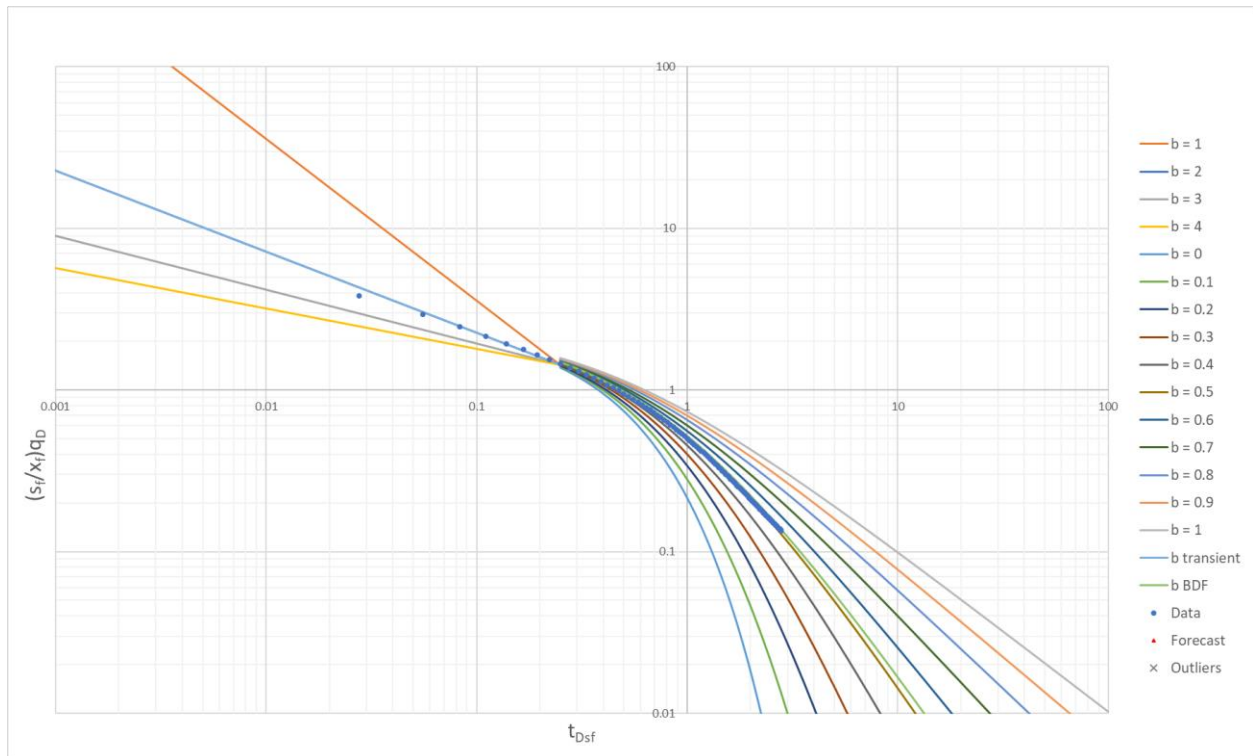


Fig. 3.3: Simulated Gas Well Type Curve Match. An early period of transient period flow, corresponding to a b_{TR} value of 2, was followed by a transition to BDF characterized by a b_{BDF} value of 0.525. The presence of BDF in the data allowed for a unique match to be made.

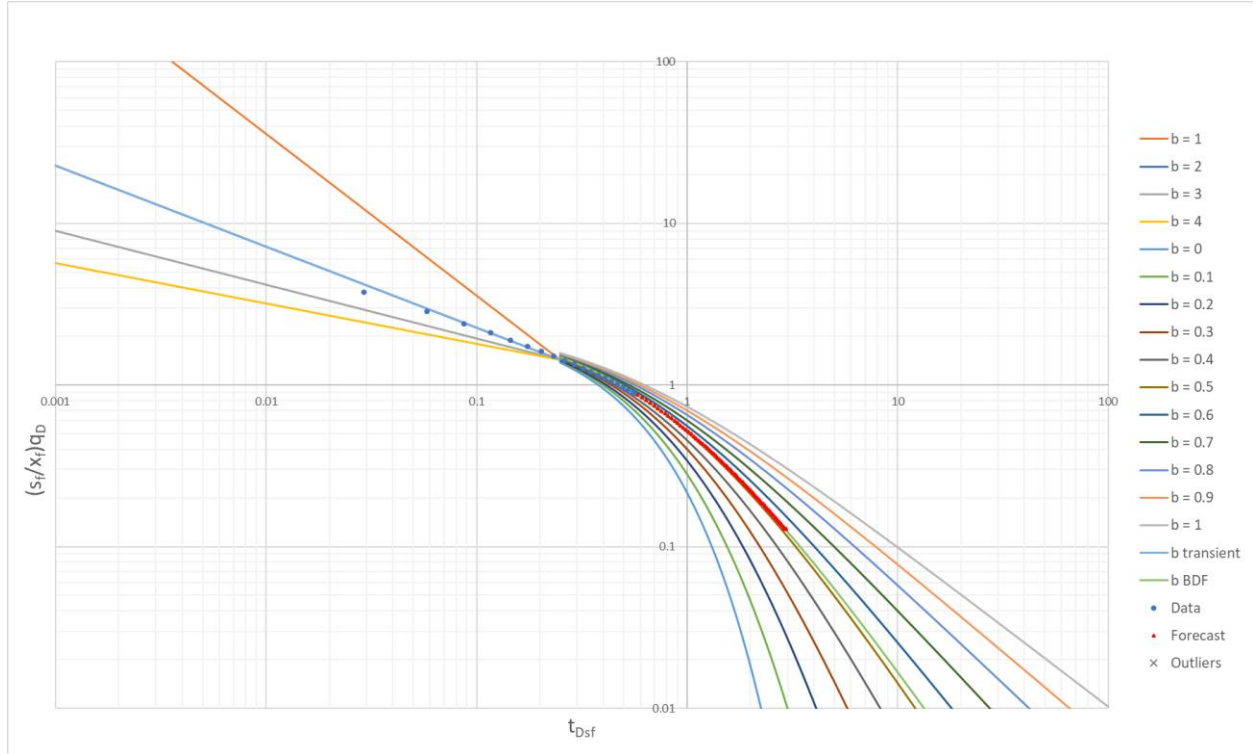


Fig 3.4: Simulated Gas Well – Forecast Testing. The simulated production data was truncated and reproduced using the previously discussed forecasting methodology. As can be seen by comparison to Fig. 3.3, the forecast closely agrees with the simulated data.

3.2 Field Study – Midland Basin Data Set

To provide an example field application, the methodology proposed in this thesis was applied to a set of 140 multi-fractured horizontal oil wells from the Wolfcamp Formation in the West Texas Midland Basin. None of the 140 wells were determined to have made the transition to BDF, and therefore all wells were analyzed assuming a transition from transient flow at a specified minimum decline rate, at which point a transition region would begin prior to the start of BDF. In all cases, BDF was modeled using a b_{BDF} of 0.3, which is consistent with typical values for solution gas drive oil wells. Future production was projected to 30 years, and corresponding EUR's were calculated for each well.

The wells in the data set were subdivided into three groups – so-called “good” wells with relatively minimal noise and clear transient trends, “bad” wells that were difficult to characterize, be it due to noisy data or operational changes, and “early-time” time wells with production histories shorter than one year. Once all wells within a set were analyzed individually, their production profiles and EUR’s were scaled to a common 30 scaled-year basis, and P90, P50, and P10 type wells were constructed.

3.2.1 Input Parameters

In order to calculate permeability and fracture half-length for a matched well, various reservoir, completions, and operational properties must be known or assumed. The permeability calculation requires input values for fracture spacing, porosity, and viscosity and total compressibility at initial reservoir conditions, and the fracture half-length calculation is dependent upon the calculated permeability, fracture spacing, viscosity and FVF at initial reservoir conditions, lateral length, net pay, and drawdown.

Optimally, these required input values would be thoroughly tracked and reported for each well, but, in reality, they are not typically known and instead must be assumed. For the purpose of this analysis, ranges of reasonable values for each input parameter (apart from lateral length, which was regularly recorded) were determined, based upon the limited reporting of the data set and typical properties in the Wolfcamp Formation (Blomquist, 2016). Properties were selected from this range on a well-by-well basis, with an effort made to select complementary inputs (e.g. large values of total compressibility, associated with lower depths, were coupled with smaller drawdown values). **Table 3.2** shows the selected ranges for the aforementioned input parameters.

Parameter	Min	Max
μ , cP	0.465	0.695
B, RB/STB	1.34	1.37
ϕ	0.07	0.12
h, ft	-	200
ct, psi-1	1.10E-05	1.95E-05
sf, ft	200	300
Δp , psi	1750	4000

Table 3.2: Range of Input Parameters for Wolfcamp Formation Data Set. Ranges were determined based upon reported values from the data set and from typical formation properties.

3.2.2 “Good” Wells

The “good” wells consisted of a set of 46 wells with clear transient trends and minimal noise and outliers. Each well was matched to the type curve using the procedure outlined in section 2.2.3 for wells still experiencing transient flow, and its corresponding permeability and fracture half-length were calculated. Production was then forecast to a lifetime of 30 years, at which point EUR was determined.

A diagnostic plot, type curve match, and forecast for an example well from the set are shown below in **Figs. 3.5, 3.6, and 3.7**. The diagnostic plot shows a clear transient trend and no definitive evidence indicating BDF has begun, which would manifest as a unit-slope straight line in the rate/MBT data. The best-fit logarithmic straight line exhibits a negative half slope, suggesting a b_{TR} value of 2. The well was forced to transition from transient flow at a specified decline rate of 15%/year and was matched to the type curve based upon this forced transition

point. Permeability and fracture half-length were calculated to be 4.4×10^{-4} mD and 287.3 ft, respectively, and EUR after 30 years was forecast to be 700.6 MSTB.

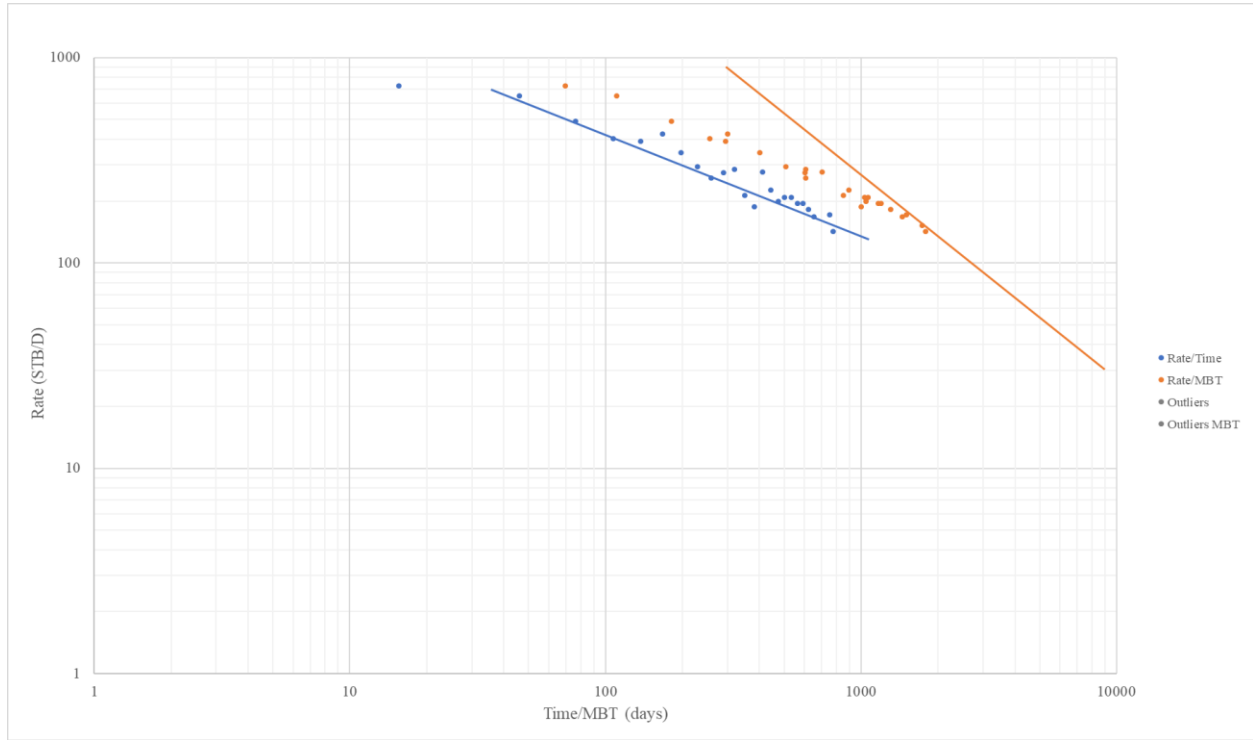


Fig. 3.5: Well 119 Diagnostic Plot. The blue line through the Rate/Time data shows the logarithmic straight-line transient trend, which begins with the second datapoint. The orange logarithmic unit-slope straight line next to the Rate/MBT data is meant to help identify the BDF regime. As a unit-slope trend has not developed in the Rate/MBT data, the well has not yet transitioned to BDF.

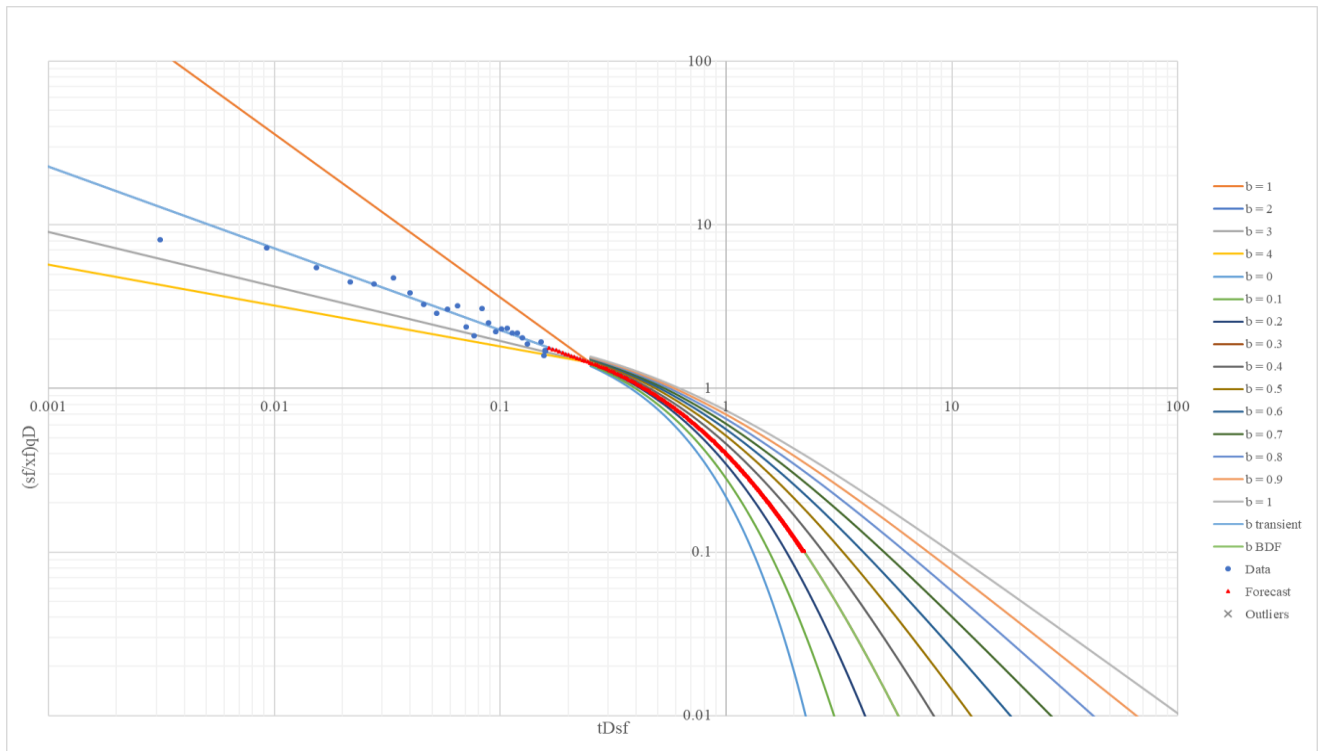


Fig. 3.6: Well 119 Type Curve Match. This well exhibits a pure-linear trend during transient flow, after which it was forced to transition to a BDF regime with a b_{BDF} value of 0.3.

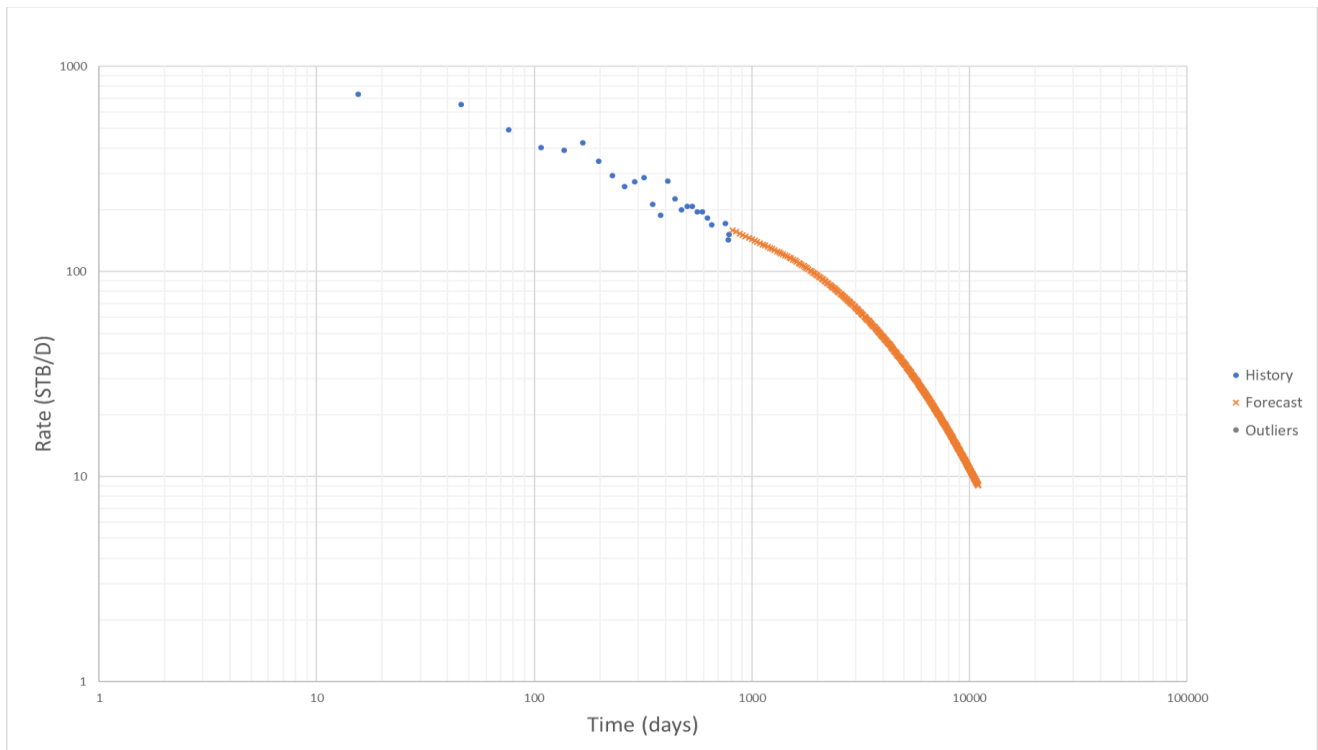


Fig. 3.7: Well 119 Production History and Forecast

All other wells in the set were analyzed in a similar fashion, and all plots and results can be found in Appendix A.

The range of transient b-values for wells from the “good” set is shown in **Fig. 3.8** below. Values range from 1.25 to 2.6, with the highest concentration of wells falling between 1.6 and 2. **Fig. 3.9** shows a histogram of calculated permeabilities. Despite the small sample size of only 46 wells, the results clearly approximate a lognormal distribution, with an average permeability of 4.75×10^{-4} mD, a median of 4.54×10^{-4} mD, and a range from 2.11×10^{-4} mD to 9.07×10^{-4} mD. This coincides with expectations, as permeability naturally tends to be distributed lognormally. Calculated fracture half-lengths are summarized in **Fig. 3.10** and are distributed far more randomly. Because fracture half-length is influenced largely by completion design as opposed to by natural processes, such a distribution seems reasonable. The average fracture half-length is 232.5 ft, the median is 234.7 ft, and values range from 137.6 ft to a maximum of 343.9 ft, although only one well crosses the 300 ft threshold.

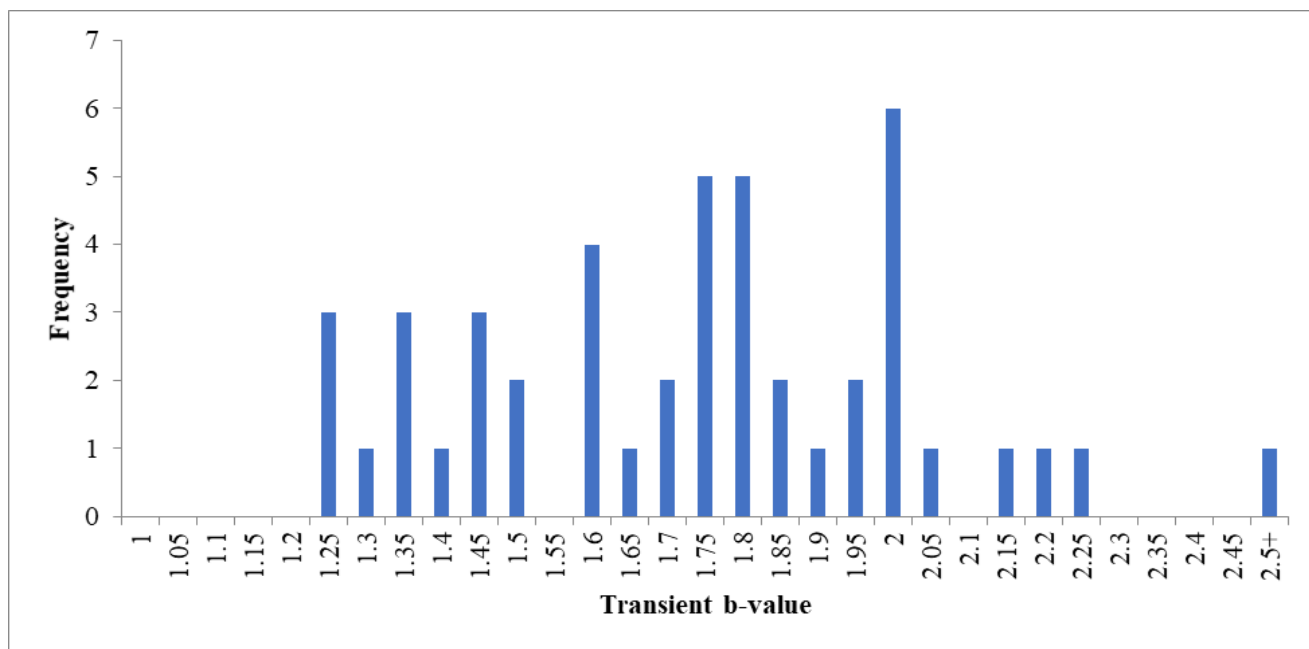


Fig. 3.8: Histogram of b_{TR} -Values – “Good” Well Set. Values of b_{TR} range from 1.25 to 2.6, with the highest concentration falling between 1.6 and 2.

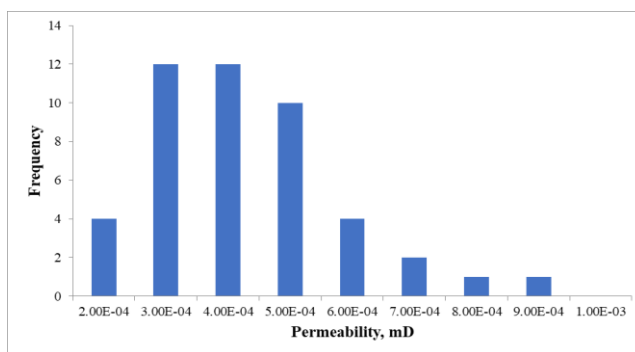


Fig. 3.9: Histogram of Calculated Permeabilities – “Good” Well Set. The distribution of permeabilities clearly approximates a lognormal distribution, as would be expected.

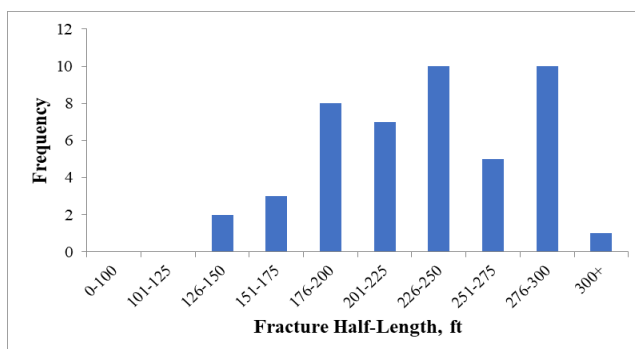


Fig. 3.10: Histogram of Calculated Fracture Half-Lengths – “Good” Well Set. The randomness is likely due to the fact that fracture half-length is determined more by completion design as opposed to by natural processes.

Prior to scaling, the distribution of EURs for wells in the “good” set also appears to be approximately lognormal. The average unscaled EUR, 498.2 MSTB, is slightly higher than the median, 441.4 MSTB, and values range from a minimum of 132.5 MSTB to a maximum of 1,193.1 MSTB. Because EUR is largely a function of multiplicative process (i.e. areal extent multiplied by net pay multiplied by porosity multiplied by recovery factor, etc.), this result is expected. The distribution of unscaled EURs is shown in **Fig. 3.11** on the following page.

The primary aim of this analysis is to construct type wells by using representative rate/time production profiles. Because each well’s EUR is a function of its unique set of reservoir, completion, and operational properties, wells cannot simply be ranked in order by increasing EUR. Doing so and then, for example, using the well corresponding to the 90th percentile of EUR to construct a P10 type well would yield misleading and incorrect results, as that particular well’s EUR would only be in the 90th percentile by virtue of comparisons to dissimilar wells with dissimilar properties. Therefore, to accurately rank wells for the purpose of type well construction, they must first be scaled to a common set of reference parameters. It is typically appropriate to select reference parameters that are representative of the anticipated properties of the newly drilled or soon-to-be drilled wells in question. However, for the purpose of this analysis, all wells were scaled to average values, summarized in **Table 3.3**.

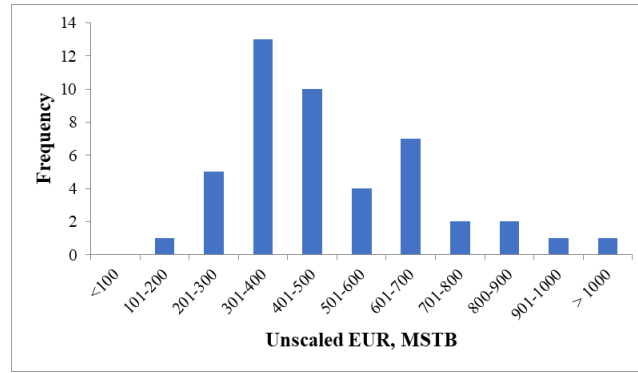


Fig. 3.11: Histogram of Unscaled EURs – “Good” Well Set. The distribution of EURs appears to be approximately lognormal. This result is expected because EUR is largely a function of multiplicative processes (areal extent multiplied by net pay multiplied by porosity multiplied by recovery factor, etc.).

Ref. k	4.47E-04	mD
Ref. s_f	258.1	ft
Ref. h	188.4	ft
Ref. L_w	7856.4	ft
Ref. x_f	231.5	ft
Ref. Δp	2576.2	psi

Table 3.3: Scaling Reference Parameters – “Good” Well Set. Reference parameters were determined by averaging values for all wells in the “good” well set.

After determining scaling factors for each well, rate/time profiles were reconstructed and scaled EURs were calculated. The scaled distribution of EURs is entirely dissimilar to the unscaled and appears roughly uniform. The range narrowed substantially, with both extremes moving closer to the mean; the minimum EUR increased from 132.5 MSTB to 227.4 MSTB while the maximum decreased from 1,193 MSTB to 697.4 MSTB. The mean and median EURs were quite close to one another, 491.4 MSTB and 495.0 MSTB, respectively. The distribution of scaled EURs can be seen in **Fig. 3.12**, and **Table 3.4** summarizes both the scaled and unscaled EUR of each well. **Figs. 3.13 and 3.14** are plots of the unscaled and scaled production profiles

of all wells, respectively, and were included to further highlight the pronounced effect of scaling. The vertical spread between production profiles is visibly reduced on the scaled plot, with all profiles being pulled more closely together.

Scaling all production profiles to a common set of reference parameters facilitates the ultimate end goal of this analysis, the construction of type wells. The wells were ordered by ascending scaled EUR, and the production profiles of those corresponding to the 10th, 50th, and 90th percentile, respectively, were used to construct P90, P50, and P10 type wells. To smooth the type wells, the historical rate data for each selected well was replaced by rates calculated using its transient model, as was presented in section 2.2.3. The resulting type wells can be seen in **Fig. 3.15**.

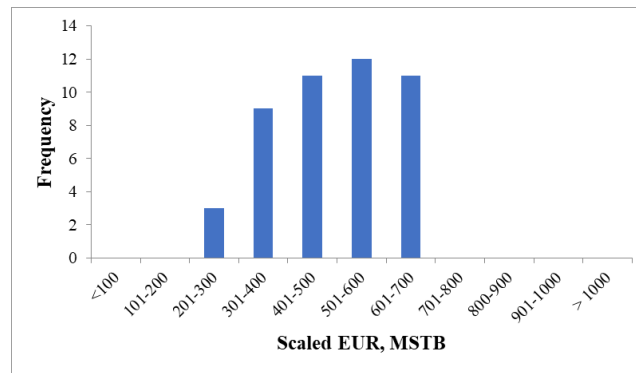


Fig. 3.12: Histogram of Scaled EURs – “Good” Well Set. Scaling the EURs transformed the distribution from approximately lognormal to approximately uniform.

Well	Unscaled EUR	Scaled EUR	Well	Unscaled EUR	Scaled EUR
6	446.9	644.8	83	599.7	405.8
7	554.8	572.2	84	442.1	229.4
13	466.4	558.0	88	908.3	547.3
14	819.8	517.2	89	1193.1	684.4
19	591.2	697.4	93	416.6	368.0
21	655.8	355.5	99	351.3	633.7
22	664.5	595.0	100	440.6	417.1
29	369.0	387.3	103	132.5	633.3
32	226.0	416.9	106	407.9	430.9
35	392.2	372.5	111	355.4	482.8
36	397.9	543.7	112	349.6	372.7
41	374.1	506.1	117	614.5	480.3
42	412.8	407.5	118	345.5	337.1
45	477.1	475.0	119	700.6	608.9
46	333.1	483.8	120	457.1	612.0
51	259.1	227.4	121	329.2	567.5
53	363.4	654.8	122	614.3	607.5
59	692.2	455.0	125	790.2	511.1
60	383.6	413.5	127	558.6	530.9
68	485.2	634.1	128	293.9	683.2
70	249.9	233.3	129	692.7	569.5
77	842.1	556.3	130	678.2	384.1
78	289.1	307.3	133	334.6	340.7

Table 3.4: Scaled and Unscaled EURs, MSTB – “Good” Well Set

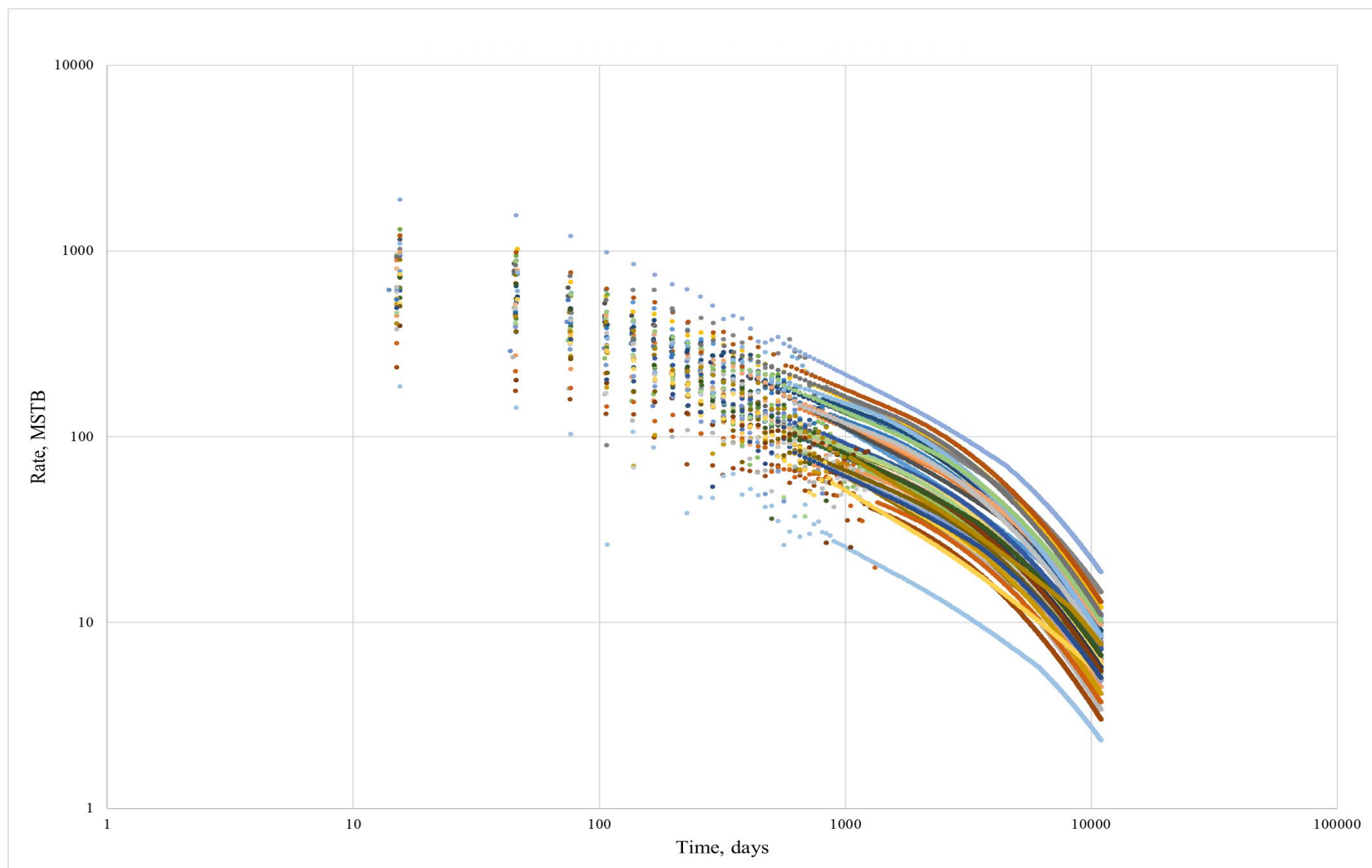


Fig. 3.13: Unscaled Production Profiles of all Wells – “Good” Well Set. This plot shows all unscaled production profiles from the “good” well set. Notice the substantial vertical spread between profiles.

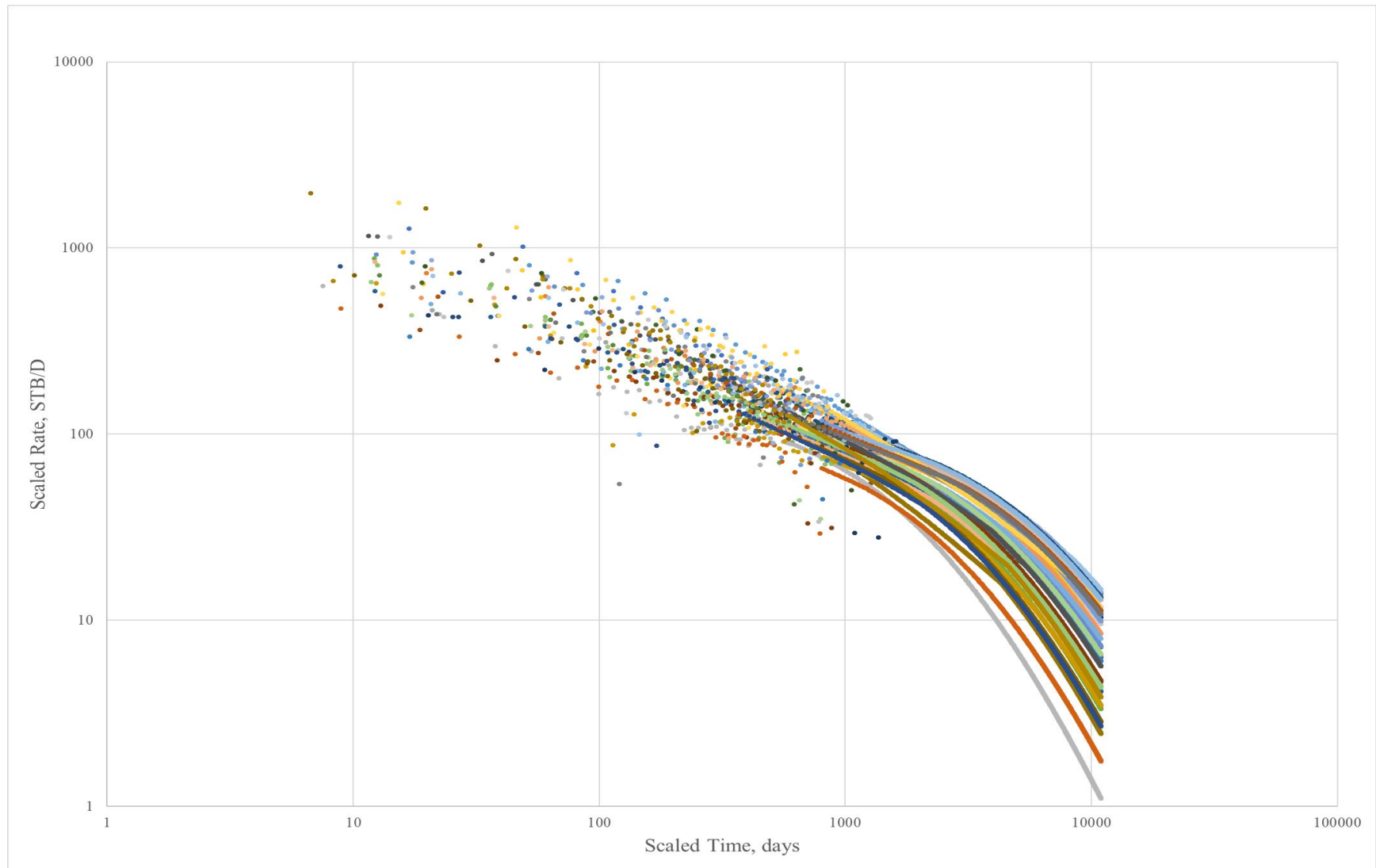


Fig. 3.14: Scaled Production Profiles of all Wells – “Good” Well Set. This plot shows all scaled production profiles from the “good” well set. The vertical spread is noticeably reduced, particularly during early and intermediate times.

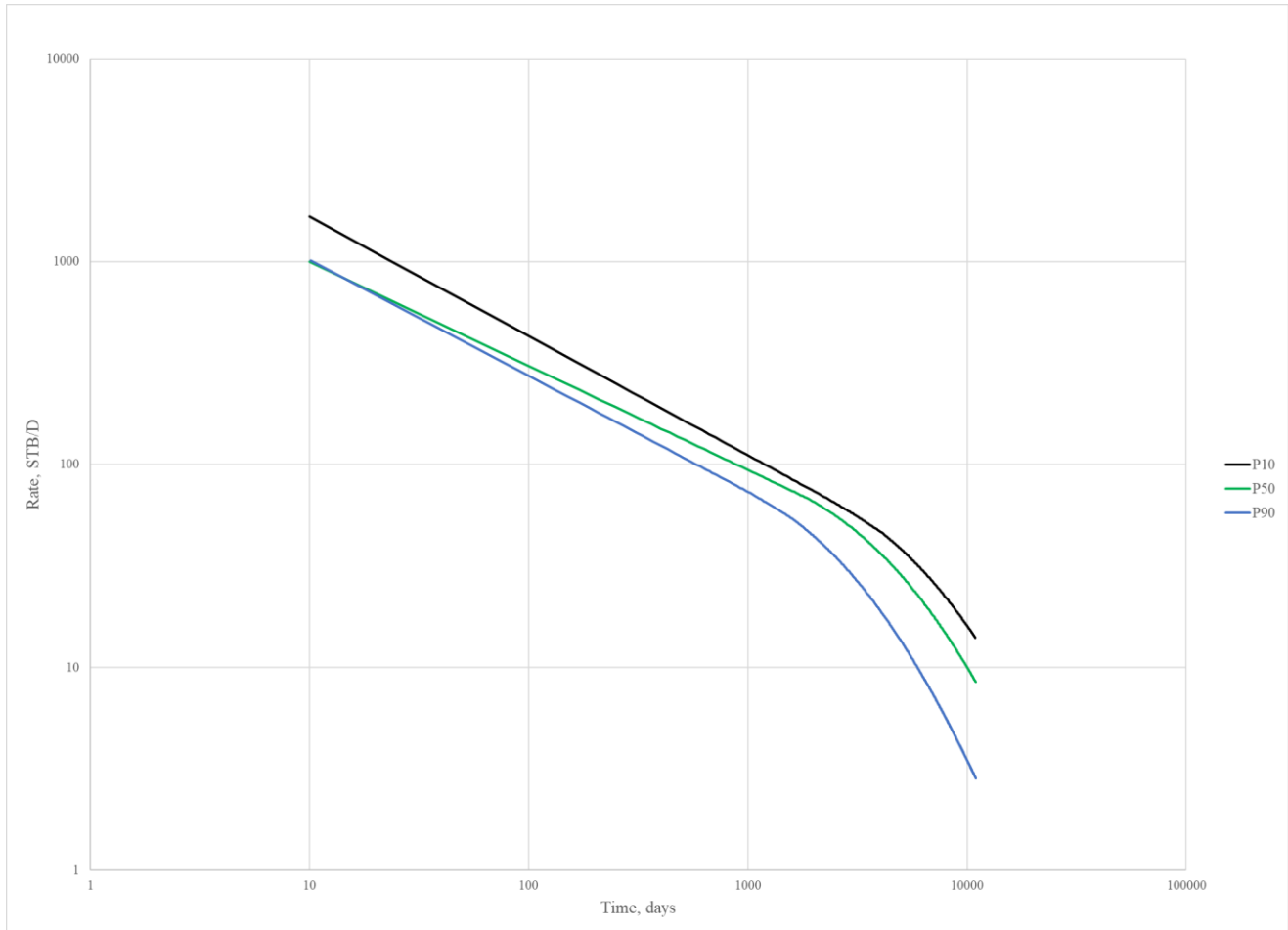


Fig. 3.15: P90, P50, and P10 Type Wells – “Good” Well Set. These three type wells were created by selecting and smoothing the production profiles of the wells from the “good” data set with scaled EURs corresponding to the 10th, 50th and 90th percentiles.

3.2.3 “Bad” Wells

The “bad” wells were a set of 24 wells with more than a year of production history whose rate/time data was more difficult to characterize, be it due to increased levels of noise or an increased number of outliers. This data set was analyzed using the same methodology as before, but due to the aforementioned issues related to data quality, the results of the analysis are of questionable accuracy as compared to those of the “good” well set.

Transient b-values for the “bad” wells ranged from 1 to 3.4, with an average of 1.6. The distribution was fairly uniform across this interval, although no wells were found to have a b_{TR} value between 1.85 and 2.15. Due to the small size of the data set, however, this is likely attributable to random chance. The distribution is shown in **Fig. 3.16**.

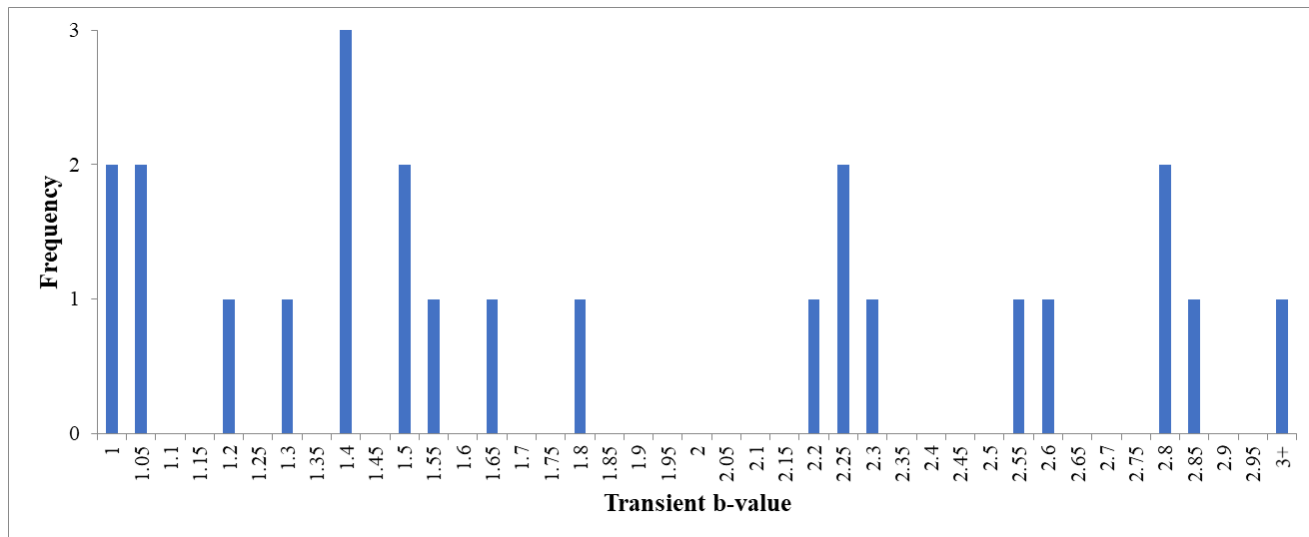


Fig. 3.16: Histogram of b_{TR} -Values – “Bad” Well Set. Values of b_{TR} range from 1 to 3.4. No wells were found to have a b_{TR} value between 1.85 and 2.15, but this is likely attributable to random chance.

Like the “good” wells, the distribution of calculated permeabilities for the “bad” wells, shown below in **Fig. 3.17**, was approximately lognormal. The average permeability was found to be 4.06×10^{-4} mD and the median 3.49×10^{-4} mD, with values ranging from a minimum of 1.68×10^{-4} mD to a maximum of 1.04×10^{-3} mD. The calculated fracture half-lengths were distributed approximately uniformly on an interval ranging from 109.9 ft to 403.3 ft, with an average half-length of 216.4 ft and a median of 214.5 ft. **Fig. 3.18** shows the distribution of fracture half-lengths.

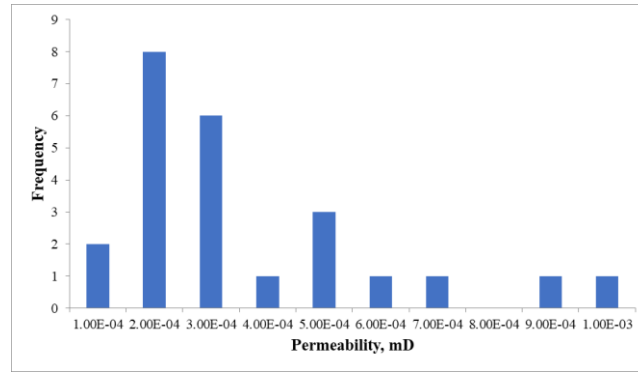


Fig. 3.17: Histogram of Calculated Permeabilities – “Bad” Well Set. As with the “good” wells, the distribution of calculated permeabilities is approximately lognormal, which is the expected result.

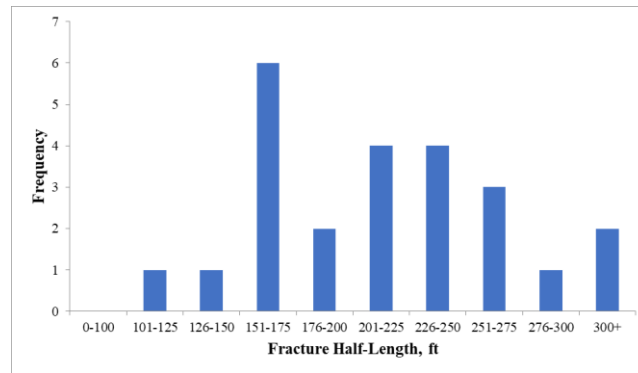


Fig. 3.18: Histogram of Calculated Fracture Half-Lengths – “Bad” Well Set. Again, the distribution of calculated fracture half-lengths is quite random, which is likely due to fracture half-length being primarily a function of completion design rather than natural processes.

All wells in the “bad” well set were scaled to the reference parameters shown in **Table 3.5**. Prior to scaling, the distribution of EURs was approximately lognormal, as per expectations, ranging from 170.4 MSTB to 904.7 MSTB, with a mean of 456.6 MSTB and a median of 398.2 MSTB. Once scaled, the range of the distribution narrowed, with the minimum increasing to 230.8 MSTB and the maximum decreasing to 773.9 MSTB. The distribution was approximately uniform across this interval, with a mean value of 485.5 MSTB and a median of 476.6 MSTB. **Figs. 3.19 and 3.20** show these distributions for unscaled and scaled EUR, respectively, and the EURs for each well are summarized in **Table 3.6**.

Ref. k	4.11E-04	mD
Ref. s_f	244.8	ft
Ref. h	196.9	ft
Ref. L_w	7562.2	ft
Ref. x_f	212.7	ft
Ref. Δp	2708.3	psi

Table 3.5: Scaling Reference Parameters – “Bad” Well Set. Reference parameters were determined by averaging properties of all wells from the “bad” well set.

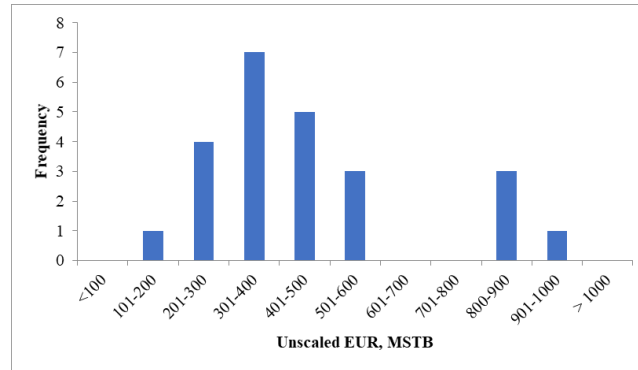


Fig. 3.19: Histogram of Unscaled EURs – “Bad” Well Set. The distribution of unscaled EURs exhibits the expected approximately lognormal shape.

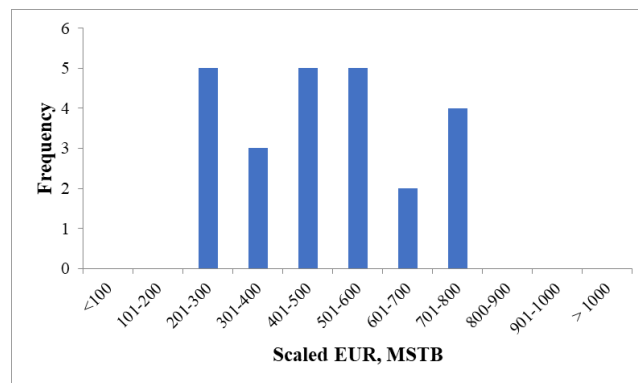


Fig. 3.20: Histogram of Scaled EURs – “Bad” Well Set. Scaling the rate/time production profiles transformed the distribution of EURs from approximately lognormal to approximately uniform.

Well	Unscaled EUR	Scaled EUR	Well	Unscaled EUR	Scaled EUR
3	267.5	773.9	65	845.5	285.3
16	341.2	230.8	69	402.5	353.2
18	400.1	773.4	80	819.3	631.2
20	547.8	447.5	90	391.4	358.5
24	396.2	648.8	92	170.4	269.9
25	369.6	569.8	96	448.6	482.1
30	327.8	709.2	108	904.7	555.7
38	424.4	413.2	134	335.0	524.2
49	550.8	445.2	135	241.5	255.8
58	493.0	277.6	136	268.4	341.0
61	859.3	471.1	140	337.9	511.9
63	296.9	726.1	141	529.8	597.6

Table 3.6: Scaled and Unscaled EURs, MSTB – “Bad” Well Set

The scaled production profiles of wells 135, 61, and 30, respectively, were used to construct the P90, P50, and P10 type wells seen in **Fig. 3.21**. Wells 135 and 30 were selected for the sake of conservatism, as they were nearest to without exceeding the 90th and 10th percentiles.

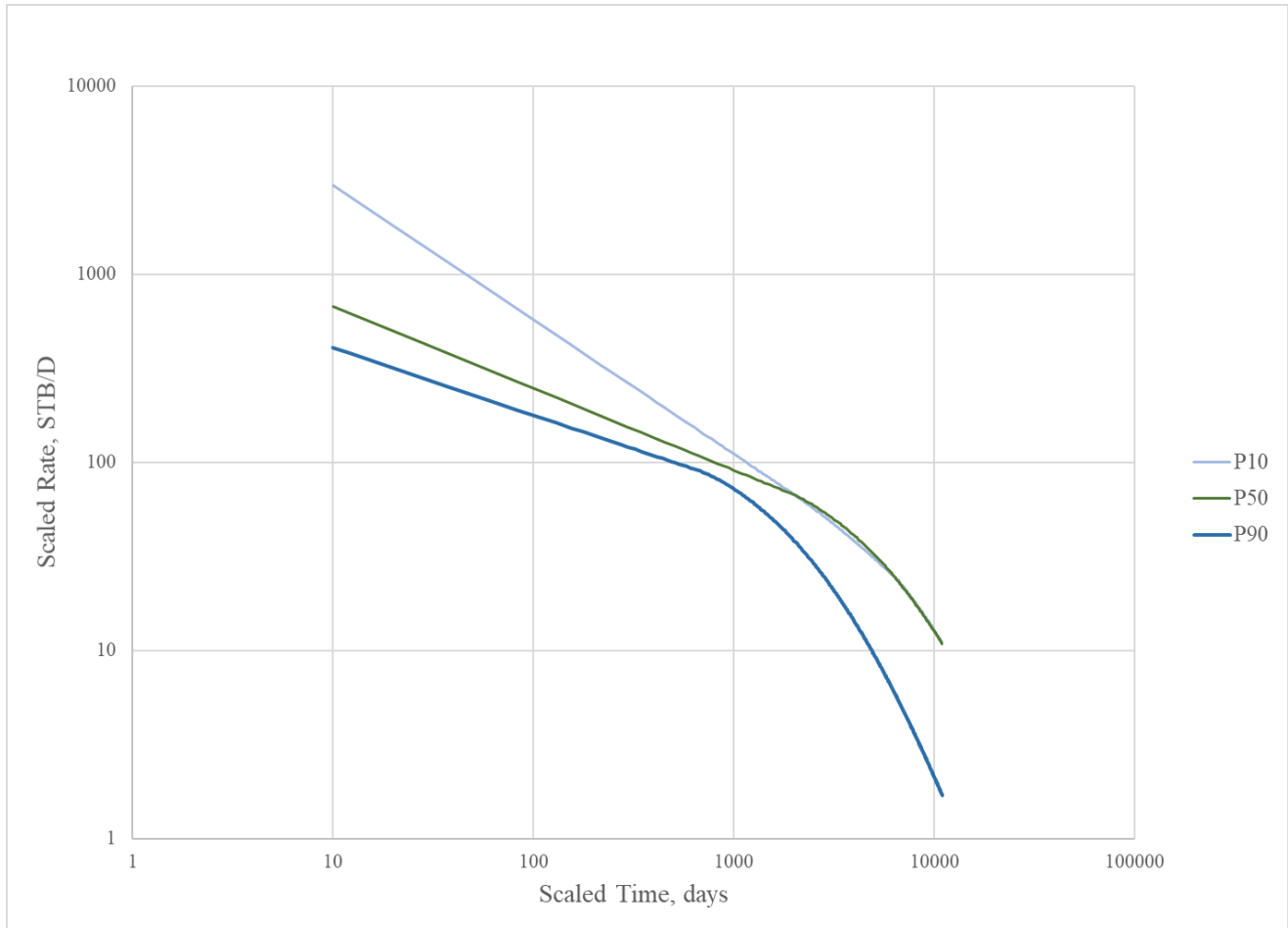


Fig. 3.21: P90, P50, and P10 Type Wells – “Bad” Well Set. Notice the overlap between the P10 and P50 type wells. Although the P10 type well produces at lower rates than the P50 type well later in their productive lives, the P10 type well nonetheless has a much larger EUR due to higher initial rates. The eventual overlap is the result of the P10 type well having a significantly steeper transient decline.

Tabulated results as well as diagnostic plots, type curve matches, and forecasts for each well in the “bad” well set can be found in Appendix A.

3.2.4 “Early” Wells

The “early” wells were all wells from the data set with production histories of less than a year. Due to the lack of available data, all results for the “early” wells set are highly speculative, as often wells were analyzed prior even to the start of transient flow.

The impact of analyzing wells based solely upon early-time data is particularly evident in the distribution of transient b-values, shown in **Fig. 3.22**. The distribution is shifted noticeably to the right, with more than two-thirds of b_{TR} values greater than or equal to 2, as compared to approximately 25% of the “good” wells and 42% of the “bad wells.” This is likely attributable to the inclusion of early off-trend data points in the analysis. Due to occurrences such as fracture fluid clean-up or changing bottomhole pressure conditions, the first months of production are often substantially off- and typically below-trend. With longer production histories, the real transient trend has time to develop and become apparent, and consequently these early-time points can be ignored and thus do not influence the analysis. In case of wells with short histories, however, these points must be considered, often resulting in incorrect characterization of the transient regime. Specifically, when the early-time points are below-trend, the resulting b_{TR} value will be too high, as the decline will appear shallower than it truly is.

Despite the aforementioned issues, the distribution of calculated permeabilities nonetheless retains the approximately lognormal shape, as can be seen in **Fig. 3.23**. Values range from 1.99×10^{-4} mD to 9.25×10^{-4} mD, with an average of 4.50×10^{-4} mD and a median of 4.01×10^{-4} mD.

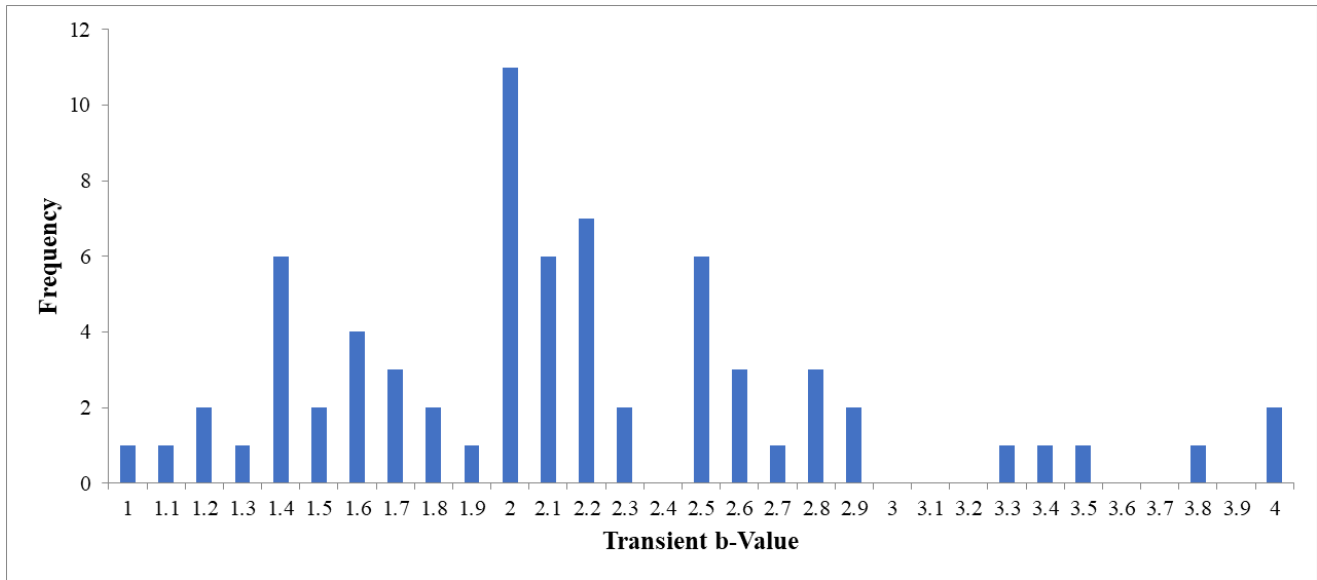


Fig. 3.22: Histogram of b_{TR} -Values – “Early” Well Set. The “early” set of wells has a much higher frequency of wells with b_{TR} values larger than 2. This is likely due to early time data distorting the true transient trend.

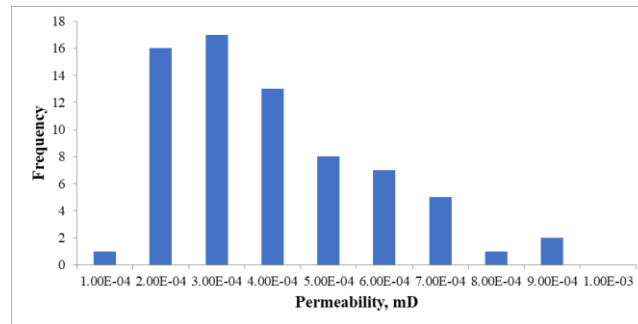


Fig. 3.23: Histogram of Calculated Permeabilities – “Early” Well Set. The distribution of calculated permeabilities displays the anticipated approximately lognormal shape.

The distribution of calculated fracture half-lengths, shown below in **Fig. 3.24**, covers a far wider interval than either of the other two sets, ranging from a minimum value of 100.7 ft to a maximum of 483.4 ft. The values toward the higher end of this spectrum are likely erroneous, as fractures substantially longer than 300 ft are unlikely and atypical. This is almost certainly a consequence of modeling the transient period with too high a b_{TR} value, as discussed above. Higher values of b_{TR} result in a slower decline, maintaining higher rates and resulting in a lower

RMP. Because fracture half-length varies inversely with RMP, this will cause the calculations to be artificially high.

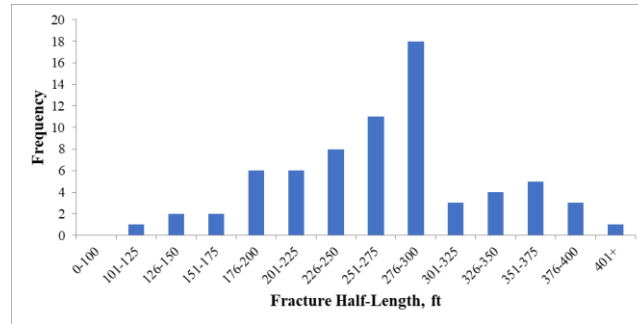


Fig. 3.24: Histogram of Calculated Fracture Half-Lengths – “Early” Well Set. Many of the calculated fracture half-lengths are far larger than would be expected, as a reasonable maximum would be closer to 300 ft. This is likely attributable to early time data resulting in artificially high values of b_{TR} , which in turn lead to higher calculated values of fracture half-length.

As with both the “good” and “bad” well sets, the unscaled EUR distribution for the “early” wells exhibits the anticipated lognormal shape. The average unscaled EUR is 622.0 MSTB, the median is 579.5 MSTB, and values range from 139.3 MSTB to 1318.2 MSTB. After forecasting unscaled production, the “early” wells were scaled to the set of reference parameters found in **Table 3.7**. The scaled distribution is again approximately uniform, with all but two wells spanning an interval from 339.3 MSTB to 851.1 MSTB. With scaled EURs of 1046.4 MSTB and 1386.5 MSTB, respectively more than 20% and 60% higher than the maximum of this range, the two aberrant wells should both be considered outliers. Excluding them, the mean scaled EUR is 610.0 MSTB and the median is 637.7 MSTB. **Figs. 3.25 and 3.26** summarize the two distributions, and calculated EURs for each well are tabulated in **Table 3.8**.

Ref. k	4.50E-04	mD
Ref. s_f	237.1	ft
Ref. h	194.3	ft
Ref. L_w	8294.8	ft
Ref. x_f	270.7	ft
Ref. Δp	2622.9	psi

Table 3.7: Scaling Reference Parameters – “Early” Well Set. Reference parameters were determined by averaging properties of all wells from the “early” well set.

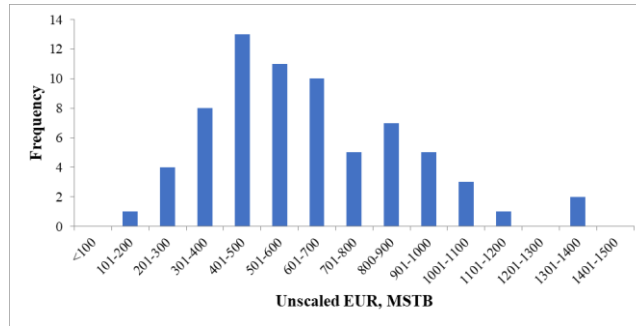


Fig. 3.25: Histogram of Unscaled EURs – “Early” Well Set. The distribution of Unscaled EURs exhibits the expected lognormal shape.

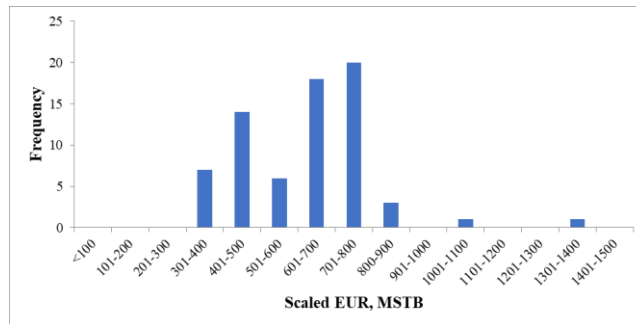


Fig. 3.26: Histogram of Scaled EURs – “Early” Well Set. The two EURs outside the interval from 339.3 MSTB to 851.1 MSTB should be considered outliers and were excluded from consideration for type well construction.

Well	EUR	Scaled EUR	Well	EUR	Scaled EUR	Well	EUR	Scaled EUR
1	432.9	556.5	50	246.3	492.0	101	504.1	497.0
2	991.8	733.8	52	420.1	339.3	102	236.6	573.3
4	339.9	385.0	54	895.1	673.3	104	271.3	435.3
5	489.4	617.2	55	909.2	728.2	105	552.3	385.8
8	324.3	808.9	56	684.1	671.8	107	485.3	420.0
9	552.1	645.1	57	525.1	494.7	109	400.6	520.2
10	723.2	607.1	64	782.3	811.9	110	579.6	792.1
11	402.8	725.5	66	480.7	580.2	113	929.7	776.6
12	841.2	731.9	67	625.2	418.4	114	560.2	637.3
15	625.4	715.4	71	831.1	496.7	116	883.1	702.1
17	526.6	482.8	72	269.0	680.5	123	708.1	666.9
23	430.4	520.5	73	706.4	621.9	124	514.9	603.9
26	1091.8	769.8	74	326.4	344.9	126	821.0	684.5
27	349.4	1046.3	76	429.7	431.7	131	345.5	371.5
28	611.5	617.4	79	788.6	678.5	132	318.2	1386.5
31	699.7	688.4	81	1037.7	743.7	137	1318.2	741.4
33	500.0	465.8	82	393.0	746.9	138	451.9	610.0
34	625.1	792.1	85	579.5	638.1	139	335.8	591.8
37	902.3	791.6	86	495.2	724.0	142	1185.7	851.1
39	632.3	393.4	87	1310.8	708.4	143	662.3	664.8
40	598.2	448.7	91	426.3	448.3			
43	1081.0	738.7	94	887.3	754.9			
44	139.3	389.7	95	813.8	748.5			
47	419.4	468.2	97	692.1	767.2			
48	952.0	689.7	98	641.8	429.6			

Table 3.8: Scaled and Unscaled EURs, MSTB – “Early” Well Set

With scaled EURs of 393.4 MSTB, 638.1 MSTB, and 791.6 MSTB, Wells 39, 85, and 37, respectively, were used to construct P90, P50, and P10 type wells for the “early” wells. These type wells are plotted below in **Fig. 3.27**.

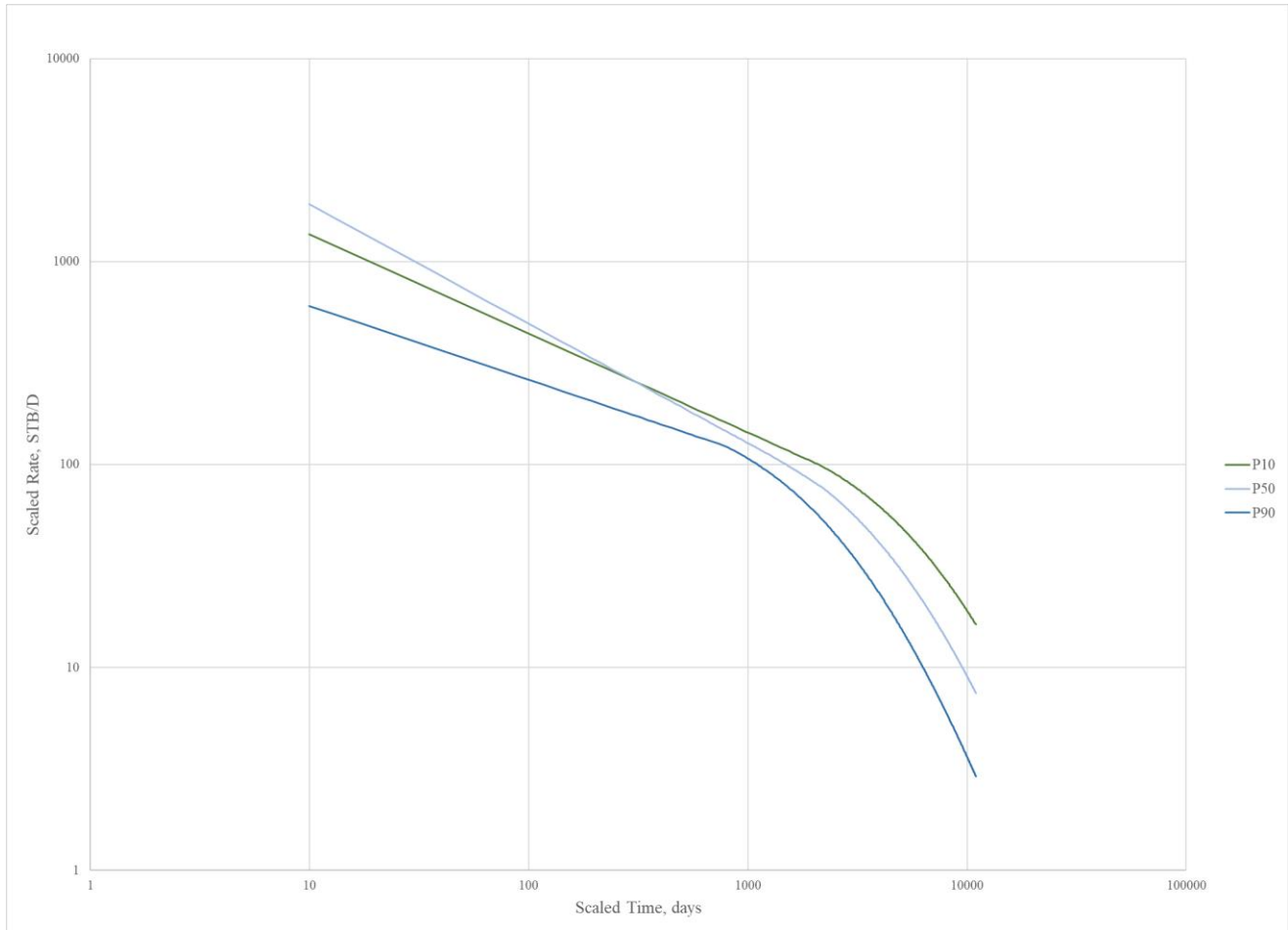


Fig. 3.27: P90, P50, and P10 Type Wells – “Early” Well Set. Notice that the P50 type well actually begins above the P10 type well. This is possible because, despite higher initial rates, the P50 type well has a much steeper transient decline and thus spends the majority of its life producing at a lower rate than the P10 type well.

Tabulated results as well as diagnostic plots, type curve matches, and forecasts for each well in the “early” well set can be found in Appendix A.

3.3 The Issue of Uncertainty

Each well from the previously discussed field application was analyzed in a decidedly deterministic fashion. A single value for each input parameter was selected, a minimum decline rate was specified, and a transition to a BDF regime with a set b-value was forced, resulting in a single forecast with a single corresponding set of calculated parameters (permeability, fracture

half-length, and EUR). These singular forecasts were then aggregated across all wells, scaled, and ranked, after which the results were used to construct the desired type wells.

There is nothing inherently wrong with such an approach, assuming that all inputs - the reservoir, completion, and operational parameters, the specified minimum decline rate, and the b_{BDF} value – are known with certainty. Problematically, however, very few, if any, of these things will ever be certain. As such, these singular forecasts are disingenuous; they misrepresent the level of uncertainty associated with the entire premise of forecasting a well relying upon nothing but its production history and a set of assumed inputs.

In reality, inputs could take any value from within a range, or distribution, of values. For the wells being analyzed, it was asserted that porosity could range between 7% and 12%, but choosing the correct value for any particular well from within this range would be nearly impossible; any selection would be purely arbitrary, as any other value could have just as reasonably been assumed. This principle holds true for most every other input parameter, although a few, such as lateral length, for example, should be known with a least some degree of certainty.

Rather than simply assuming values, it is therefore better to acknowledge this uncertainty by determining a range of possible outcomes using Monte Carlo Simulation, each one generated by randomly sampling values of input parameters from their respective distributions. This would result in a distribution of possible forecasts, each with their own corresponding calculated parameters, for every well.

The type wells from the field application example were constructed by ranking the scaled EURs corresponding to each well's deterministic forecast and selecting the production profiles of wells of the appropriate percentiles. This procedure could be adapted to a more statistical approach by again using Monte Carlo simulation. A single complete set of analyzed wells could be created by randomly sampling an outcome for every one of the wells in the set. Repeating this procedure for a sufficiently large number of iterations would result in the creation of a distribution of complete sets. After scaling every complete set of wells within the distribution to the same set of reference parameters, type wells could be constructed for each at selected levels of uncertainty (e.g. P90, P50, and P10). Aggregating these type wells across all complete sets would result in distributions of type wells for each level of uncertainty (e.g. the P90 type wells from each set would comprise the distribution of P90 type wells). It seems reasonable that, given a sufficiently large number of complete sets, the final type wells could then be constructed by averaging the wells in these distributions. Such an approach would help to avoid the pitfalls associated with the deterministic alternative, which constructed type wells based upon only one of an infinite set of possible outcomes. By using a large number of possible outcomes to construct the type wells, the inherent uncertainty is addressed and reflected in the results.

4. CONCLUSIONS AND RECOMMENDATIONS FOR FUTURE WORK

4.1 Conclusions

1. The new type curve presented in this thesis effectively maintains the functionality of Wattenbarger's type curve, allowing for the calculation of matrix permeability and fracture half-length from field production data, while additionally providing means by which future production may be forecast.
2. Wells that have not yet undergone the transition to BDF may be matched to the type curve and forecast by assuming a minimum nominal decline rate at which point transient flow concludes. After this, forecast production can be described by a transition period using an intermediate b -value that smoothly connects the end of transient flow to the beginning of BDF. Wells undergoing steeper decline during the transient period (corresponding to lower values of b_{TR}) experience longer transition regions. The BDF regime can then be modeled by assuming a value of b_{BDF} , typically 0.3 in the case of solution gas drive oil reservoirs.
3. Determining appropriate reference parameters, scaling production profiles, and ranking by scaled EUR provides a basis by which statistical type wells (e.g. P90, P50, and P10) may be constructed. It should be noted, however, that these type wells are only fully-representative for wells with properties equivalent to the assumed reference parameters; predicting performance of well with different properties requires scaling to a differing set of reference parameters.
4. Using the methodology outlined in this thesis to analyze wells with short production histories (approximately one year or less) may yield inaccurate results. Early rate data is oftentimes

distorted by phenomena such as fracture fluid clean-up or changing bottomhole/operational conditions, and consequently the correct transient trend may be obscured. In most cases, early off-trend data will fall below the true trend, resulting in an apparent transient period characterized by far too shallow a decline (far too high a b_{TR} value). Using an artificially inflated b_{TR} value when analyzing a well will result in incorrectly high calculated values of fracture half-length and EUR. Therefore, inaccuracies associated with the inclusion of only early-time data in the analysis may be mitigated by assuming lower values of b_{TR} than are suggested by a best fit straight line of the logarithmic rate/time data.

4.2 Recommendations for Future Work

I recommend that further efforts be made to incorporate a statistical approach to the construction of type wells, as was discussed in section 3.3, into the methodology outlined in this thesis. Using a deterministic approach, as was done for the example field application, is likely to yield misleading results that misrepresent the true level of uncertainty.

NOMENCLATURE

BDF	Boundary-dominated flow
EUR	Estimated ultimate recovery
MBT	Material balance time, t, days or years
MFHW	Multi-fractured horizontal well
RMP	Rate match point
TMP	Time match point
B	Initial formation volume factor, dimensionless, RB/STB, RB/scf, or rcf/scf
b_{BDF}	Arps' BDF b-value
b_{TR}	Transient b-value
c_t	Total compressibility, psi^{-1}
d	Nominal decline rate, $1/t$, days^{-1} or years^{-1}
h	Net pay, L, ft
k	Permeability, L^2 , mD
L_w	Well lateral length, L, ft
$m(p_i)$	Initial average reservoir pseudopressure, m/Lt^3 , psia^2/cP
$m(p_{wf})$	Flowing bottomhole pseudopressure, m/Lt^3 , psia^2/cP
N_p	Cumulative oil production, L^3 , MSTB
p_i	Initial average reservoir pressure, m/Lt^2 , psia
p_{wf}	Flowing bottomhole pressure, m/Lt^2 , psia
q	Production rate, L^3/t , STB/D or Mscf/D
q'	Rate scaling factor
q_{DSF}	Dimensionless rate, $(\text{STB/D})(\text{RB/STB})(\text{cP})/(\text{mD}\cdot\text{ft}\cdot\text{psia})$

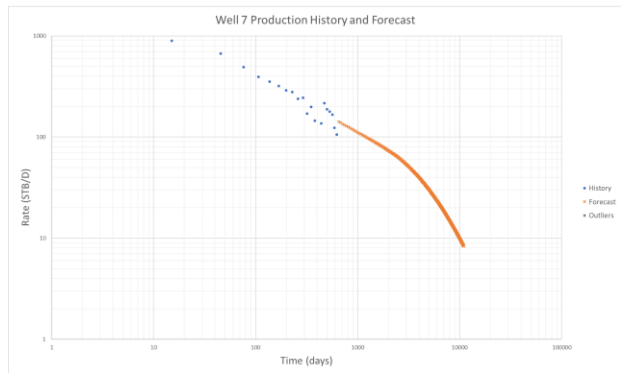
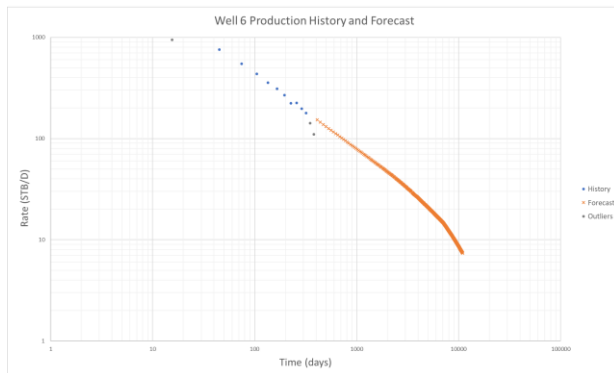
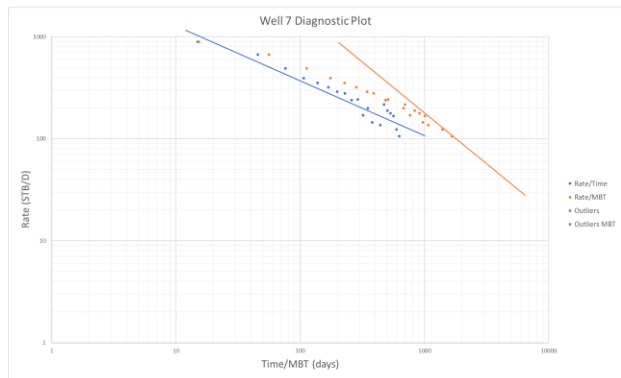
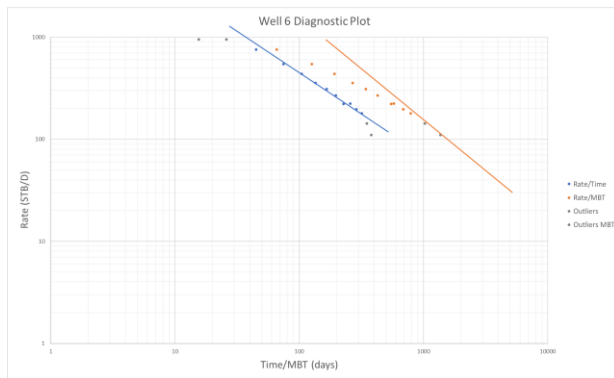
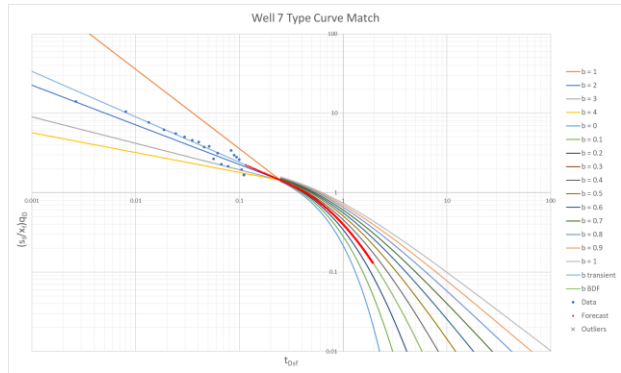
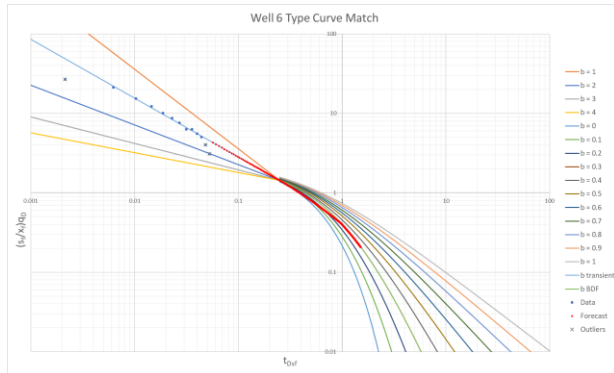
q_{sc}	Scaled rate, L^3/t , STB/D or Mscf/D
$q_{transition}$	Rate at the end of transient flow, L^3/t , STB/D or Mscf/D
s_f	Fracture spacing, L, ft
T	Reservoir temperature, T, °R
t	Time, days or years
t'	Time scaling factor
t_{BDF}	Time at the beginning of BDF, t, days or years
t_{DSF}	Dimensionless time, $(mD \cdot days)/(cP \cdot psi^{-1} \cdot ft^2)$
t_{sc}	Scaled time, t, days or years
$t_{transition}$	Time at the end of transient flow, t, days or years
x_f	Fracture half-length, L, ft
μ	Viscosity, m/lt, cP
ϕ	Porosity

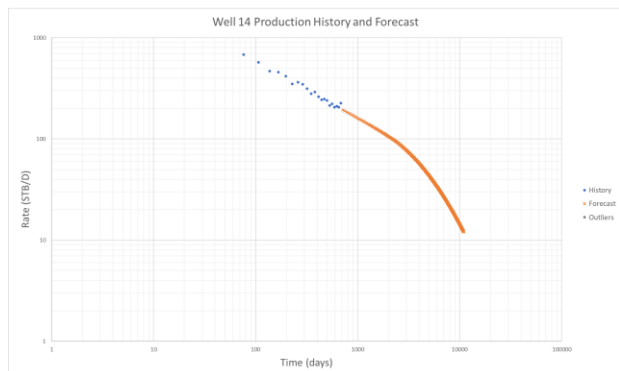
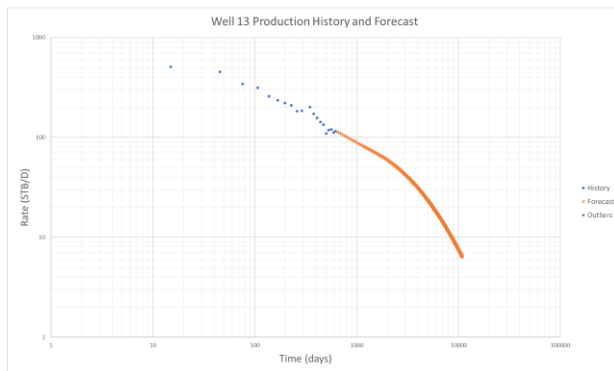
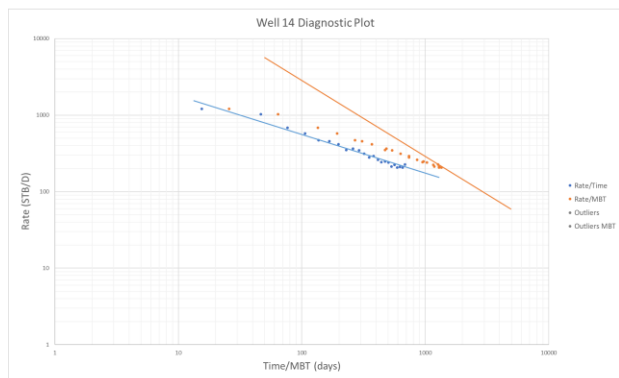
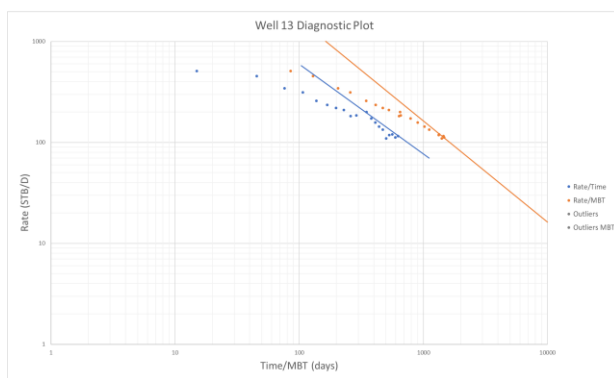
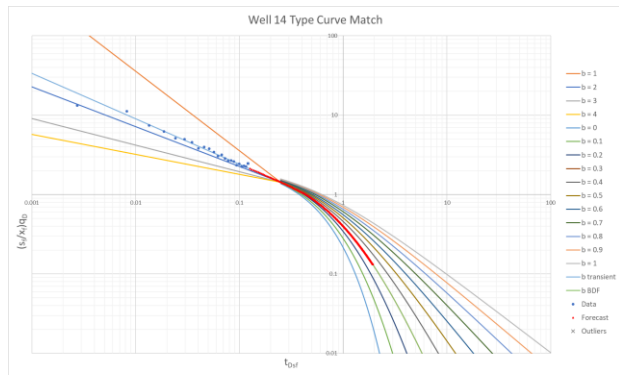
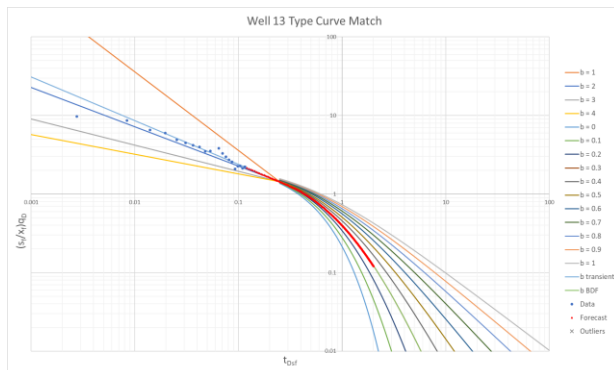
REFERENCES

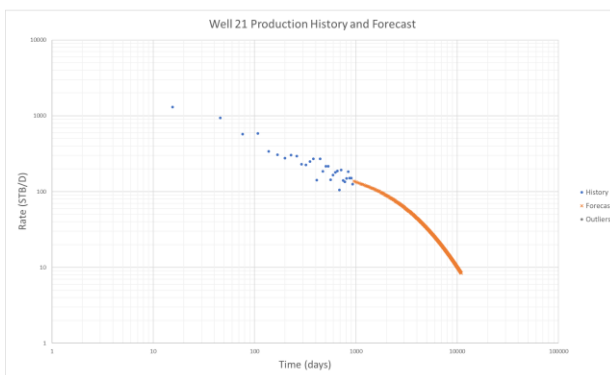
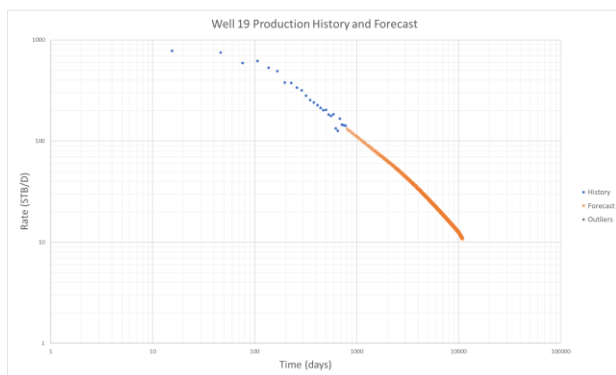
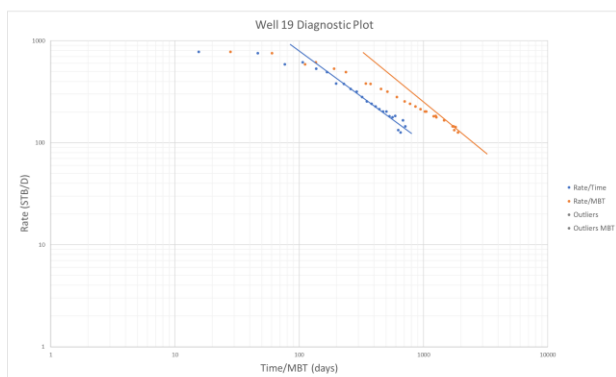
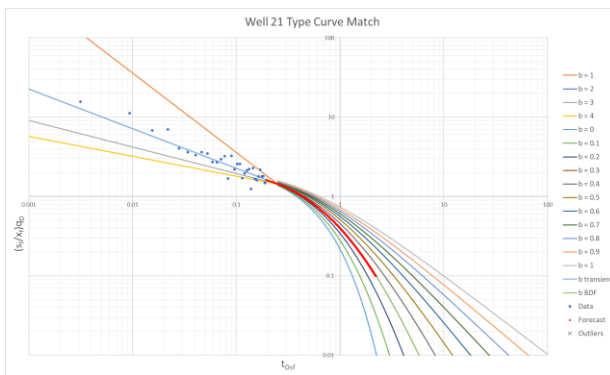
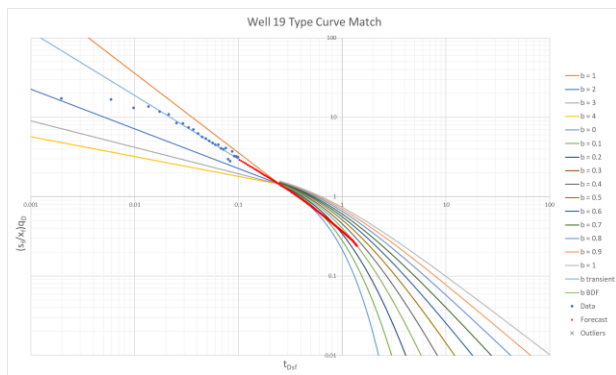
- Carter, R. D. 1985. Type Curves for Finite Radial and Linear Gas-Flow Systems: Constant-Terminal-Pressure Case. Society of Petroleum Engineers. doi:10.2118/12917-PA
- Chaudhary, N. L., & Lee, W. J. (2016, May 10). Detecting and Removing Outliers in Production Data to Enhance Production Forecasting. Society of Petroleum Engineers. doi:10.2118/179958-MS
- Chen, H.-Y., & Teufel, L. W. 2000. A New Rate-Time Type Curve for Analysis of Tight-Gas Linear and Radial Flows. Society of Petroleum Engineers. doi:10.2118/63094-MS
- Fetkovich, M. J. 1980. Decline Curve Analysis Using Type Curves. Society of Petroleum Engineers. doi:10.2118/4629-PA
- Freeborn, R., Russell, B., & Keinick, W. E. 2012. Creating Analogs, Fact and Fiction. Society of Petroleum Engineers. doi:10.2118/162630-MS
- Freeborn, R., & Russell, B. 2016. Creating More-Representative Type Wells. Society of Petroleum Engineers. doi:10.2118/175967-PA
- Rastogi, A., & Lee, W. J. 2015. Methodology for Construction of Type Wells for Production Forecasting in Unconventional Reservoirs. Unconventional Resources Technology Conference. doi:10.15530/URTEC-2015-2152273
- Russell, B., & Freeborn, R. 2012. A Practical Guide to Unconventional Petroleum Evaluation. Society of Petroleum Engineers. doi:10.2118/158867-MS
- Wattenbarger, R. A., El-Banbi, A. H., Villegas, M. E., & Maggard, J. B. (1998, January 1). Production Analysis of Linear Flow Into Fractured Tight Gas Wells. Society of Petroleum Engineers. doi:10.2118/39931-MS

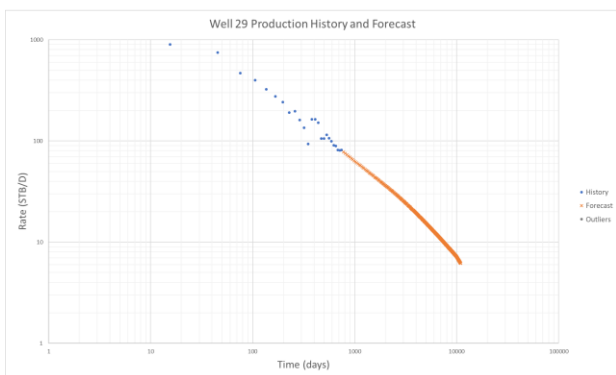
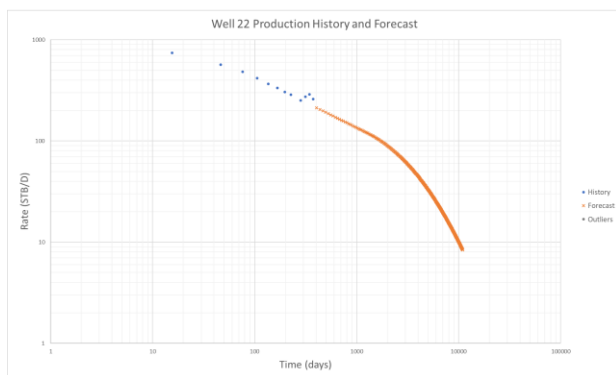
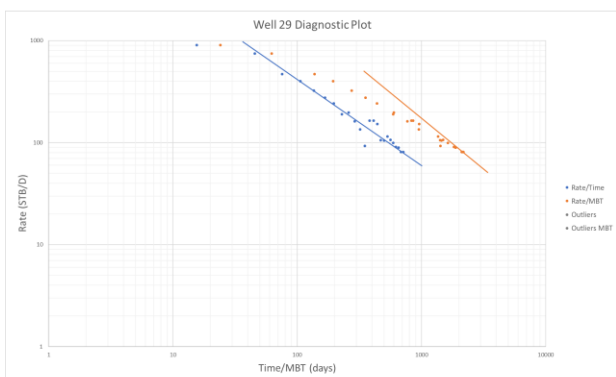
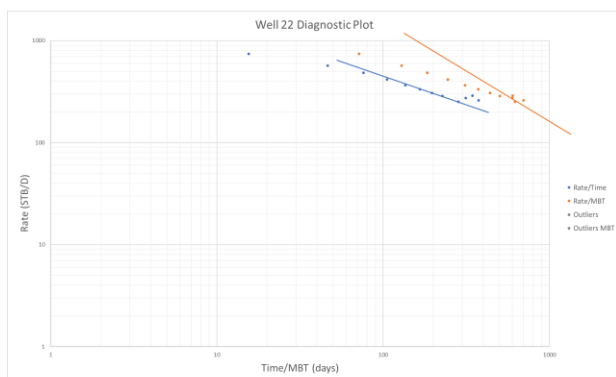
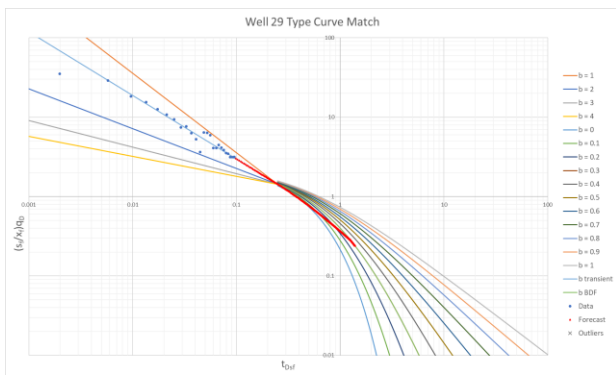
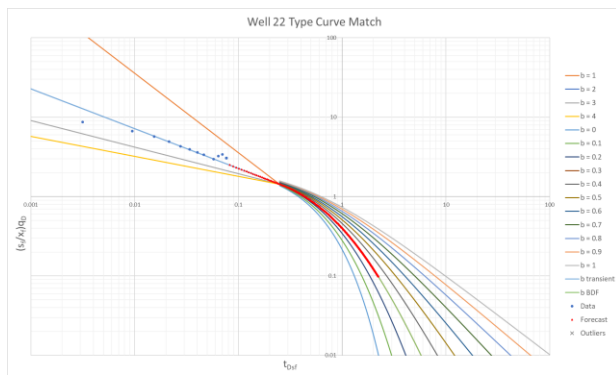
APPENDIX A

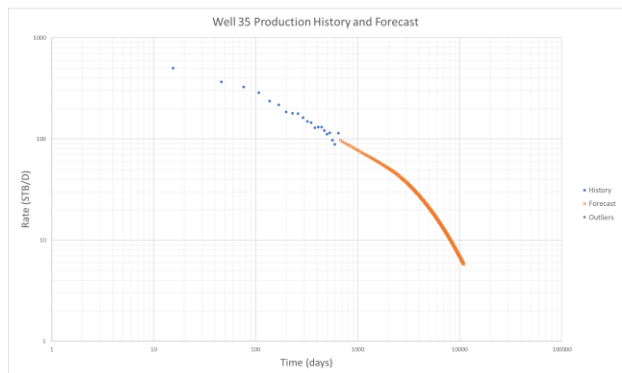
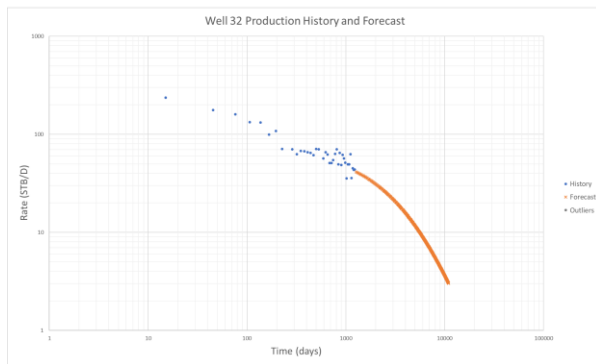
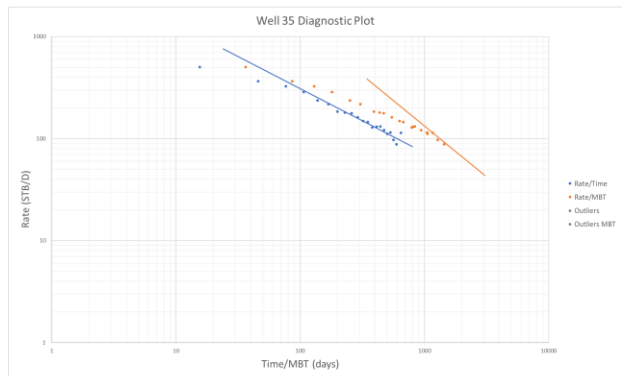
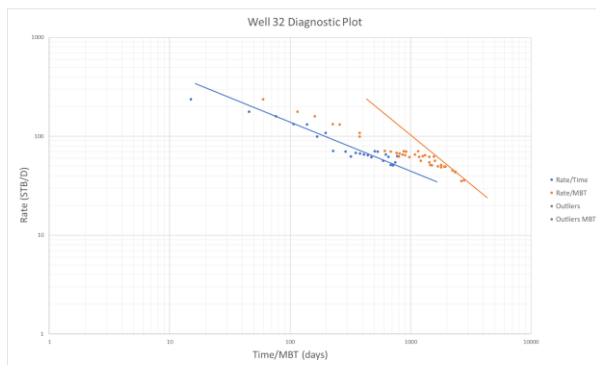
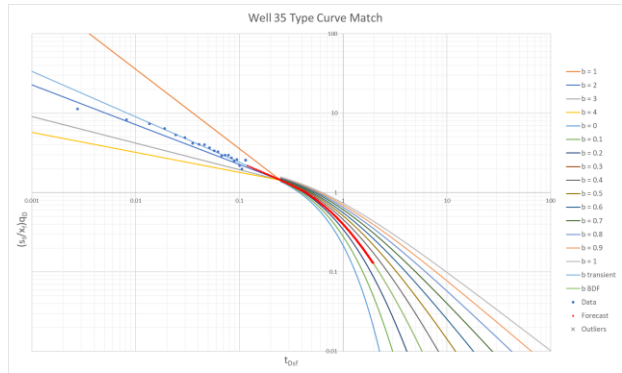
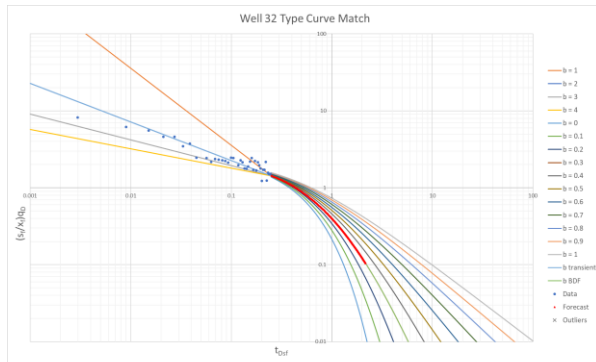
“Good” Well Set Plots and Results

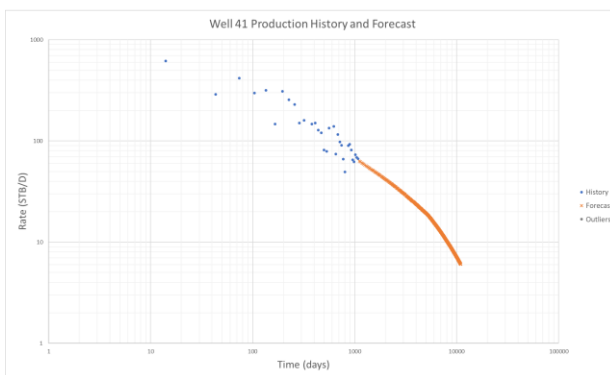
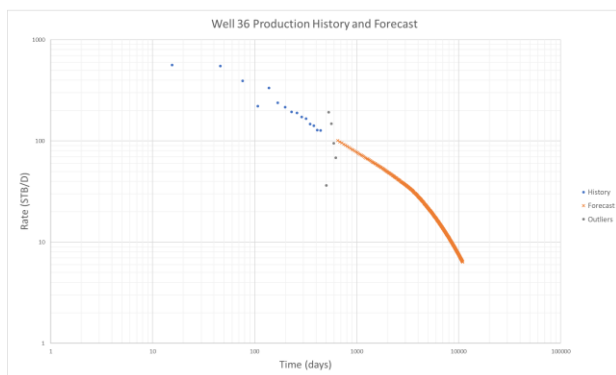
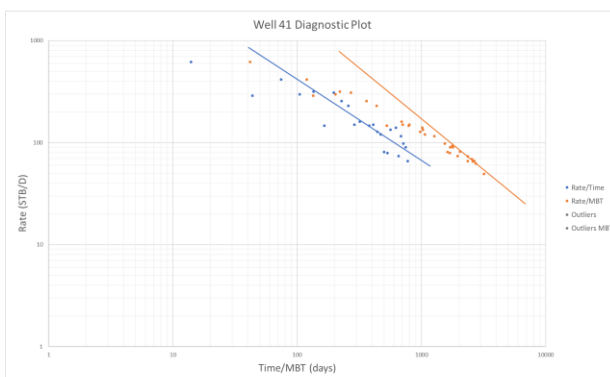
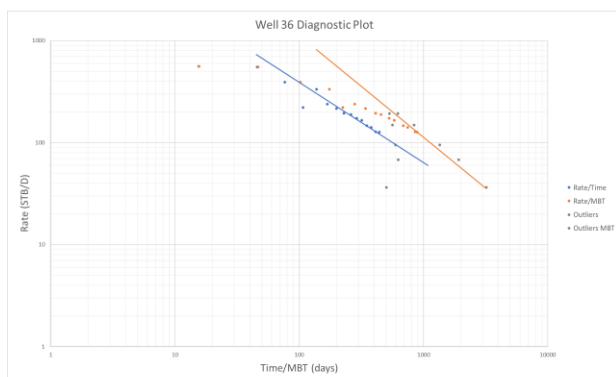
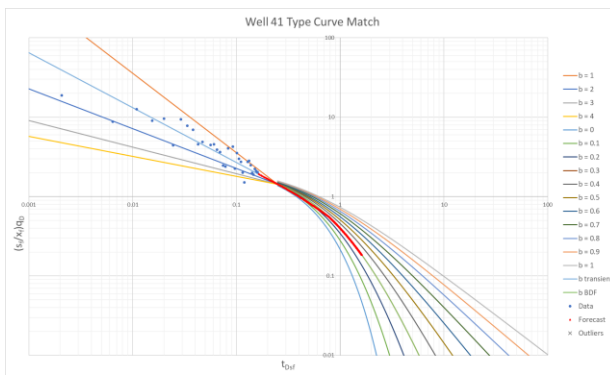
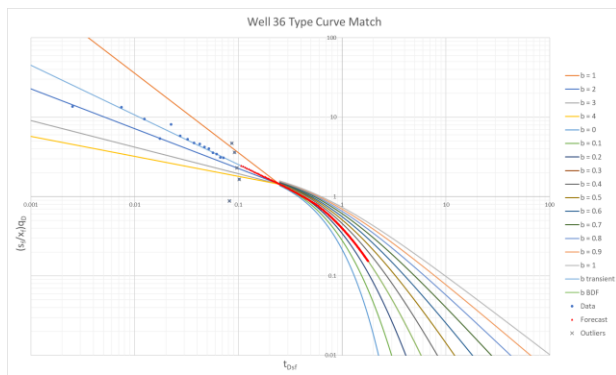


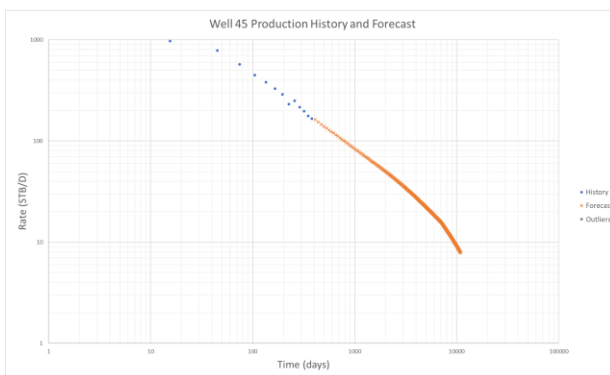
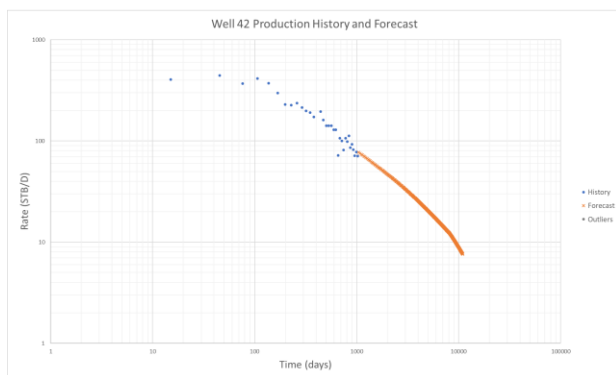
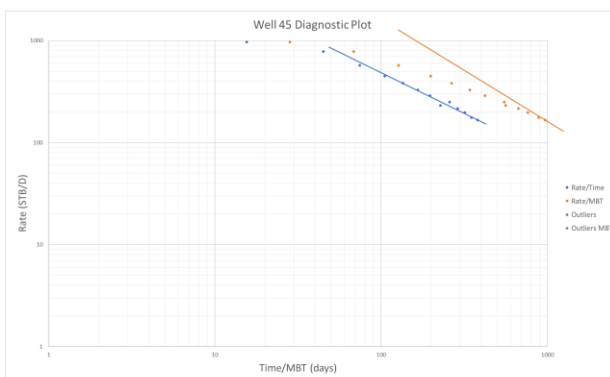
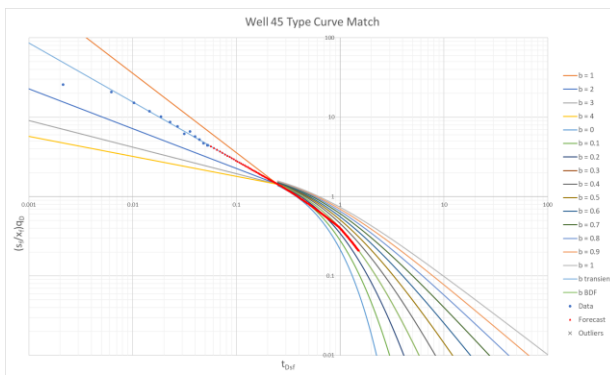
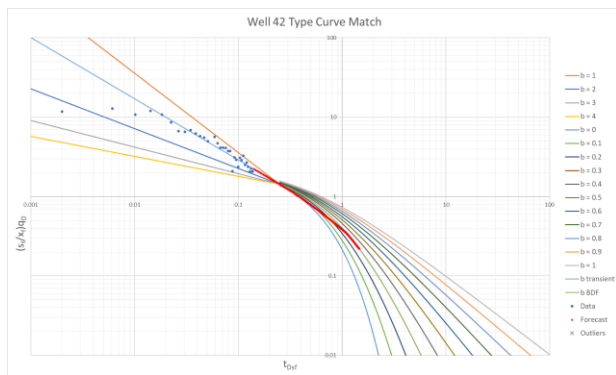


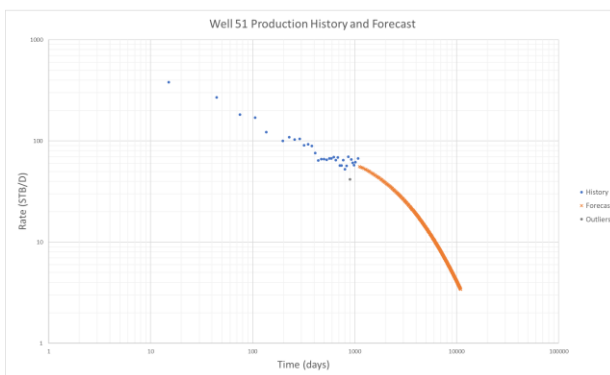
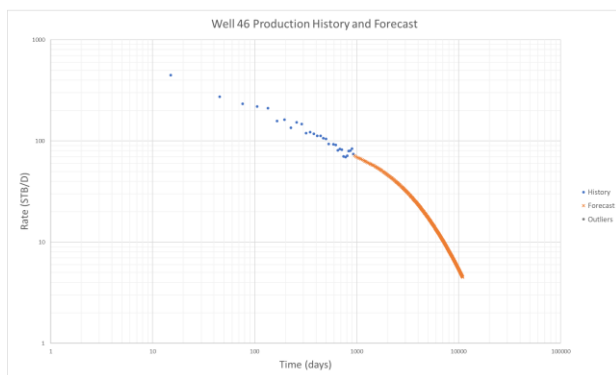
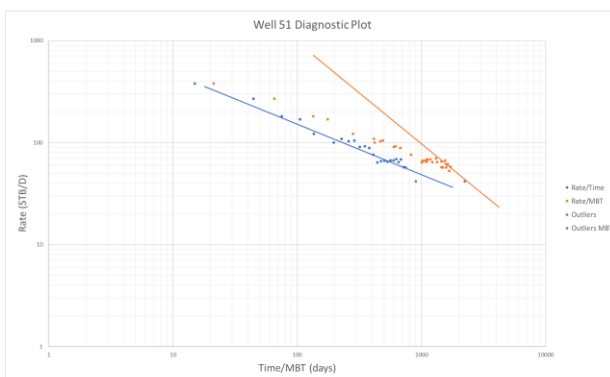
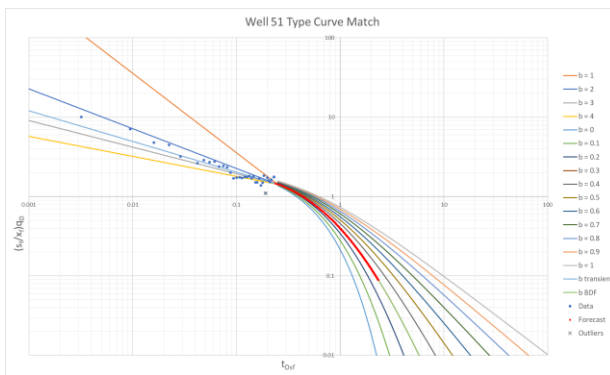
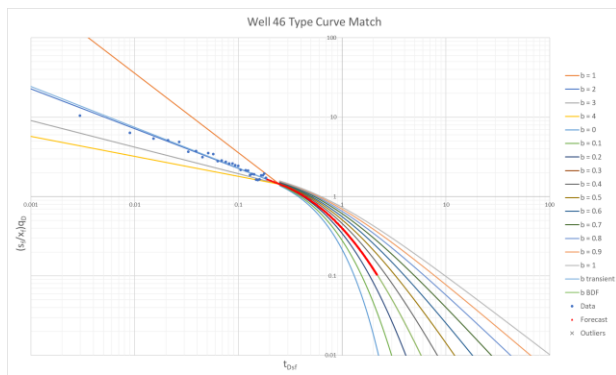


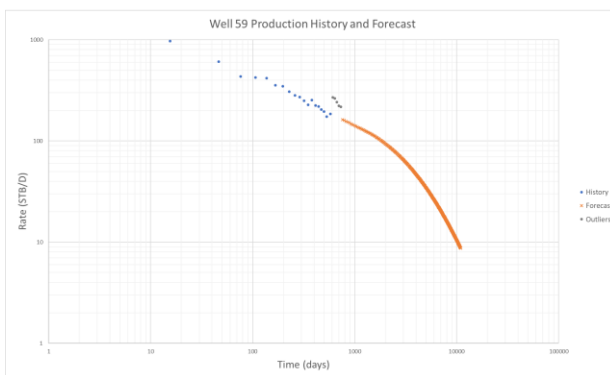
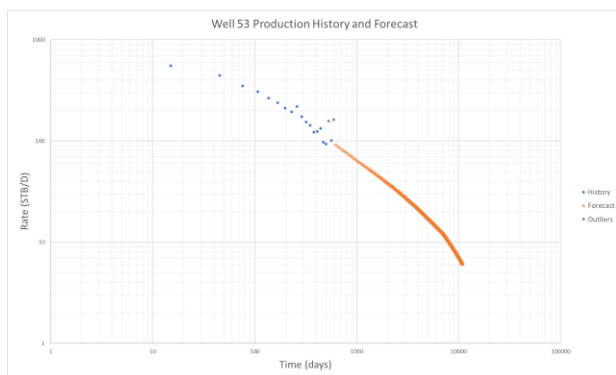
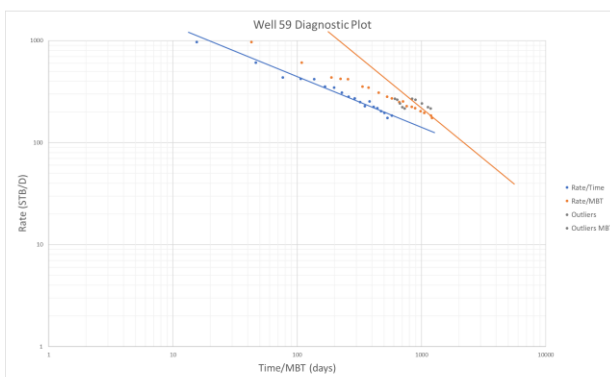
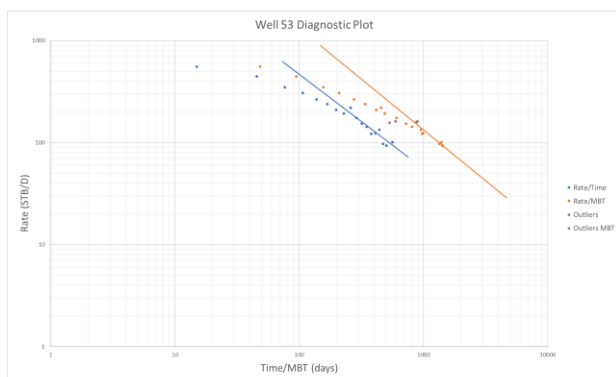
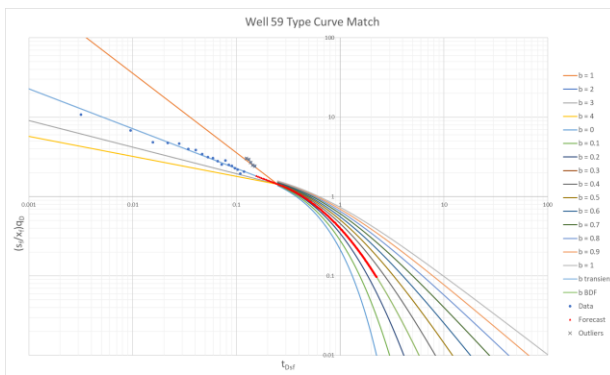
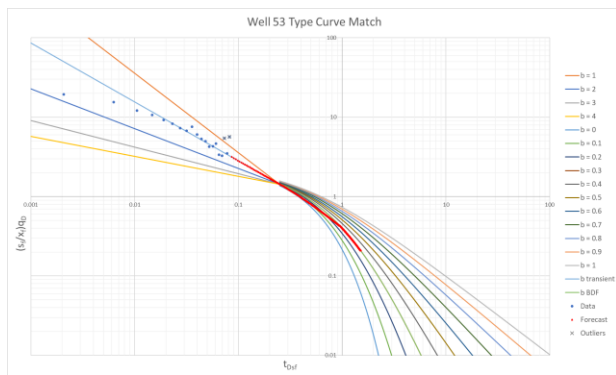


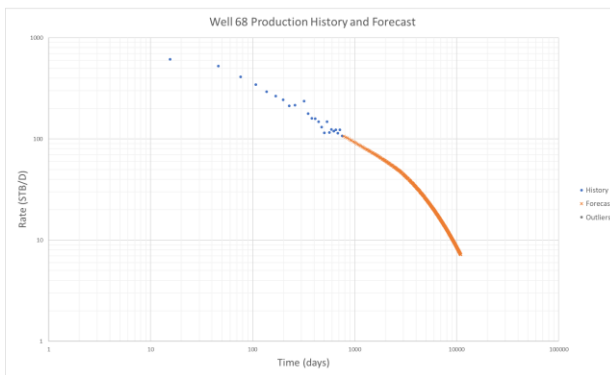
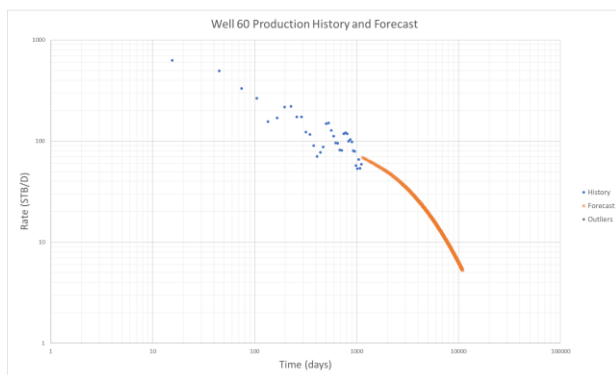
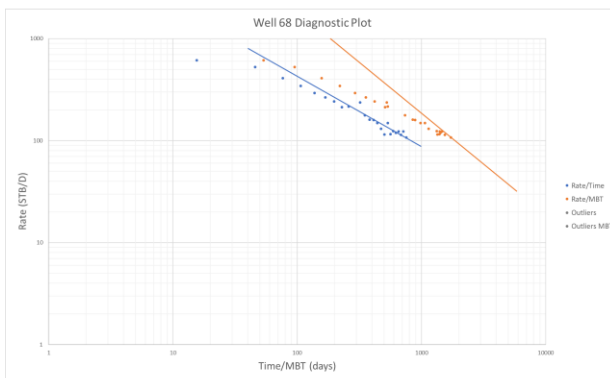
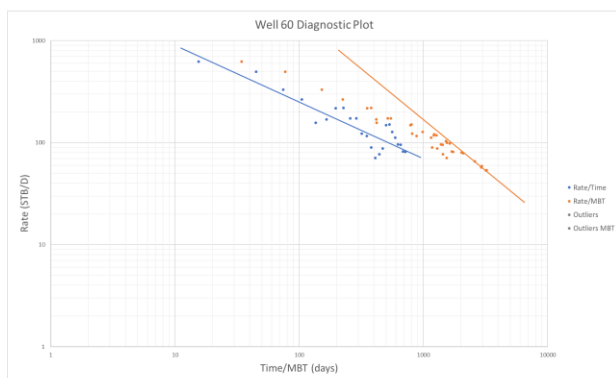
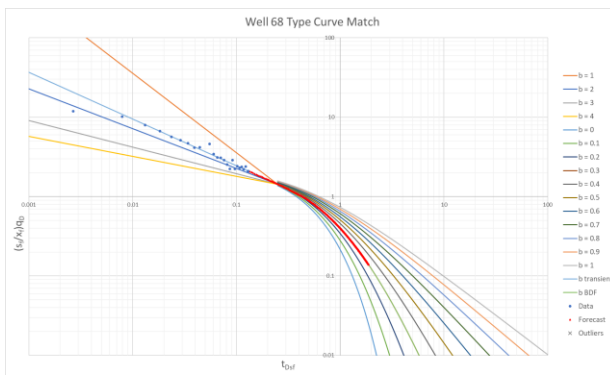
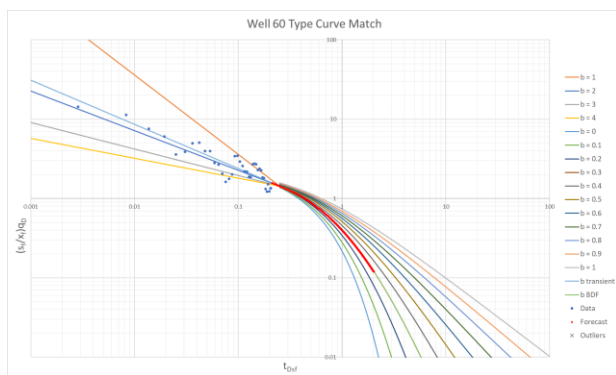


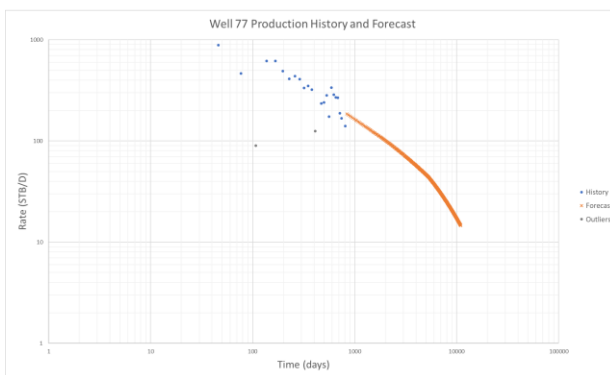
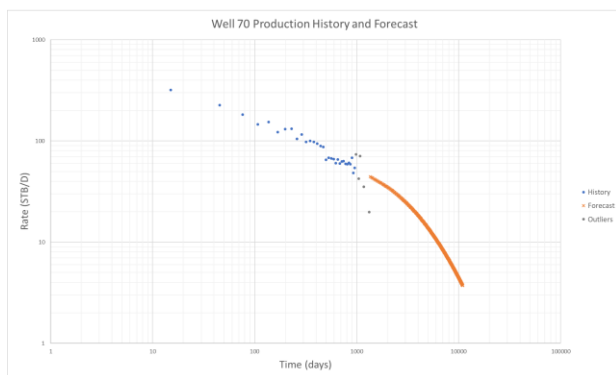
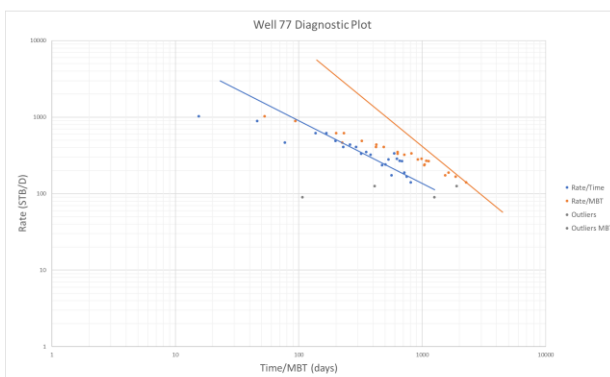
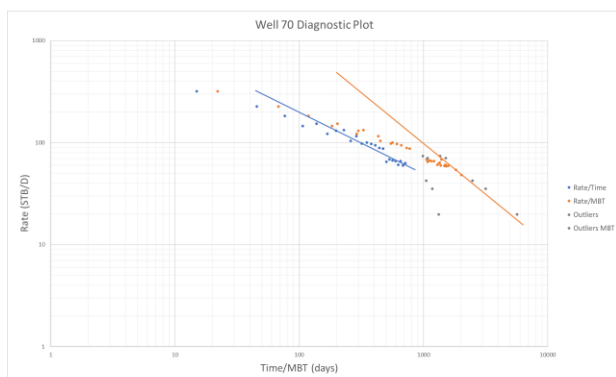
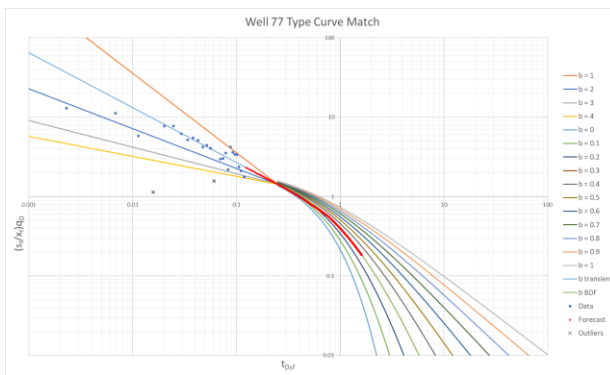
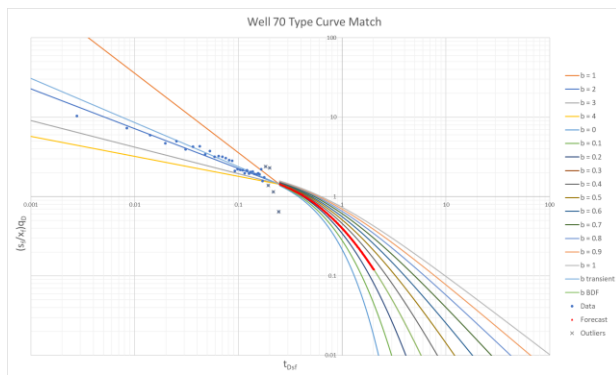


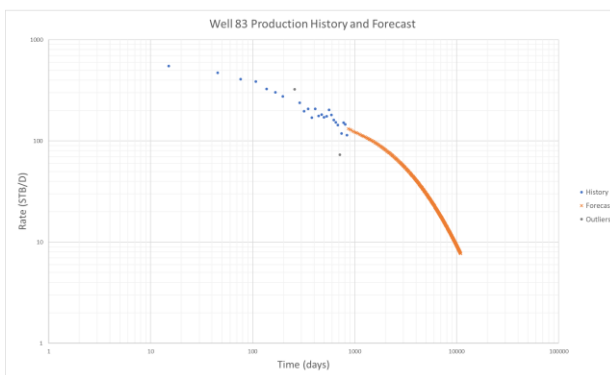
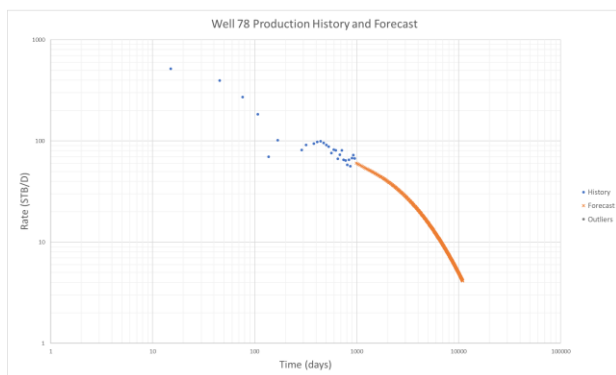
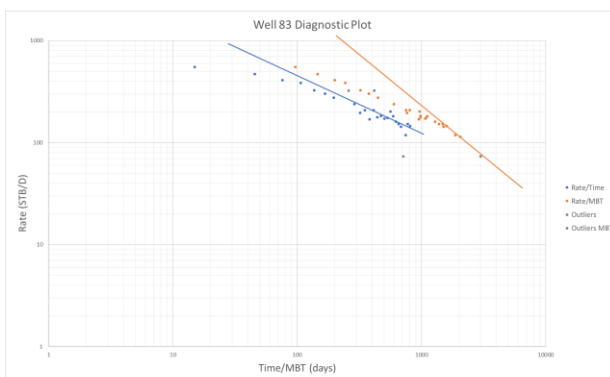
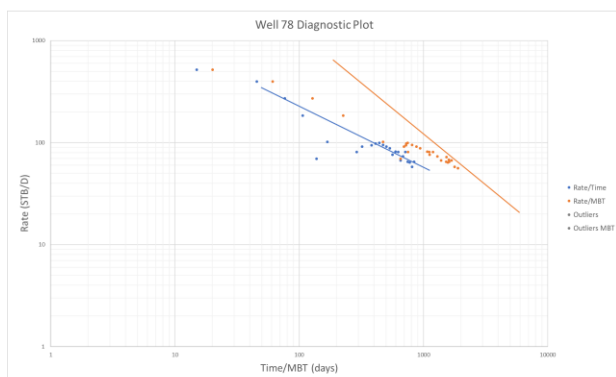
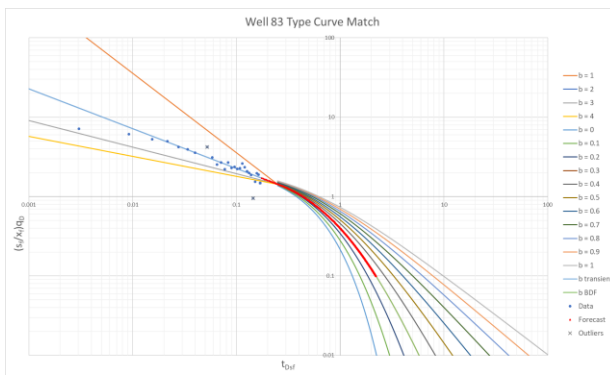
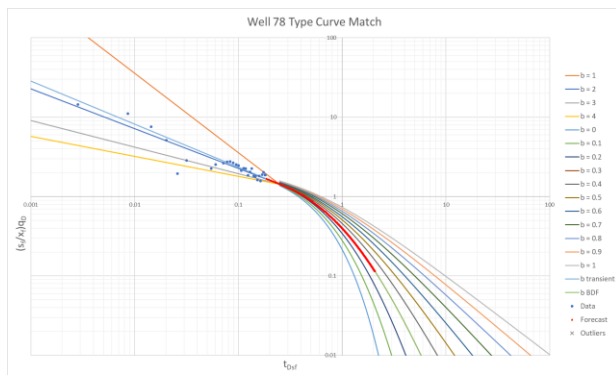


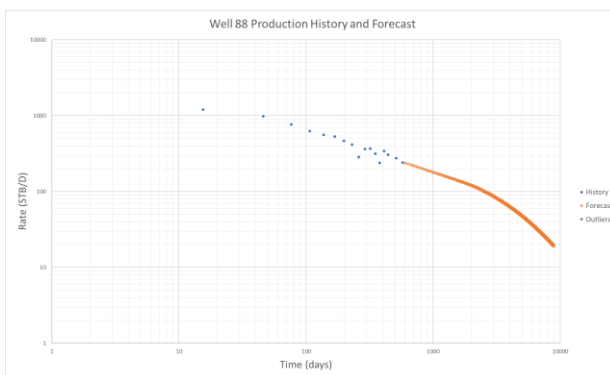
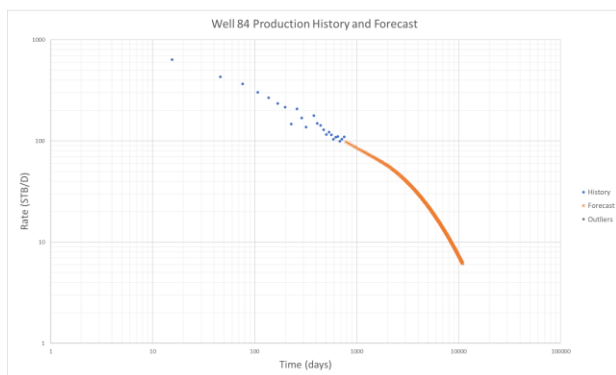
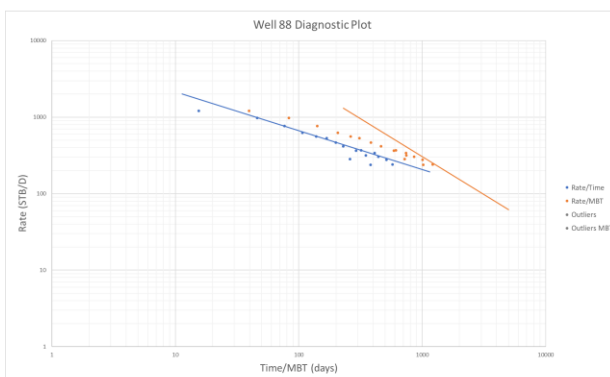
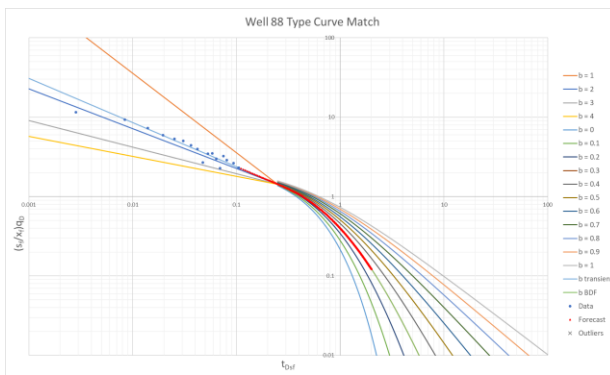
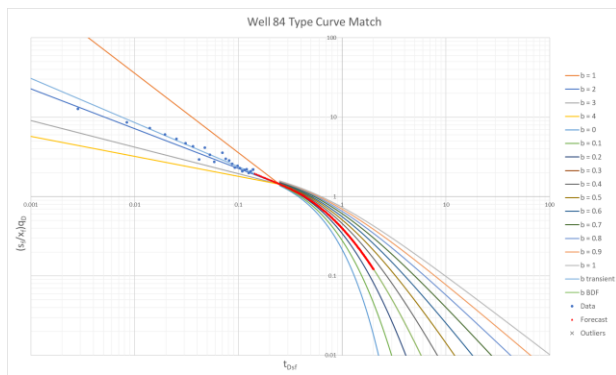


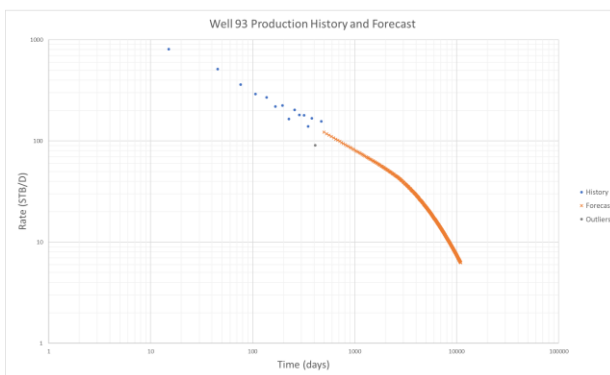
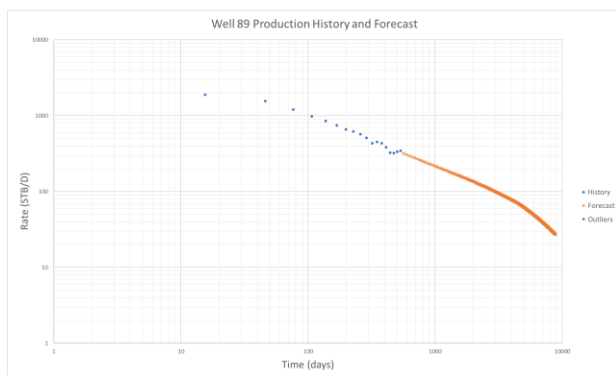
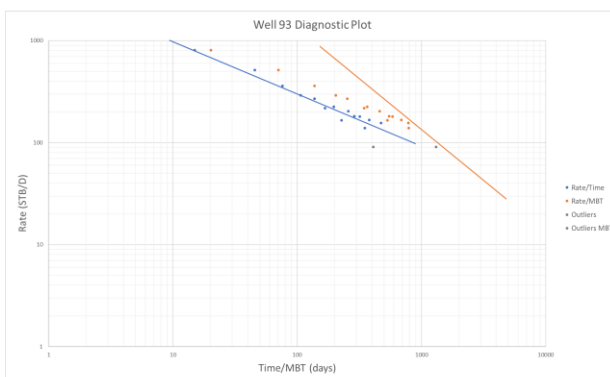
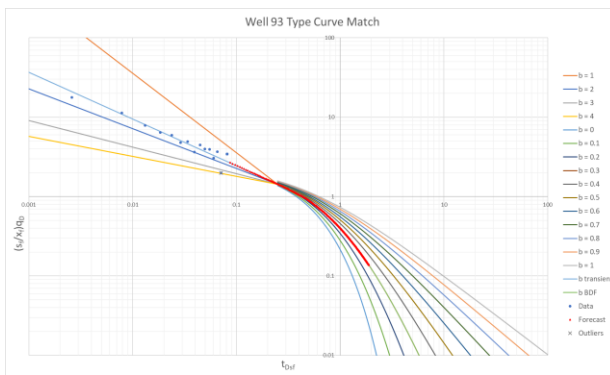
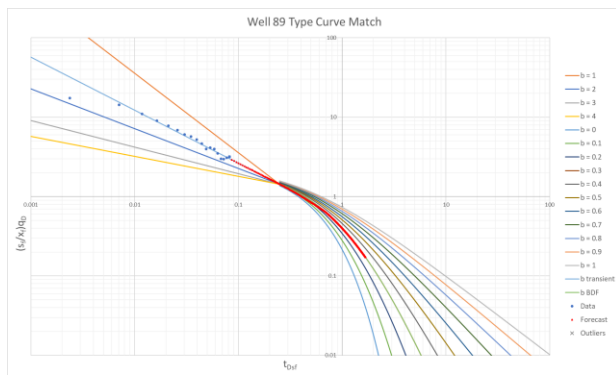


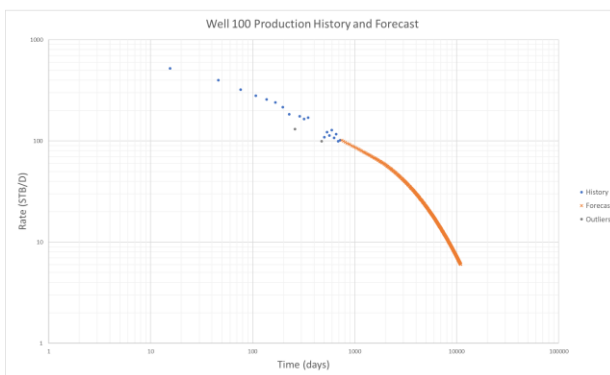
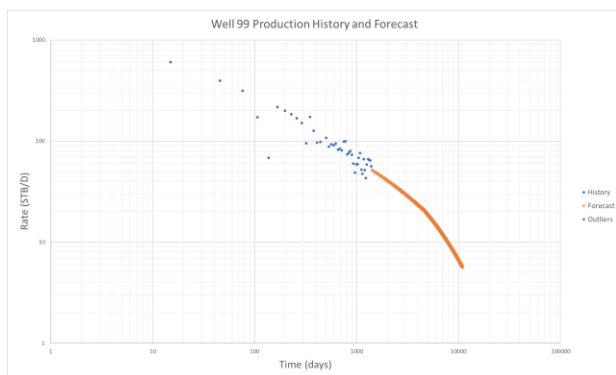
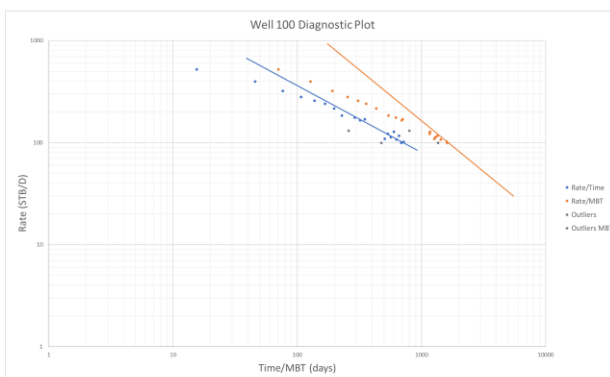
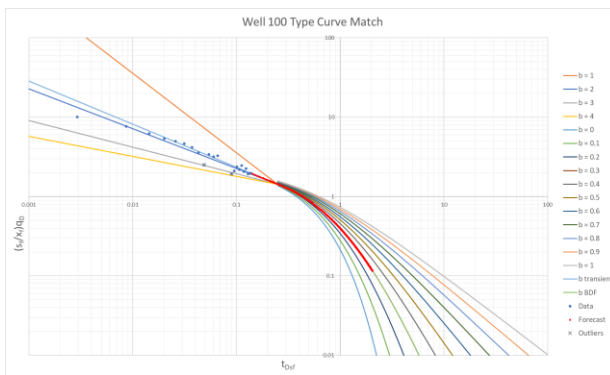
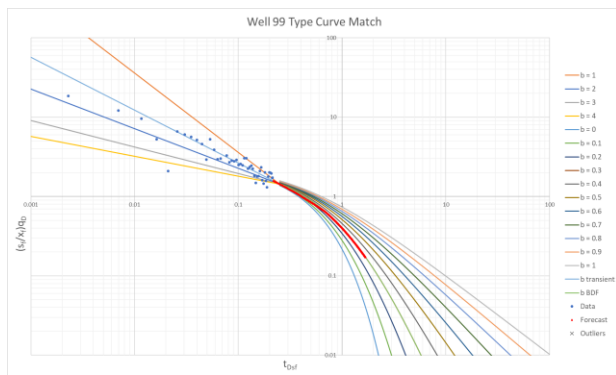


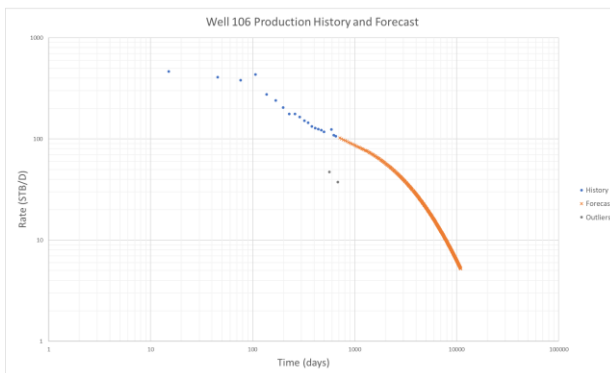
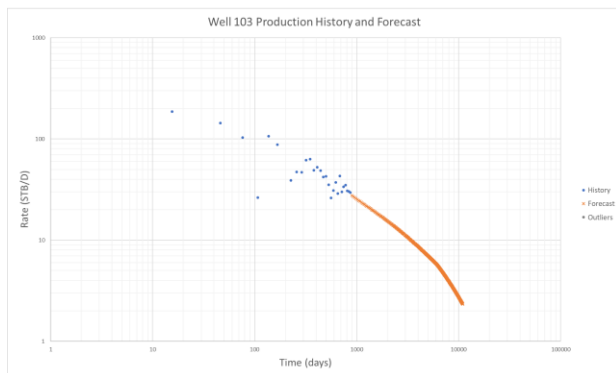
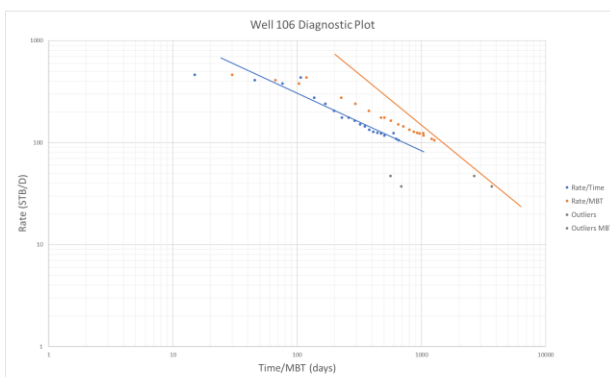
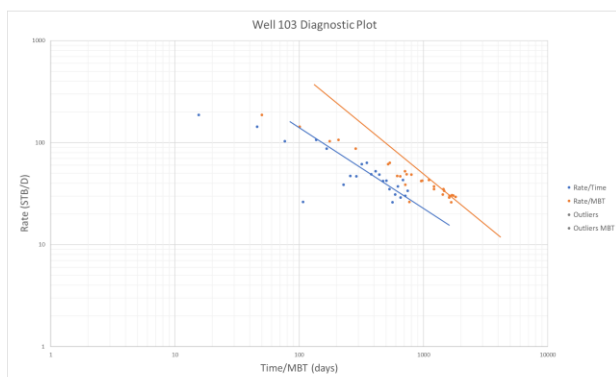
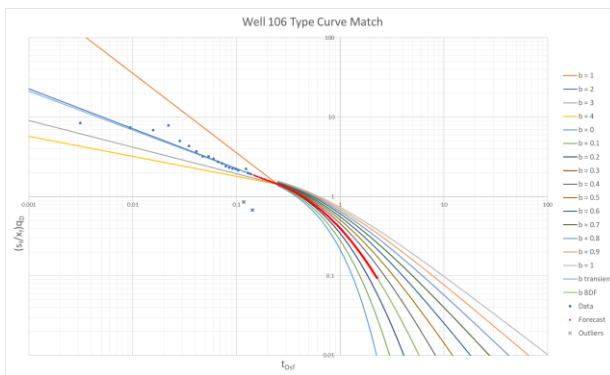
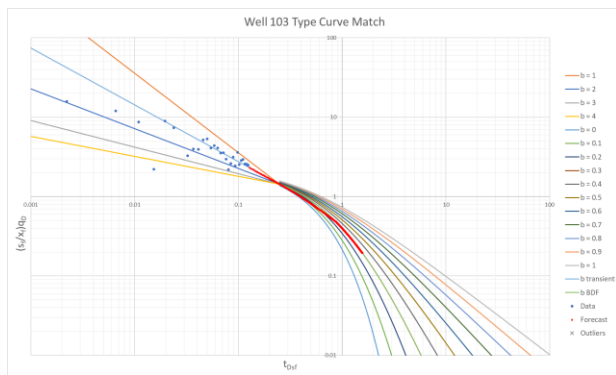


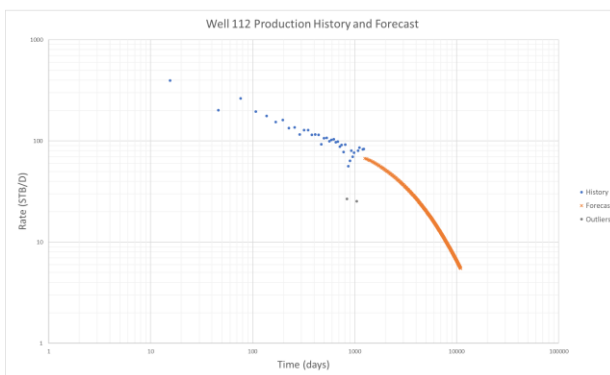
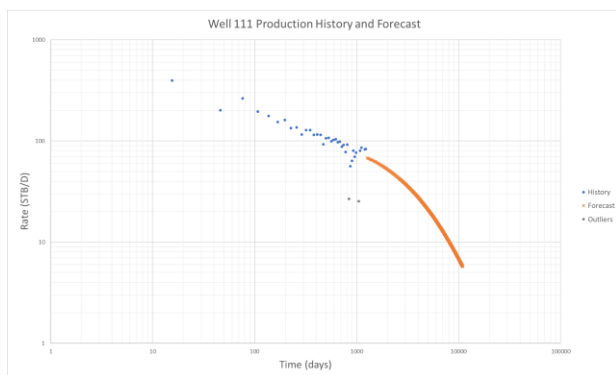
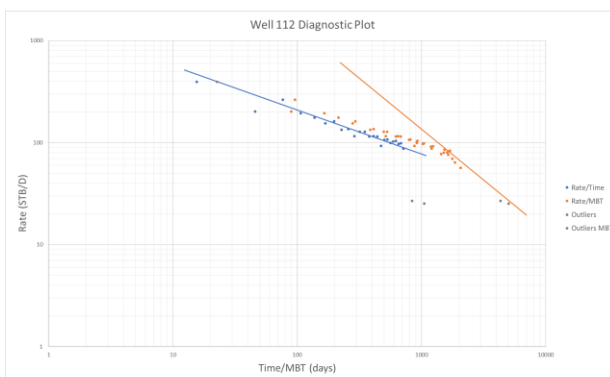
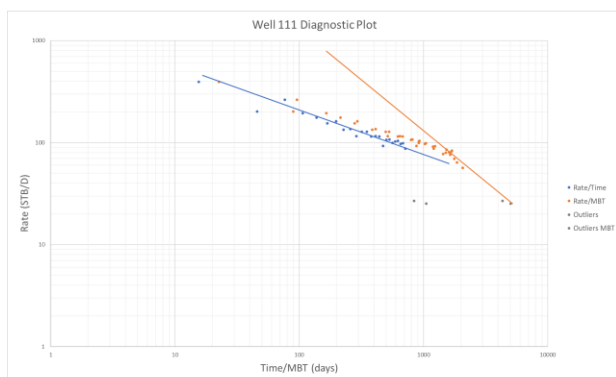
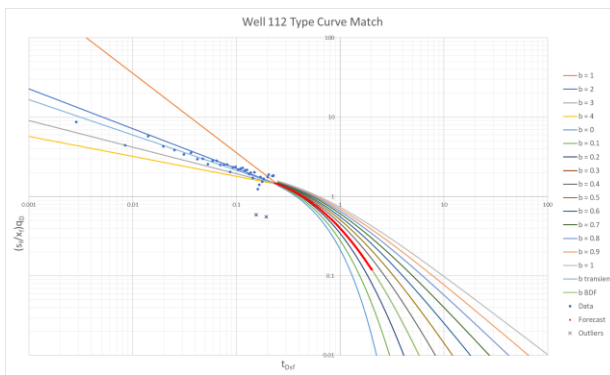
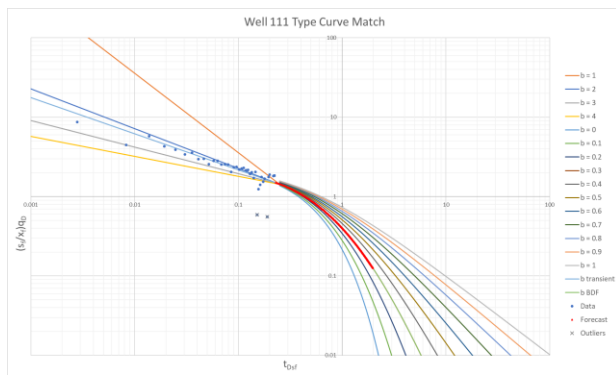


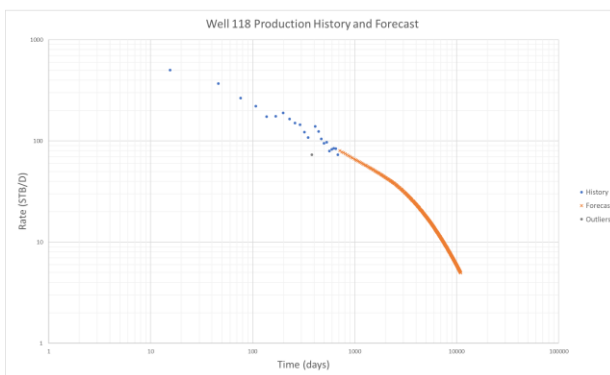
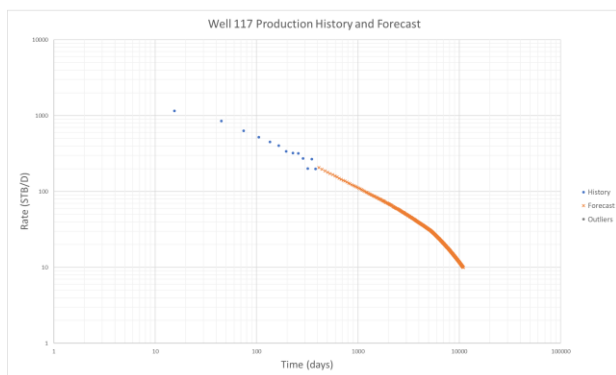
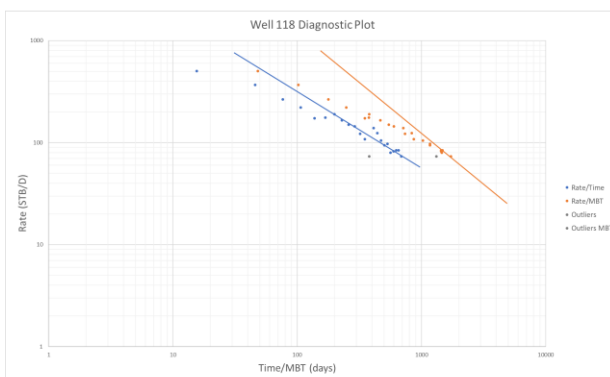
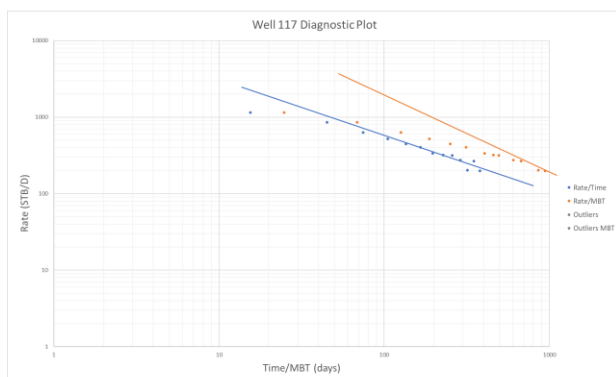
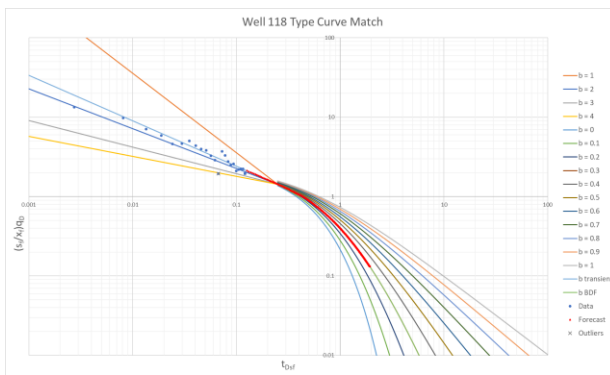
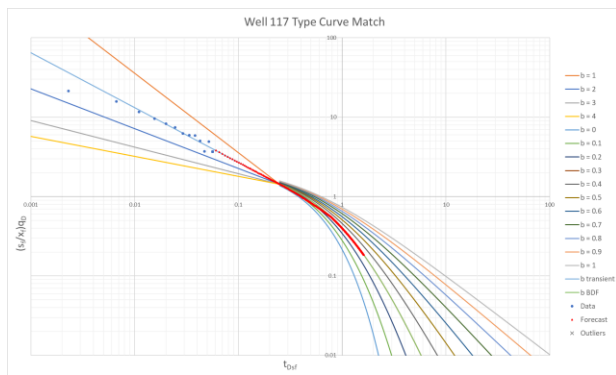


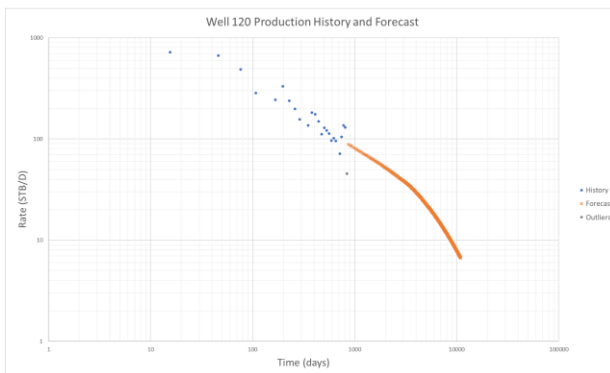
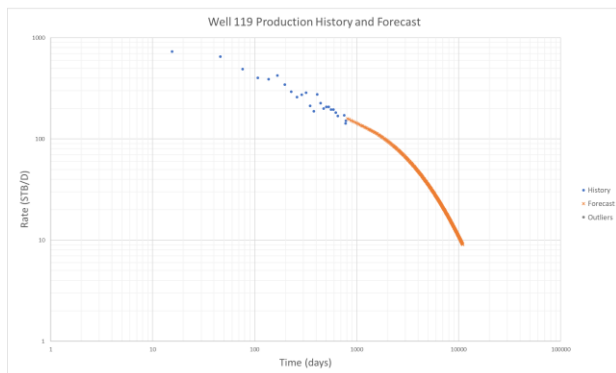
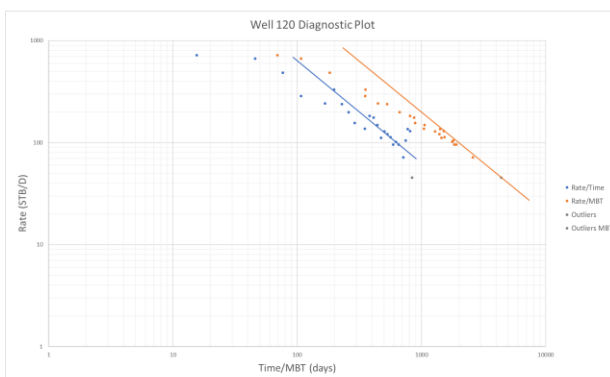
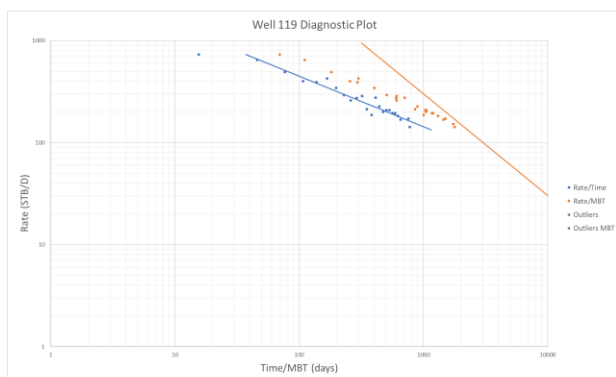
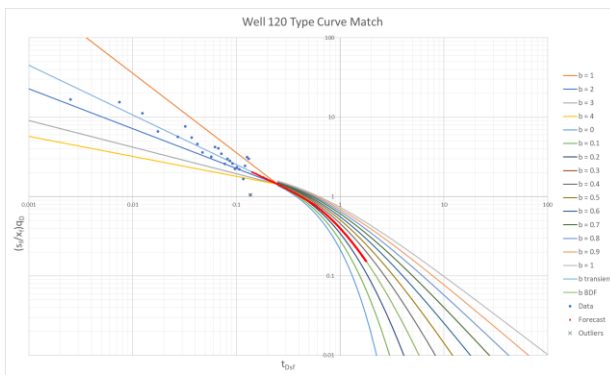
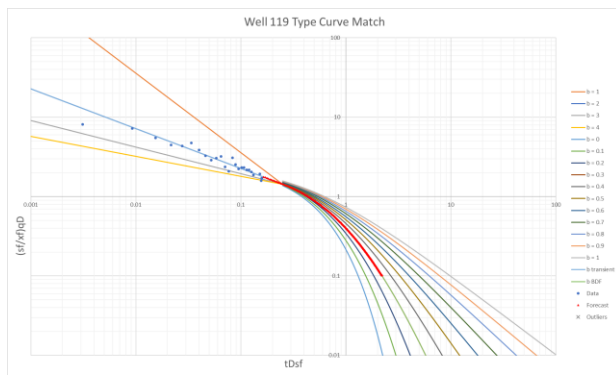


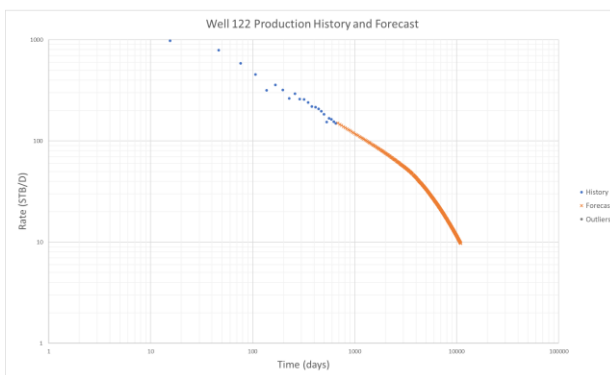
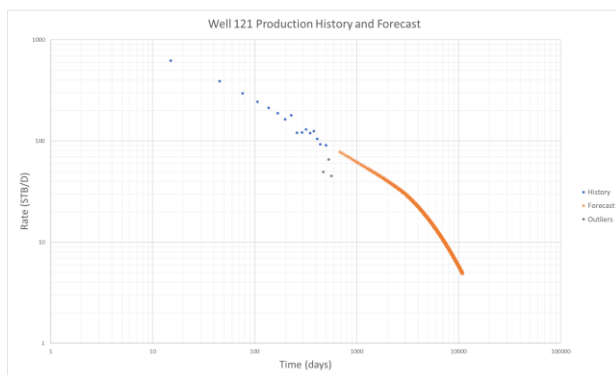
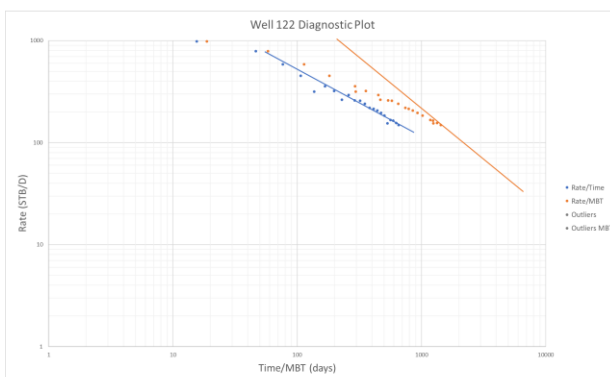
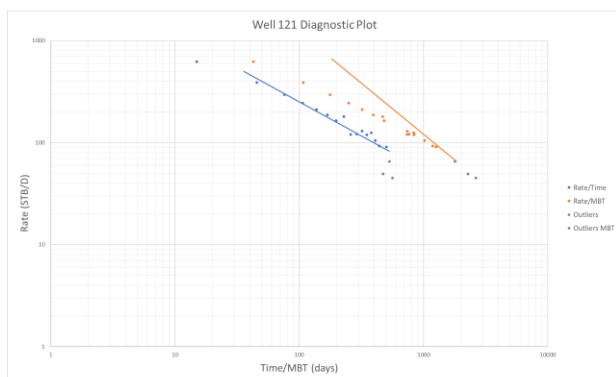
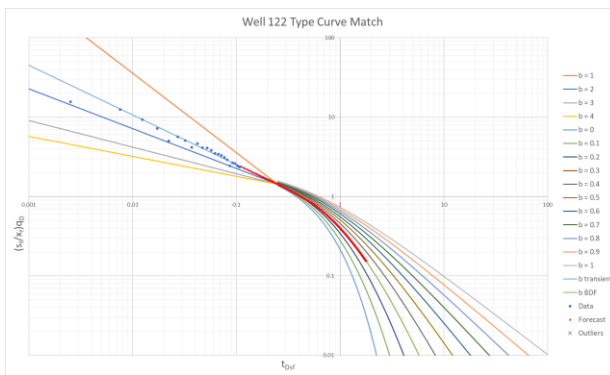
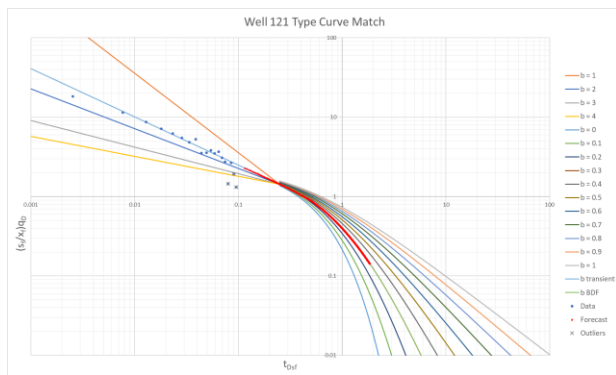


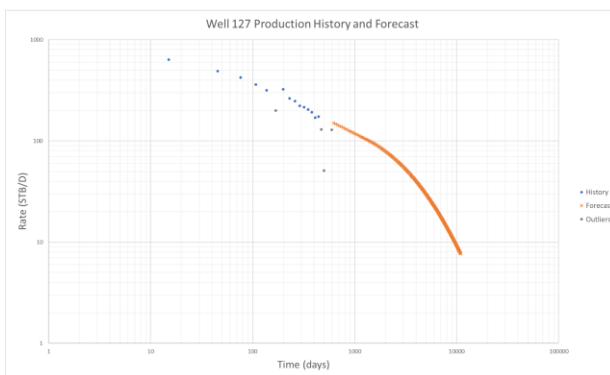
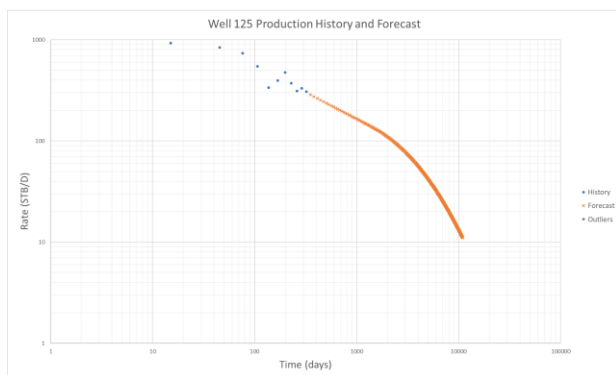
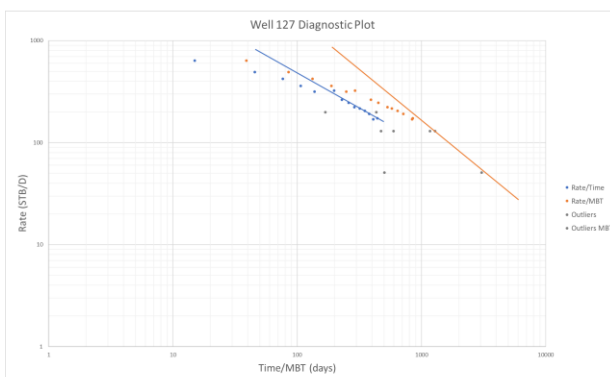
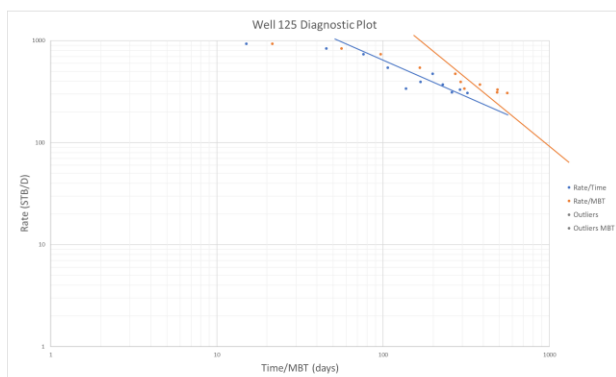
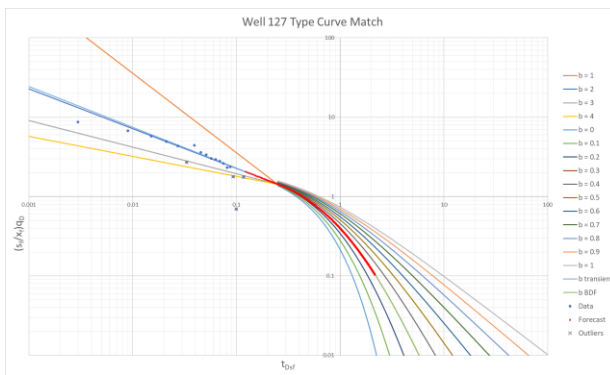
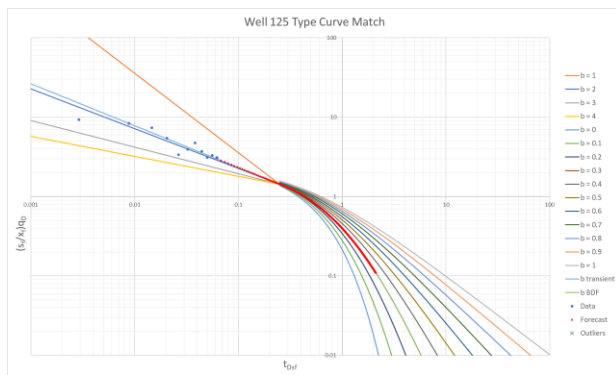


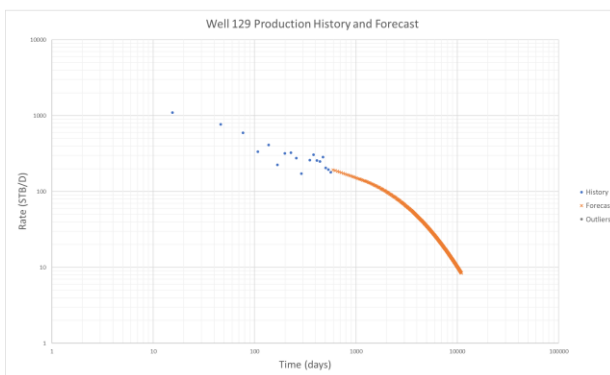
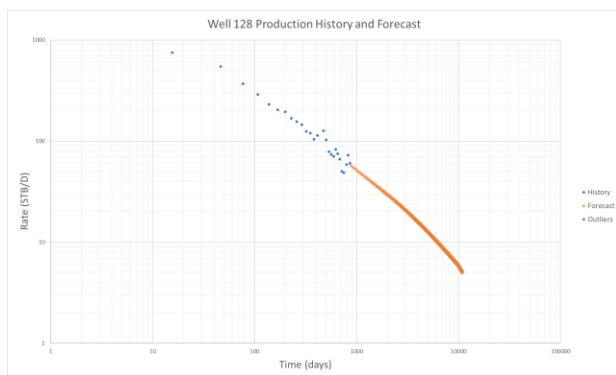
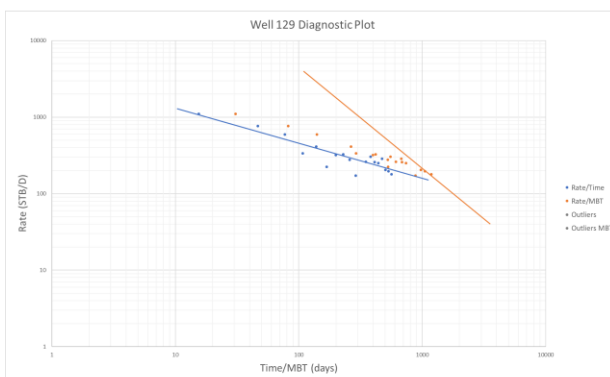
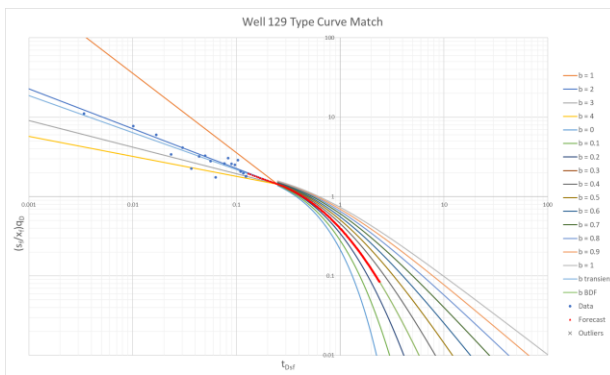
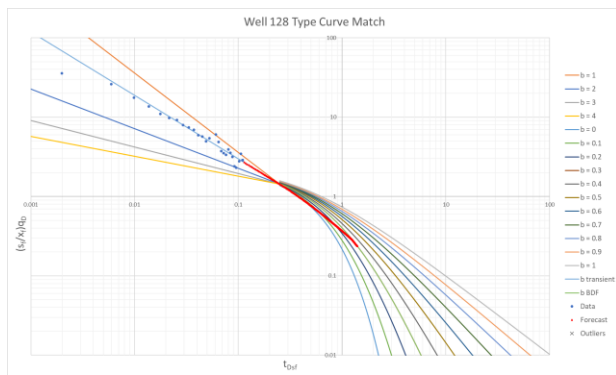


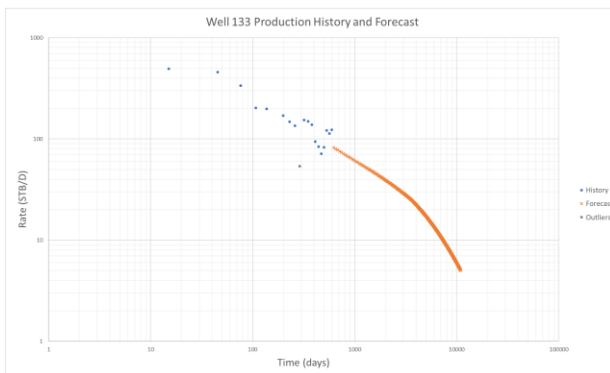
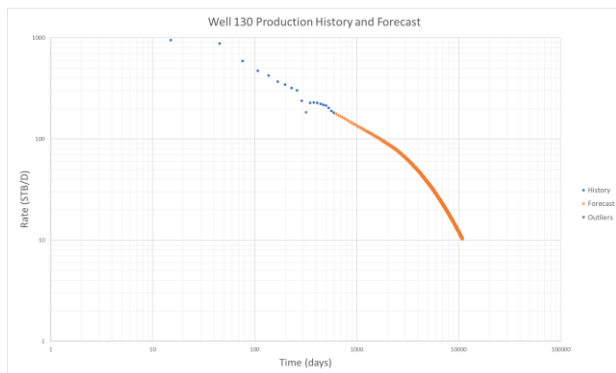
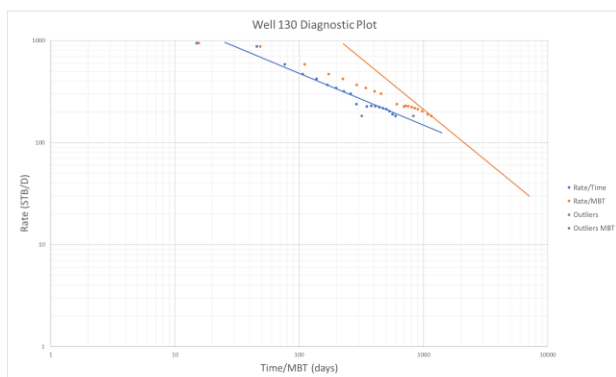
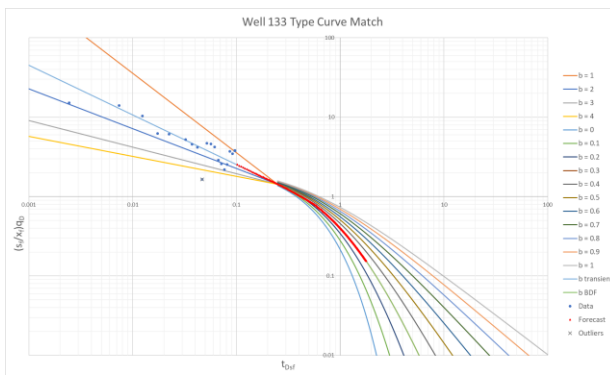
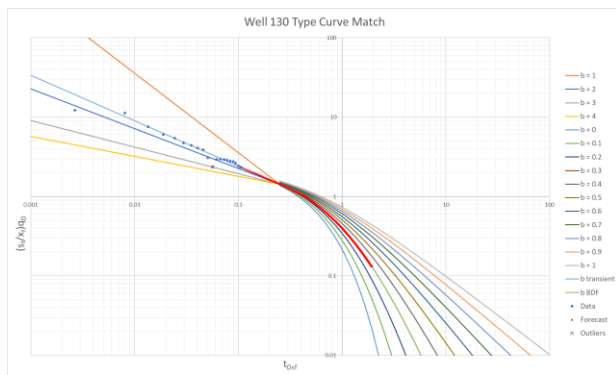










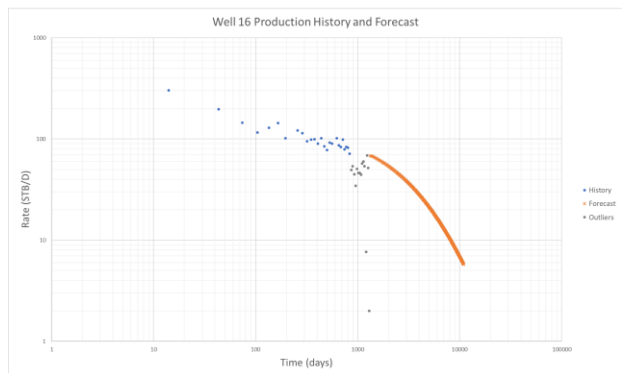
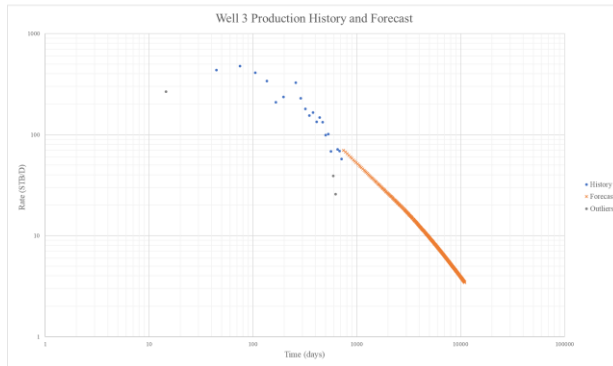
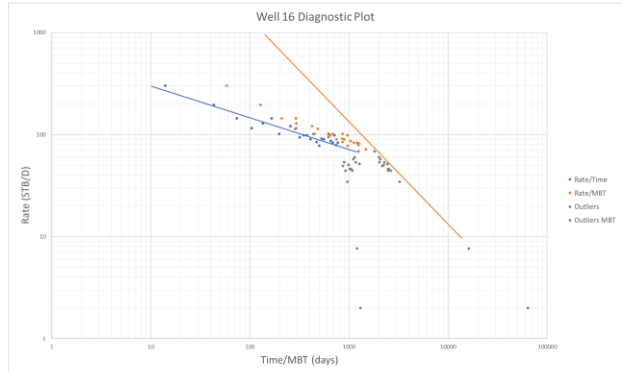
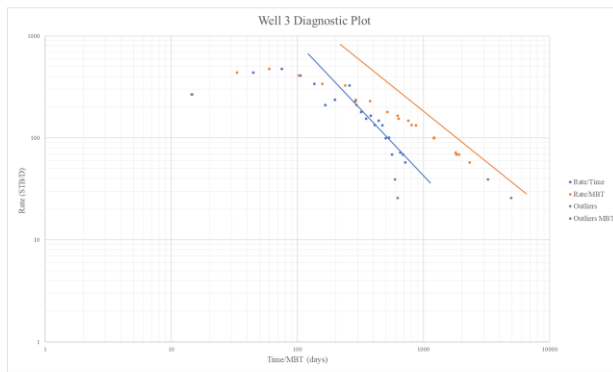
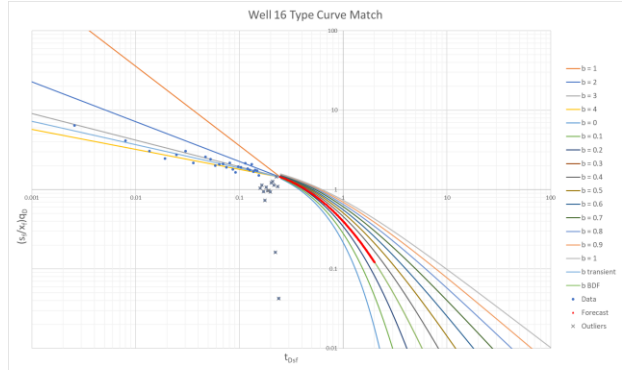
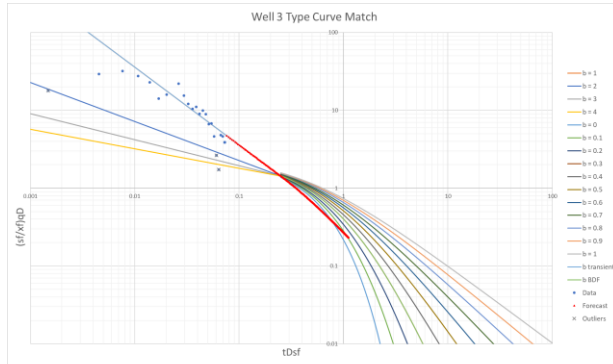


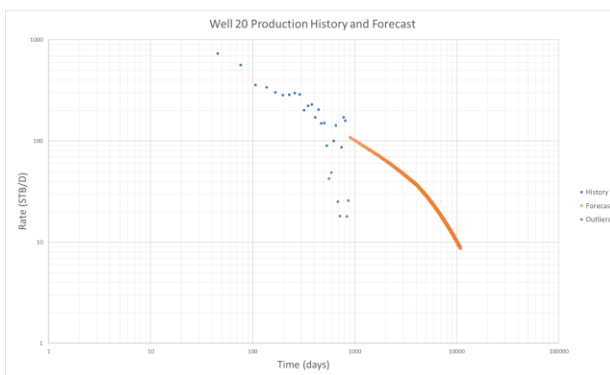
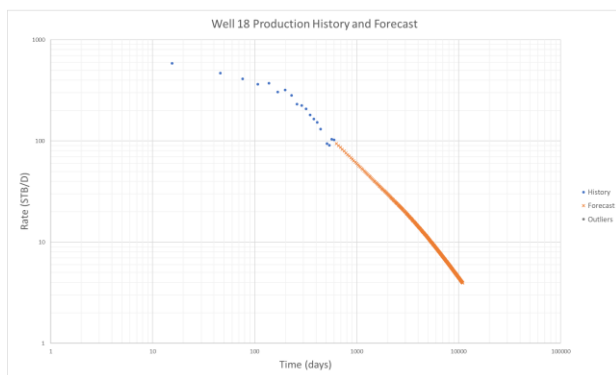
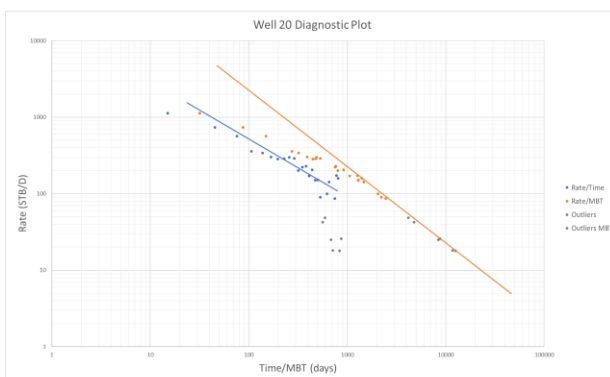
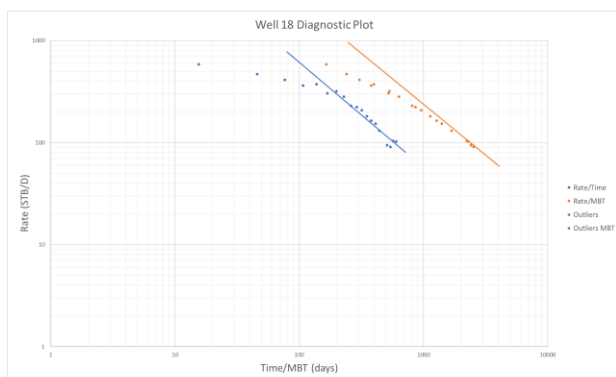
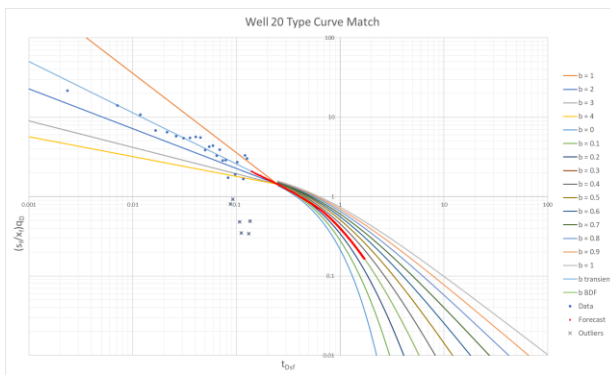
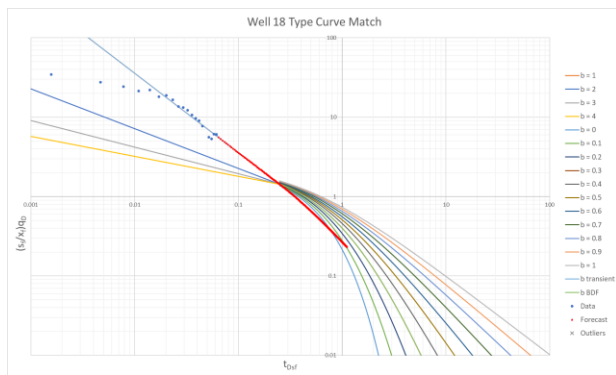
Well	6	7	13	14	19	21	22	29	32	35	36	41	42	45	46	51
μ , cP	0.65	0.60	0.65	0.64	0.64	0.55	0.64	0.55	0.70	0.60	0.65	0.63	0.55	0.70	0.60	0.50
B, RB/STB	1.35	1.34	1.35	1.35	1.35	1.36	1.36	1.35	1.35	1.35	1.35	1.35	1.35	1.35	1.35	1.35
ϕ	0.11	0.12	0.11	0.11	0.12	0.08	0.12	0.07	0.09	0.09	0.11	0.09	0.08	0.12	0.10	0.07
h, ft	200	200	200	200	200	200	200	200	100	200	200	175	200	200	200	150
c_t , psi ⁻¹	1.88E-05	1.85E-05	1.80E-05	1.70E-05	1.95E-05	1.50E-05	1.90E-05	1.50E-05	1.70E-05	1.40E-05	1.80E-05	1.80E-05	1.60E-05	1.20E-05	1.80E-05	1.15E-05
L_w , ft	8017	7080	7727	7125	9414	8002	10350	7274	7513	7189	7402	7762	6594	8107	7433	9996
s_f , ft	250	225	250	225	200	300	200	300	300	250	250	250	300	350	225	250
Δp , psi	2000	2000	2000	3250	1750	4100	1750	2250	2925	2800	1800	2925	2925	4000	1900	4000
D_{min} , year ⁻¹	0.15	0.15	0.15	0.15	0.15	0.15	0.15	0.15	0.15	0.15	0.15	0.15	0.15	0.15	0.15	0.12
History, days	381	625	625	686	778	930	375	747	1234	647	626	1081	1022	381	928	1082
b_{TR}	1.35	1.75	1.80	1.75	1.25	2.00	2.00	1.25	2.00	1.75	1.60	1.45	1.30	1.35	1.95	2.60
b_{BDF}	0.30	0.30	0.30	0.30	0.30	0.30	0.30	0.30	0.30	0.30	0.30	0.30	0.30	0.30	0.30	0.30
$t_{transition}$, years	5.0	3.9	3.7	3.9	5.4	3.4	3.4	5.4	3.5	3.9	4.2	4.6	5.1	5.0	3.5	3.2
t_{BDF} , years	19.4	6.6	5.6	6.6	27.2	4.0	4.0	27.2	4.3	6.2	9.6	14.4	22.5	19.4	4.0	3.4
TMP	1.38E-04	1.77E-04	1.84E-04	1.77E-04	1.27E-04	2.03E-04	2.04E-04	1.27E-04	1.98E-04	1.78E-04	1.62E-04	1.48E-04	1.33E-04	1.38E-04	1.98E-04	2.13E-04
RMP	2.82E-02	1.57E-02	1.91E-02	1.09E-02	2.23E-02	1.19E-02	1.18E-02	3.89E-02	3.47E-02	2.25E-02	2.43E-02	3.03E-02	2.90E-02	2.66E-02	2.32E-02	2.63E-02
k, mD	4.57E-04	4.51E-04	5.86E-04	4.22E-04	3.01E-04	4.75E-04	4.66E-04	2.61E-04	7.53E-04	3.31E-04	5.16E-04	3.73E-04	3.34E-04	6.68E-04	4.28E-04	2.11E-04
x_f , ft	187.8	286.3	224.9	290.4	221.8	255.5	245.1	284.6	209.9	238.7	232.8	167.5	253.4	141.4	206.9	178.7
t'	1.09	1.33	1.40	1.24	1.12	0.79	1.73	0.43	1.25	0.79	1.23	0.89	0.55	0.81	1.26	0.50
q'	1.35	0.82	0.91	0.53	1.08	0.67	0.57	2.19	1.54	1.16	1.16	1.49	1.63	1.18	1.20	1.64
EUR, MSTB	446.9	554.8	466.4	819.8	591.2	655.8	664.5	369.0	226.0	392.2	397.9	374.1	412.8	477.1	333.1	259.1
Scaled EUR, MSTB	644.8	572.2	558.0	517.2	697.4	355.5	595.0	387.3	416.9	372.5	543.7	506.1	407.5	475.0	483.8	227.4

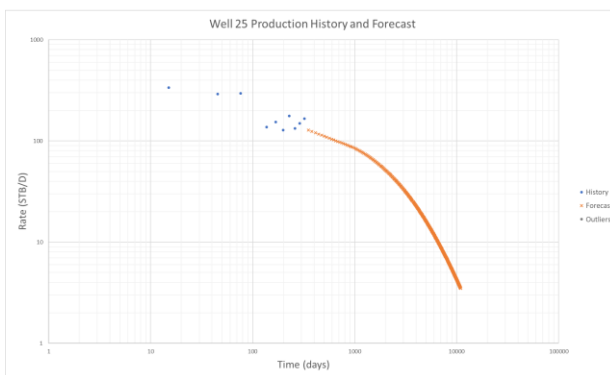
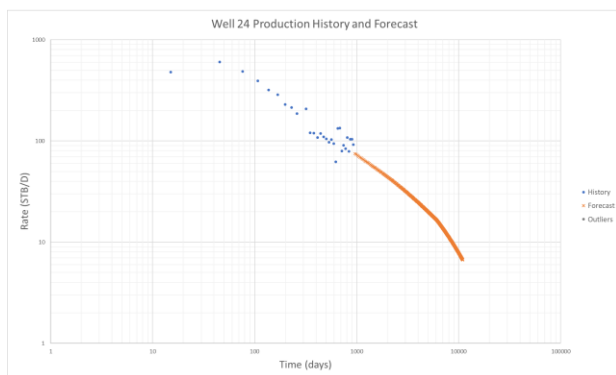
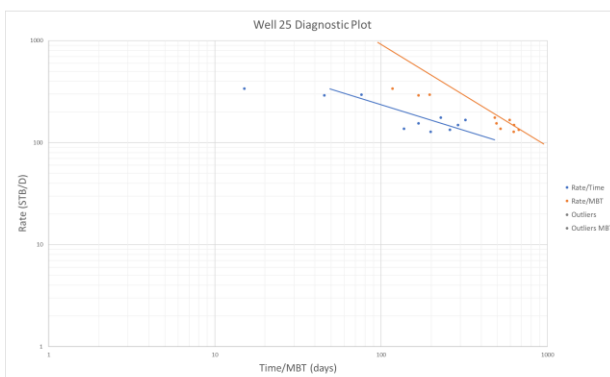
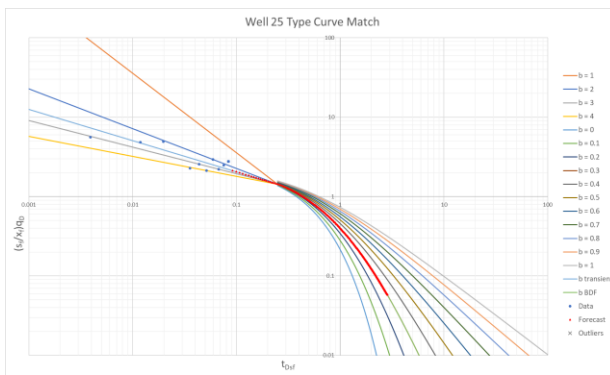
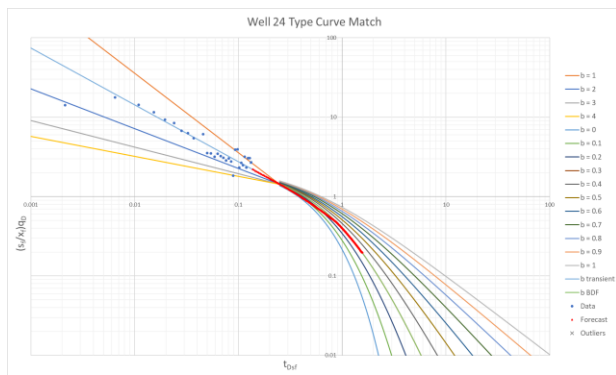
Well	53	59	60	68	70	77	78	83	84	88	89	93	99	100	103	106
μ , cP	0.63	0.67	0.55	0.64	0.68	0.65	0.69	0.66	0.55	0.65	0.64	0.65	0.50	0.55	0.69	0.60
B, RB/STB	1.35	1.35	1.35	1.35	1.35	1.35	1.35	1.35	1.35	1.35	1.34	1.35	1.35	1.35	1.35	1.35
φ	0.11	0.10	0.09	0.12	0.07	0.11	0.09	0.09	0.09	0.11	0.12	0.08	0.11	0.10	0.12	0.09
h, ft	200	175	200	200	150	200	150	200	200	200	200	200	175	200	100	200
c_t , psi ⁻¹	1.90E-05	1.65E-05	1.60E-05	1.95E-05	1.15E-05	1.90E-05	1.20E-05	1.60E-05	1.55E-05	1.85E-05	1.95E-05	1.55E-05	1.90E-05	1.40E-05	1.95E-05	1.75E-05
L_w , ft	6818	9143	6822	7074	6807	9700	7898	7935	7055	9538	7674	7627	7820	9834	6965	7710
s_f , ft	225	250	200	300	275	225	300	225	300	250	300	275	300	300	275	275
Δp , psi	2000	2750	2500	1800	4000	2250	4000	3250	3000	2500	2750	2925	2000	2925	1800	2300
D_{min} , year ⁻¹	0.15	0.15	0.15	0.15	0.15	0.15	0.15	0.15	0.15	0.15	0.15	0.15	0.15	0.15	0.15	0.15
History, days	595	732	1112	755	1326	808	961	838	754	575	534	472	1387	720	868	686
b_{TR}	1.35	2.00	1.80	1.70	1.80	1.45	1.85	2.00	1.80	1.80	1.50	1.70	1.50	1.85	1.40	2.05
b_{BDF}	0.30	0.30	0.30	0.30	0.30	0.30	0.30	0.30	0.30	0.30	0.30	0.30	0.30	0.30	0.30	0.30
$t_{transition}$, years	5.0	3.3	3.7	4.0	3.7	4.6	3.6	3.4	3.7	3.7	4.5	4.0	4.5	3.6	4.8	3.3
t_{BDF} , years	18.9	3.9	5.6	7.5	5.6	14.4	5.1	4.0	5.7	5.9	12.3	7.3	12.3	5.1	16.7	3.5
TMP	1.38E-04	2.05E-04	1.85E-04	1.72E-04	1.84E-04	1.48E-04	1.89E-04	2.03E-04	1.83E-04	1.83E-04	1.53E-04	1.73E-04	1.53E-04	1.88E-04	1.43E-04	2.08E-04
RMP	3.47E-02	1.12E-02	2.29E-02	1.93E-02	3.24E-02	1.26E-02	2.79E-02	1.30E-02	1.99E-02	9.49E-03	9.19E-03	2.19E-02	3.05E-02	1.93E-02	8.40E-02	1.81E-02
k, mD	3.63E-04	5.60E-04	2.18E-04	9.07E-04	3.01E-04	3.83E-04	4.99E-04	3.85E-04	5.00E-04	5.98E-04	8.10E-04	4.16E-04	5.68E-04	5.15E-04	6.89E-04	5.86E-04
x_f , ft	177.4	291.2	246.9	244.5	246.4	298.8	180.0	248.2	224.3	287.3	343.9	230.6	180.7	165.7	137.6	230.4
t'	1.07	1.33	0.81	1.50	0.59	1.13	0.83	1.13	0.83	1.42	1.34	0.82	0.94	0.85	1.36	1.15
q'	1.71	0.52	1.29	0.94	1.48	0.60	1.25	0.61	1.12	0.45	0.45	1.05	1.90	1.09	3.77	0.94
EUR, MSTB	363.4	692.2	383.6	485.2	249.9	842.1	289.1	599.7	442.1	908.3	1193.1	416.6	351.3	440.6	132.5	407.9
Scaled EUR, MSTB	654.8	455.0	413.5	634.1	233.3	556.3	307.3	405.8	229.4	547.3	684.4	368.0	633.7	417.1	633.3	430.9

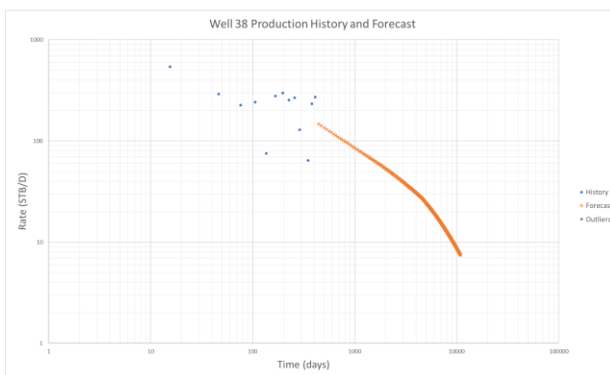
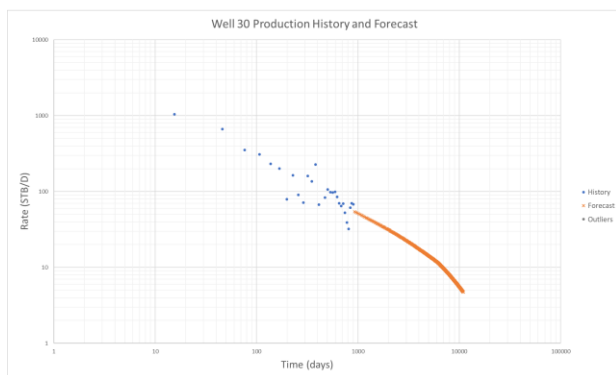
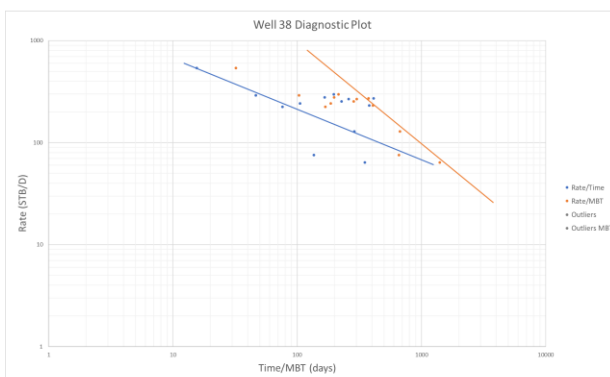
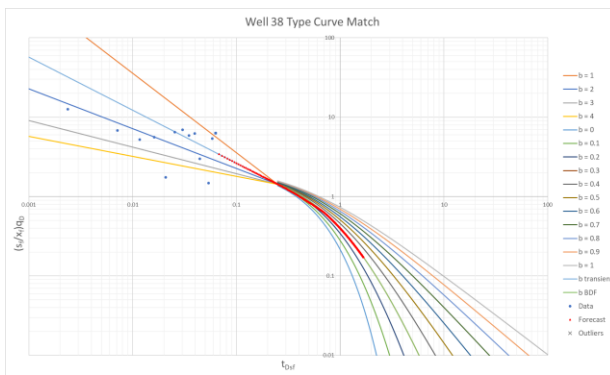
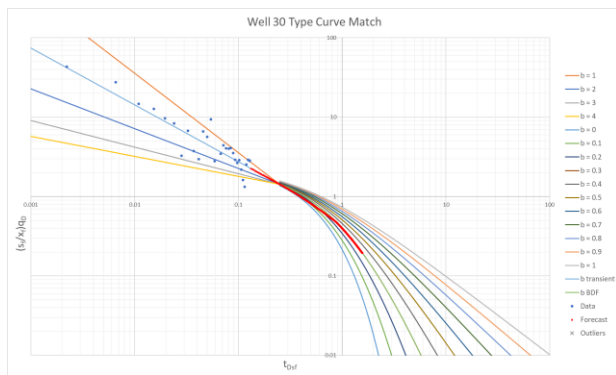
Well	111	112	117	118	119	120	121	122	125	127	128	129	130	133
μ , cP	0.62	0.55	0.58	0.58	0.60	0.65	0.60	0.64	0.65	0.64	0.63	0.60	0.58	0.59
B, RB/STB	1.35	1.35	1.34	1.35	1.34	1.35	1.35	1.34	1.35	1.35	1.35	1.35	1.35	1.35
ϕ	0.11	0.09	0.09	0.07	0.12	0.11	0.11	0.12	0.11	0.11	0.11	0.12	0.08	0.07
h , ft	200	200	200	200	200	200	175	200	200	200	150	200	200	200
c_i , psi ⁻¹	1.80E-05	1.65E-05	1.75E-05	1.55E-05	1.92E-05	1.85E-05	1.78E-05	1.92E-05	1.80E-05	1.90E-05	1.90E-05	1.90E-05	1.65E-05	1.50E-05
L_w , ft	7046	7046	8001	7328	8056	7962	7736	7263	7468	7855	6996	7634	9676	7954
s_F , ft	225	300	225	300	200	250	225	200	250	250	250	250	300	275
Δp , psi	2000	2400	2750	2750	2000	2100	2200	2100	2925	2000	2000	2925	2925	2925
D_{min} , year ⁻¹	0.12	0.12	0.15	0.15	0.15	0.15	0.15	0.15	0.15	0.15	0.15	0.15	0.15	0.15
History, days	1234	1233	381	687	785	839	656	655	321	595	858	565	595	595
b_{TR}	2.20	2.25	1.45	1.75	2.00	1.60	1.65	1.60	1.90	1.95	1.25	2.15	1.75	1.60
b_{BDF}	0.30	0.30	0.30	0.30	0.30	0.30	0.30	0.30	0.30	0.30	0.30	0.30	0.30	0.30
$t_{transition}$, years	3.8	3.7	4.6	3.9	3.4	4.2	4.0	4.2	3.5	3.5	5.3	3.1	3.9	4.2
t_{BDF} , years	4.1	4.0	14.4	6.7	4.1	9.6	8.1	9.5	4.7	4.0	26.8	3.5	6.6	9.5
TMP	1.80E-04	1.85E-04	1.48E-04	1.76E-04	2.01E-04	1.62E-04	1.69E-04	1.63E-04	1.93E-04	1.98E-04	1.28E-04	2.19E-04	1.77E-04	1.63E-04
RMP	2.20E-02	2.20E-02	1.84E-02	2.65E-02	1.12E-02	2.32E-02	2.93E-02	1.59E-02	9.98E-03	1.36E-02	4.76E-02	1.01E-02	1.29E-02	3.07E-02
k , mD	4.43E-04	5.06E-04	2.53E-04	3.95E-04	4.40E-04	5.31E-04	3.97E-04	3.60E-04	6.13E-04	6.53E-04	4.16E-04	7.39E-04	4.76E-04	3.01E-04
x_F , ft	218.4	251.6	268.5	236.6	287.3	189.0	167.2	275.8	290.6	271.3	181.2	216.2	284.9	198.7
t'	1.30	0.84	0.74	0.65	1.64	1.26	1.17	1.34	1.46	1.56	0.99	1.76	0.79	0.59
q'	1.10	1.24	1.00	1.42	0.58	1.10	1.52	0.78	0.48	0.67	2.34	0.52	0.69	1.61
EUR, MSTB	355.4	349.6	614.5	345.5	700.6	457.1	329.2	614.3	790.2	558.6	293.9	692.7	678.2	334.6
Scaled EUR, MSTB	482.8	372.7	480.3	337.1	608.9	612.0	567.5	607.5	511.1	530.9	683.2	569.5	384.1	340.7

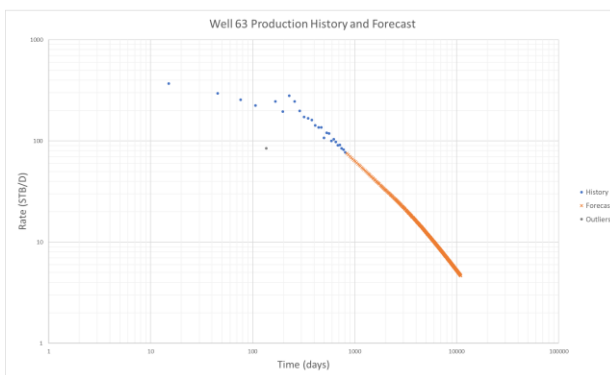
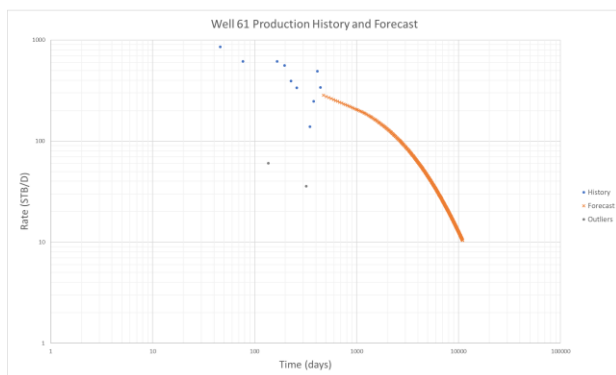
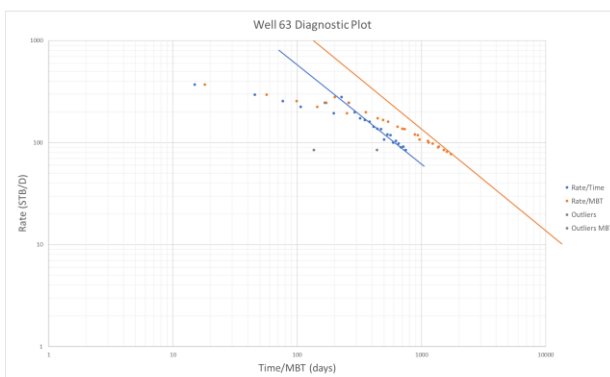
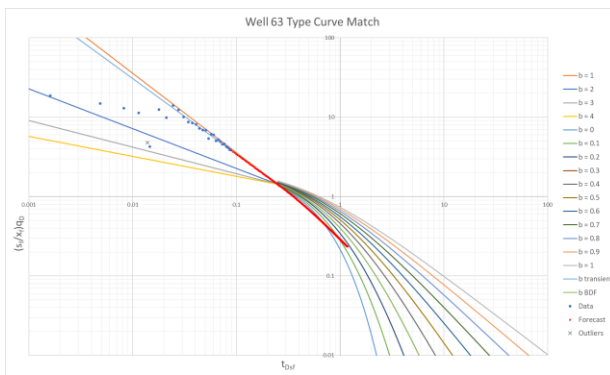
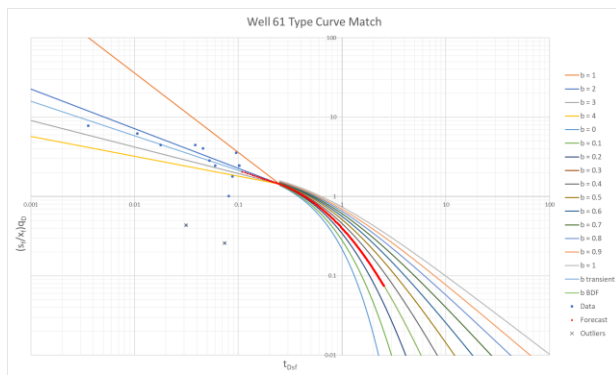
“Bad” Well Set Plots and Results

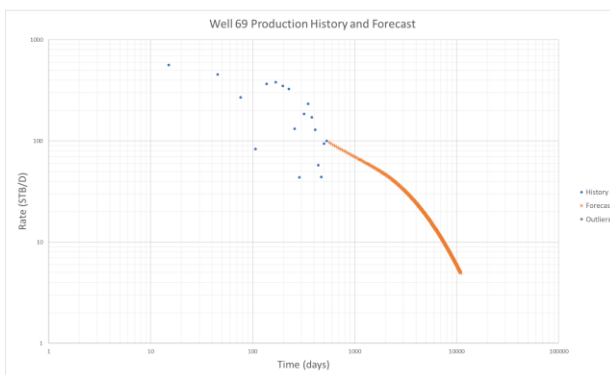
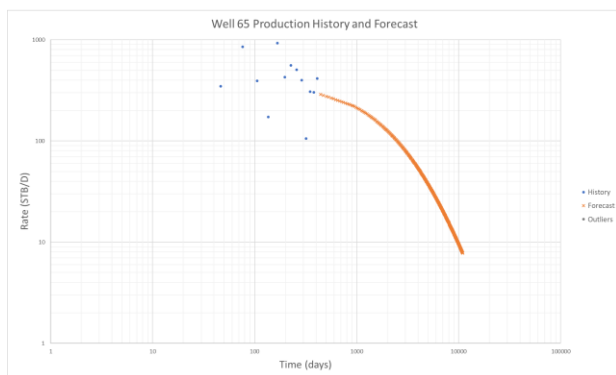
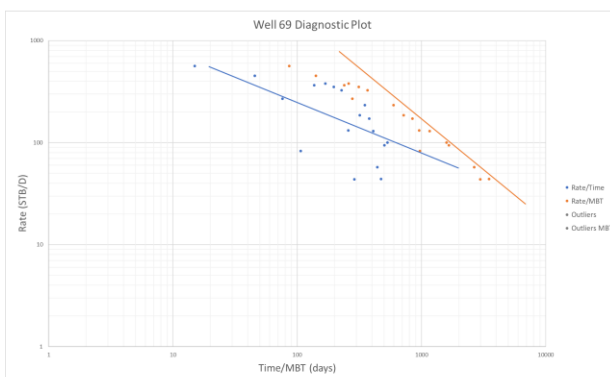
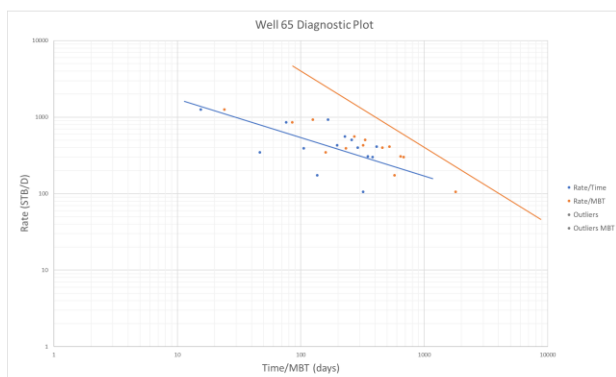
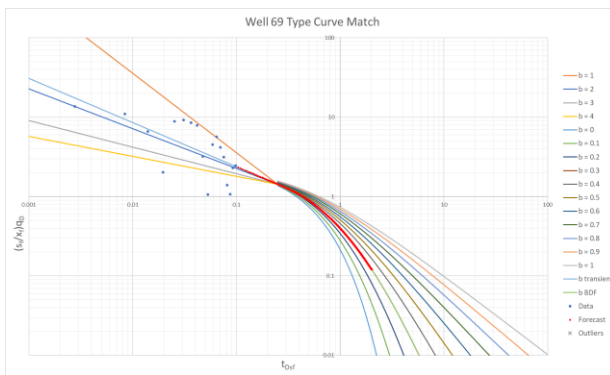
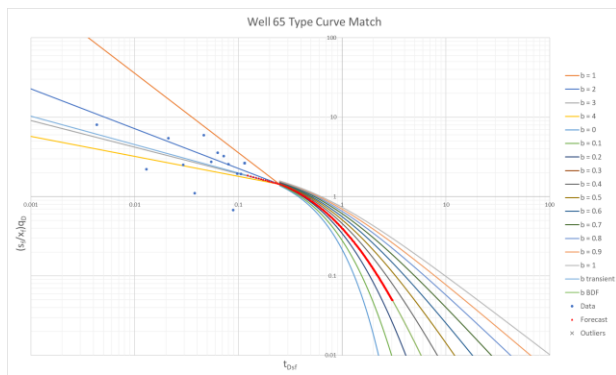


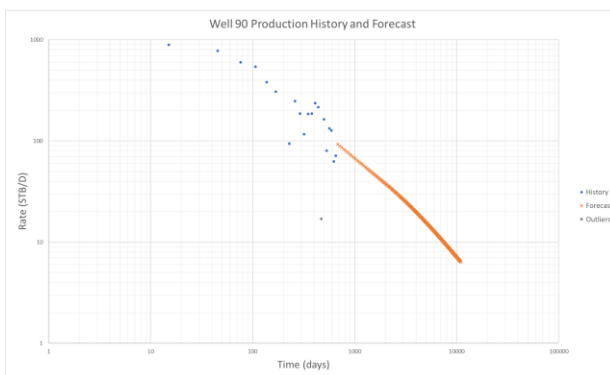
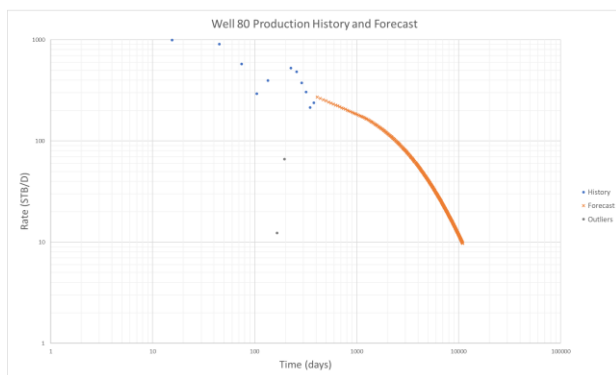
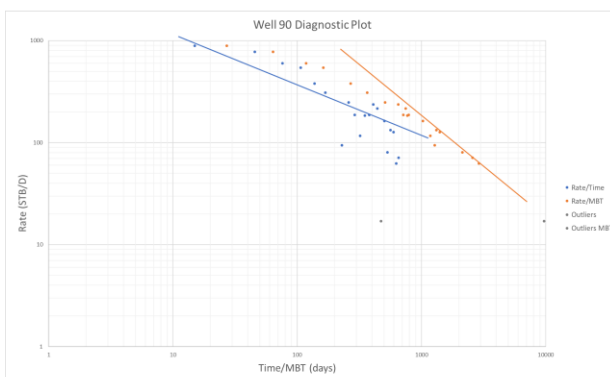
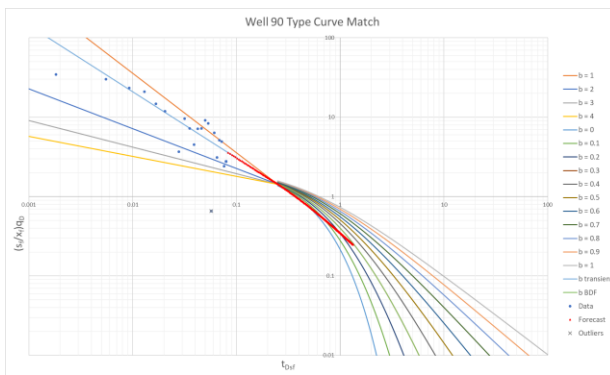
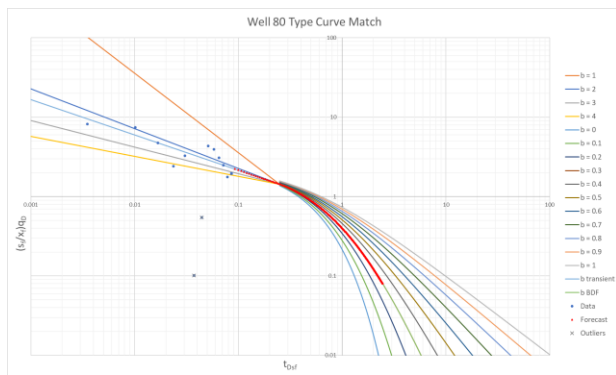


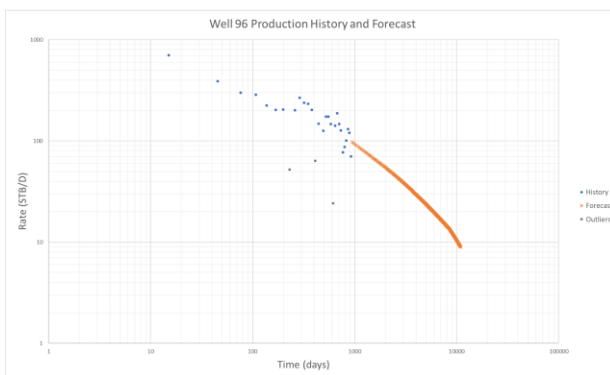
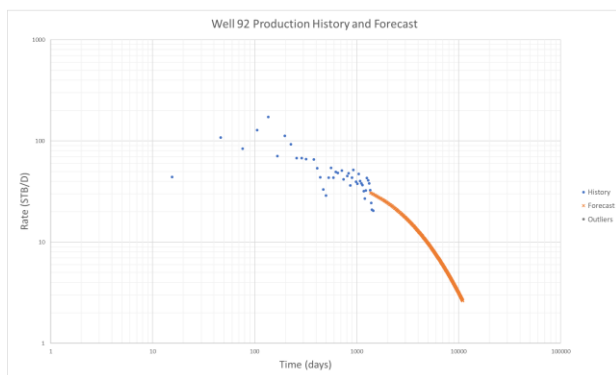
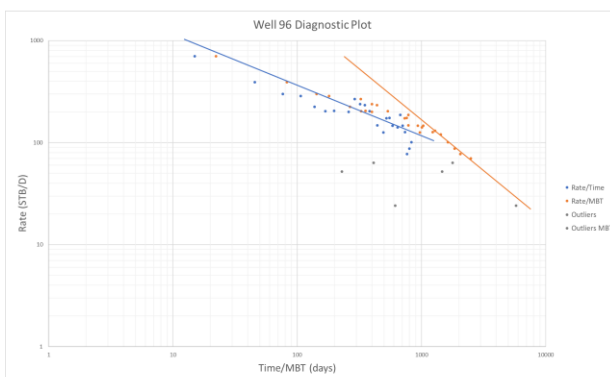
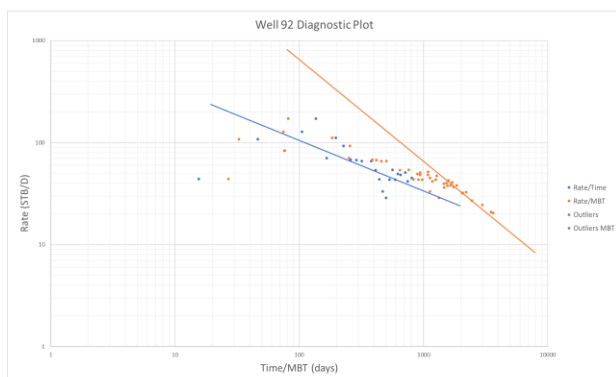
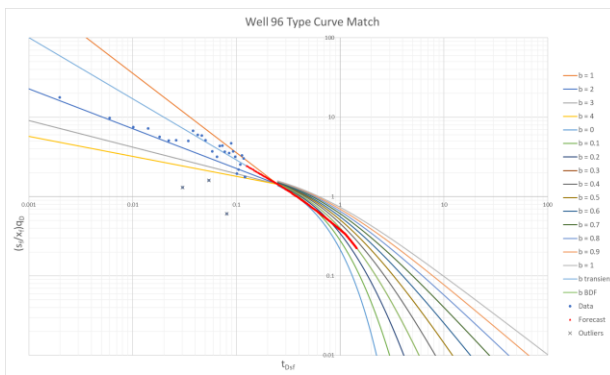
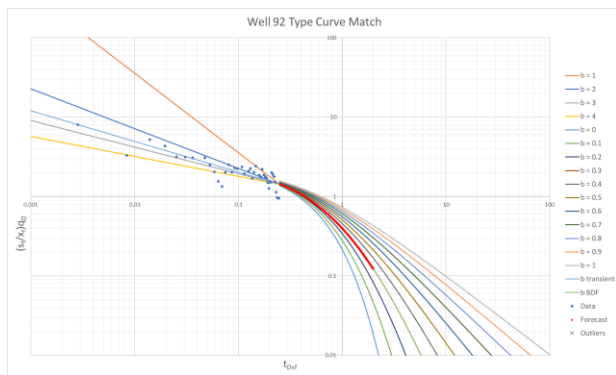


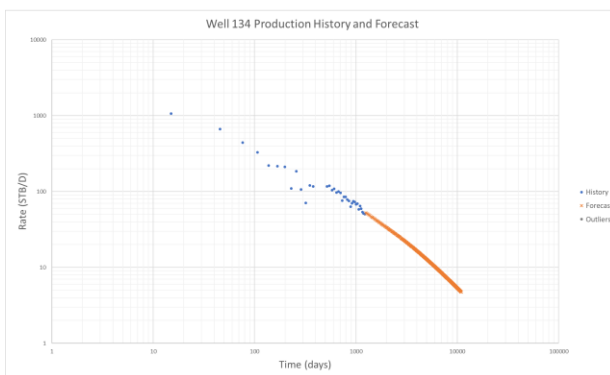
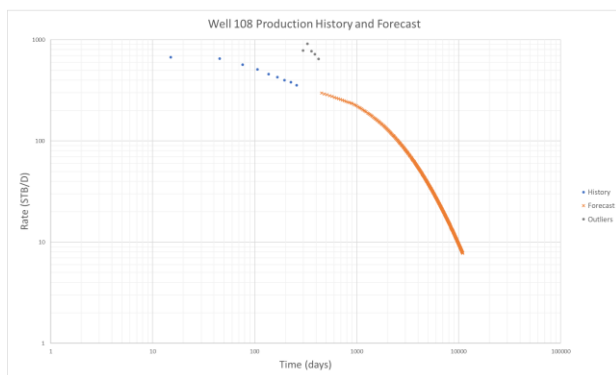
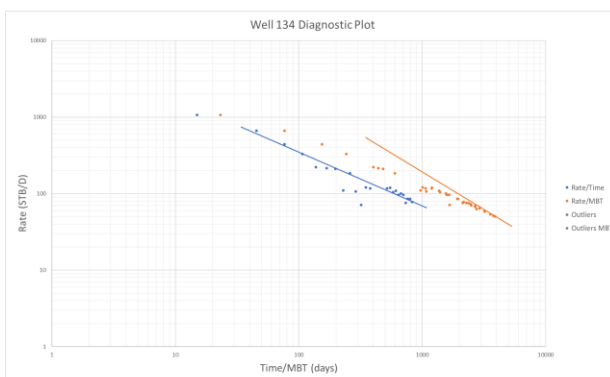
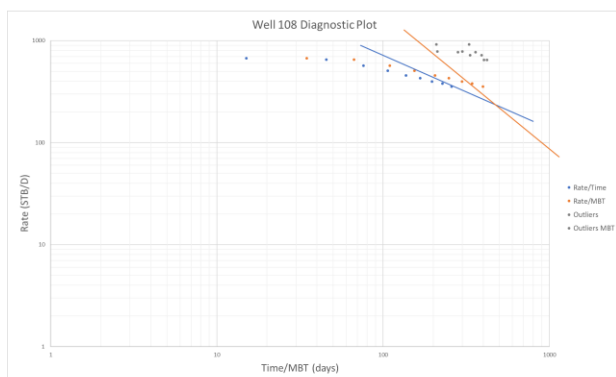
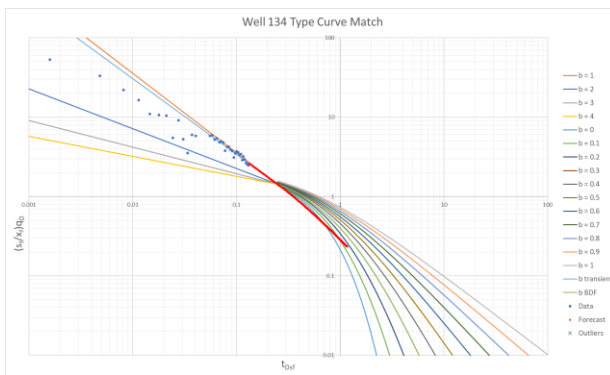
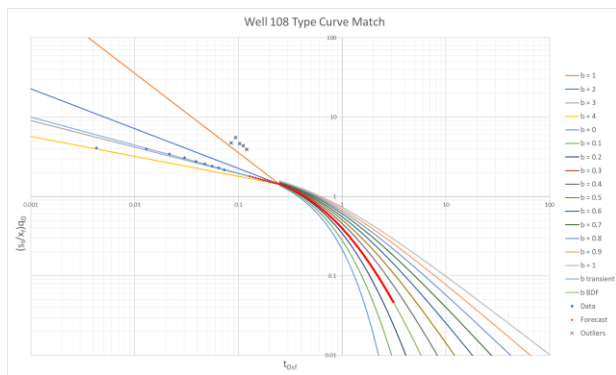


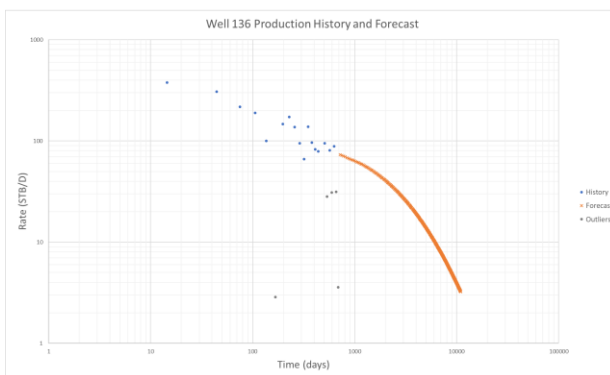
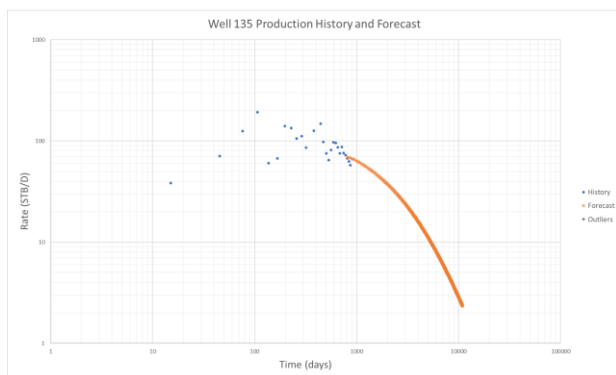
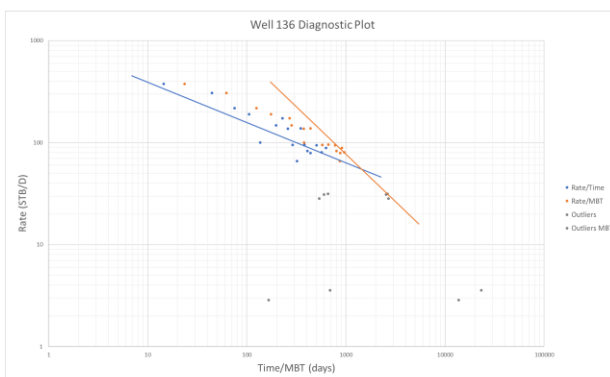
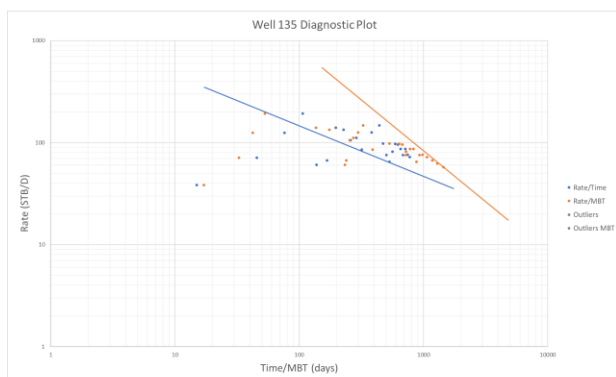
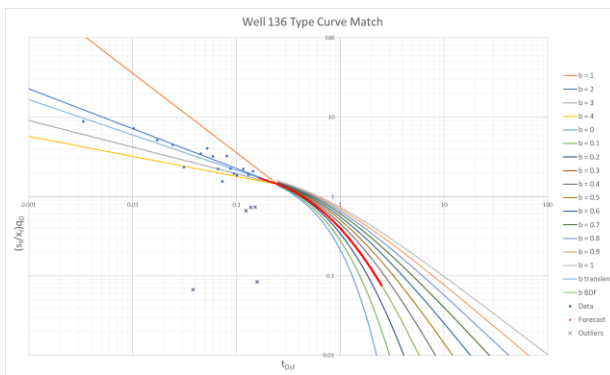
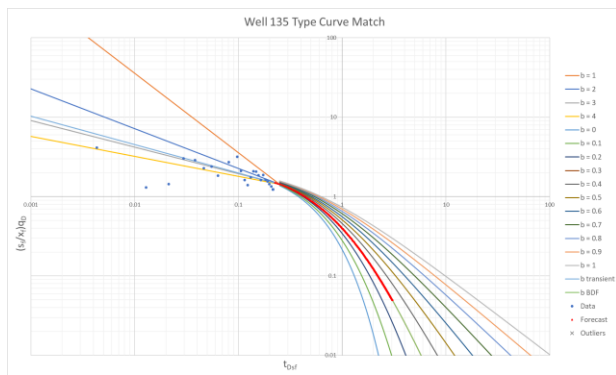


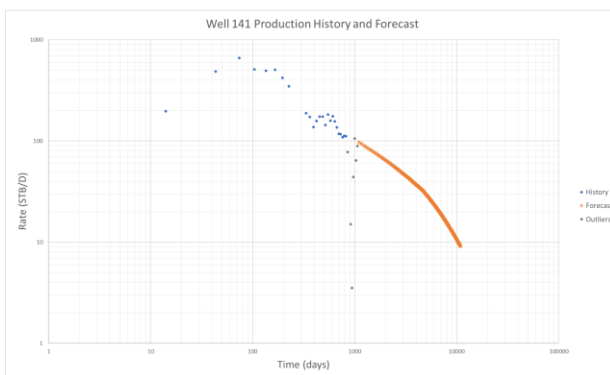
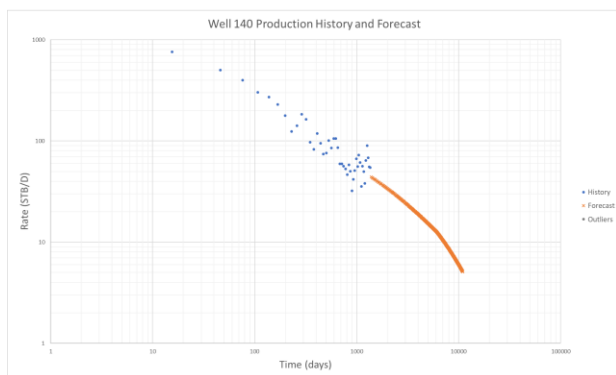
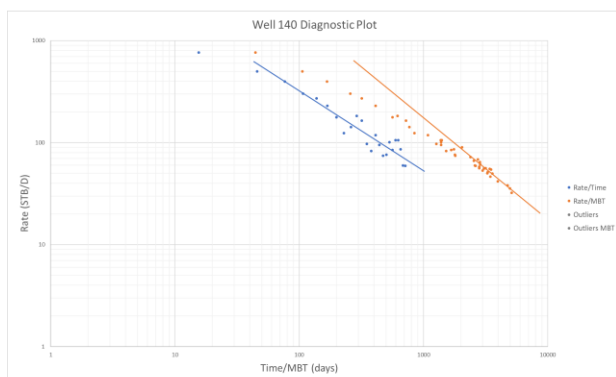
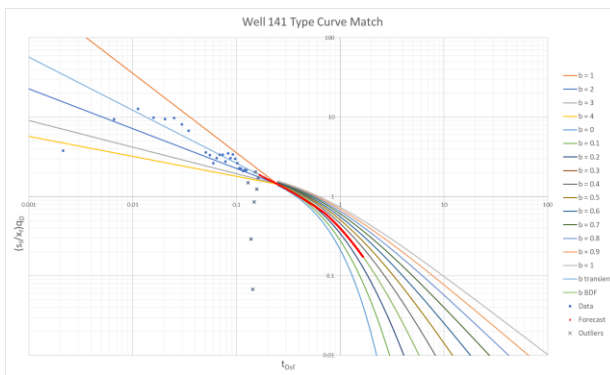
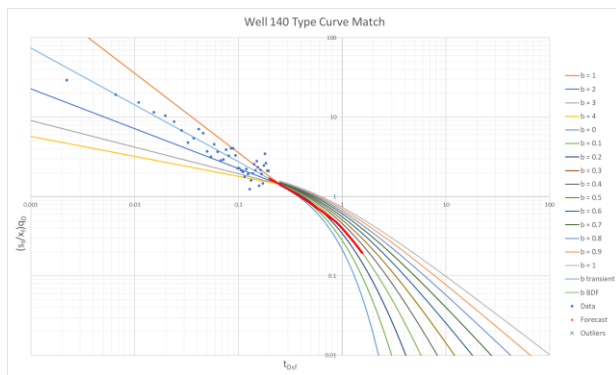






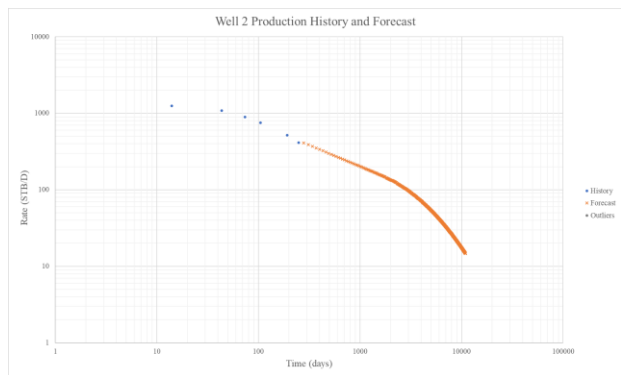
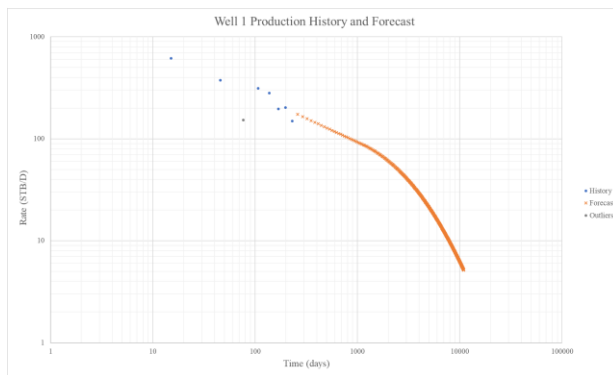
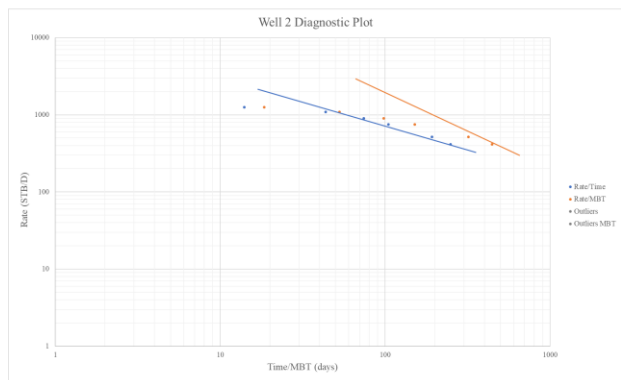
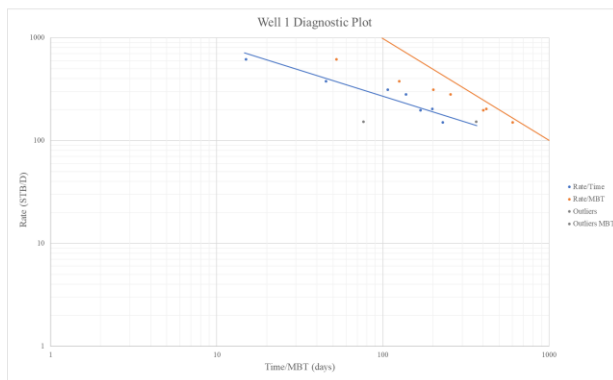
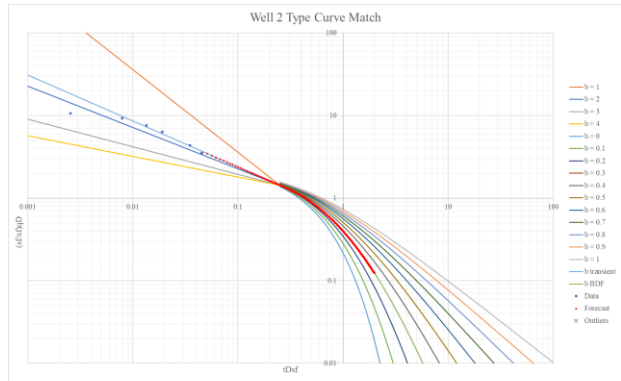
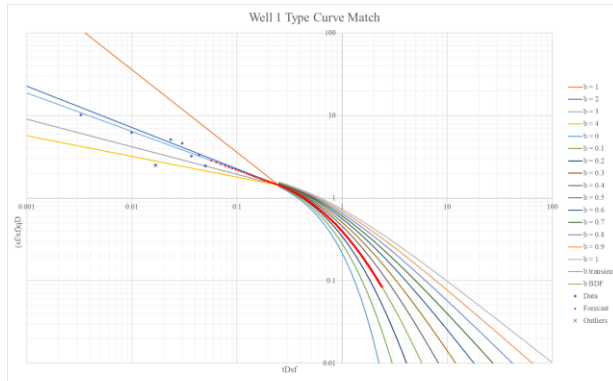


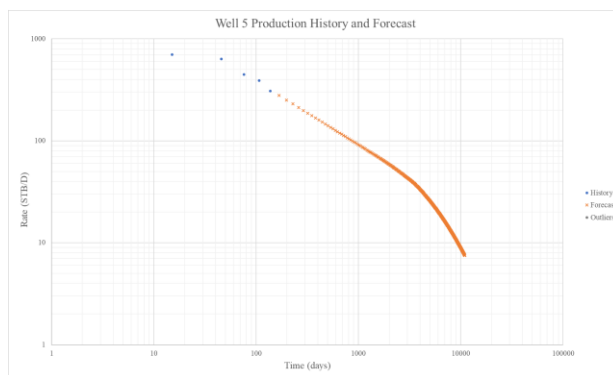
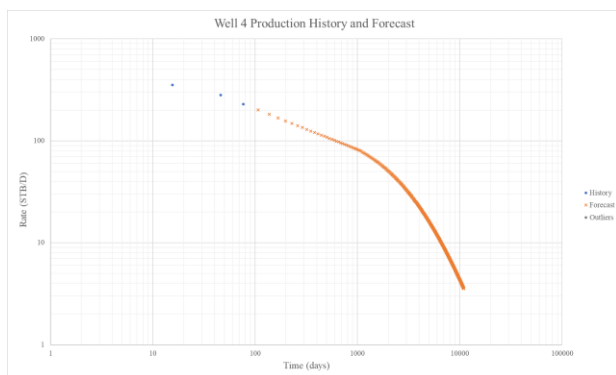
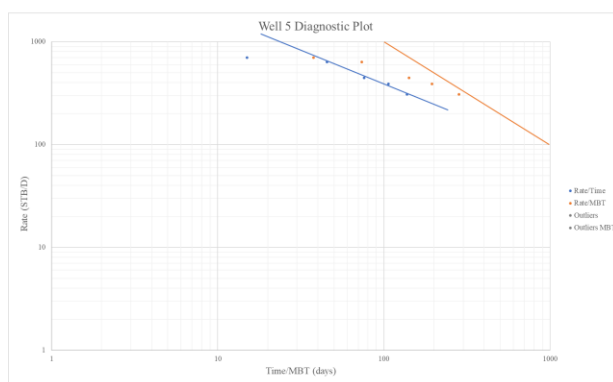
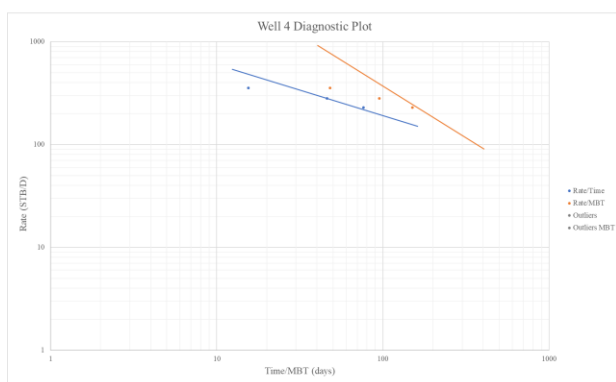
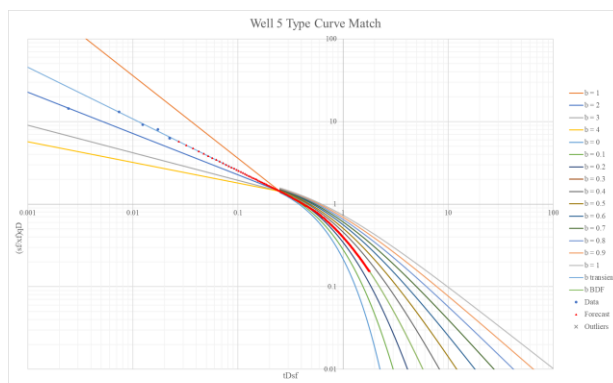
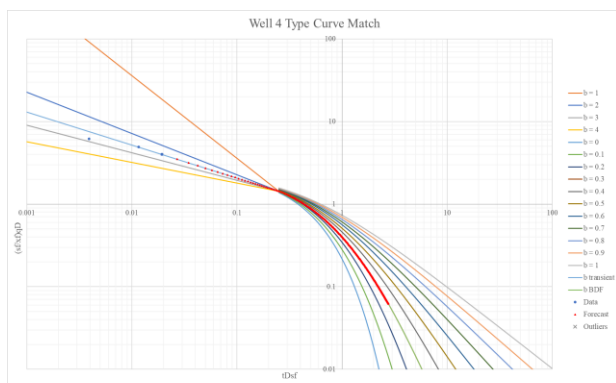


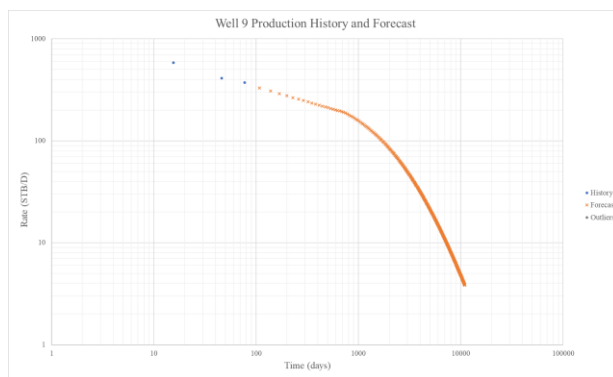
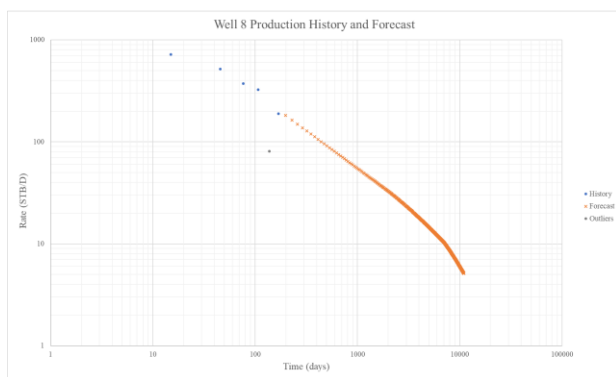
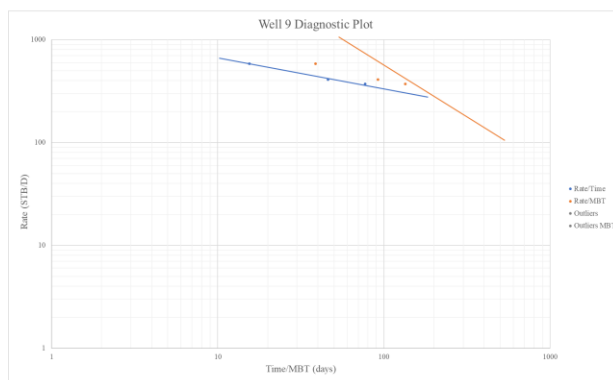
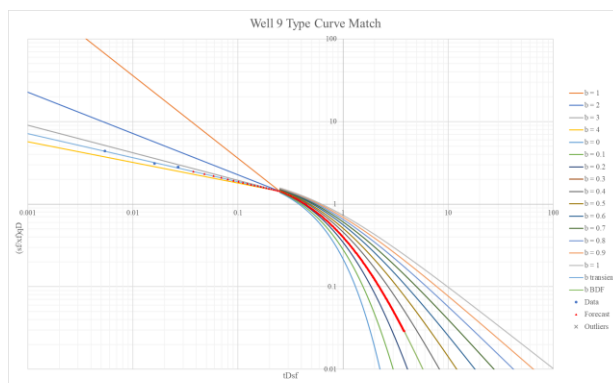
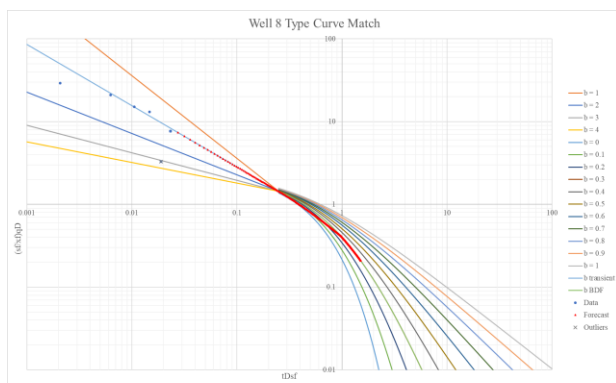


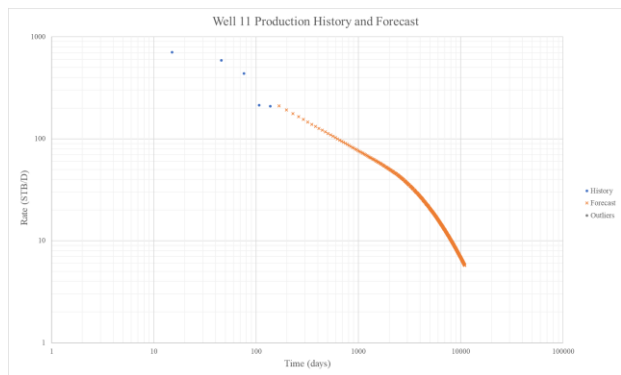
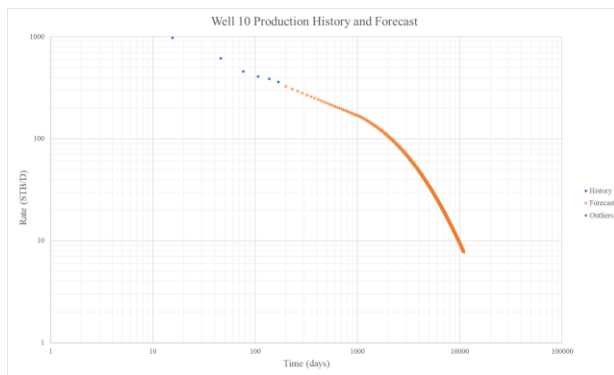
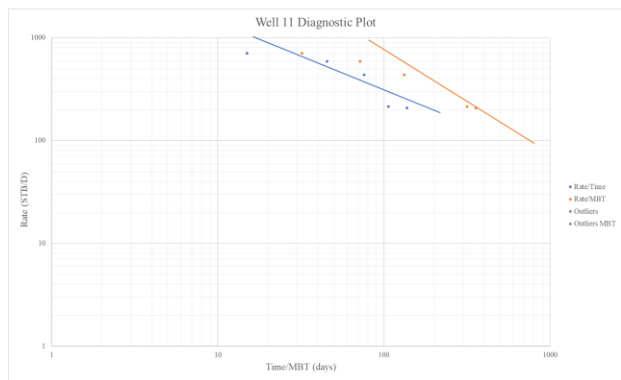
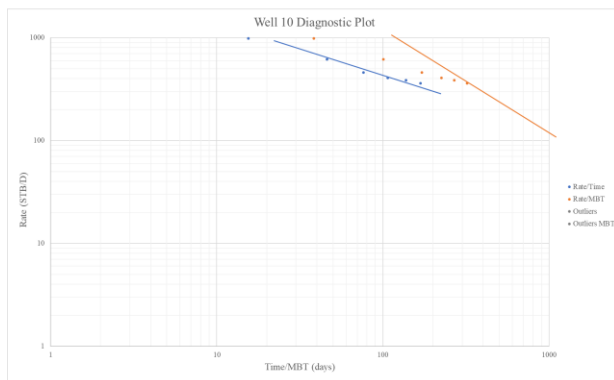
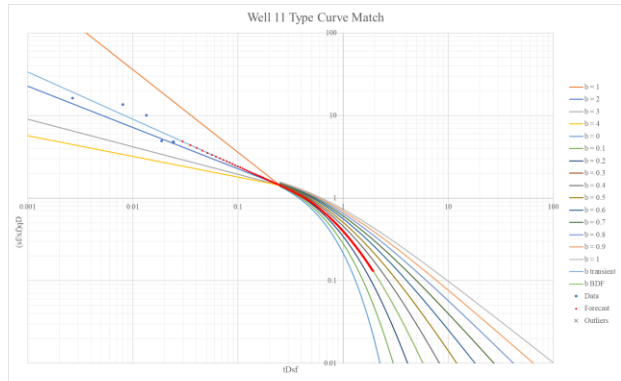
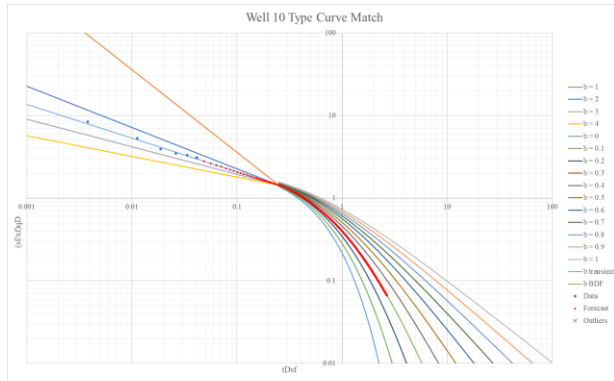
Well	3	16	18	20	24	25	30	38	49	58	61	63	65	69	80	90	96	108	134	135	136	140	141
μ , cP	0.65	0.64	0.65	0.58	0.63	0.64	0.63	0.50	0.55	0.65	0.65	0.65	0.55	0.55	0.57	0.55	0.60	0.64	0.55	0.50	0.55	0.55	0.64
B, RB/STB	1.35	1.35	1.35	1.35	1.35	1.35	1.35	1.35	1.34	1.36	1.34	1.35	1.37	1.35	1.35	1.35	1.35	1.35	1.35	1.35	1.35	1.36	1.35
ϕ	0.12	0.07	0.10	0.09	0.12	0.12	0.11	0.09	0.11	0.08	0.11	0.12	0.08	0.07	0.09	0.07	0.10	0.12	0.09	0.07	0.08	0.09	0.12
h, ft	200	200	150	200	200	200	200	200	200	200	200	125	200	200	200	200	200	200	200	200	200	200	200
c_t , psi ⁻¹	1.95E-05	1.80E-05	1.75E-05	1.65E-05	1.90E-05	1.92E-05	1.90E-05	1.60E-05	1.65E-05	1.20E-05	1.85E-05	1.95E-05	1.35E-05	1.50E-05	1.75E-05	1.40E-05	1.75E-05	1.95E-05	1.70E-05	1.40E-05	1.65E-05	1.65E-05	1.90E-05
L_w , ft	6850	7551	8747	8489	7696	7694	6125	6831	7104	7346	9498	7080	10169	6840	6852	7697	6826	9798	6756	8154	6696	7882	7770
s_o , ft	200	250	300	200	300	250	225	200	200	300	225	300	200	200	250	300	250	250	250	200	200	275	250
Δp , psi	2000	2250	2000	2925	2000	2000	2000	2925	3250	4000	2750	2000	3750	2925	3000	2925	2500	2925	2925	2925	2925	2925	2000
D_{min} , year ⁻¹	0.15	0.08	0.15	0.15	0.15	0.15	0.15	0.15	0.15	0.15	0.15	0.15	0.15	0.15	0.15	0.15	0.15	0.15	0.15	0.15	0.15	0.15	0.15
History, days	716	1301	603	869	931	321	900	412	808	381	442	808	412	533	381	656	919	422	1220	778	690	1357	1065
b_{TR}	1.00	3.40	1.00	1.55	1.40	2.55	1.40	1.50	2.20	1.65	2.30	1.00	2.80	1.80	2.25	1.20	1.30	2.85	1.05	2.80	2.25	1.40	1.50
b_{BDF}	0.30	0.30	0.30	0.30	0.30	0.30	0.30	0.30	0.30	0.30	0.30	0.30	0.30	0.30	0.30	0.30	0.30	0.30	0.30	0.30	0.30	0.30	0.30
$t_{transition}$, years	6.7	3.7	6.7	4.4	4.8	2.6	4.8	4.5	3.0	4.0	3.0	6.7	2.5	3.7	3.0	5.6	5.2	2.4	6.4	2.5	3.0	4.8	4.5
t_{BDF} , years	80.6	3.8	73.3	11.2	16.8	2.8	16.7	12.3	3.3	8.0	3.2	56.6	2.6	5.6	4.0	32.8	23.2	2.5	58.5	2.6	3.2	16.8	12.7
TMP	1.02E-04	1.18E-04	1.02E-04	1.56E-04	1.43E-04	2.60E-04	1.43E-04	1.53E-04	2.25E-04	1.69E-04	2.31E-04	1.02E-04	2.78E-04	1.85E-04	2.38E-04	1.22E-04	1.32E-04	2.85E-04	1.07E-04	2.78E-04	2.30E-04	1.43E-04	1.52E-04
RMP	6.74E-02	2.38E-02	5.89E-02	1.91E-02	2.94E-02	1.66E-02	4.15E-02	2.32E-02	1.15E-02	1.84E-02	7.24E-03	5.68E-02	6.38E-03	2.43E-02	1.20E-02	3.87E-02	2.51E-02	6.06E-03	4.97E-02	2.15E-02	2.35E-02	3.84E-02	1.93E-02
k, mD	2.45E-04	2.34E-04	4.11E-04	2.13E-04	7.28E-04	9.40E-04	3.76E-04	1.75E-04	3.55E-04	3.76E-04	6.12E-04	5.51E-04	2.61E-04	1.68E-04	5.28E-04	2.33E-04	3.42E-04	1.04E-03	2.21E-04	2.14E-04	2.64E-04	3.48E-04	5.44E-04
x_i , ft	109.9	403.3	176.0	219.7	164.6	158.0	159.7	235.9	220.4	276.5	269.1	201.9	334.9	256.7	262.6	233.0	244.4	209.2	151.4	173.5	173.2	129.6	232.7
r'	0.89	0.55	0.67	0.77	1.18	2.19	1.08	0.64	1.29	0.61	1.76	0.89	0.95	0.61	1.23	0.38	0.80	2.43	0.52	0.78	0.96	0.67	1.27
q'	3.19	1.15	2.79	1.01	1.44	0.80	2.03	1.43	0.65	0.87	0.35	2.69	0.35	1.36	0.65	2.17	1.29	0.29	2.78	1.33	1.31	2.14	0.94
EUR, MSTB	267.5	341.2	400.1	547.8	396.2	369.6	327.8	424.4	550.8	493.0	859.3	296.9	845.5	402.5	819.3	391.4	448.6	904.7	335.0	241.5	268.4	337.9	529.8
Scaled EUR, MSTB	773.9	230.8	773.4	447.5	648.8	569.8	709.2	413.2	445.2	277.6	471.1	726.1	285.3	353.2	631.2	358.5	482.1	555.7	524.2	255.8	341.0	511.9	597.6

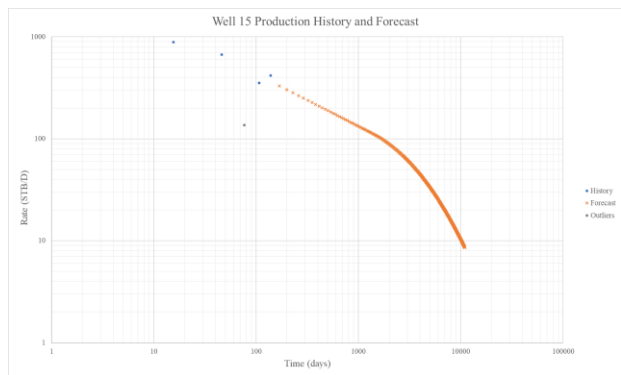
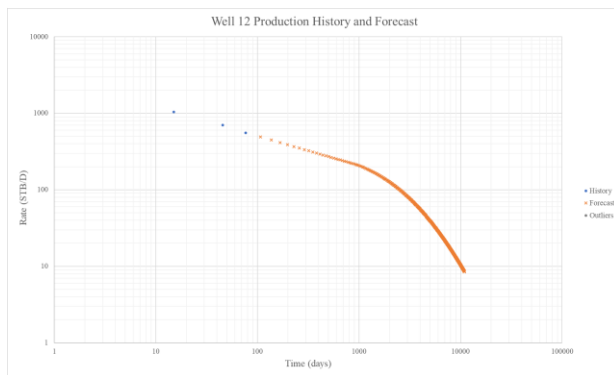
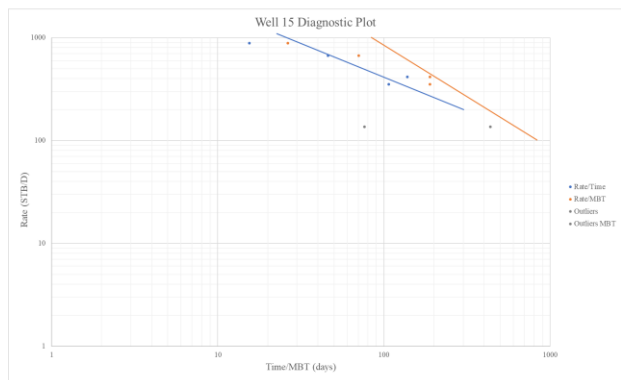
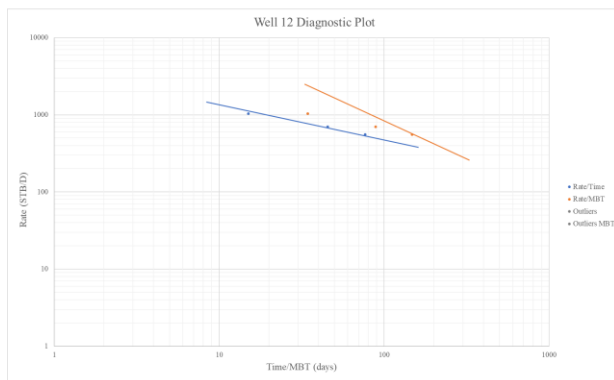
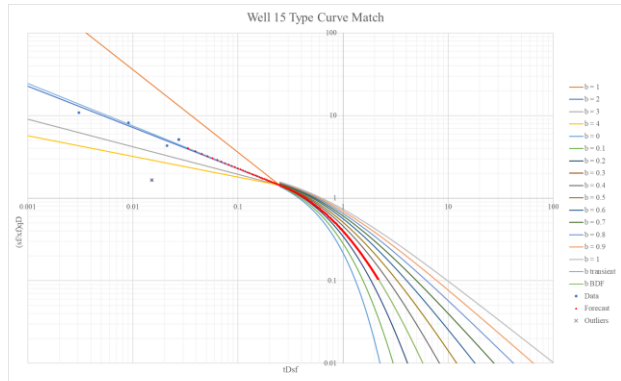
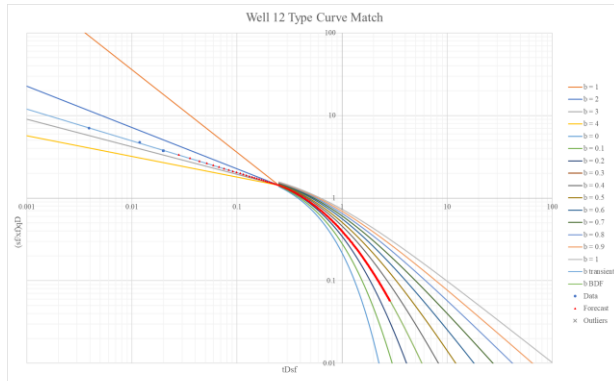
“Early” Well Set Plots and Results

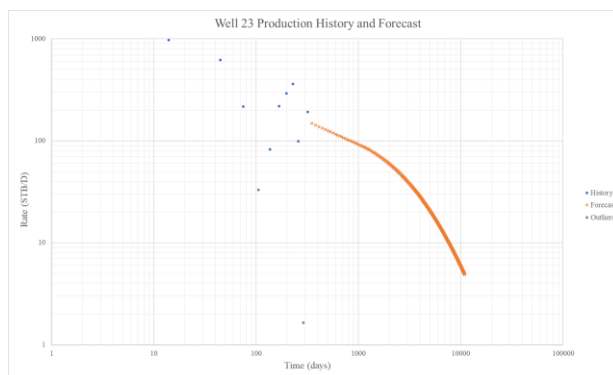
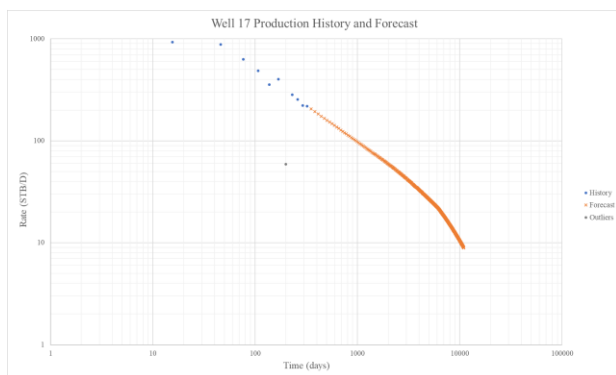
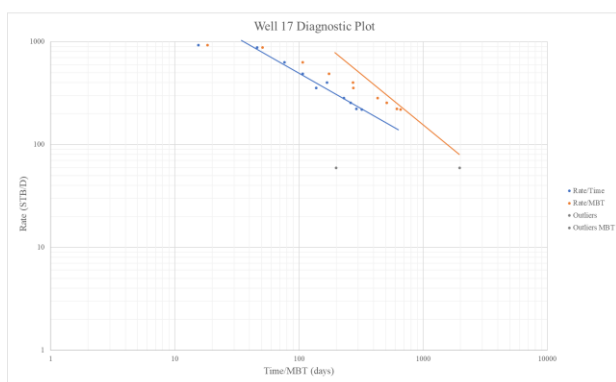
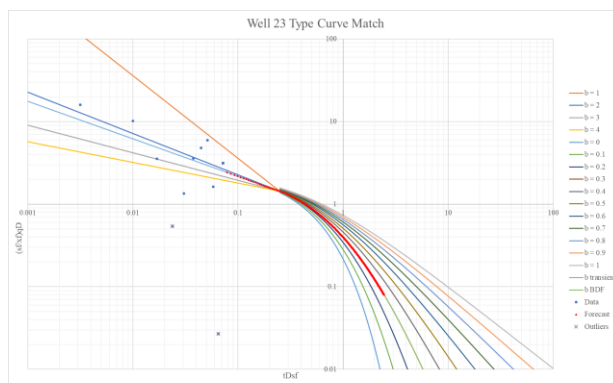
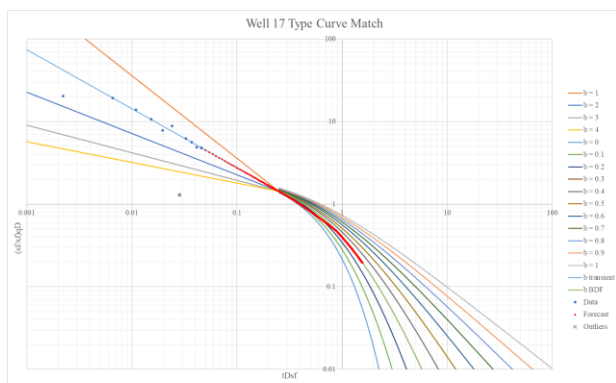


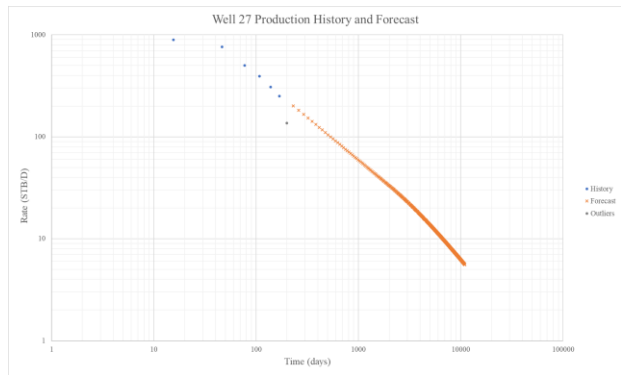
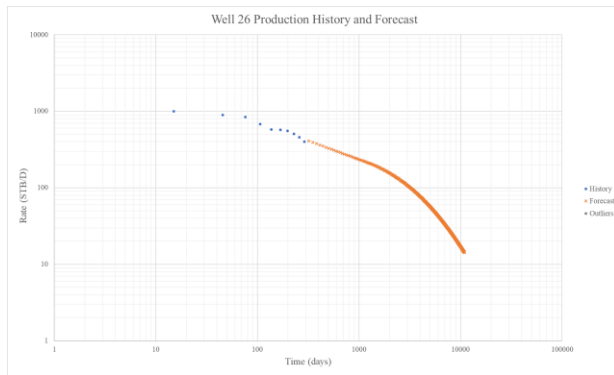
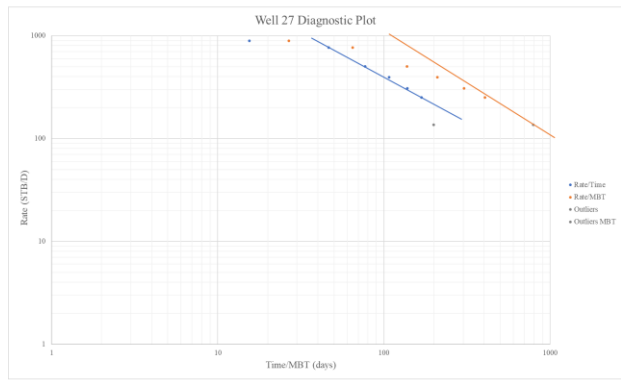
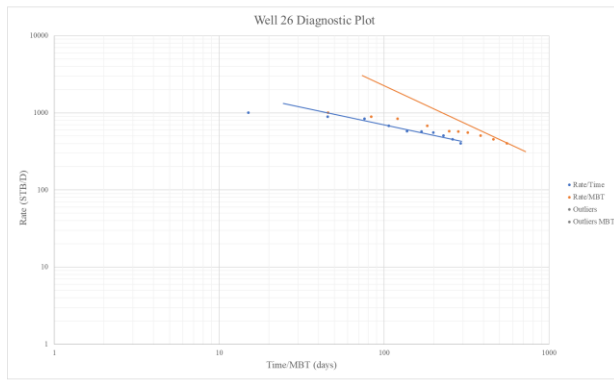
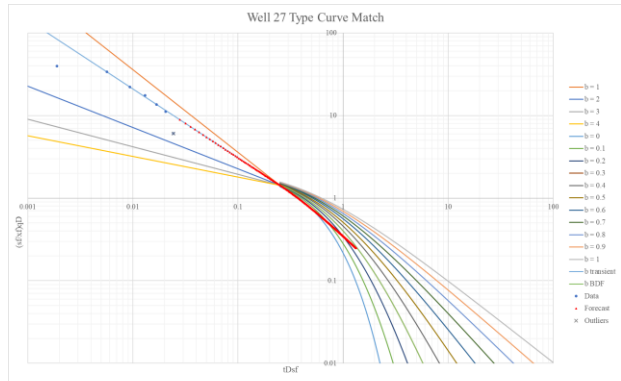
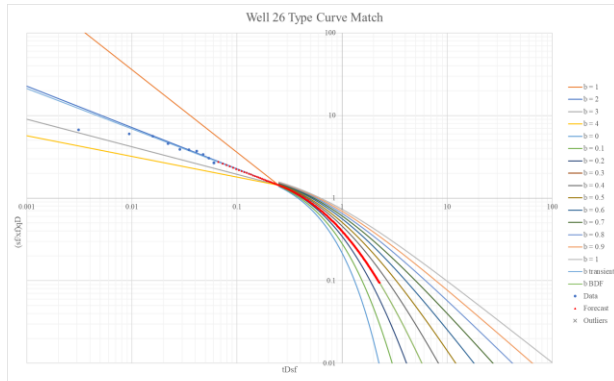


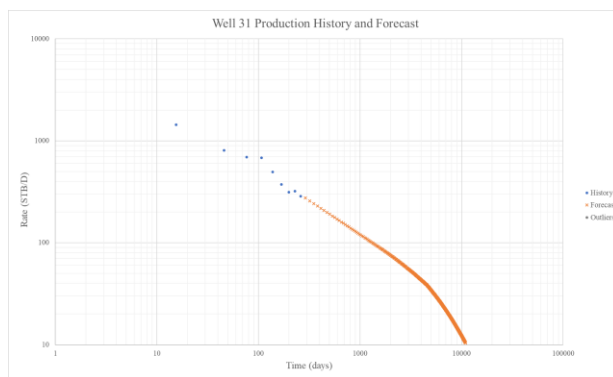
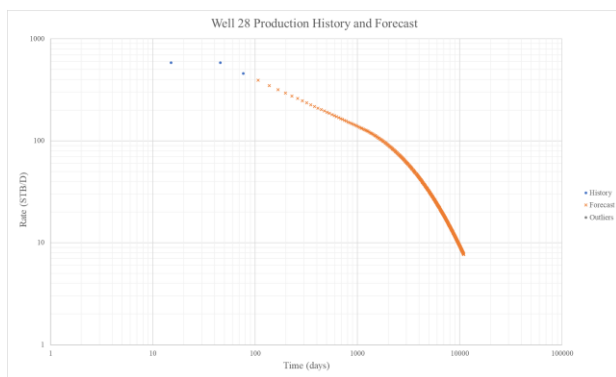
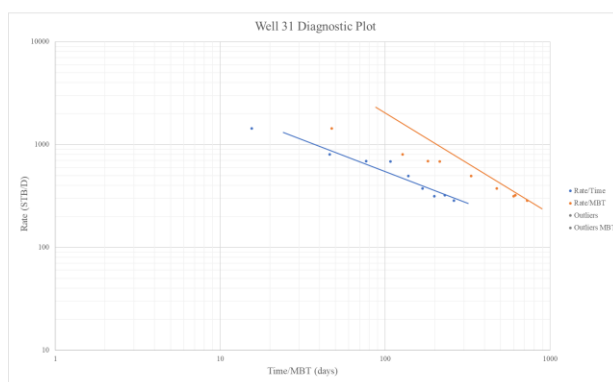
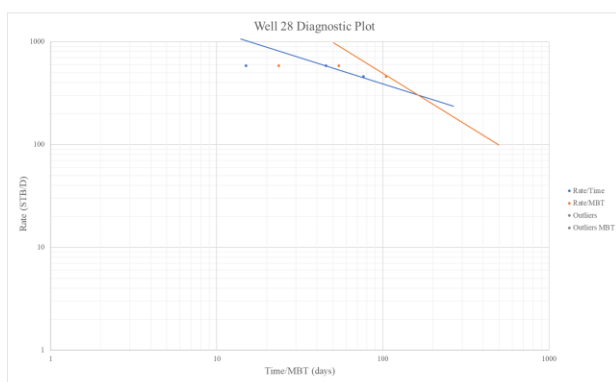
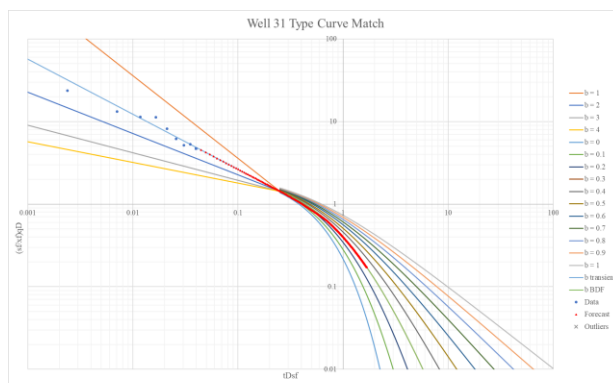
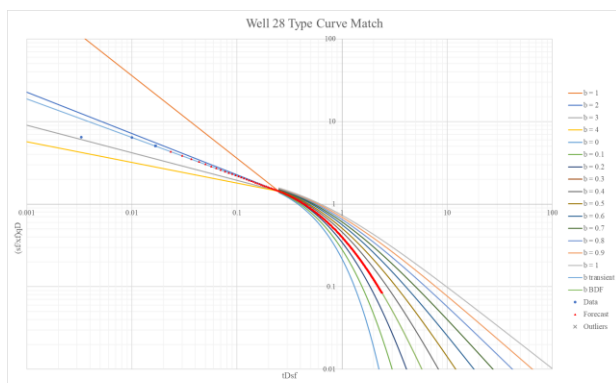


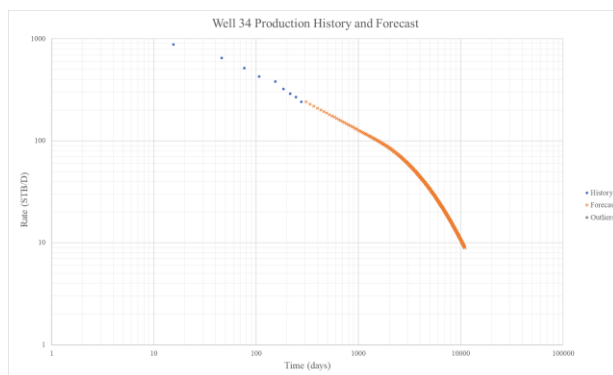
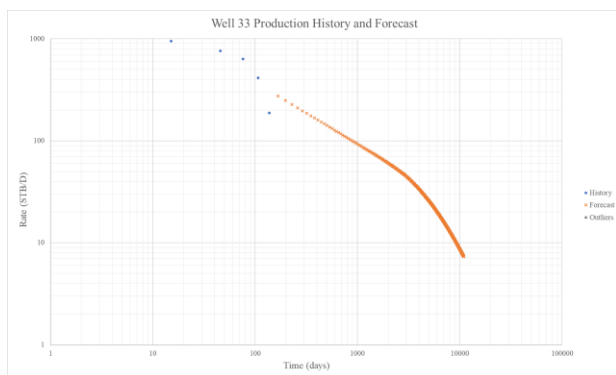
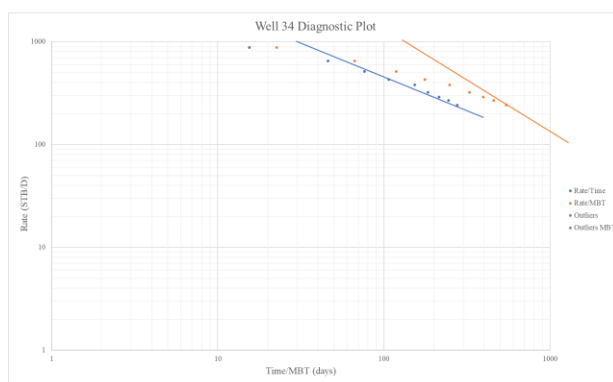
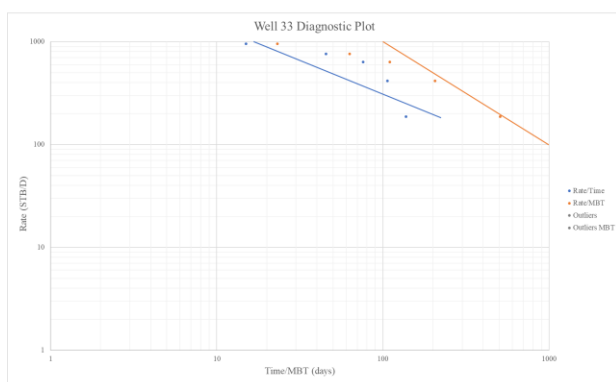
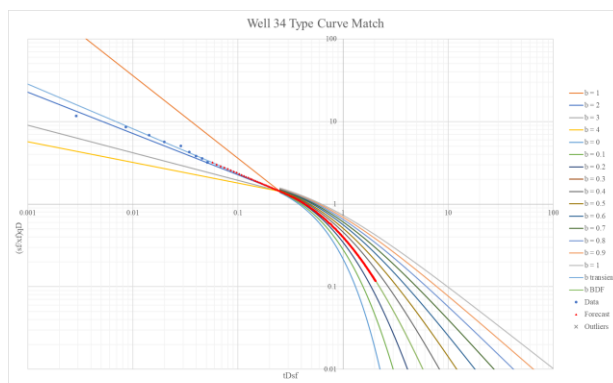
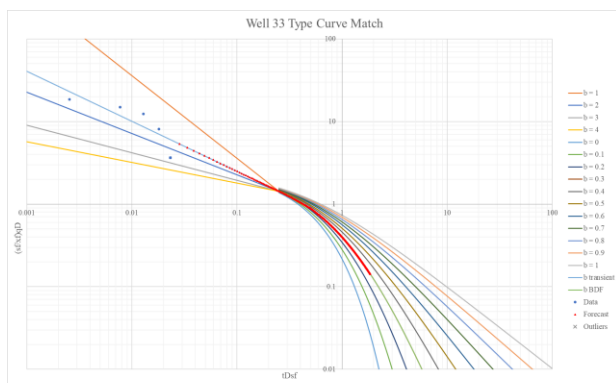


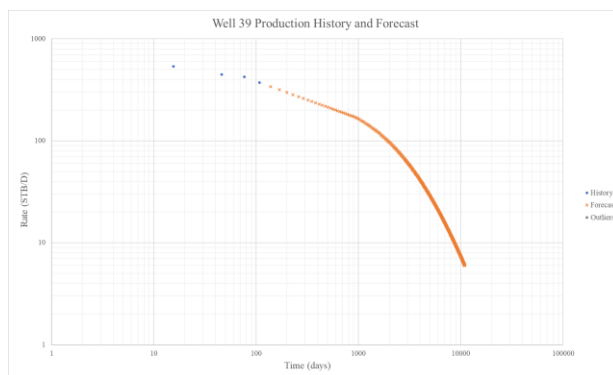
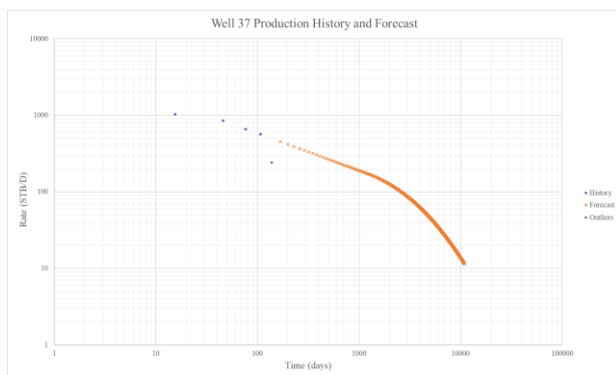
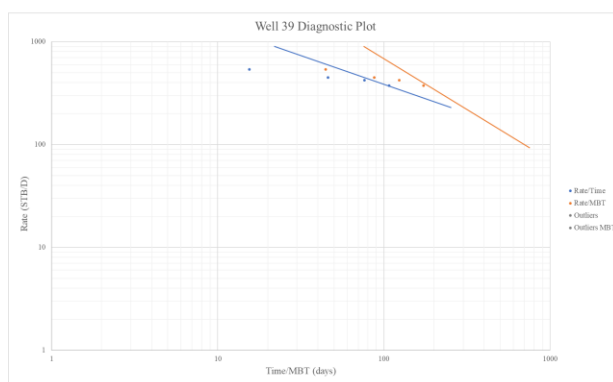
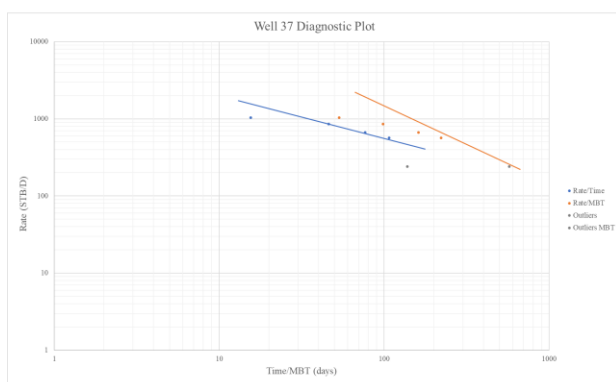
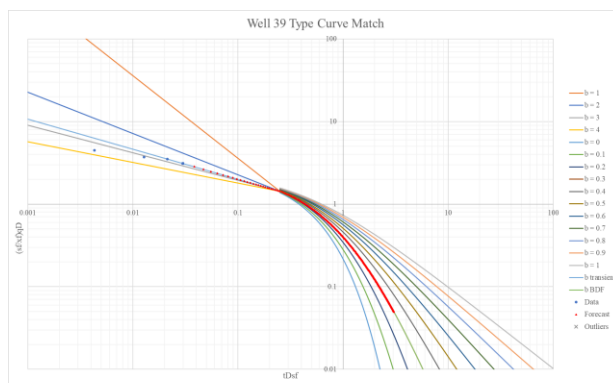
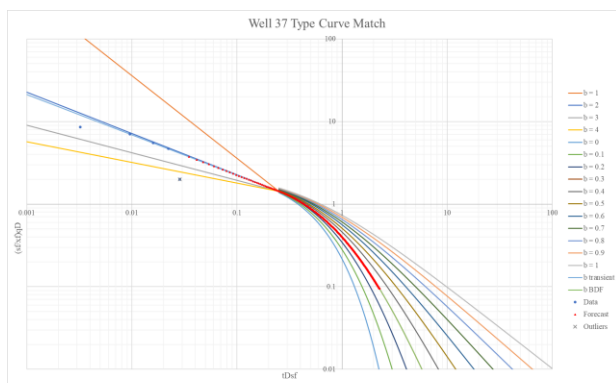


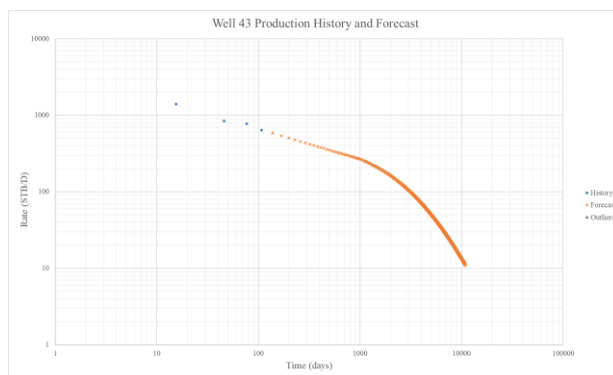
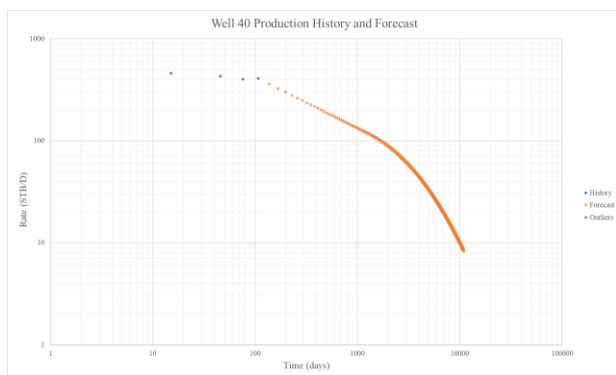
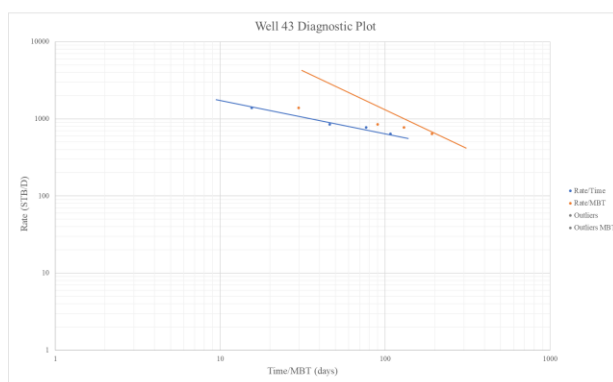
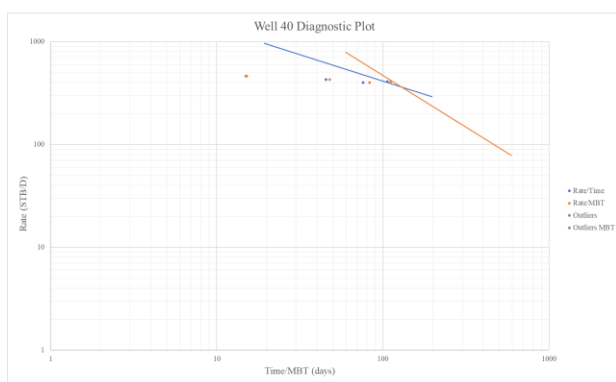
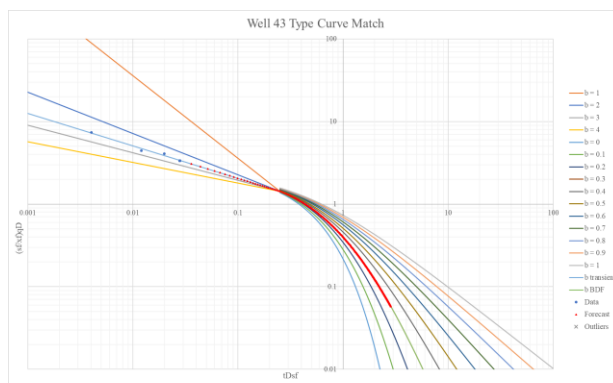
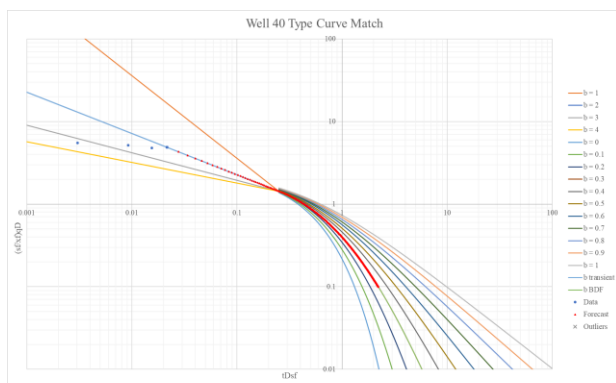


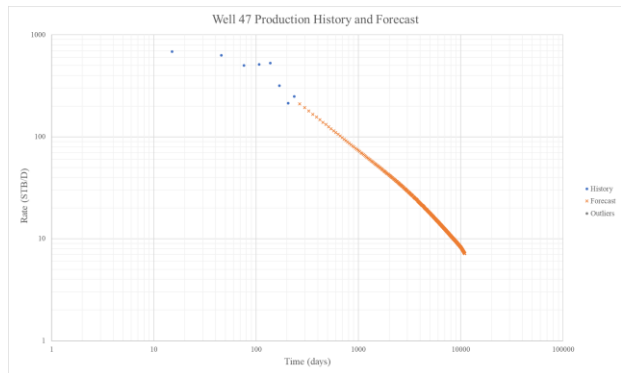
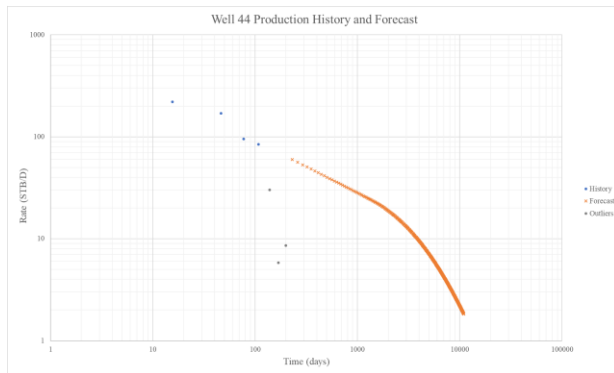
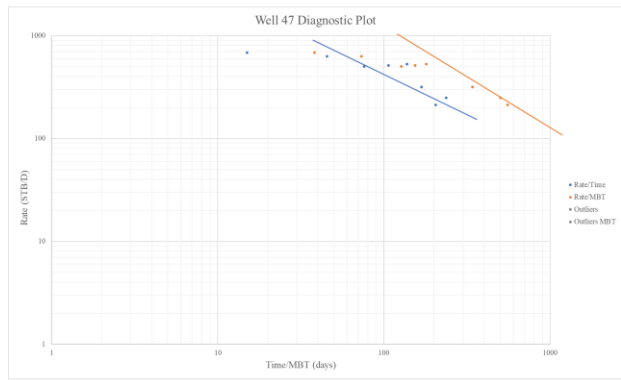
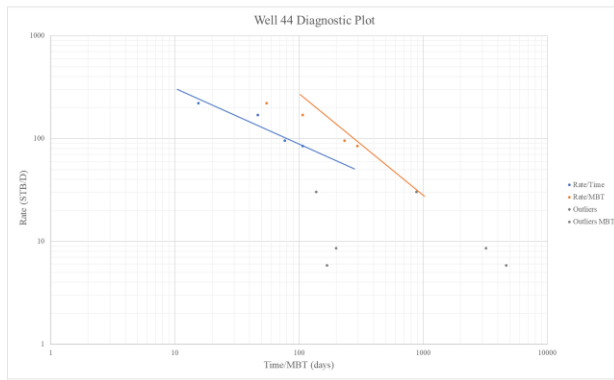
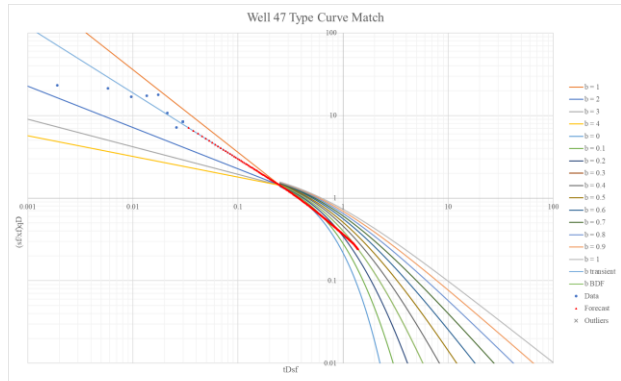
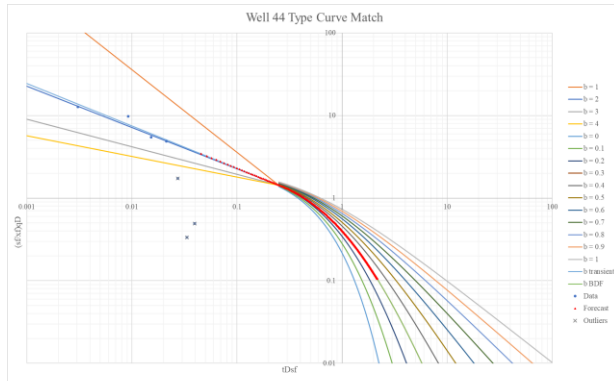


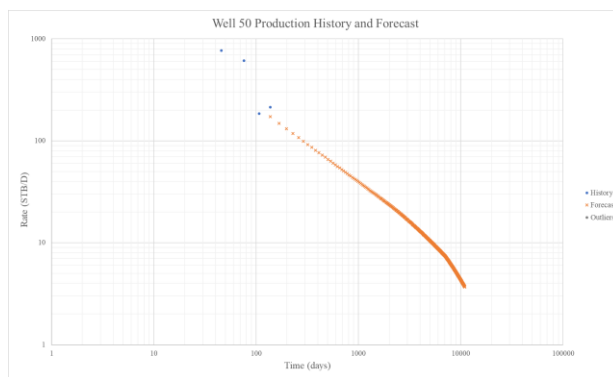
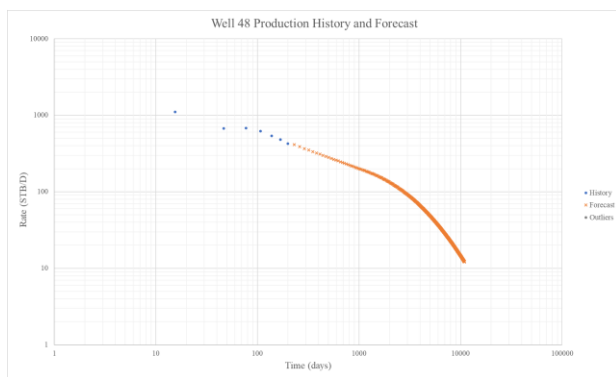
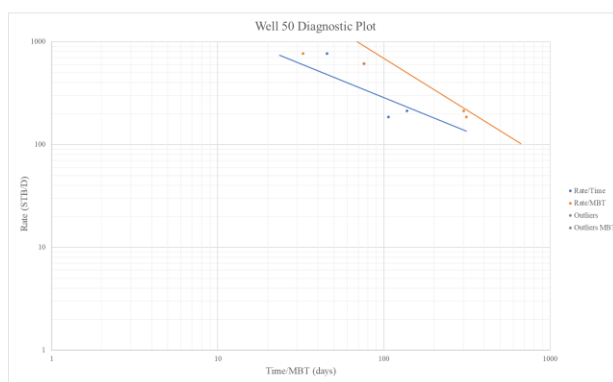
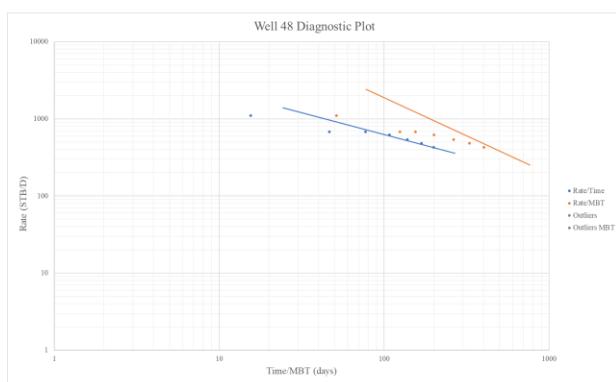
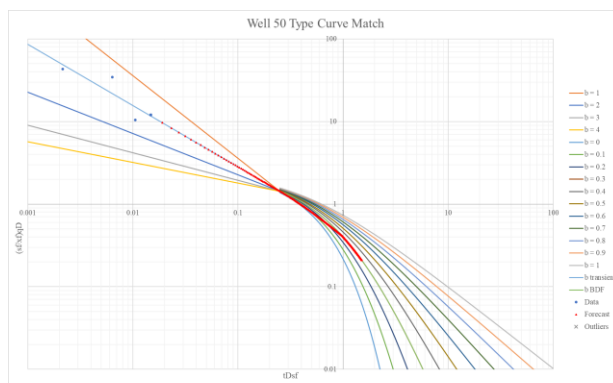
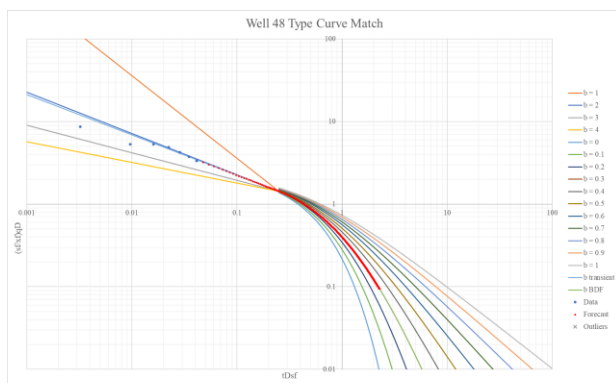


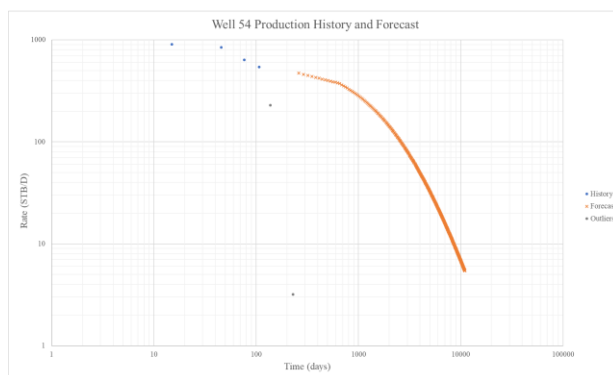
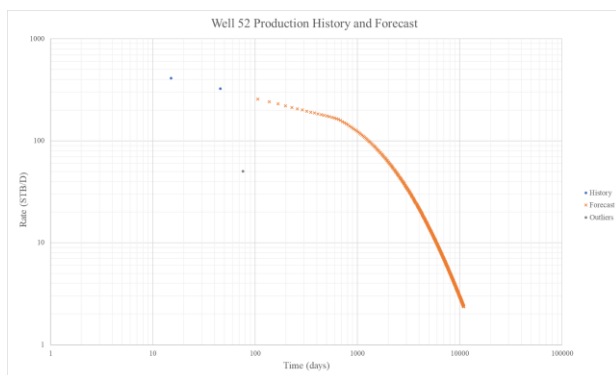
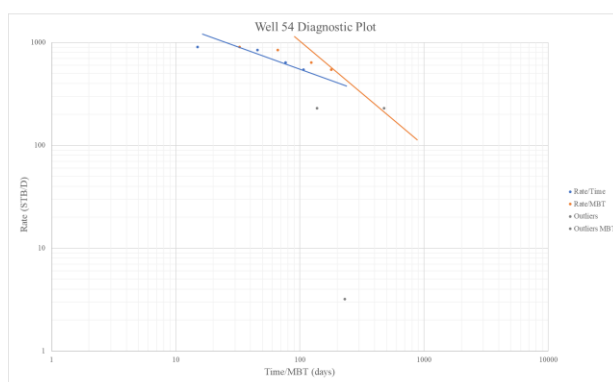
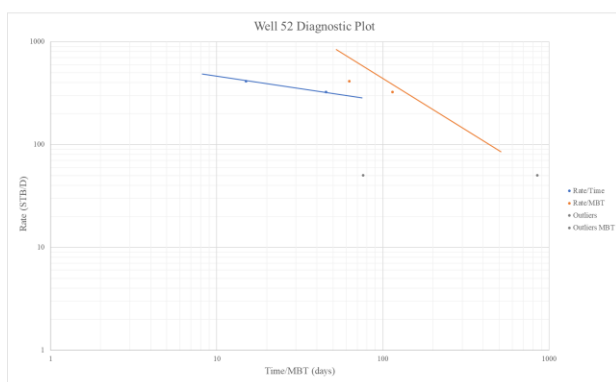
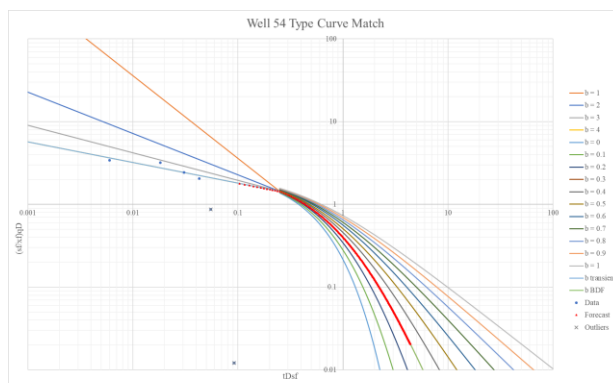
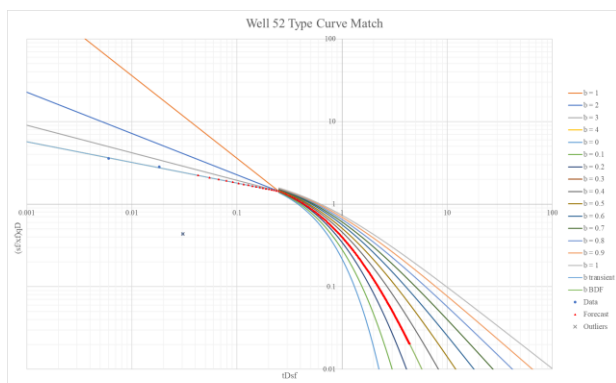


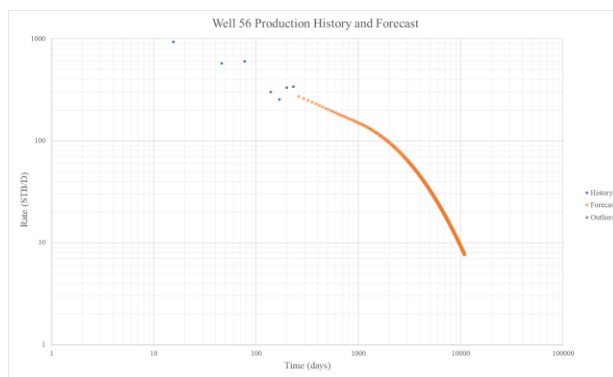
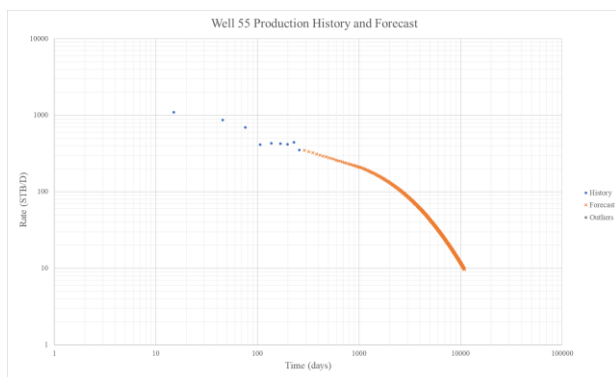
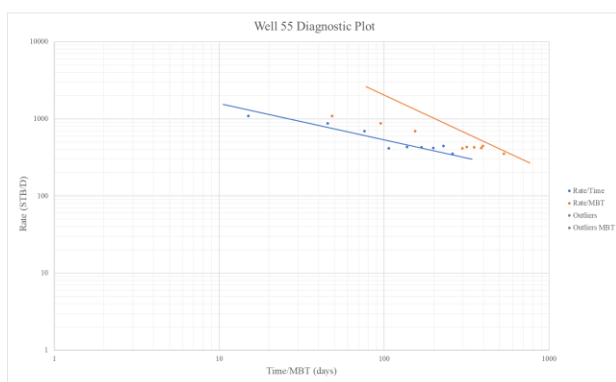
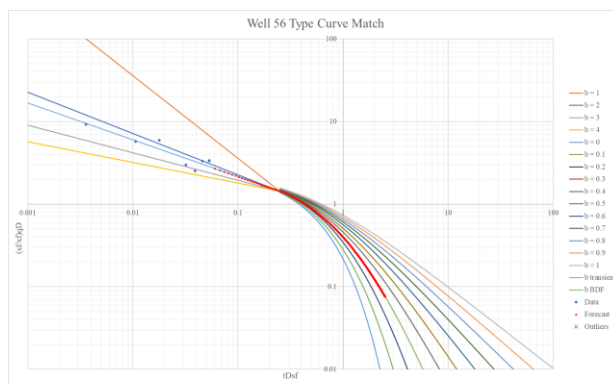
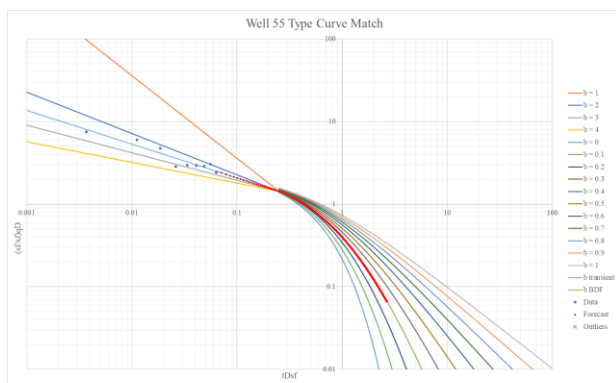


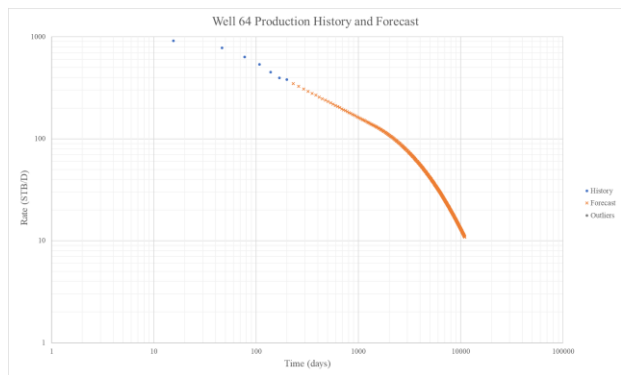
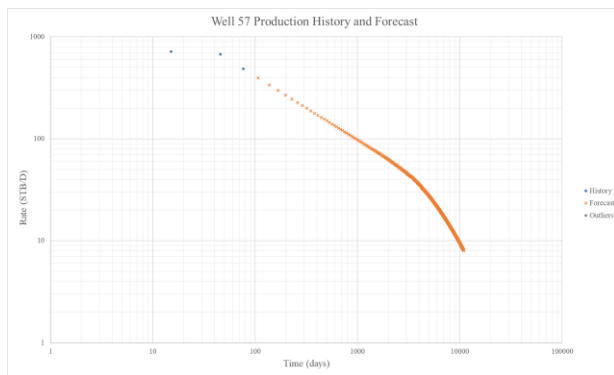
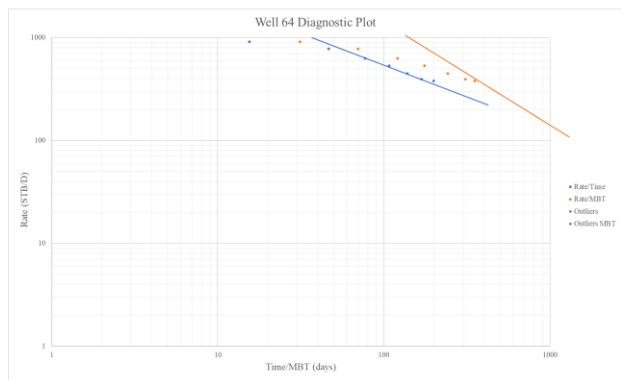
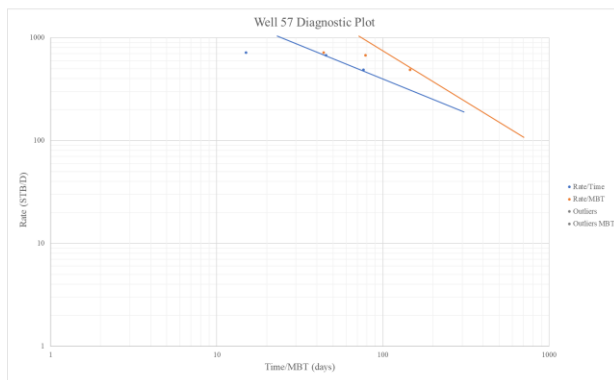
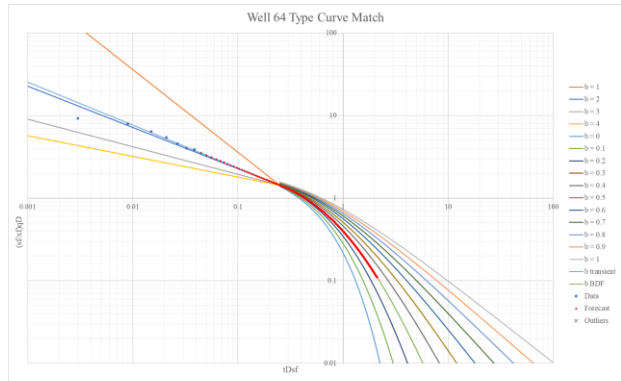
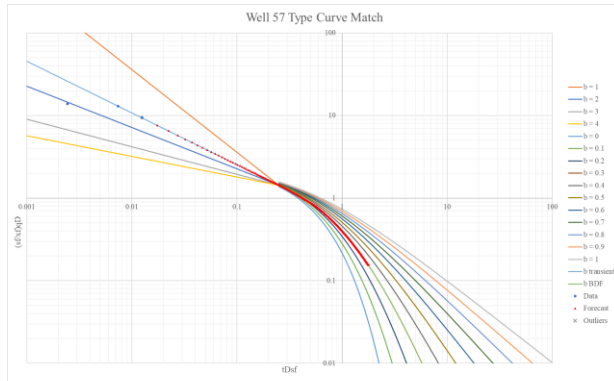


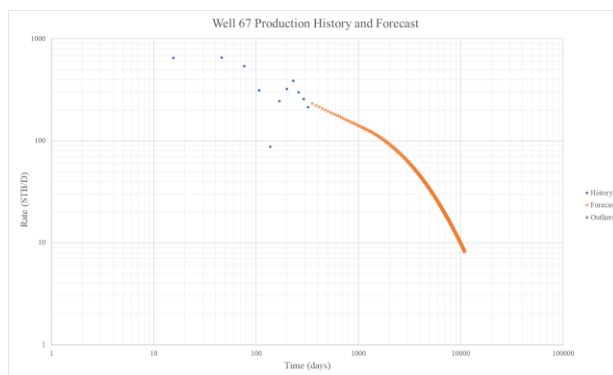
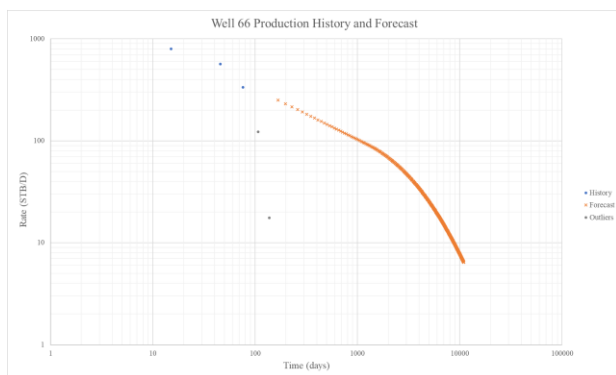
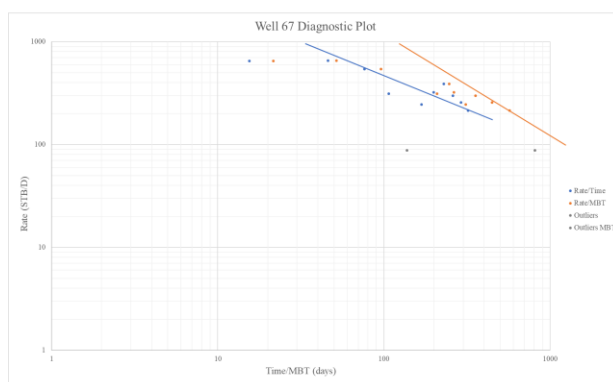
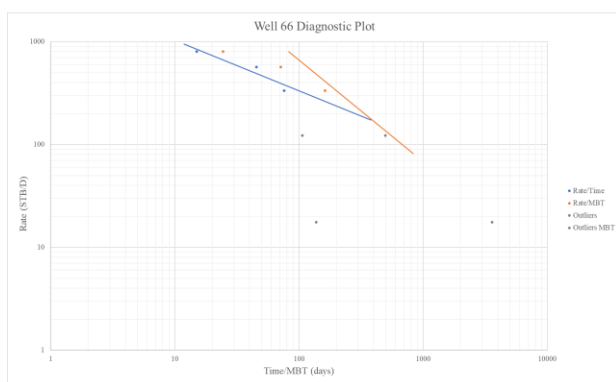
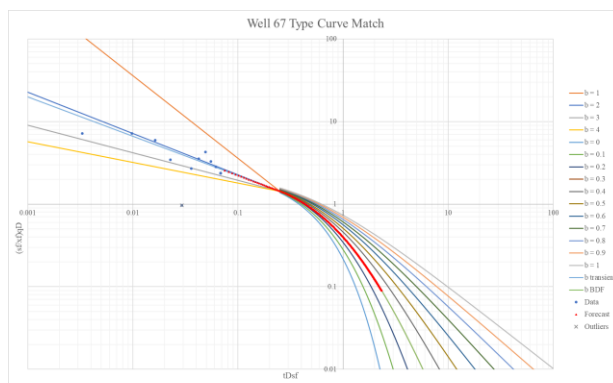
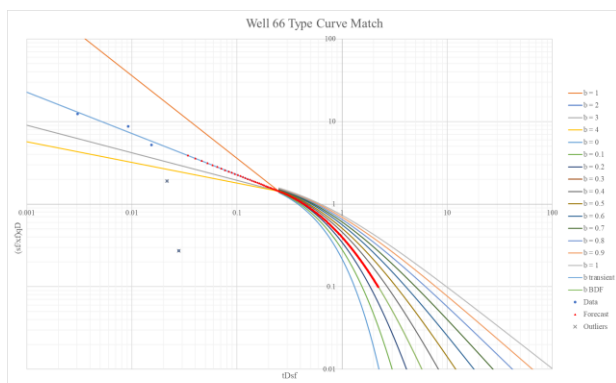


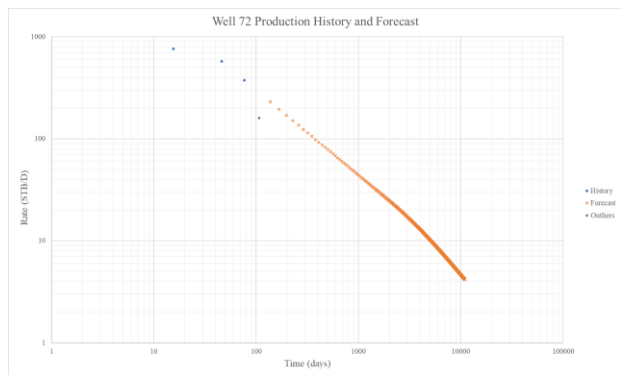
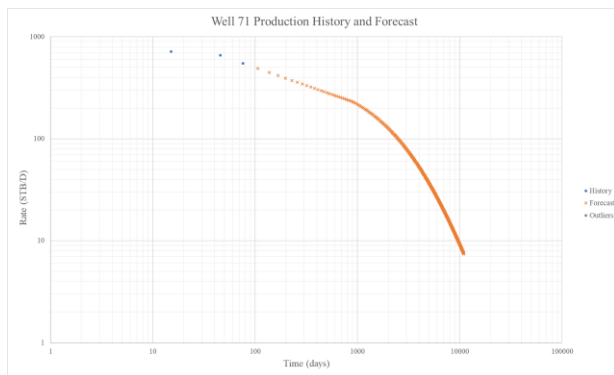
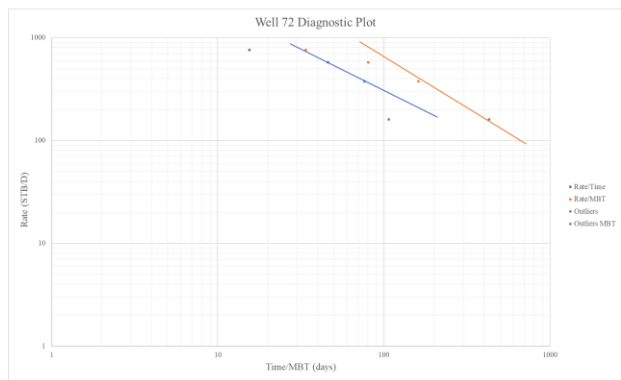
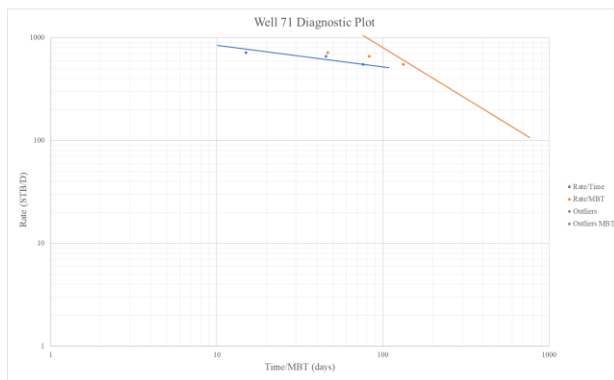
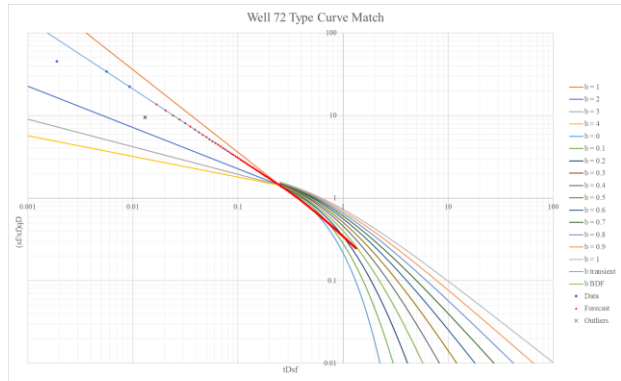
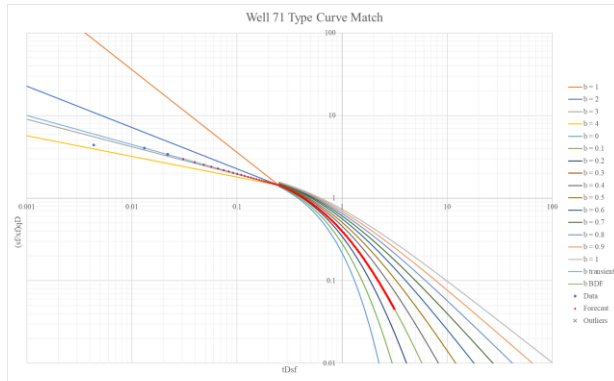


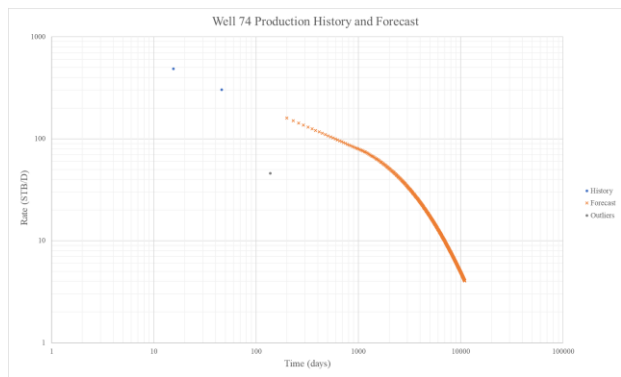
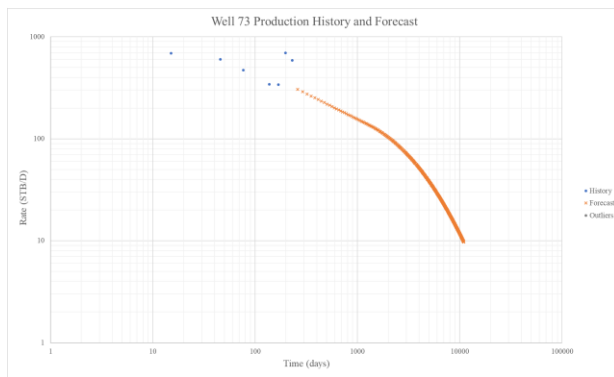
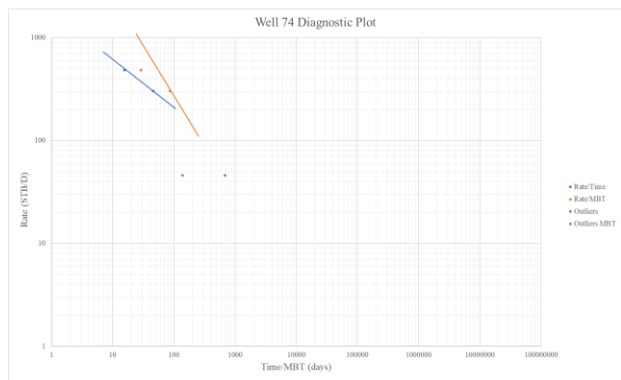
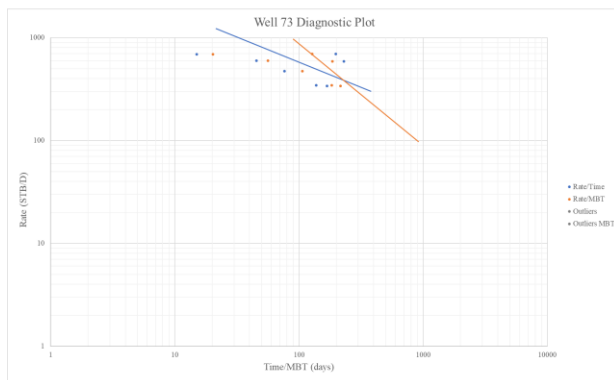
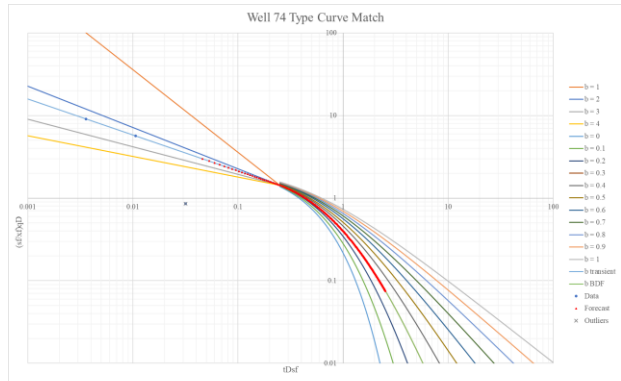
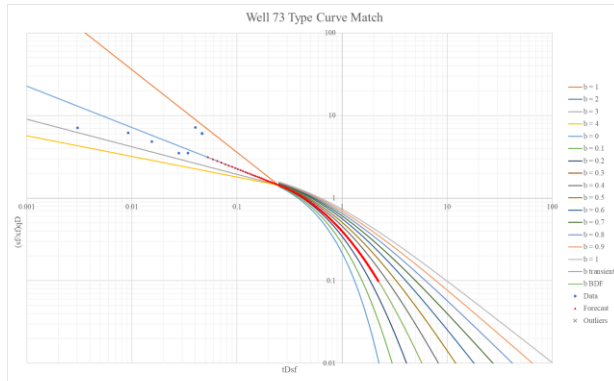


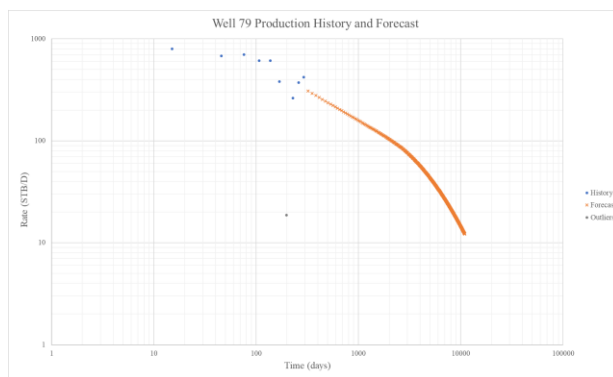
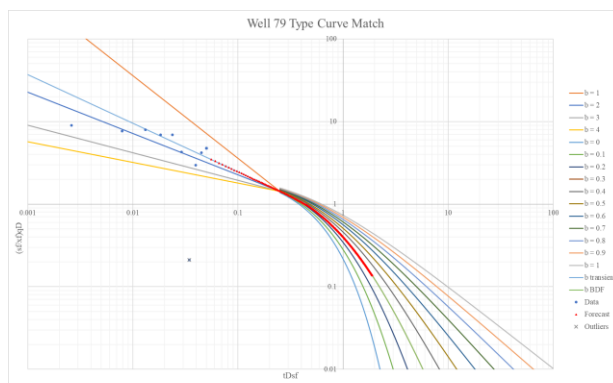
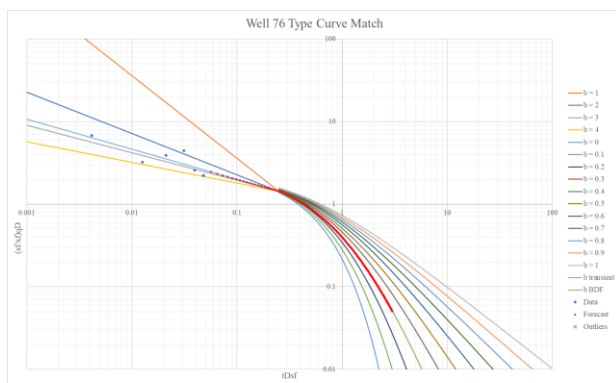


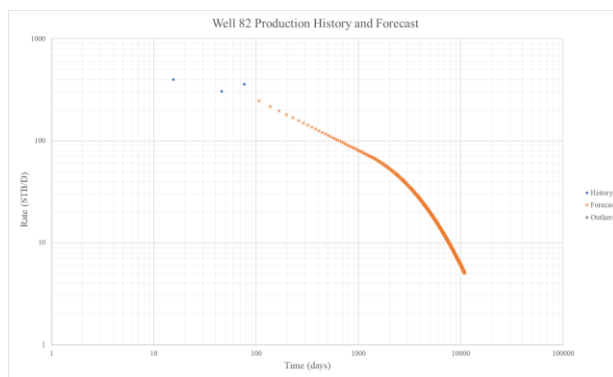
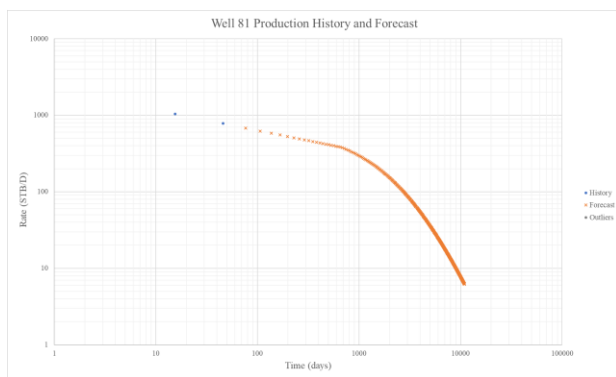
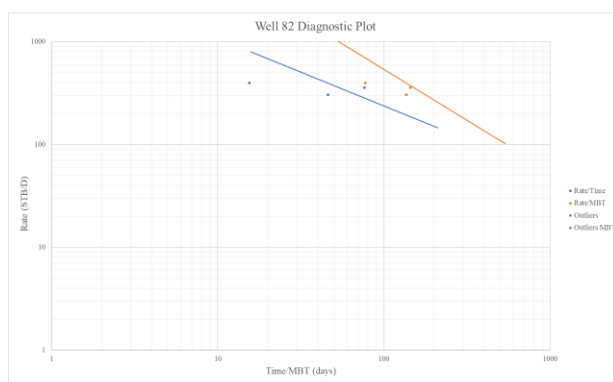
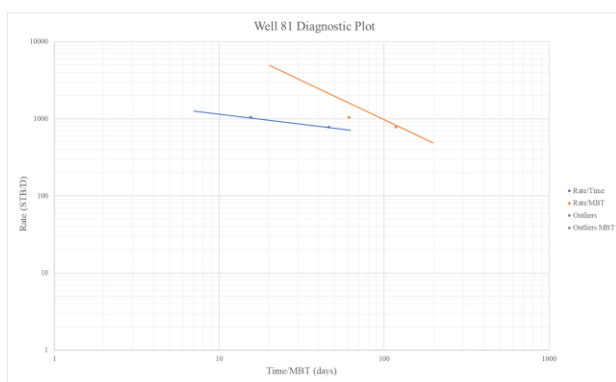
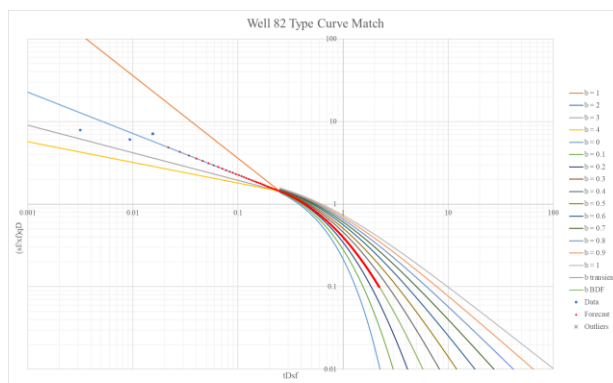
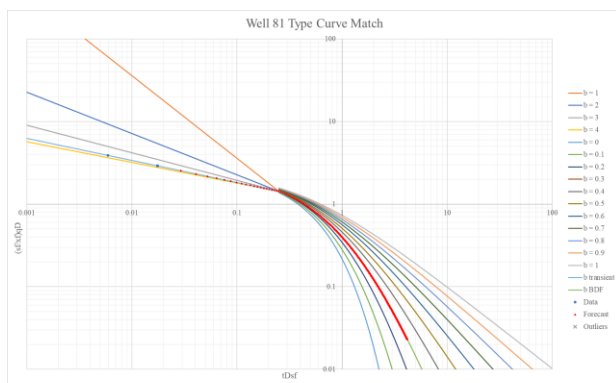


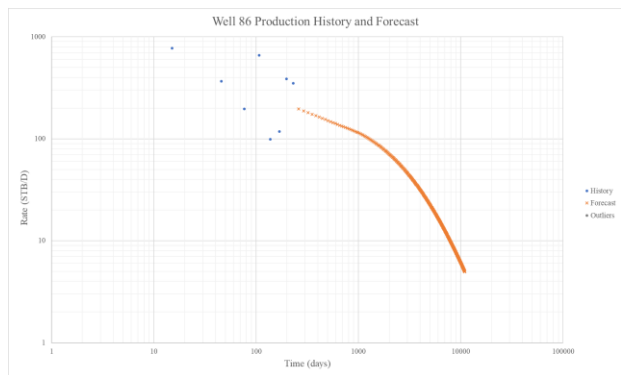
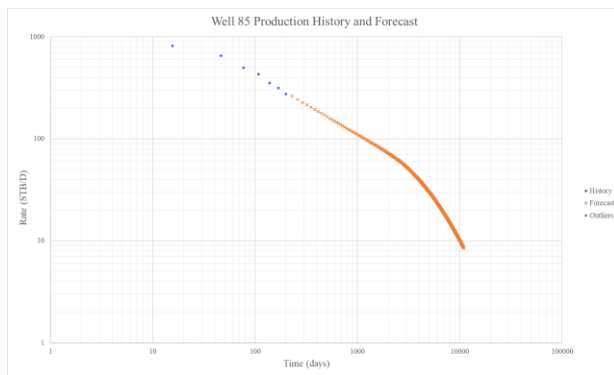
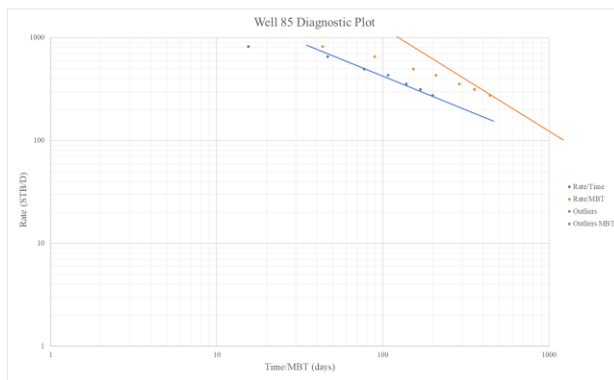
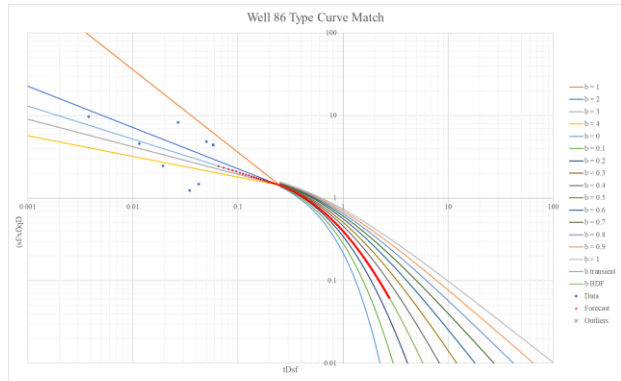
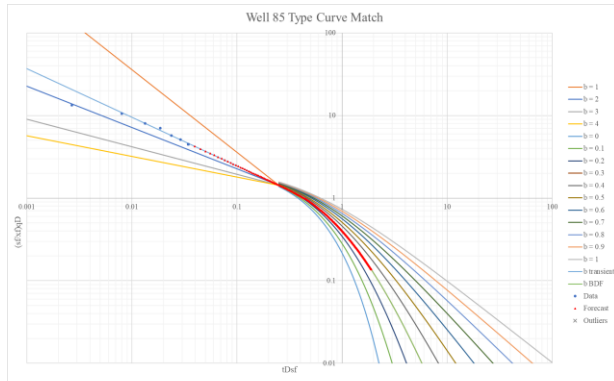


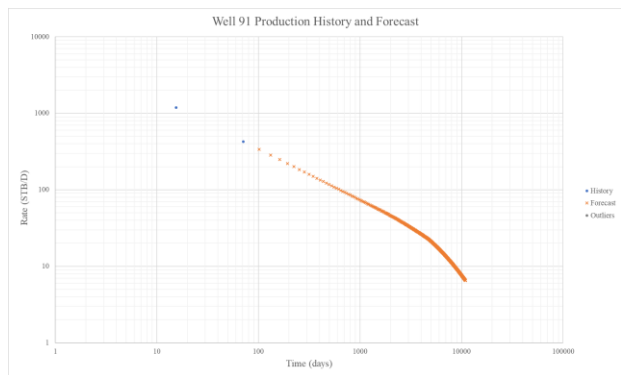
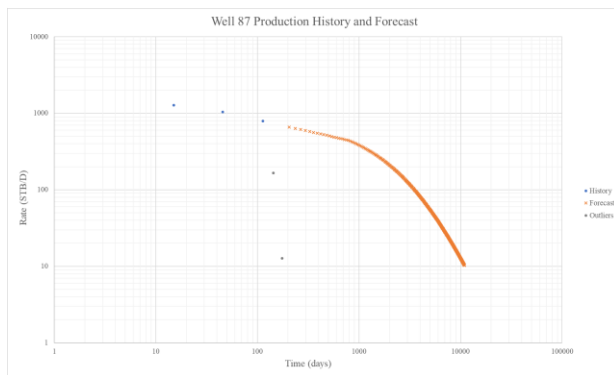
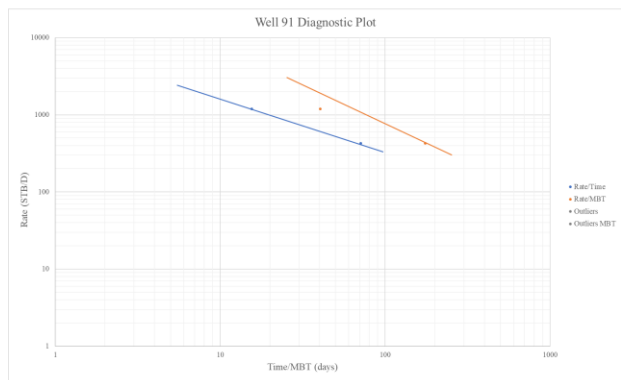
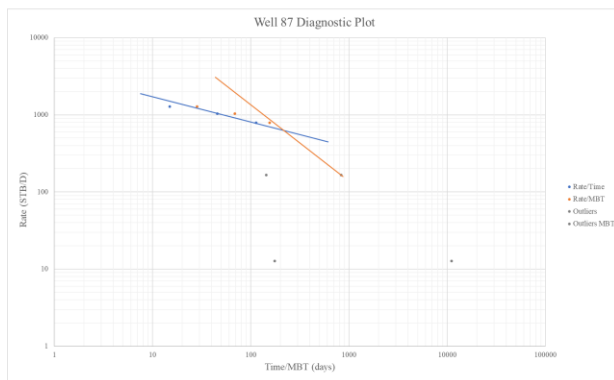
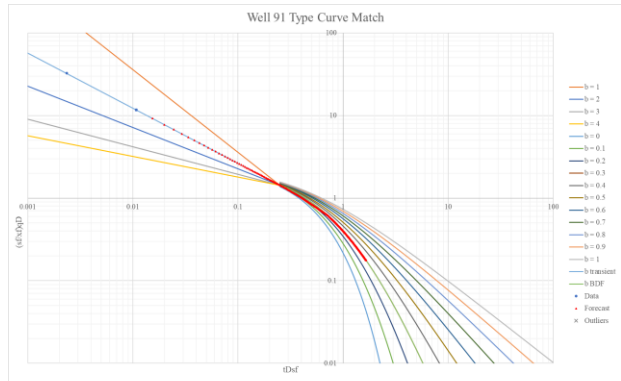
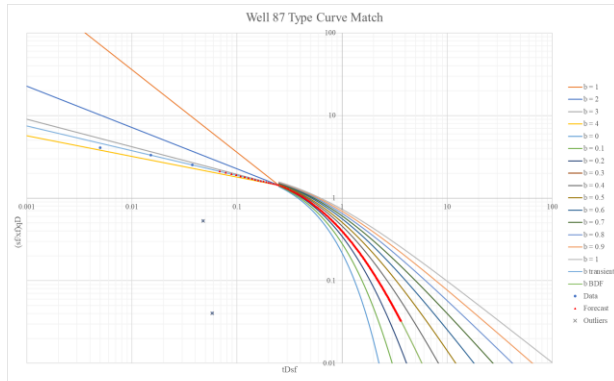


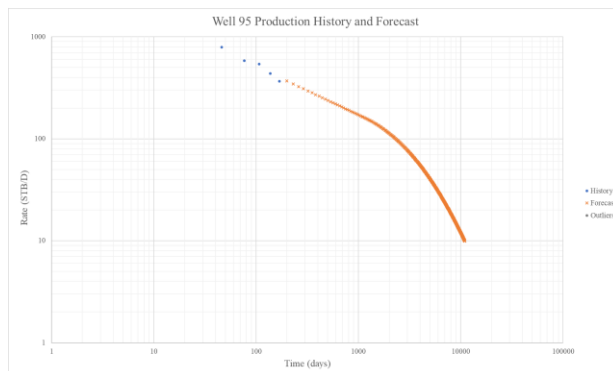
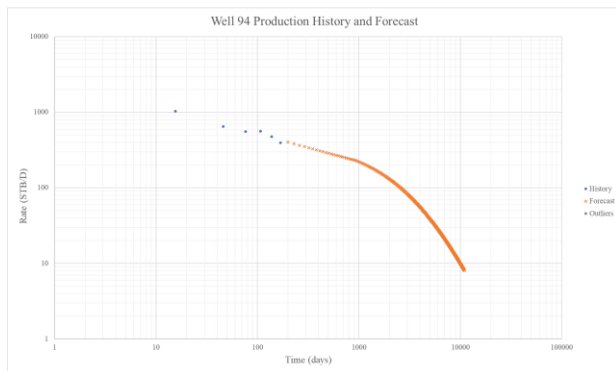
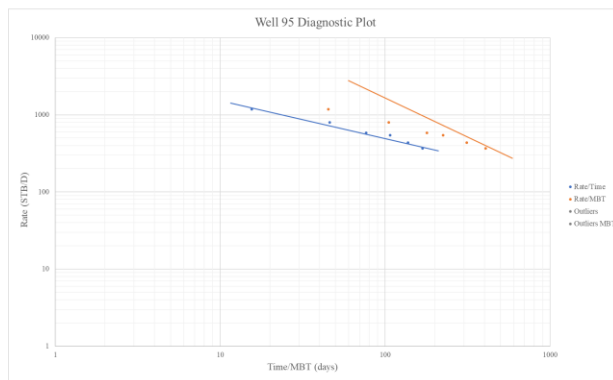
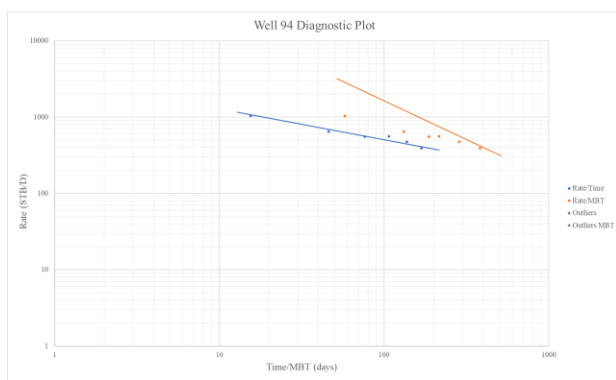
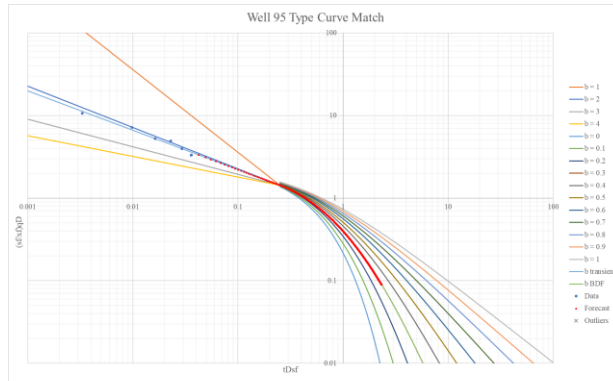
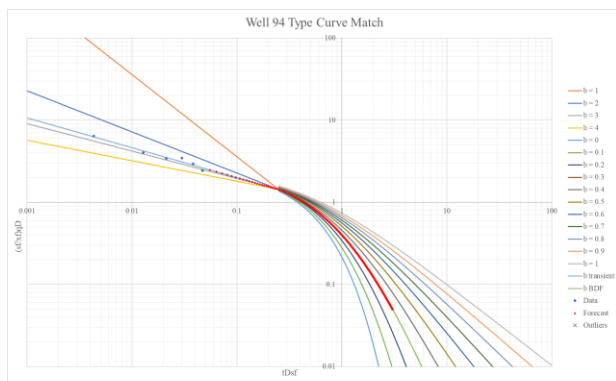


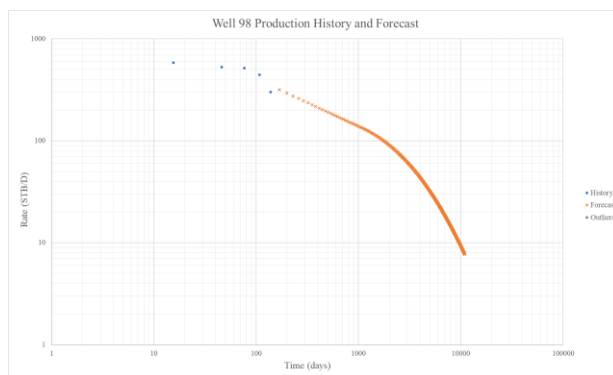
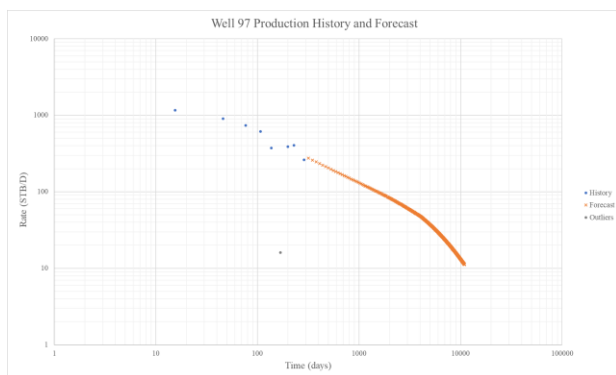
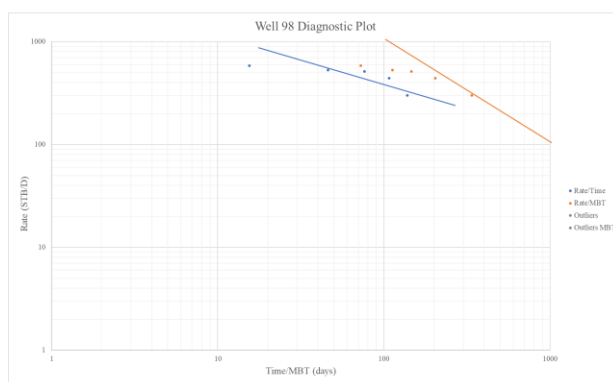
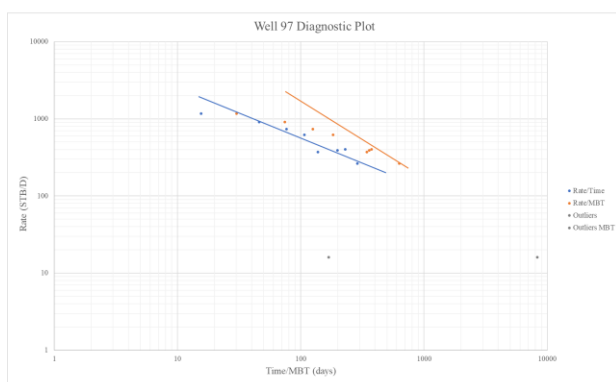
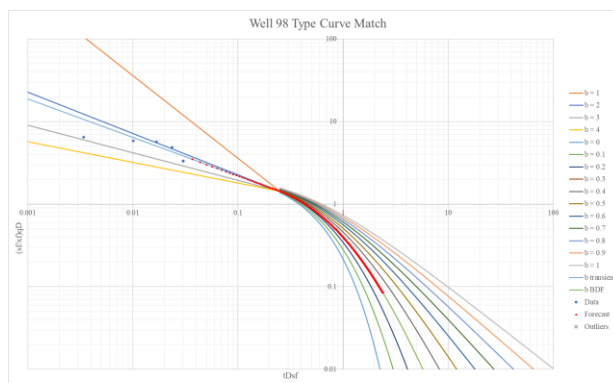
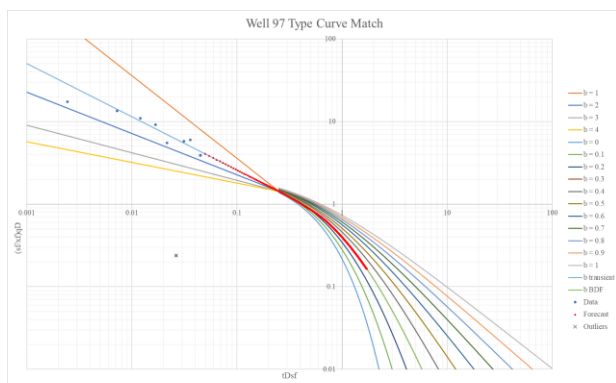


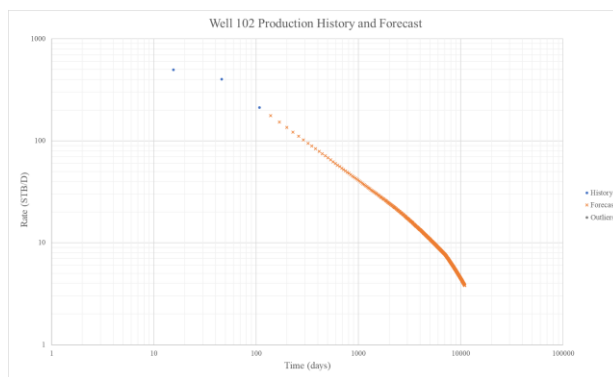
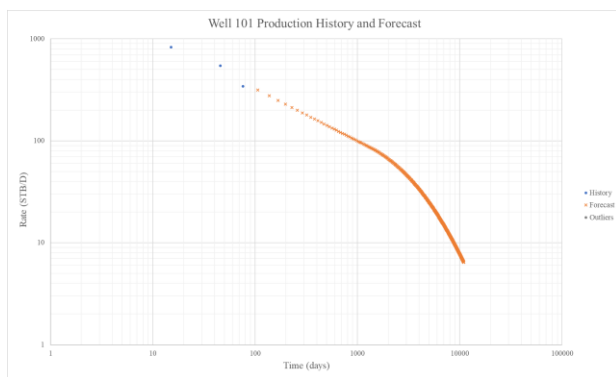
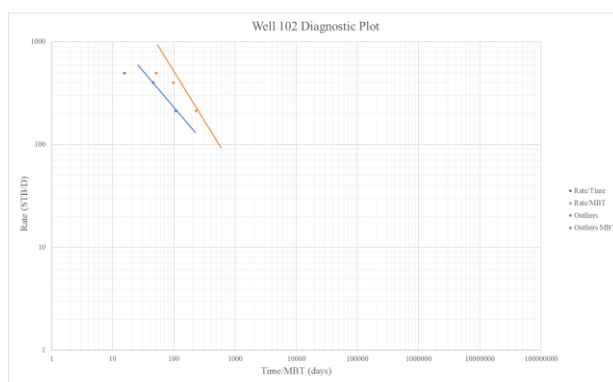
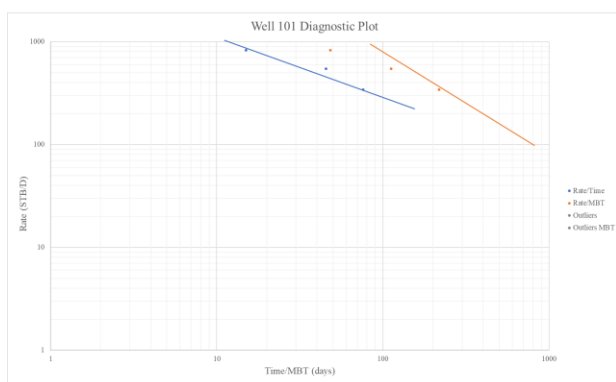
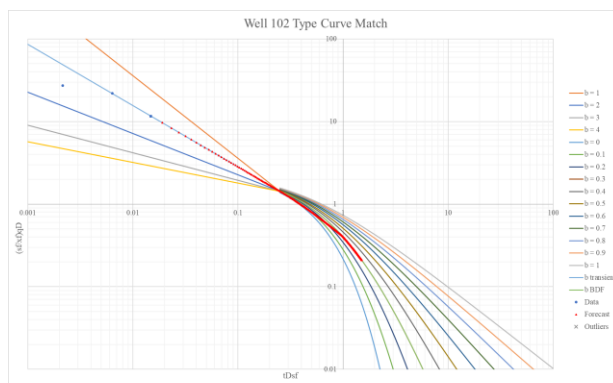
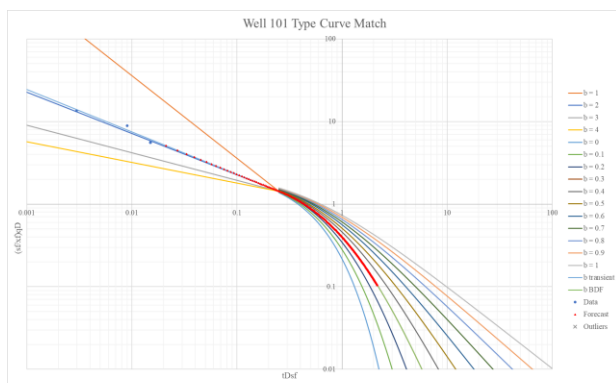


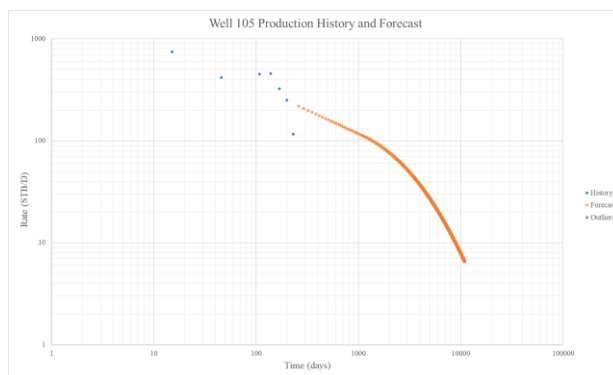
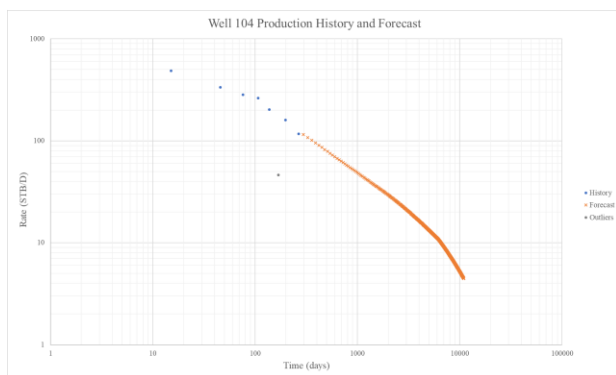
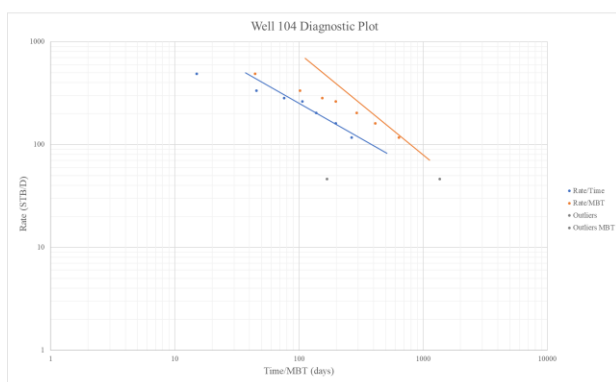
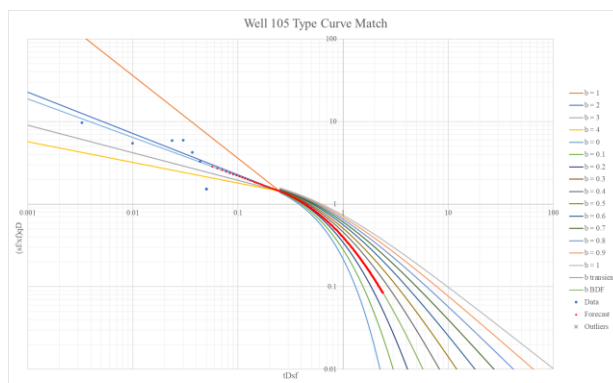
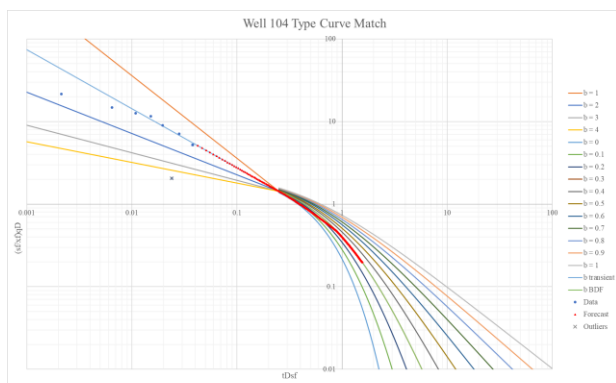


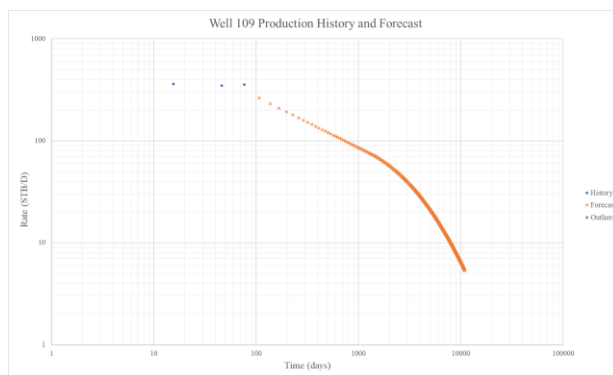
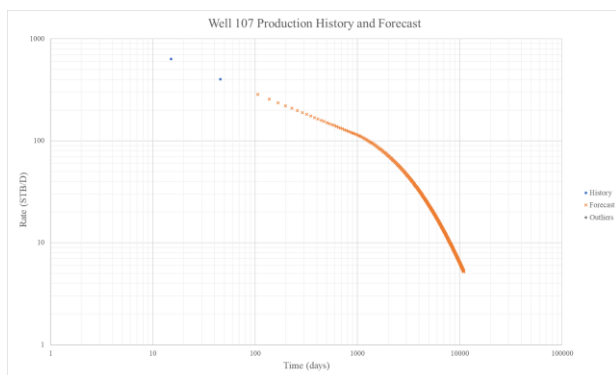
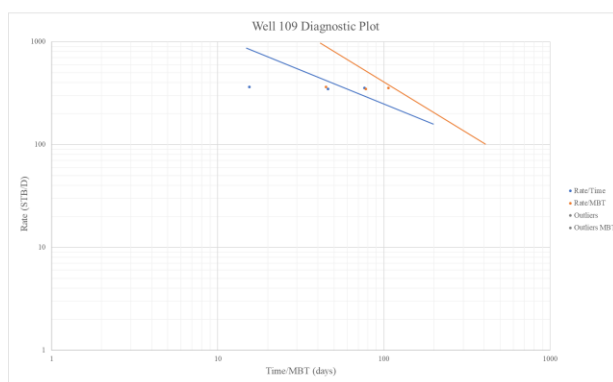
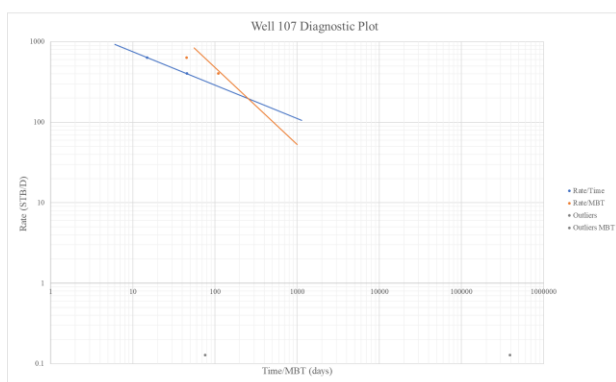
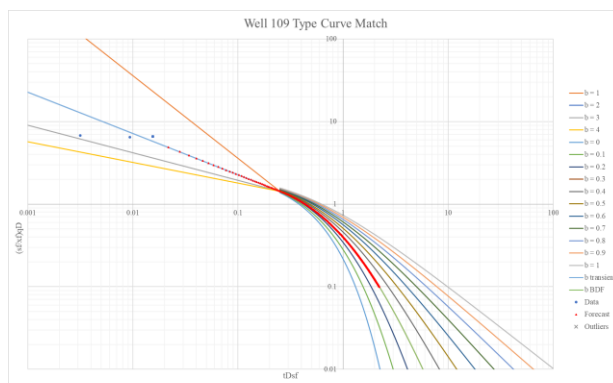
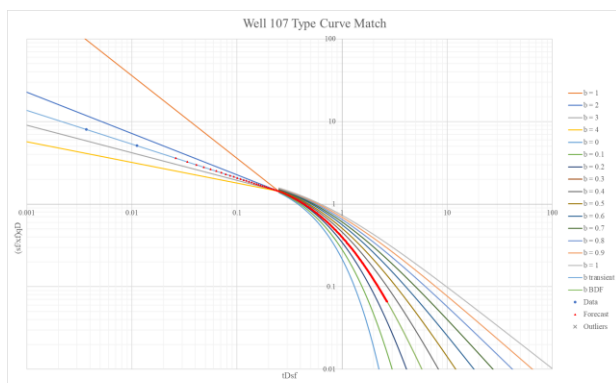


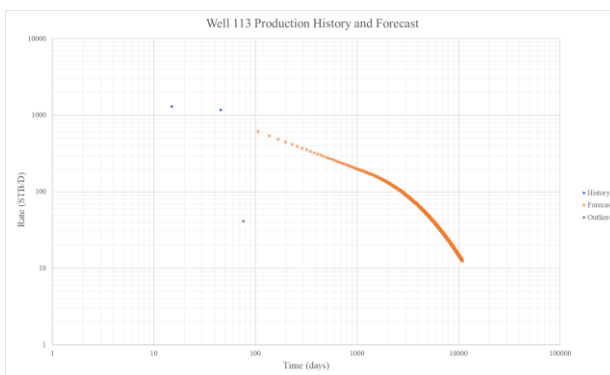
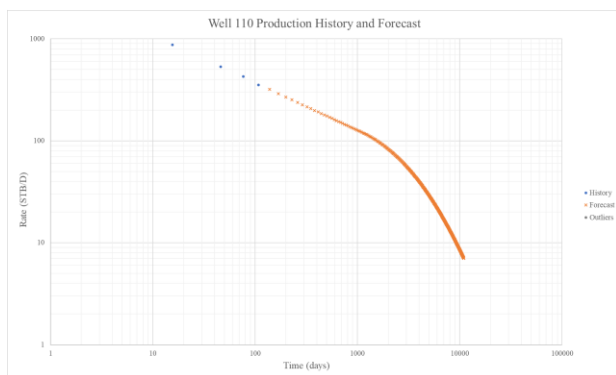
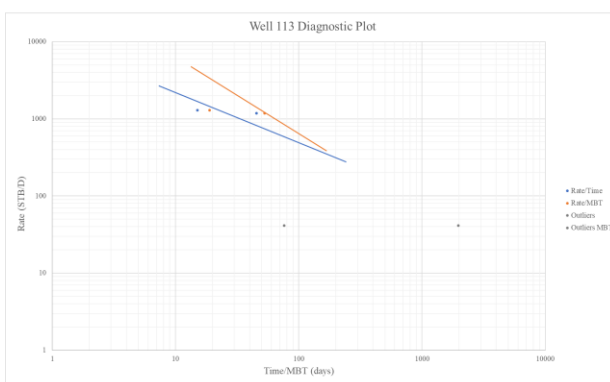
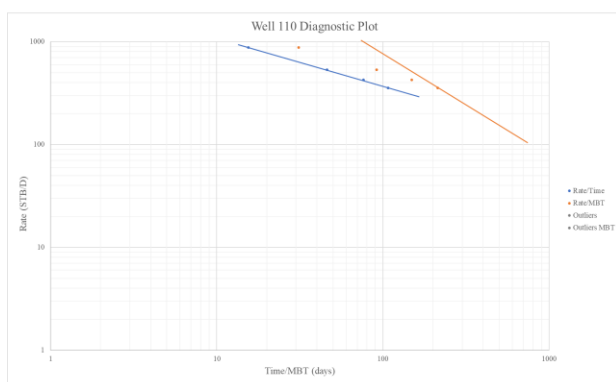
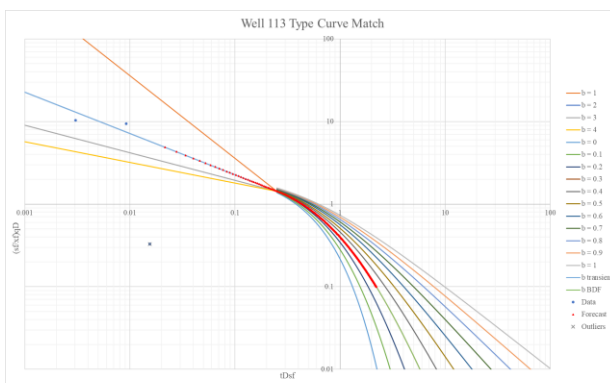
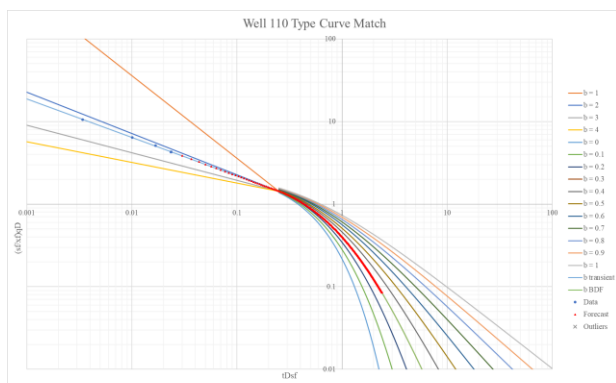


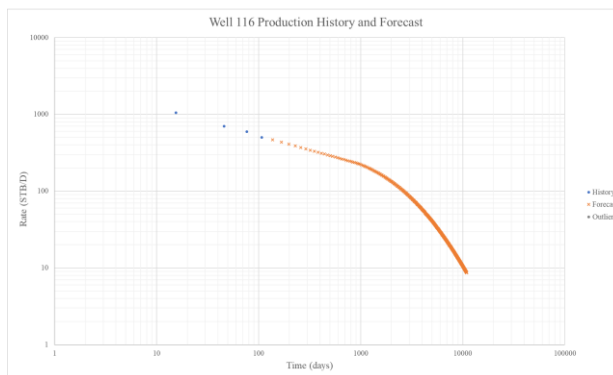
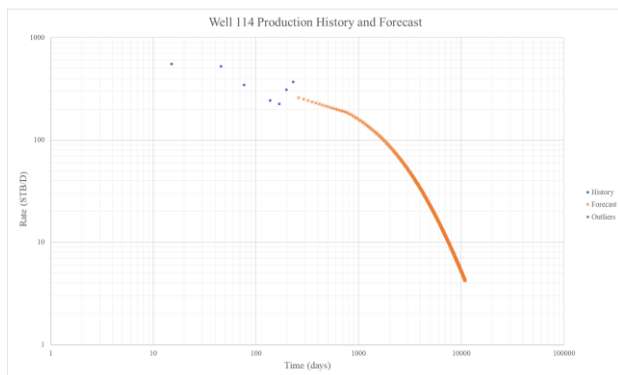
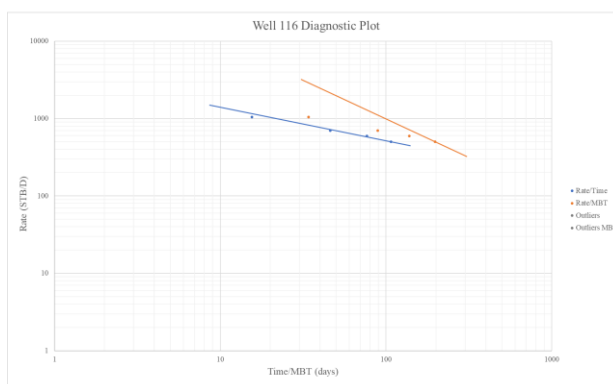
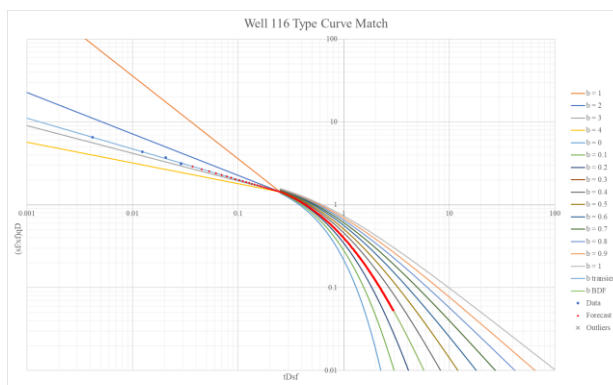
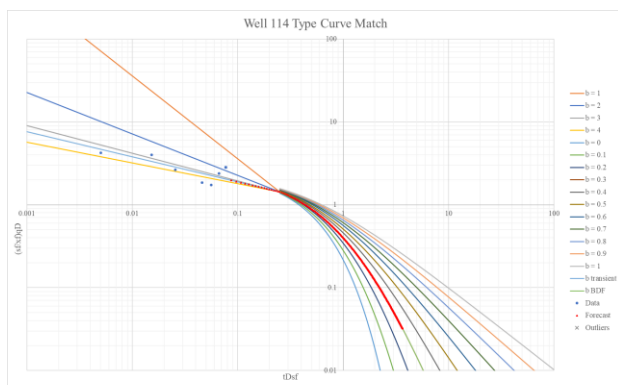


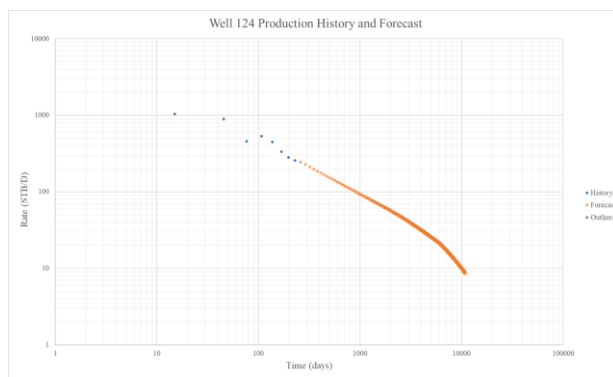
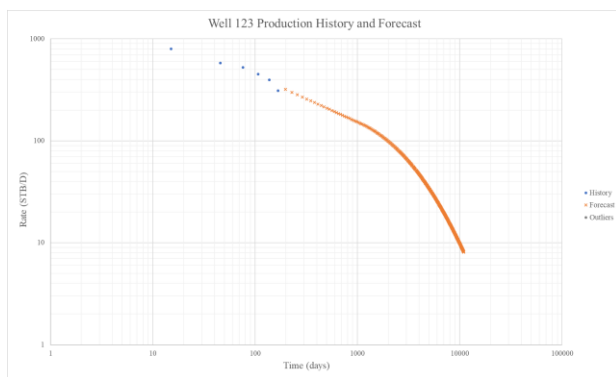
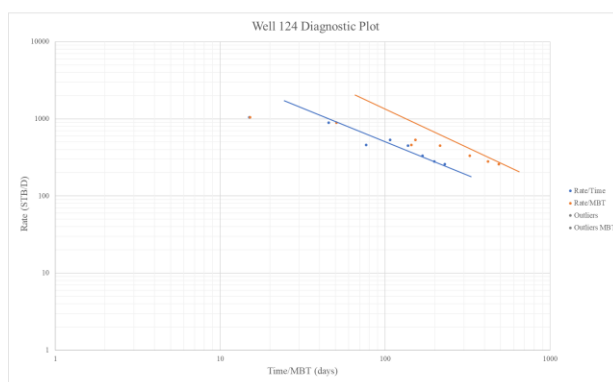
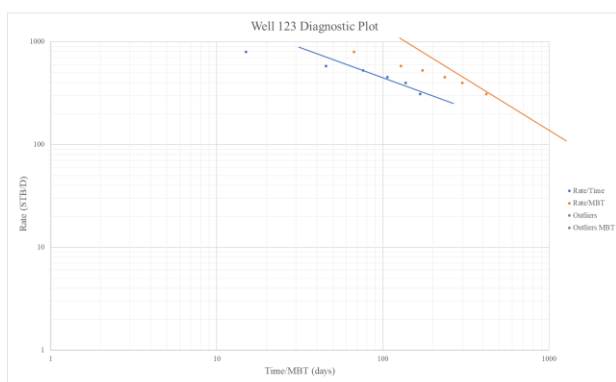
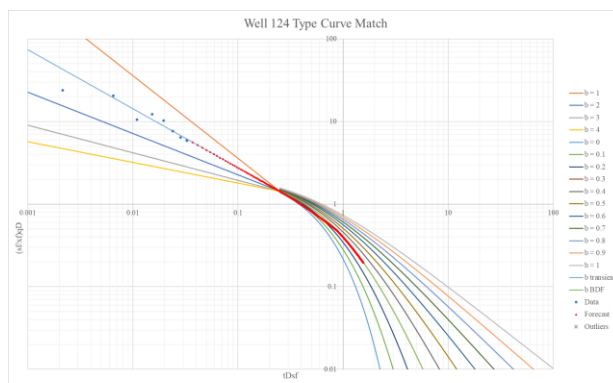
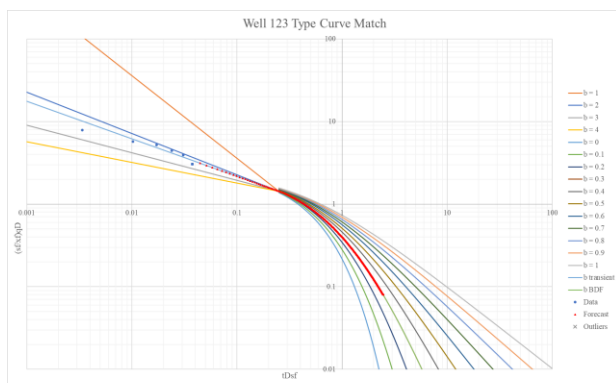


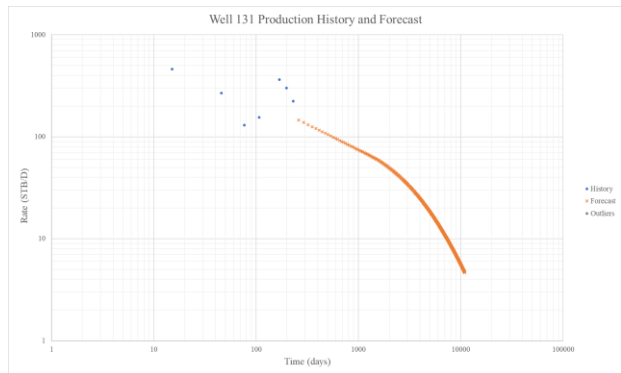
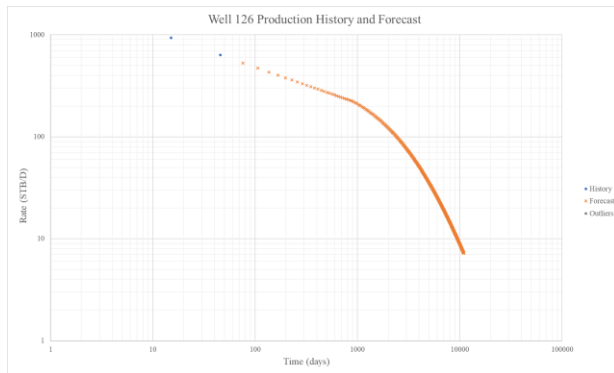
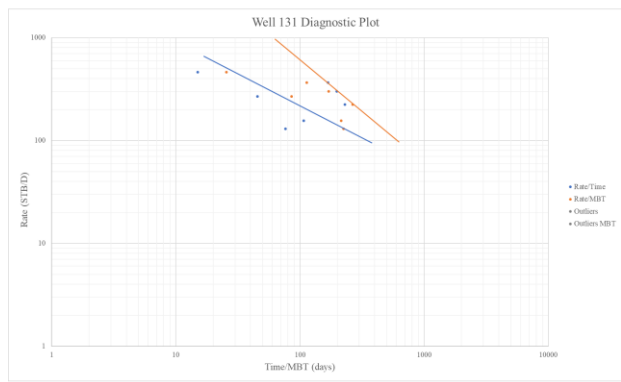
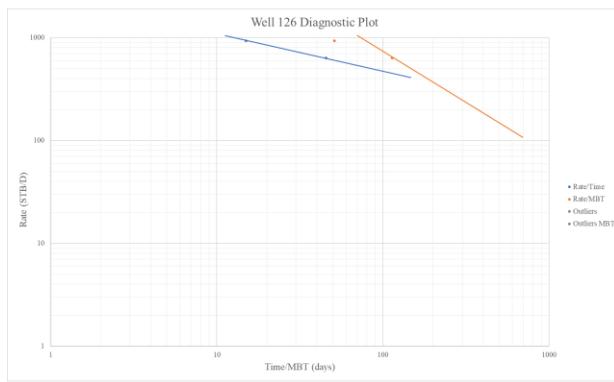
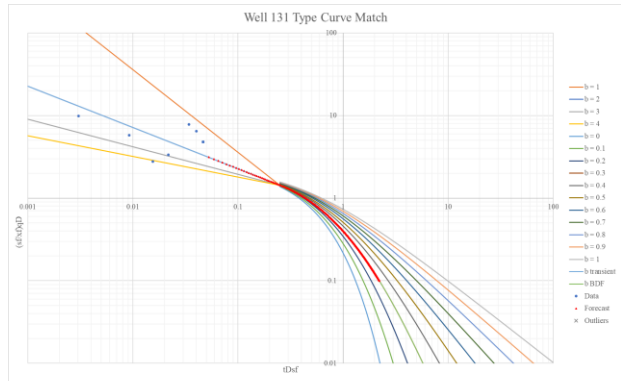
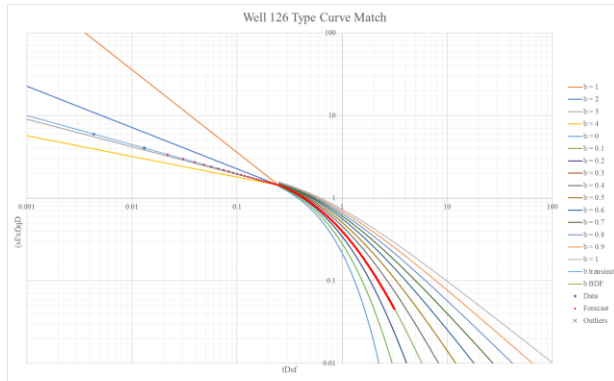


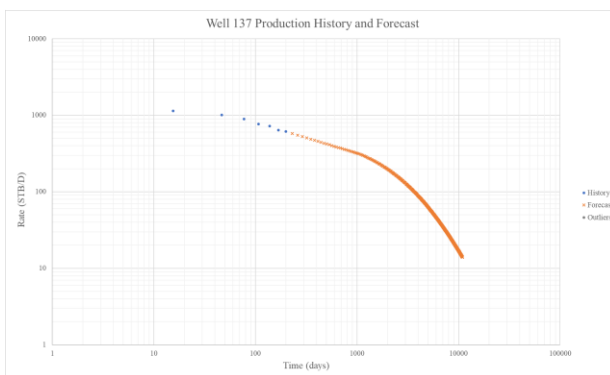
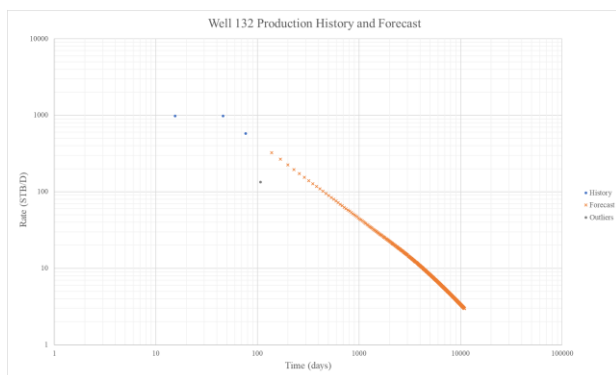
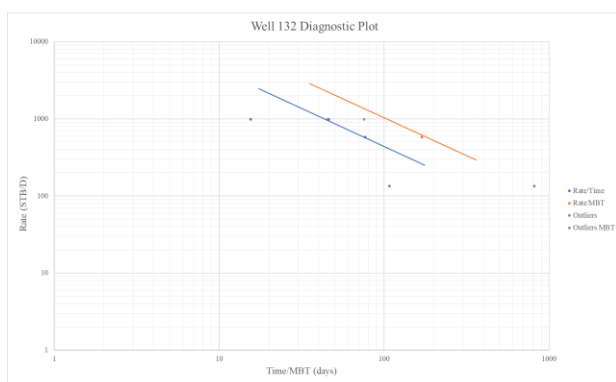
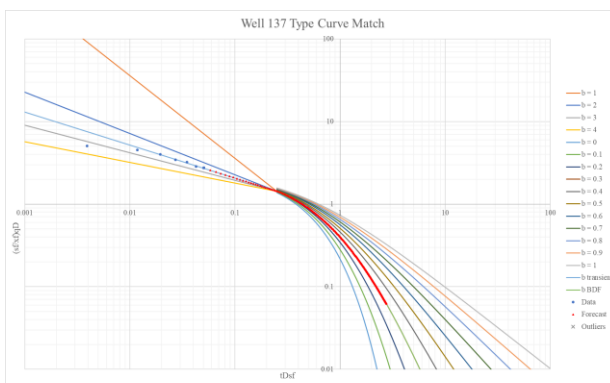
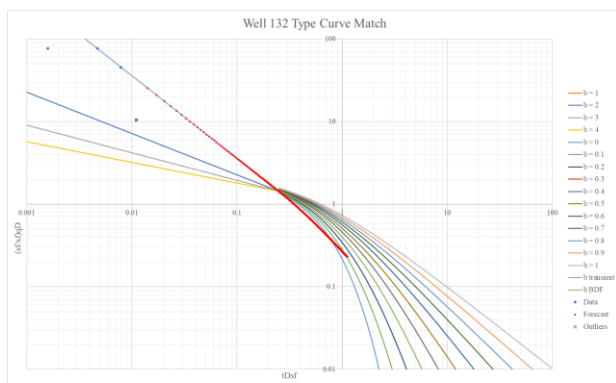


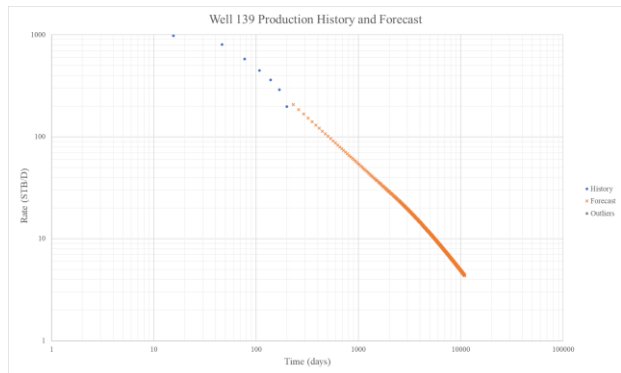
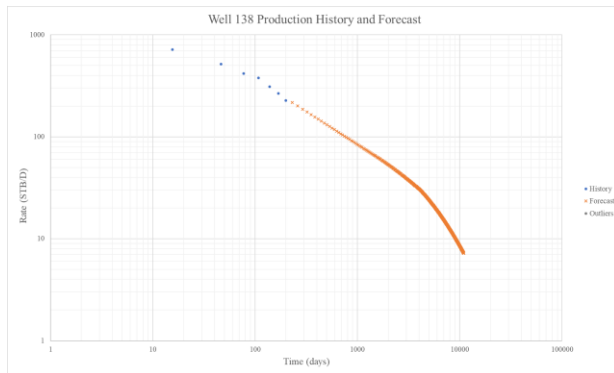
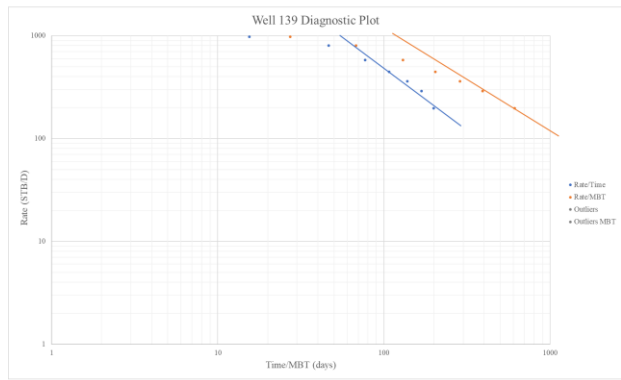
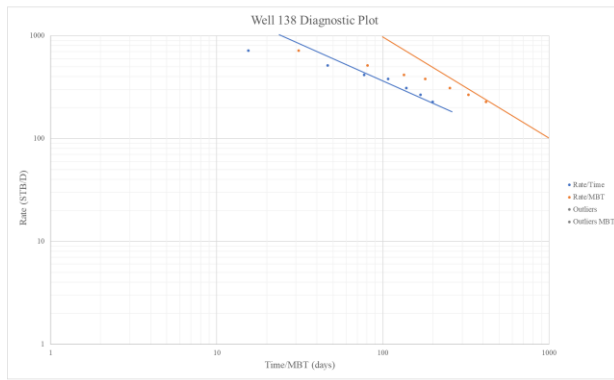
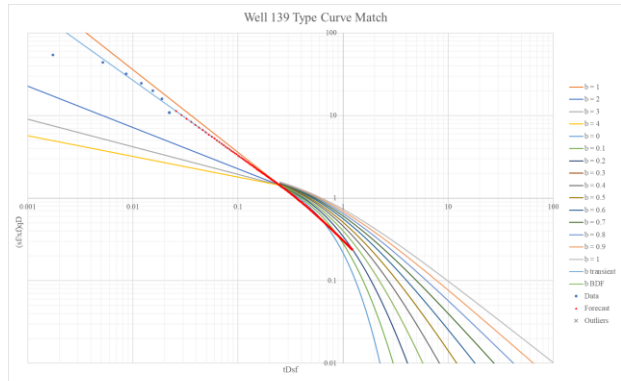
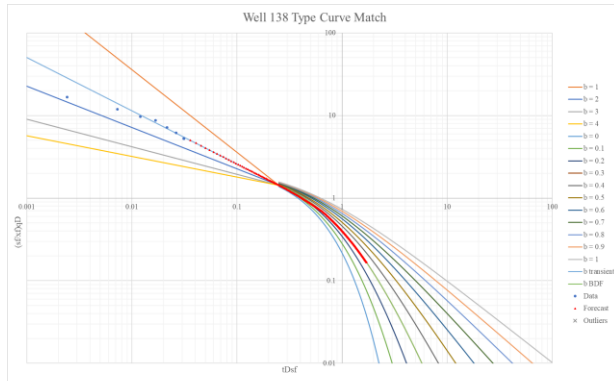


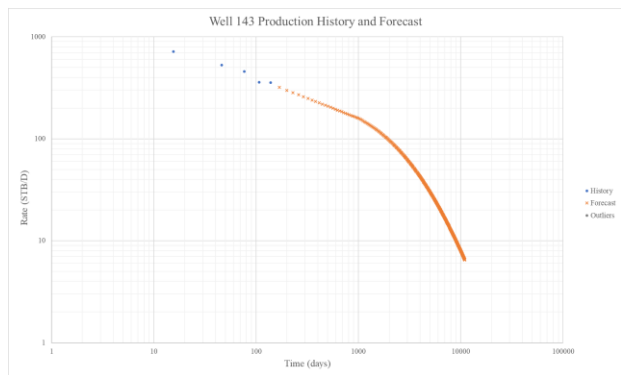
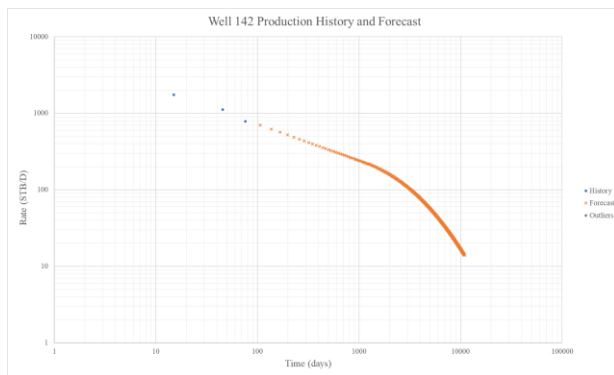
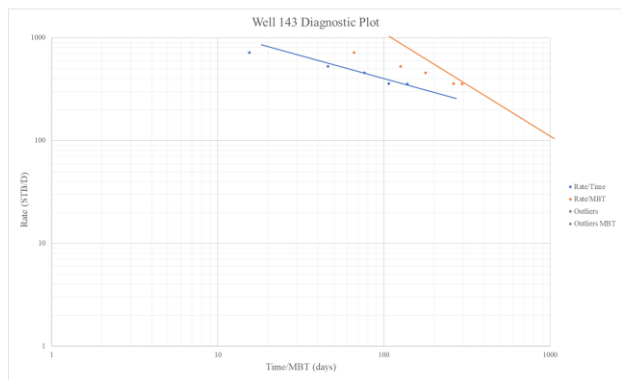
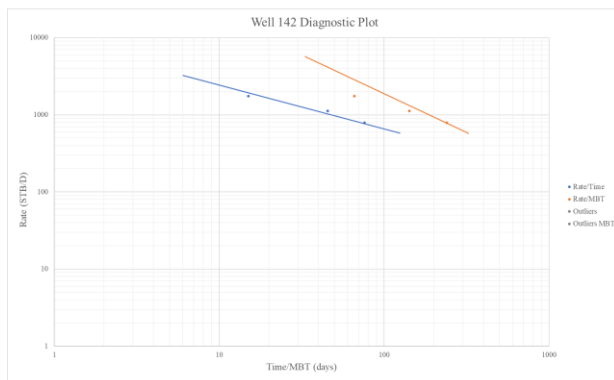
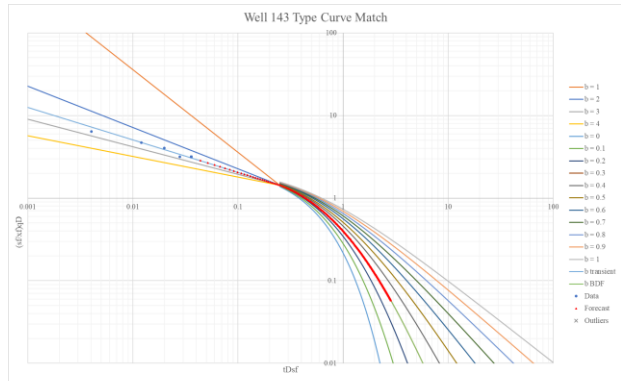
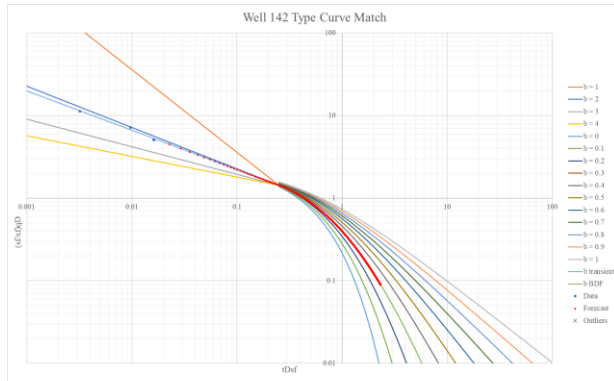












Well	1	2	4	5	8	9	10	11	12	15	17	23	26	27	28
μ , cP	0.55	0.58	0.50	0.60	0.60	0.60	0.60	0.65	0.65	0.55	0.55	0.55	0.60	0.60	0.58
B, RB/STB	1.35	1.34	1.35	1.35	1.35	1.35	1.35	1.35	1.35	1.35	1.35	1.35	1.35	1.35	1.35
φ	0.09	0.11	0.07	0.09	0.10	0.11	0.10	0.10	0.12	0.11	0.07	0.08	0.12	0.12	0.10
h , ft	200	200	200	200	150	200	200	200	200	200	200	200	200	150	200
c_r , psi ⁻¹	1.75E-05	1.85E-05	1.50E-05	1.70E-05	1.80E-05	1.90E-05	1.75E-05	1.90E-05	1.95E-05	1.85E-05	1.60E-05	1.70E-05	1.90E-05	1.90E-05	1.80E-05
L_w , ft	6940	9498	9524	9776	6970	7508	9146	4562	7168	7284	9686	6448	10244	7535	7731
s_F , ft	250	225	200	250	250	200	300	200	200	200	250	200	250	300	250
Δp , psi	2500	2850	2500	2750	2250	2000	2500	2500	2250	2500	2900	2750	2250	1950	2750
D_{min} , year ⁻¹	0.15	0.15	0.15	0.15	0.15	0.15	0.15	0.15	0.15	0.15	0.15	0.15	0.15	0.15	0.15
History, days	230	249	77	138	169	77	169	138	77	138	322	320	291	200	77
b_{TR}	2.15	1.80	2.50	1.60	1.35	3.45	2.45	1.75	2.60	1.95	1.40	2.20	2.05	1.20	2.15
b_{BDF}	0.30	0.30	0.30	0.30	0.30	0.30	0.30	0.30	0.30	0.30	0.30	0.30	0.30	0.30	0.30
$t_{transition}$, years	3.1	3.8	2.7	4.2	5.0	2.0	2.8	3.9	2.6	3.5	4.8	3.0	3.3	5.6	3.1
t_{BDF} , years	3.5	5.9	2.9	9.5	19.4	2.0	3.0	6.6	2.8	4.3	16.8	3.3	3.8	32.9	3.5
TMP	2.19E-04	1.82E-04	2.53E-04	1.63E-04	1.38E-04	3.49E-04	2.45E-04	1.77E-04	2.61E-04	1.98E-04	1.43E-04	2.25E-04	2.08E-04	1.22E-04	2.19E-04
RMP	1.65E-02	8.46E-03	1.74E-02	2.05E-02	4.06E-02	7.53E-03	8.56E-03	2.30E-02	6.78E-03	1.22E-02	2.20E-02	1.64E-02	6.68E-03	4.43E-02	1.10E-02
k , mD	4.42E-04	4.29E-04	2.10E-04	3.68E-04	3.68E-04	6.92E-04	9.14E-04	3.44E-04	6.26E-04	3.50E-04	2.17E-04	2.66E-04	7.01E-04	5.91E-04	5.59E-04
x_f , ft	260.3	282.9	220.0	176.2	204.2	293.5	288.4	275.2	363.0	270.8	245.6	272.3	331.9	179.1	262.1
t'	0.88	1.06	0.66	0.74	0.74	2.16	1.27	1.08	1.96	1.09	0.43	0.83	1.40	0.82	1.12
q'	1.43	0.71	1.67	1.64	3.24	0.60	0.68	1.69	0.50	1.06	1.91	1.43	0.53	3.53	0.92
EUR, MSTB	432.9	991.8	339.9	489.4	324.3	552.1	723.2	402.8	841.2	625.4	526.6	430.4	1091.8	349.4	611.5
Scaled EUR, MSTB	556.5	733.8	385.0	617.2	808.9	645.1	607.1	725.5	731.9	715.4	482.8	520.5	769.8	1046.3	617.4

Well	31	33	34	37	39	40	43	44	47	48	50	52	54	55	56
μ , cP	0.60	0.60	0.62	0.65	0.55	0.50	0.65	0.55	0.55	0.60	0.50	0.50	0.50	0.60	0.55
B, RB/STB	1.35	1.40	1.35	1.35	1.35	1.35	1.34	1.35	1.35	1.35	1.35	1.35	1.35	1.35	1.35
φ	0.09	0.07	0.12	0.12	0.07	0.08	0.12	0.07	0.07	0.11	0.07	0.07	0.12	0.12	0.10
h , ft	200	200	200	200	200	200	200	100	200	200	150	200	200	200	200
c_r , psi ⁻¹	1.85E-05	1.65E-05	1.90E-05	1.95E-05	1.60E-05	1.55E-05	1.95E-05	1.40E-05	1.40E-05	1.85E-05	1.40E-05	1.40E-05	1.95E-05	1.80E-05	1.85E-05
L_w , ft	8000	7356	4498	7291	9463	9515	9500	9088	9552	10401	9789	9567	7449	6938	7260
s_F , ft	250	225	250	200	200	200	200	300	300	200	300	200	200	250	250
Δp , psi	2700	3500	2500	2250	3500	3500	2000	2925	2925	2750	2925	2925	3000	2750	2750
D_{min} , year ⁻¹	0.15	0.15	0.15	0.15	0.15	0.15	0.15	0.15	0.15	0.15	0.15	0.15	0.15	0.15	0.15
History, days	261	138	276	138	108	107	108	200	236	200	107	76	230	260	230
b_{TR}	1.50	1.65	1.85	2.05	2.75	2.00	2.55	1.95	1.25	2.05	1.35	4.00	4.00	2.45	2.25
b_{BDF}	0.30	0.30	0.30	0.30	0.30	0.30	0.30	0.30	0.30	0.30	0.30	0.30	0.30	0.30	0.30
$t_{transition}$, years	4.5	4.0	3.7	3.3	2.5	3.4	2.6	3.5	5.4	3.3	5.0	1.7	1.7	2.8	3.0
t_{BDF} , years	12.3	8.0	5.3	3.8	2.6	4.0	2.8	4.3	27.5	3.8	19.4	1.7	1.8	3.0	3.2
TMP	1.53E-04	1.69E-04	1.86E-04	2.08E-04	2.78E-04	2.03E-04	2.60E-04	1.98E-04	1.27E-04	2.08E-04	1.38E-04	4.01E-04	4.00E-04	2.45E-04	2.31E-04
RMP	1.65E-02	1.95E-02	1.32E-02	8.28E-03	8.32E-03	1.20E-02	5.27E-03	5.74E-02	3.37E-02	7.81E-03	5.64E-02	8.68E-03	3.79E-03	6.87E-03	9.92E-03
k , mD	3.57E-04	2.35E-04	6.50E-04	4.99E-04	2.71E-04	1.99E-04	6.26E-04	3.79E-04	2.43E-04	3.82E-04	2.39E-04	3.09E-04	7.36E-04	7.84E-04	5.80E-04
x_F , ft	281.9	254.4	382.8	366.8	282.0	241.8	392.3	163.8	206.6	268.6	147.9	253.7	305.5	349.1	286.0
t'	0.71	0.58	1.30	1.56	0.85	0.62	1.96	0.53	0.34	1.20	0.33	0.97	2.30	1.57	1.16
q'	1.31	1.51	1.02	0.61	0.72	1.14	0.39	4.99	2.94	0.62	5.41	0.83	0.36	0.55	0.86
EUR, MSTB	699.7	500.0	625.1	902.3	632.3	598.2	1081.0	139.3	419.4	952.0	246.3	420.1	895.1	909.2	684.1
Scaled EUR, MSTB	688.4	465.8	792.1	791.6	393.4	448.7	738.7	389.7	468.2	689.7	492.0	339.3	673.3	728.2	671.8

Well	57	64	66	67	71	72	73	74	76	79	81	82	85	86	87
μ , cP	0.60	0.60	0.60	0.55	0.53	0.65	0.65	0.50	0.55	0.58	0.50	0.55	0.60	0.55	0.50
B, RB/STB	1.35	1.34	1.35	1.35	1.35	1.35	1.35	1.35	1.35	1.35	1.35	1.35	1.35	1.34	1.34
φ	0.07	0.12	0.09	0.07	0.09	0.07	0.10	0.07	0.08	0.11	0.12	0.11	0.09	0.11	0.12
h , ft	200	200	200	200	200	200	200	200	200	200	200	200	200	200	200
c_t , psi ⁻¹	1.70E-05	1.95E-05	1.80E-05	1.65E-05	1.60E-05	1.95E-05	1.85E-05	1.40E-05	1.55E-05	1.75E-05	1.95E-05	1.85E-05	1.80E-05	1.85E-05	1.95E-05
L_w , ft	7502	6914	7271	10515	9782	9429	9665	6902	8009	9587	9644	4638	7610	6764	8000
s_F , ft	225	200	275	225	200	300	200	300	225	250	200	200	250	250	200
Δp , psi	2900	2250	2750	3000	3250	1900	3000	2925	3250	2750	2000	2500	2500	2250	2500
D_{min} , year ⁻¹	0.15	0.15	0.15	0.15	0.15	0.15	0.15	0.15	0.15	0.15	0.15	0.15	0.15	0.15	0.15
History, days	77	200	138	322	76	107	230	169	174	291	46	77	200	230	175
b_{TR}	1.60	1.92	2.00	2.10	2.85	1.20	2.00	2.30	2.75	1.70	3.75	2.00	1.70	2.50	3.35
b_{BDF}	0.30	0.30	0.30	0.30	0.30	0.30	0.30	0.30	0.30	0.30	0.30	0.30	0.30	0.30	0.30
$t_{transition}$, years	4.2	3.5	3.4	3.2	2.4	5.6	3.4	3.0	2.5	4.0	1.8	3.4	4.0	2.7	2.1
t_{BDF} , years	9.5	4.7	4.0	3.6	2.5	32.8	4.0	3.2	2.6	7.3	1.8	4.0	7.3	2.9	2.1
TMP	1.63E-04	1.93E-04	2.03E-04	2.13E-04	2.88E-04	1.22E-04	2.03E-04	2.31E-04	2.76E-04	1.73E-04	3.82E-04	2.03E-04	1.73E-04	2.52E-04	3.32E-04
RMP	1.92E-02	1.01E-02	1.55E-02	1.10E-02	6.14E-03	5.93E-02	1.03E-02	1.87E-02	1.23E-02	1.13E-02	3.73E-03	1.98E-02	1.62E-02	1.25E-02	3.19E-03
k , mD	2.32E-04	4.28E-04	5.89E-04	2.71E-04	3.44E-04	3.84E-04	3.85E-04	4.01E-04	3.77E-04	4.54E-04	7.03E-04	3.58E-04	4.14E-04	6.97E-04	6.13E-04
x_F , ft	298.9	336.2	238.0	283.4	298.9	137.2	217.3	283.0	220.4	256.1	376.2	255.3	280.6	245.6	483.4
t'	0.57	1.34	0.97	0.67	1.08	0.53	1.20	0.56	0.93	0.91	2.20	1.12	0.83	1.40	1.92
q'	1.53	0.82	1.24	0.96	0.56	4.37	0.75	1.80	1.07	0.93	0.36	1.72	1.29	1.10	0.31
EUR, MSTB	525.1	782.3	480.7	625.2	831.1	269.0	706.4	326.4	429.7	788.6	1037.7	393.0	579.5	495.2	1310.8
Scaled EUR, MSTB	494.7	811.9	580.2	418.4	496.7	680.5	621.9	344.9	431.7	678.5	743.7	746.9	638.1	724.0	708.4

Well	91	94	95	97	98	101	102	104	105	107	109	110	113	114	116
μ , cP	0.50	0.65	0.60	0.60	0.50	0.55	0.65	0.65	0.50	0.60	0.65	0.58	0.65	0.55	0.60
B, RB/STB	1.35	1.34	1.34	1.35	1.35	1.35	1.35	1.35	1.35	1.35	1.35	1.35	1.34	1.35	1.34
ϕ	0.07	0.12	0.11	0.11	0.07	0.08	0.07	0.07	0.07	0.07	0.08	0.12	0.12	0.11	0.12
h , ft	200	200	200	200	200	200	150	200	200	200	200	200	200	200	200
c_r , psi ⁻¹	1.40E-05	1.95E-05	1.90E-05	1.90E-05	1.60E-05	1.55E-05	1.80E-05	1.40E-05	1.40E-05	1.65E-05	1.80E-05	1.95E-05	1.95E-05	1.85E-05	1.88E-05
L_w , ft	10289	7283	8000	7167	9685	7963	9607	7106	10819	9688	9737	5880	8000	6924	9601
s_F , ft	300	225	200	250	225	200	300	275	300	250	200	225	200	250	200
Δp , psi	2925	2250	2500	2300	3250	3100	1850	2925	2925	2500	2600	2250	2200	2600	2250
D_{min} , year ⁻¹	0.15	0.15	0.15	0.15	0.15	0.15	0.15	0.15	0.15	0.15	0.15	0.15	0.15	0.15	0.15
History, days	71	169	169	287	138	76	108	266	230	76	77	108	76	230	107
b_{TR}	1.50	2.75	2.10	1.55	2.15	1.95	1.35	1.40	2.15	2.45	2.00	2.15	2.00	3.30	2.70
b_{BDF}	0.30	0.30	0.30	0.30	0.30	0.30	0.30	0.30	0.30	0.30	0.30	0.30	0.30	0.30	0.30
$t_{transition}$, years	4.5	2.5	3.2	4.4	3.1	3.5	5.0	4.8	3.1	2.8	3.4	3.1	3.4	2.0	2.5
t_{BDF} , years	13.0	2.6	3.6	11.1	3.5	4.3	19.4	16.9	3.5	3.0	4.0	3.5	4.0	2.1	2.7
TMP	1.51E-04	2.78E-04	2.13E-04	1.57E-04	2.19E-04	1.98E-04	1.38E-04	1.42E-04	2.19E-04	2.45E-04	2.03E-04	2.19E-04	2.03E-04	3.35E-04	2.69E-04
RMP	2.72E-02	6.18E-03	9.03E-03	1.48E-02	1.10E-02	1.63E-02	5.46E-02	4.43E-02	1.31E-02	1.27E-02	1.87E-02	1.20E-02	7.98E-03	7.65E-03	6.22E-03
k , mD	2.62E-04	8.46E-04	4.22E-04	4.63E-04	2.44E-04	2.13E-04	4.02E-04	2.71E-04	3.79E-04	4.19E-04	3.00E-04	5.94E-04	4.87E-04	9.25E-04	5.52E-04
x_F , ft	199.4	363.8	297.6	317.3	285.0	245.8	191.3	188.7	273.4	278.0	175.6	296.7	359.5	257.9	306.2
t'	0.36	2.09	1.32	0.93	0.60	0.67	0.56	0.45	0.53	0.84	0.94	1.47	1.52	1.85	1.72
q'	2.62	0.46	0.73	1.18	1.06	1.41	4.02	3.26	1.25	1.01	1.37	0.99	0.59	0.67	0.50
EUR, MSTB	426.3	887.3	813.8	692.1	641.8	504.1	236.6	271.3	552.3	485.3	400.6	579.6	929.7	560.2	883.1
Scaled EUR, MSTB	448.3	754.9	748.5	767.2	429.6	497.0	573.3	435.3	385.8	420.0	520.2	792.1	776.6	637.3	702.1

Well	123	124	126	131	132	137	138	139	142	143
μ , cP	0.55	0.55	0.60	0.50	0.65	0.65	0.55	0.55	0.60	0.60
B, RB/STB	1.34	1.35	1.35	1.35	1.37	1.34	1.35	1.35	1.34	1.35
ϕ	0.10	0.08	0.11	0.07	0.12	0.12	0.09	0.07	0.12	0.11
h, ft	200	200	200	200	200	200	200	200	200	200
c_t , psi ⁻¹	1.80E-05	1.75E-05	1.90E-05	1.40E-05	1.95E-05	1.95E-05	1.65E-05	1.55E-05	1.95E-05	1.85E-05
L_w , ft	8021	8004	9380	7943	7452	10443	6958	7743	9419	9607
s_F , ft	200	250	200	300	300	200	250	300	200	250
Δp , psi	2500	2750	2250	3150	1750	2500	2900	3000	2150	2350
D_{min} , year ⁻¹	0.15	0.15	0.15	0.15	0.15	0.15	0.15	0.15	0.15	0.15
History, days	168	230	46	230	108	200	200	200	76	138
b_{TR}	2.20	1.40	2.85	2.00	1.00	2.50	1.55	1.10	2.10	2.55
b_{BDF}	0.30	0.30	0.30	0.30	0.30	0.30	0.30	0.30	0.30	0.30
$t_{transition}$, years	3.0	4.8	2.4	3.4	6.7	2.7	4.4	6.1	3.2	2.6
t_{BDF} , years	3.3	16.7	2.5	4.0	72.6	2.9	11.2	47.6	3.6	2.8
TMP	2.25E-04	1.43E-04	2.88E-04	2.03E-04	1.02E-04	2.52E-04	1.56E-04	1.12E-04	2.13E-04	2.60E-04
RMP	9.86E-03	2.29E-02	6.37E-03	2.14E-02	7.81E-02	4.46E-03	2.31E-02	5.51E-02	6.42E-03	8.89E-03
k, mD	3.52E-04	2.71E-04	5.71E-04	3.52E-04	5.51E-04	6.06E-04	3.15E-04	2.37E-04	4.73E-04	7.49E-04
x_F , ft	299.1	240.4	299.1	227.6	100.7	348.3	223.6	156.2	369.3	238.4
t'	1.10	0.54	1.79	0.49	0.77	1.90	0.63	0.33	1.48	1.50
q'	0.87	1.99	0.51	2.06	5.69	0.33	2.01	4.79	0.52	0.71
EUR, MSTB	708.1	514.9	821.0	345.5	318.2	1318.2	451.9	335.8	1185.7	662.3
Scaled EUR, MSTB	666.9	603.9	684.5	371.5	1386.5	741.4	610.0	591.8	851.1	664.8

APPENDIX B

Derivation of Eq. 2.4

Wattenbarger's "short-term" approximation (1998) is given by

$$\frac{1}{q_D} = \frac{\pi}{2} \sqrt{\pi \left(\frac{y_e}{x_f} \right)^2 t_{Dye}} \quad (\text{B-1})$$

Rearranging Eq. B-1 and substituting in q_{Ds_f} for q_D , t_{Ds_f} for t_{Dye} , and $s_f/2$ for y_e , we arrive upon the equation for the transient stem corresponding to $b_{TR} = 2$:

$$\left(\frac{s_f}{x_f} \right) q_D = \left(\frac{4}{\pi^{1.5}} \right) (t_{Ds_f})^{-0.5} \quad (\text{B-2})$$

Taking the logarithm of both sides and splitting terms yields

$$\log \left(\left(\frac{s_f}{x_f} \right) q_D \right) = \log \left(\frac{4}{\pi^{1.5}} \right) - \frac{1}{2} \log (t_{Ds_f}) \quad (\text{B-3})$$

which is the equation of a logarithmic negative half-slope straight line. Observing that the slope of the logarithmic straight line is equal to $-1/b_{TR}$, the general equation for the transient stems is given by

$$\log\left(\left(\frac{s_f}{x_f}\right) q_D\right) = \log(c_1) - \frac{1}{b_{TR}} \log(t_{Dsf}) \quad (\text{B-3})$$

where c_1 is a currently unknown constant but can be solved for by forcing all transient stems to converge at a given point. Defining $t_{Dsf,Con}$ as dimensionless time at which all transient stems converge, the corresponding dimensionless convergence rate can be determined by equating Eqs. B-2 and B-3:

$$\log\left(\frac{4}{\pi^{1.5}}\right) - \frac{1}{2} \log(t_{Dsf,Con}) = \log(c_1) - \frac{1}{b_{TR}} \log(t_{Dsf,Con}) \quad (\text{B-5})$$

Rearranging Eq. B-4 to solve for $\log(c_1)$,

$$\log(c_1) = \log\left(\frac{4}{\pi^{1.5}}\right) + \left(\frac{1}{b_{TR}} - \frac{1}{2}\right) \log(t_{Dsf,Con}) \quad (\text{B-6})$$

Substituting Eq. B-6 into Eq. B-3 and solving for $(s_f/x_f)q_D$, we arrive upon the general equation for the transient stems in terms of an arbitrary dimensionless convergence time:

$$\left(\frac{s_f}{x_f}\right) q_D = \left(\frac{4}{\pi^{1.5}}\right) (t_{Dsf,Con})^{\frac{1}{b_{TR}} - \frac{1}{2}} (t_{Dsf})^{-\frac{1}{b_{TR}}} \quad (\text{B-7})$$

Per Wattenbarger, transient flow concludes at a dimensionless time of 0.25 (1998). Substituting this value into Eq. B-7, we arrive upon Eq. 2.4, the final form of the general equation for the transient stems:

$$\left(\frac{s_f}{x_f}\right) q_D = \left(\frac{4}{\pi^{1.5}}\right) (0.25)^{\frac{1}{b_{TR}} - \frac{1}{2}} (t_{Ds f})^{-\frac{1}{b_{TR}}} \quad (2.4)$$

Derivation of Eq. 2.9

Wattenbarger's long-term approximation (1998), describing the period of exponential decline following the end of transient flow, is given by

$$\frac{1}{q_D} = \frac{\pi}{4} \exp\left(\frac{\pi^2}{4} t_{Dye}\right) \quad (B-8)$$

Rearranging and substituting in $q_{Ds f}$ for q_D , $t_{Ds f}$ for t_{Dye} , and $s_f/2$ for y_e , we arrive upon the equation for the BDF stem corresponding to $b = 0$:

$$\left(\frac{s_f}{x_f}\right) q_D = \frac{8}{\pi} \exp\left(-\frac{\pi^2}{4} t_{Ds f}\right) \quad (B-9)$$

It is assumed that the form of the hyperbolic BDF stems is similar to Arps' definition. Under this assumption, the general form is given by

$$\left(\frac{s_f}{x_f}\right) q_D = c_1 / (1 + c_2 b_{BDF} t_{DSf})^{\frac{1}{b_{BDF}}} \quad (\text{B-10})$$

For this equation to be valid, it must equal Eq. B-9 in the limit as b_{BDF} goes to zero. Evaluating this limit,

$$\lim_{b_{BDF} \rightarrow 0} \left(\frac{s_f}{x_f}\right) q_D = c_1 \exp(-c_2 t_{DSf}) \quad (\text{B-11})$$

In order to solve for the two unknown constants, c_1 and c_2 , we must provide another set of equations. Taking the derivative with respect to t_{DSf} of both Eq. B-9 and Eq. B-10 yields, respectively

$$\frac{d\left[\left(\frac{s_f}{x_f}\right) q_D\right]}{dt_{DSf}} = \left(-\frac{\pi^2}{4}\right) \left(\frac{8}{\pi}\right) \exp\left(-\frac{\pi^2}{4} t_{DSf}\right) \quad (\text{B-12})$$

and

$$\frac{d\left[\left(\frac{s_f}{x_f}\right) q_D\right]}{dt_{DSf}} = -c_1 c_2 / (1 + c_2 b_{BDF} t_{DSf})^{1 + \frac{1}{b_{BDF}}} \quad (\text{B-13})$$

Again, for Eq. B-10 to be valid, Eq. B-13 must equal Eq. B-12 in the limit as b_{BDF} goes to zero.

Evaluating this limit,

$$\lim_{b_{BDF} \rightarrow 0} \frac{d \left[\left(\frac{s_f}{x_f} \right) q_{Dsf} \right]}{dt_{Dsf}} = -c_1 c_2 \exp(-c_2 t_{Dsf}) \quad (\text{B-14})$$

Equating Eqs. B-12 and B-14

$$-c_1 c_2 \exp(-c_2 t_{Dsf}) = \left(-\frac{\pi^2}{4} \right) \left(\frac{8}{\pi} \right) \exp \left(-\frac{\pi^2}{4} t_{Dsf} \right) \quad (\text{B-15})$$

and solving for c_1 ,

$$c_1 = \frac{\left(\frac{\pi^2}{4} \right) \left(\frac{8}{\pi} \right) \exp \left(-\frac{\pi^2}{4} t_{Dsf} \right)}{c_2 \exp(-c_2 t_{Dsf})} \quad (\text{B-16})$$

Substituting the definition of c_1 into Eq. B-11 and equating it to Eq. B-9,

$$\frac{8}{\pi} \exp \left(-\frac{\pi^2}{4} t_{Dsf} \right) = \frac{\left(\frac{\pi^2}{4} \right) \left(\frac{8}{\pi} \right) \exp \left(-\frac{\pi^2}{4} t_{Dsf} \right)}{c_2 \exp(-c_2 t_{Dsf})} \exp(-c_2 t_{Dsf}) \quad (\text{B-17})$$

Canceling like terms and rearranging to solve for c_2 ,

$$c_2 = \frac{\pi^2}{4} \quad (\text{B-18})$$

Substituting the definition of c_2 into Eq. B-11 and equating it to Eq. B-9,

$$\frac{8}{\pi} \exp\left(-\frac{\pi^2}{4} t_{Dsf}\right) = c_1 \exp\left(-\frac{\pi^2}{4} t_{Dsf}\right) \quad (\text{B-19})$$

and c_1 therefore equals

$$c_1 = \frac{8}{\pi} \quad (\text{B-20})$$

Having derived the definitions of both c_1 and c_2 , we can now substitute them into Eq. B-10 to arrive upon the general form of the hyperbolic BDF stems, Eq. 2.9:

$$\left(\frac{s_f}{x_f}\right) q_D = \frac{8}{\pi} / \left(1 + \frac{\pi^2}{4} b_{BDF} t_{Dsf}\right)^{\frac{1}{b_{BDF}}} \quad (2.9)$$

Derivation of Eqs. 2.22 and 2.23

Wattenbarger (1998) defines dimensionless oil rate as:

$$q_D = \frac{141.2qB\mu}{kh(p_i - p_{wf})} \quad (\text{B-21})$$

And dimensionless gas rate as:

$$q_D = \frac{1424q_g T}{kh(m(p_i) - m(p_{wf}))} \quad (\text{B-22})$$

These definitions, however, presume production from a single fracture. As such, they must be modified to correct for the presence of multiple fractures. Assuming that a well with L_w/x_f fractures will produce at rates L_w/s_f higher than an equivalent well with only one fracture, the reported rate of the MFHW will be L_w/s_f times too high. Thus, Eqs. B-21 and B-22 must be modified in the following way:

$$q_D = \frac{141.2(\frac{s_f}{L_w})qB\mu}{kh(p_i - p_{wf})} = \left(\frac{s_f}{L_w}\right) \frac{141.2qB\mu}{kh(p_i - p_{wf})} \quad (\text{Eq. 2.22})$$

and

$$q_D = \frac{1424(\frac{s_f}{L_w})q_g T}{kh(m(p_i) - m(p_{wf}))} = \left(\frac{s_f}{L_w}\right) \frac{1424q_g T}{kh(m(p_i) - m(p_{wf}))} \quad (\text{Eq. 2.23})$$

Derivation of Eq. 2.30

The definition of the RMP is given by

$$RMP = \frac{\left(\frac{s_f}{x_f}\right)q_D}{q} \quad (B-23)$$

Rearranging to solve for rate,

$$q = \frac{\left(\frac{s_f}{x_f}\right)q_D}{RMP} \quad (B-24)$$

Therefore,

$$q_{i,BDF} = \frac{\left[\left(\frac{s_f}{x_f}\right)q_D\right]_{i,BDF}}{RMP} \quad (B-25)$$

Substituting in the general equation for the hyperbolic BDF stems, Eq. 2.9, and recognizing that

$t_{Dsf} = 0$ when $t = 0$, we arrive upon the expression for $q_{i,BDF}$, Eq. 2.30.

$$q_{i,BDF} = \frac{\frac{8}{\pi} \left(1 + \frac{\pi^2}{4} b_{BDF}(0)\right)^{\frac{1}{b_{BDF}}}}{RMP} = \frac{8}{\pi} \left(\frac{1}{RMP}\right) \quad (2.30)$$

Derivation of Eq. 2.31

The definition of nominal decline rate is

$$d = -\frac{1}{q} \frac{dq}{dt} \quad (\text{B-26})$$

and $(s_f/x_f)q_D$ during BDF is given by Eq. 2.9

$$\left(\frac{s_f}{x_f}\right) q_D = \frac{8}{\pi} / \left(1 + \frac{\pi^2}{4} b_{BDF} t_{Dsf}\right)^{\frac{1}{b_{BDF}}} \quad (2.9)$$

Recalling the definition of the RMP,

$$RMP = \frac{\left(\frac{s_f}{x_f}\right) q_D}{q} \quad (\text{B-27})$$

substituting it into Eq. B-26, and using the chain rule to expand the derivative term,

$$d = -\frac{RMP}{\left(\frac{s_f}{x_f}\right) q_D} \frac{dq}{d\left[\left(\frac{s_f}{x_f}\right) q_D\right]} \frac{d\left[\left(\frac{s_f}{x_f}\right) q_D\right]}{dt_{Dsf}} \frac{dt_{Dsf}}{dt} \quad (\text{B-28})$$

The derivative of q with respect to $(s_f/x_f)q_D$ can be found by rearranging and differentiating Eq.

B-27:

$$\frac{dq}{d\left[\left(\frac{s_f}{x_f}\right)q_D\right]} = \frac{1}{RMP} \quad (\text{B-29})$$

The second of the derivative terms in Eq. B-28 can be found by differentiating the general equation of the hyperbolic BDF stems, Eq. 2.9:

$$\frac{d\left[\left(\frac{s_f}{x_f}\right)q_D\right]}{dt_{Dsf}} = -\left(\frac{\pi^2}{4}\right)\left(\frac{8}{\pi}\right) / \left(1 + \frac{\pi^2}{4} b_{BDF} t_{Dsf}\right)^{\frac{1}{b_{BDF}}-1} \quad (\text{B-30})$$

The final derivative term of Eq. B-28 can be using the definition of the TMP:

$$TMP = \frac{t_{Dsf}}{t} \quad (\text{B-31})$$

Rearranging and differentiating yields

$$\frac{dt_{Dsf}}{dt} = TMP \quad (\text{B-32})$$

Substituting Eqs. 2.9, B-29, B-30, and B-32 into Eq. B-28,

$$d_{BDF} = \frac{(RMP)(TMP)}{RMP} \left[\frac{\left(\frac{\pi^2}{4}\right)\left(\frac{8}{\pi}\right)}{\left(1 + \frac{\pi^2}{4} b_{BDF} t_{Dsf}\right)^{\frac{1}{b_{BDF}} - 1}} \right] / \left[\frac{\frac{8}{\pi}}{\left(1 + \frac{\pi^2}{4} b_{BDF} t_{Dsf}\right)^{\frac{1}{b_{BDF}}}} \right] \quad (B-33)$$

Recognizing that $t_{Dsf} = 0$ when $t = 0$ and canceling like terms, we arrive upon Eq. 2.31:

$$d_{i,BDF} = (TMP) \left(\frac{\pi^2}{4}\right) \quad (2.31)$$

Derivation of Eq. 2.54

The cumulative production at any given point may be calculated by integrating the rate function with respect to time:

$$N_p = \int_0^{t_2} q dt \quad (B-34)$$

Therefore, the scaled EUR, forecast to scaled time $t_{life,sc}$, is given by

$$EUR_{sc} = \int_0^{t_{2,sc}=t_{life,sc}} q_{sc} dt_{sc} \quad (B-35)$$

The definitions of q_{sc} and t_{sc} are, respectively,

$$q_{sc} = q'q \quad (B-36)$$

and

$$t_{sc} = t' t \quad (\text{B-37})$$

Differentiating Eq. B-37,

$$dt_{sc} = t' dt \quad (\text{B-38})$$

Substituting Eqs. B-36 and B-38 into Eq. B-35,

$$EUR_{sc} = \int_{t_{1,sc}=0}^{t_{2,sc}=t_{life,sc}} q' q t' dt \quad (\text{B-39})$$

Using Eq. B-37 to convert the limits of integration from scaled time to unscaled time and pulling the constants outside the integral,

$$EUR_{sc} = q' t' \int_0^{t_2 = t_{life,sc}/t'} q dt \quad (\text{B-40})$$

which is simply the cumulative production after an unscaled time of $t_{life,sc}/t'$ multiplied by the rate and time scaling factors. Thus, we arrive upon Eq. 2.54:

$$EUR_{sc} = q' t' N_p(t = \frac{t_{life,sc}}{t'}) \quad (2.54)$$